



Addendum Cover Page

Complete only applicable items.

QA: QA

1. Total Pages: 312

2. Addendum to (Title): Multiscale Thermohydrologic Model			
3. DI (including Revision and Addendum No.): ANL-EBS-MD-000049 REV 03 AD 01			
	Printed Name	Signature	Date
4. Originator	Thomas A. Buscheck	<i>Thomas A. Buscheck</i>	8/23/07
5. Independent Technical Reviewer	Jean Younker	<i>Jean Younker</i>	8/23/07
6. Checker	John Leem	<i>John Leem</i>	8/23/07
7. QCS / QA Reviewer	Charles Beach	<i>Charles P. Beach</i>	8-23-07
8. Responsible Manager / Technical Lead	Ernest Hardin	<i>Ernest Hardin</i>	8/23/07
9. Responsible Manager	Geoff Freeze	<i>Geoff Freeze</i>	8/24/07
10. Remarks For clarity, Figures 6.3-77(a), 6.3-78(a), and 6.3-79(a) were replaced without alteration to the data; the plot curves now correspond to the legends. See also the editorial change on p. 6-47(a).			
Change History			
11. Revision and Addendum No.	12. Description of Change		
REV 03 AD 01	This addendum addresses the following CRs: 6521, 6543, 6730, 7191, 7892, 7969, 9740, 10733 and 10846.		

GAF
8/30/07

INTENTIONALLY LEFT BLANK

CONTENTS

	Page
ACRONYMS AND ABBREVIATIONS	xvii[a]
1[a]. PURPOSE	1-1[a]
2[a]. QUALITY ASSURANCE	2-1[a]
3[a]. USE OF SOFTWARE	3-1[a]
3.1[a] SOFTWARE	3-1[a]
3.1.1[a] Qualified Software	3-1[a]
4[a]. INPUTS	4-1[a]
4.1[a] PARAMETERS/DATA	4-1[a]
4.1.1[a] Qualification for Intended Use of Outside Sources	4-8[a]
4.2[a] YUCCA MOUNTAIN REVIEW PLAN ACCEPTANCE CRITERIA	4-12[a]
4.2.1[a] Acceptance Criterion 1 – System Description and Model Integration Are Adequate	4-12[a]
4.2.2[a] Acceptance Criterion 2 – Data Are Sufficient for Model Justification	4-13[a]
4.2.3[a] Acceptance Criterion 3 – Data Uncertainty Is Characterized and Propagated through the Model Abstraction	4-13[a]
4.2.4[a] Acceptance Criterion 4 – Model Uncertainty Is Characterized and Propagated through the Model Abstraction	4-14[a]
4.2.5[a] Acceptance Criterion 5 – Model Abstraction Output Is Supported by Objective Comparisons	4-14[a]
5[a]. ASSUMPTIONS	5-1[a]
5.1[a] BOUNDARY CONDITIONS	5-1[a]
5.1.1[a] Ground-Surface Relative Humidity	5-1[a]
5.1.2[a] Ambient Percolation Flux above Repository Horizon	5-1[a]
5.1.3[a] Barometric Pressure Fluctuations at the Ground Surface	5-1[a]
5.1.4[a] Timing of Climate Change Influence on Percolation Flux above Repository	5-1[a]
5.1.5[a] Water Table Rise	5-1[a]
5.2[a] HEAT FLOW PROCESSES	5-1[a]
5.2.1[a] Mountain-Scale Heat Flow	5-1[a]
5.2.2[a] Drift-Scale Heat Flow	5-1[a]
5.2.3[a] Waste Package Emplacement	5-1[a]
5.3[a] MATERIAL PROPERTIES	5-1[a]
5.3.1[a] Hydrologic Properties	5-1[a]
5.3.2[a] Thermal Properties	5-3[a]

CONTENTS (Continued)

	Page
5.4[a]	WASTE PACKAGE MODELING.....5-3[a]
5.4.1[a]	Average Waste Package Diameter and Location above Invert5-3[a]
5.4.2[a]	Waste Package Sequence along Drifts.....5-4[a]
5.5[a]	RELATIVE HUMIDITY IN EMPLACEMENT DRIFTS.....5-5[a]
5.6[a]	CONDENSATE DRAINAGE AROUND EMPLACEMENT DRIFTS5-5[a]
5.7[a]	GAS- AND LIQUID-PHASE FLOW IN THE LONGITUDINAL DIRECTION ALONG EMPLACEMENT DRIFTS (THE COLD-TRAP EFFECT)5-5[a]
5.8[a]	PROPERTIES OF HOST-ROCK RUBBLE FOR LOW- PROBABILITY-SEISMIC COLLAPSED-DRIFT SCENARIO5-5[a]
5.8.1[a]	Bulk Density of Host-Rock Rubble5-5[a]
6[a].	MODEL DISCUSSION.....6-1[a]
6.1[a]	YUCCA MOUNTAIN THERMOHYDROLOGY CONCEPTUAL MODEL6-1[a]
6.2[a]	THE MULTISCALE THERMOHYDROLOGIC MODELING APPROACH6-1[a]
6.2.1[a]	Overview of the MSTHM.....6-1[a]
6.2.2[a]	Incorporating the Unsaturated Zone Hydrology Model in the MSTHM.....6-1[a]
6.2.3[a]	Governing Equations for Unsaturated Zone Thermohydrology6-1[a]
6.2.4[a]	MSTHM Calculation Sequence6-1[a]
6.2.5[a]	SMT Submodels.....6-1[a]
6.2.6[a]	LDTH Submodels6-1[a]
6.2.7[a]	SDT Submodels6-1[a]
6.2.8[a]	DDT Submodels.....6-1[a]
6.2.9[a]	SMT and SDT Submodels for the Low-Probability-Seismic Collapsed-Drift Scenario6-2[a]
6.2.10[a]	LDTH Submodels for the Low-Probability-Seismic Collapsed-Drift Scenario6-2[a]
6.2.11[a]	DDT Submodels for the Low-Probability-Seismic Collapsed-Drift Scenario6-2[a]
6.2.12[a]	Modifications to MSTHM Implementation for TSPA.....6-2[a]
6.2.13[a]	Overview of Model Input Revisions.....6-7[a]
6.2.14[a]	Current SMT Submodel.....6-11[a]
6.2.15[a]	Current SDT Submodels6-12[a]
6.2.16[a]	Current LDTH Submodels.....6-14[a]
6.2.17[a]	Current DDT Submodels6-18[a]
6.2.18[a]	Current LDTH Submodels for the Low-Probability-Seismic Collapsed-Drift Case.....6-23[a]

CONTENTS (Continued)

	Page
6.2.19[a] Current DDT Submodels for the Low-Probability-Seismic Collapsed-Drift Case.....	6-23[a]
6.2.20[a] Repository-Averaged Generic LDTH Submodels	6-23[a]
6.2.21[a] Direction of Ventilation Implemented in LDTH and SDT Submodels	6-24[a]
6.3[a] MSTHM RESULTS.....	6-24[a]
6.3.1[a] TSPA-LA Base Case.....	6-24[a]
6.3.2[a] Parameter-Uncertainty Sensitivity Analyses	6-24[a]
6.3.3[a] Mass Flux in the Invert	6-24[a]
6.3.4[a] Combined Influences of Percolation Flux and Host-Rock Thermal Conductivity Uncertainty on the TSPA-LA Base Case	6-25[a]
6.3.5[a] Summary of the Range of Thermal-Hydrologic Conditions for the TSPA-LA Base Case	6-25[a]
6.3.6[a] Relationship between Relative Humidity on the Waste Package and Drip Shield and Temperature on the Drift Wall.....	6-25[a]
6.3.7[a] Influence of a Low-Probability-Seismic Collapsed-Drift Scenario on In-Drift Thermal-Hydrologic Conditions	6-25[a]
6.3.8[a] Comparison of Results for the TSPA-LA Base Case with Those for the FY01 Supplemental Science and Performance Analyses (SSPA)	6-25[a]
6.3.9[a] Influence of Host-Rock Hydrologic-Property Variability and Uncertainty	6-25[a]
6.3.10[a] Influence of Pseudo-Permeability on In-Drift Temperature and Relative Humidity	6-25[a]
6.3.11[a] Influence of Invert Hydrologic-Property Variability and Uncertainty.....	6-25[a]
6.3.12[a] Influence of Ventilation Heat-Removal Efficiency Uncertainty.....	6-25[a]
6.3.13[a] Relationship between Temperature and Relative Humidity on Waste Packages.....	6-26[a]
6.3.14[a] Sensitivity Analysis of the Influence of the Simplified Thermal-Hydrologic Stratigraphy in the Current LDTH Submodels	6-26[a]
6.3.15[a] Data Flow between Current MSTHM DTNs.....	6-32[a]
6.3.16[a] Current MSTHM Results for the TSPA Base Case.....	6-37[a]
6.3.17[a] Current MSTHM Results for the Low-Probability-Seismic Collapsed-Drift Case.....	6-46[a]
6.3.18[a] Analysis of In-Drift Vapor Flow and Condensation Using the Three-Dimensional Pillar-Scale Thermal-Hydrologic Model	6-53[a]

CONTENTS (Continued)

	Page
6.3.19[a] Influence of Invert Depth on Thermal-Hydrologic Conditions	6-57[a]
6.4[a] COMPARISON AGAINST AN ALTERNATIVE CONCEPTUAL MODEL	6-66[a]
6.5[a] FEPS	6-66[a]
7[a]. MODEL VALIDATION	7-1[a]
7.1[a] CONFIDENCE BUILDING DURING MODEL DEVELOPMENT TO ESTABLISH SCIENTIFIC BASIS AND ACCURACY FOR INTENDED USE.....	7-1[a]
7.2[a] CONFIDENCE BUILDING AFTER MODEL DEVELOPMENT TO SUPPORT THE SCIENTIFIC BASIS OF THE MODEL	7-1[a]
7.3[a] COMPARISON OF NUFT THERMAL-HYDROLOGIC MODEL AGAINST THE LARGE BLOCK TEST	7-1[a]
7.4[a] VALIDATION OF THE LDTH SUBMODEL USING THE DRIFT SCALE TEST	7-1[a]
7.4.1[a] Design and Geometry of the DST	7-1[a]
7.4.2[a] Description of Three-Dimensional Thermal-Hydrologic Model of the DST	7-1[a]
7.4.3[a] Comparison of Simulated and Field-Measured Temperatures.....	7-2[a]
7.4.4[a] Comparison of Simulated and Field-Measured Liquid-Phase Saturations in the Matrix	7-2[a]
7.4.5[a] Summary of Model Validation Using DST Data.....	7-2[a]
7.4.6[a] Updated Comparison of Simulated and Field-Measured Temperatures.....	7-2[a]
7.4.7[a] Updated Comparison of Simulated and Field-Measured Liquid-Phase Saturations in the Matrix	7-17[a]
7.4.8[a] Updated Summary of Model Validation Using DST Data	7-23[a]
7.5[a] COMPARISON OF THE MSTHM RESULTS AGAINST A MONOLITHIC THREE-DIMENSIONAL THERMAL-HYDROLOGIC MODEL	7-23[a]
7.6[a] COMPARISON OF THE MSTHM-PREDICTED IN-DRIFT TEMPERATURE DIFFERENCES AGAINST THOSE PREDICTED BY THE FLUENT CODE.....	7-23[a]
7.7[a] VALIDATION SUMMARY	7-23[a]
7.8[a] COMPARISON OF THE MSTHM RESULTS AGAINST A THREE- DIMENSIONAL PILLAR-SCALE THERMAL-HYDROLOGICAL MODEL	7-24[a]
7.9[a] UPDATED VALIDATION SUMMARY	7-35[a]

CONTENTS (Continued)

	Page
8[a]. CONCLUSIONS.....	8-1[a]
8.1[a] ANALYSIS AND MODELING CONCLUSIONS.....	8-1[a]
8.2[a] MODEL VALIDATION, UNCERTAINTIES, AND LIMITATIONS	8-1[a]
8.3[a] MODEL OUTPUTS	8-1[a]
8.4[a] YUCCA MOUNTAIN REVIEW PLAN ACCEPTANCE CRITERIA	8-3[a]
8.4.1[a] Acceptance Criterion 1 – System Description and Model Integration Are Adequate.....	8-3[a]
8.4.2[a] Acceptance Criterion 2 – Data Are Sufficient for Model Justification.....	8-5[a]
8.4.3[a] Acceptance Criterion 3 – Data Uncertainty Is Characterized and Propagated through the Model Abstraction	8-6[a]
8.4.4[a] Acceptance Criterion 4 – Model Uncertainty Is Characterized and Propagated through the Model Abstraction	8-7[a]
8.4.5[a] Acceptance Criterion 5 – Model Abstraction Output Is Supported by Objective Comparisons	8-8[a]
8.5[a] MSTHM CONDITION REPORTS	8-9[a]
8.5.1[a] CR-6521 – Incorrect Waste Package Heating for the Discrete-heat-source, Drift-scale, Thermal-conduction (DDT) Submodels of the MSTHM	8-9[a]
8.5.2[a] CR-6543 – Selecting Representative Waste Packages for TSPA Percolation Bins	8-9[a]
8.5.3[a] CR-6730 – Improve TSPA-Multiscale Temperature Abstraction.....	8-9
8.5.4[a] CR-7191 – RIT Action Items Associated with AMR ANL- EBS-MD-000049, Multiscale Thermohydrologic Model.....	8-9[a]
8.5.5[a] CR-7892 – Prediction of the Effective Thermal Conductivity of Granular Material.....	8-11[a]
8.5.6[a] CR-7969 – Lack of Documentation on Temperature Limit(s)	8-11[a]
8.5.7[a] CR-10733 – Qualified DTN: LL050500323122.060 Was Calculated Using Unqualified Data	8-11[a]
8.5.8[a] CR-10846 – Reversed Ventilation Direction in LDTH/SDT Submodels.....	8-11[a]
9[a]. INPUTS AND REFERENCES.....	9-1[a]
9.1[a] DOCUMENTS CITED	9-1[a]
9.2[a] CODES, STANDARDS, REGULATIONS, AND PROCEDURES.....	9-6[a]
9.3[a] SOURCE DATA, LISTED BY DATA TRACKING NUMBER	9-6[a]
9.4[a] OUTPUT DATA, LISTED BY DATA TRACKING NUMBER	9-8[a]
9.5[a] SOFTWARE CODES.....	9-12[a]

CONTENTS (Continued)

	Page
APPENDIX I[a]: BUILDING NUFT SUBMODELS	I-1[a]
APPENDIX II[a]: BUILDING BOUNDARY CONDITIONS FOR SUBMODELS.....	II-1[a]
APPENDIX III[a]: HEAT GENERATION FOR SUBMODELS.....	III-1[a]
APPENDIX IV[a]: BUILDING SUBMODEL MATERIAL PROPERTY FILES	IV-1[a]
APPENDIX V[a]: BUILDING SUBMODEL INPUT FILES	V-1[a]
APPENDIX VI[a]: LDTH AND DDT SUBMODEL THERMAL-RADIATION CONNECTION CALCULATION.....	VI-1[a]
APPENDIX VII[a]: EXTRACTION / MICRO-ABSTRACTION PROCESS FOR MSTHAC (BUILDING VIRTUAL LDTH AND SDT “CHIMNEY” SUBMODELS)	VII-1[a]
APPENDIX VIII[a]: BINNING CALCULATIONS	VIII-1[a]
APPENDIX IX[a]: MULTISCALE MODEL APPROACH TO THERMOHYDROLOGY AT YUCCA MOUNTAIN.....	IX-1[a]
APPENDIX X[a]: HYDROLOGIC PROPERTIES FOR THE INTERGRANULAR POROSITY OF THE INVERT	X-1[a]
APPENDIX XI[a]: THERMAL CONDUCTIVITY OF THE COLLAPSED DRIFT ZONE.....	XI-1[a]
APPENDIX XII[a]: COMPARISON OF PERCOLATION FLUXES.....	XII-1[a]
APPENDIX XIII[a]: LIST OF DATA SOURCES FOR FIGURES AND TABLES	XIII-1[a]
APPENDIX XIV[a]: QUALIFICATION OF UNQUALIFIED PROJECT DATA.....	XIV-1[a]
APPENDIX XV[a]: PREDICTION OF RH IN THE INVERT.....	XV-1[a]
APPENDIX XVI[a]: NUFT V4.0 EXECUTABLE INSTALL INFORMATION.....	XVI-1[a]

FIGURES

		Page
6.2-13[a].	SMT Submodel Mesh and UZ Flow Model Mesh, Together with Heated Repository Footprint Represented by the SMT Submodel.....	6-12[a]
6.2-14[a].	Schematic of the Stratigraphic Representation in the SDT Submodel	6-13[a]
6.2-15[a].	Schematic of the Stratigraphic Representation in the LDTH Submodel	6-15[a]
6.2-16[a].	Schematic of the Stratigraphic Representation in the DDT Submodel.....	6-18[a]
6.2-17[a].	Heated Repository Footprint of the SMT Submodel Mesh, Overlain on the UZ Flow Model Mesh and Showing the g ₉ Location.....	6-19[a]
6.2-18[a].	Distribution of the Host-Rock Units Within the Heated Repository Footprint of the SMT Submodel Mesh Overlain on the UZ Flow Model Grid.....	6-20[a]
6.2-19[a].	Heated Repository Footprint of the SMT-Submodel Mesh, Showing Panel Numbers and Contingency Drifts at the South End.....	6-21[a]
6.3-70[a].	Drift Wall Temperature (a) and Liquid-Phase Saturation (b) at the Repository Center for Different Representations of Thermal-Hydrologic Stratigraphy.....	6-28[a]
6.3-71[a].	Drift Wall Temperature (a) and Liquid-Phase Saturation (b) at the Repository Center Using the 30th and 10th Percentile Hydrologic Property Sets	6-29[a]
6.3-72[a].	Invert Temperature (a) and Liquid-Phase Saturation of the Intragranular Porosity of the Crushed Tuff in the Invert (b) at the Repository Center	6-31[a]
6.3-73[a].	Data Flow between the Output DTNs Generated by the MSTHM, Showing the Relationship between the Submodel Output DTNs and the MSTHM Output DTNs	6-32[a]
6.3-74[a].	Data Flow between the Output DTNs Generated by the MSTHM, Showing the Relationship between the Output DTNs with the Scaled Post-10,000-Year Percolation Flux Values and the DTNs with the Modified Post-10,000-Year Values	6-34[a]
6.3-75[a].	Data Flow between the Output DTNs Generated by the MSTHM, Showing How the Surrogate Cases Flow into the Five Uncertainty Cases That Were Not Directly Modeled	6-36[a]
6.3-76[a].	Range in (a) Drift Wall Temperature and (b) Waste Package Temperature for the Range of Parametric Uncertainty Addressed by the MSTHM.....	6-38[a]
6.3-77[a].	CCDF for (a) Peak Drift Wall Temperature and (b) Peak Waste Package Temperature for the Range of Parametric Uncertainty Addressed by the MSTHM.....	6-39[a]
6.3-78[a].	CCDF for the Time When Boiling Ceases on the (a) Drift Wall and (b) Waste Package for the Range of Parametric Uncertainty Addressed by the MSTHM.....	6-40[a]
6.3-79[a].	CCDF of the Maximum Lateral Extent of the Boiling-Point Isotherm (96°C) from the Drift Centerline for the Range of Parametric Uncertainty Addressed by the MSTHM	6-42[a]

FIGURES (Continued)

	Page
6.3-80[a]. Range in (a) Drift Wall and (b) Invert Liquid-Phase Saturation for the Range of Parametric Uncertainty Addressed by the MSTHM	6-44[a]
6.3-81[a]. Range in (a) Drift Wall and (b) Waste Package Relative Humidity for the Range of Parametric Uncertainty Addressed by the MSTHM	6-45[a]
6.3-82[a]. Waste Package Temperature History for the (a) DHLW/DOE SNF-Long (dhlw-11) Waste Package and the (b) 21-PWR AP CSNF (pwr1-3) Waste Package for the Nominal (Intact Drift) Case and Low and High Rubble Thermal Conductivity Collapsed-Drift Cases.....	6-48[a]
6.3-83[a]. Waste Package Relative Humidity History for the (a) DHLW/DOE SNF-Long (dhlw-11) Waste Package and the (b) 21-PWR AP CSNF (pwr1-3) Waste Package for the Nominal (Intact Drift) Case and Low and High Rubble Thermal Conductivity Collapsed-Drift Cases	6-49[a]
6.3-84[a]. Invert Liquid-Phase Saturation History for the Intragranular Porosity for the (a) DHLW/DOE SNF-Long (dhlw-11) Waste Package and the (b) 21-PWR AP CSNF (pwr1-3) Waste Package for the Nominal (Intact Drift) Case and Low and High Rubble Thermal Conductivity Collapsed-Drift Cases	6-50[a]
6.3-85[a]. Waste Package Temperature Histories and Corresponding Percentiles Showing Ranges for the DHLW/DOE SNF-Long (dhlw-11) Waste Packages for the Collapsed-Drift Case	6-51[a]
6.3-86[a]. Waste Package Temperature Histories and Corresponding Percentiles Showing Ranges for the 21-PWR AP CSNF (pwr1-3) Waste Packages for the Collapsed-Drift Case.....	6-52[a]
6.3-87[a]. CCDFs for Peak Waste Package Temperatures for CSNF and DHLW Waste Packages for Collapsed-Drift Cases Subject to Low and High Rubble K_{th}	6-53[a]
6.3-88[a]. Temperature on the Drip Shield (a) and Waste Package (b) at the Repository Center for Different Representations of In-Drift Thermal Radiation	6-55[a]
6.3-89[a]. Gas-Phase Pressure (a) and Air Mass Fraction (b) beneath the Drift Crown, above the Drip Shield Crown, and below the Drip Shield Crown at the Repository Center	6-56[a]
6.3-90[a]. Temperature on the Drift Wall (a) and Drip Shield (b) at the Repository Center for Different Representations of In-Drift Thermal Radiation	6-58[a]
6.3-91[a]. Drift Wall Liquid-Phase Saturation (a) and Drip Shield Relative Humidity (b) at the Repository Center for Different Representations of In-Drift Thermal Radiation	6-59[a]
6.3-92[a]. Invert Temperature at the Repository Center for Different Representations of In-Drift Thermal Radiation.....	6-60[a]
6.3-93[a]. Invert Liquid-Phase Saturation (a) and Relative Humidity (b) at the Repository Center for Different Representations of In-Drift Thermal Radiation	6-61[a]

FIGURES (Continued)

	Page
6.3-94[a]. Temperature on the Drift Wall (a) and Drip Shield (b) at the Repository Center for the Base Case with an Invert Depth of 0.806 m and a Case with an Updated Invert Depth of 1.32 m	6-62[a]
6.3-95[a]. Drift Wall Liquid-Phase Saturation (a) and Drip Shield Relative Humidity (b) at the Repository Center for the Base Case with an Invert Depth of 0.806 m and a Case with an Updated Invert Depth of 1.32 m.....	6-63[a]
6.3-96[a]. Invert Temperature at the Repository Center for the Base Case with an Invert Depth of 0.806 m and a Case with an Updated Invert Depth of 1.32 m	6-64[a]
6.3-97[a]. Invert Liquid-Phase Saturation (a) and Relative Humidity (b) at the Repository Center for the Base Case with an Invert Depth of 0.806 m and a Case with an Updated Invert Depth of 1.32 m.....	6-65[a]
7.4-21[a]. NUFT-Simulated and Measured Temperatures Compared along Borehole 141 at (a) 175, (b) 365, (c) 730, (d) 1,096, (e) 1,500, and (f) 2,005 Days	7-4[a]
7.4-22[a]. NUFT-Simulated and Measured Temperatures Compared along Borehole 158 at (a) 175, (b) 365, (c) 730, (d) 1,096, (e) 1,500, and (f) 2,005 Days	7-5[a]
7.4-23[a]. NUFT-Simulated and Measured Temperatures Compared along Borehole 168 at (a) 175, (b) 365, (c) 730, (d) 1,096, (e) 1,500, and (f) 2,005 Days	7-6[a]
7.4-24[a]. NUFT-Simulated and Measured Temperatures Compared along Borehole 169 at (a) 175, (b) 365, (c) 730, (d) 1,096, (e) 1,500, and (f) 2,005 Days	7-7[a]
7.4-25[a]. NUFT-Simulated and Measured Temperatures Compared along Borehole 170 at (a) 175, (b) 365, (c) 730, (d) 1,096, (e) 1,500, and (f) 2,005 Days	7-8[a]
7.4-26[a]. NUFT-Simulated and Measured Temperatures Compared along Borehole 143 at (a) 175, (b) 365, (c) 1,650, and (d) 2,005 Days	7-9[a]
7.4-27[a]. NUFT-Simulated and Measured Temperatures Compared along Borehole 164 at (a) 175, (b) 365, (c) 1,650, and (d) 2,005 Days	7-10[a]
7.4-28[a]. NUFT-Simulated and Measured Temperatures Compared along Borehole 79 at (a) 175, (b) 365, (c) 730, (d) 1,096, (e) 1,500, and (f) 2,005 Days	7-11[a]
7.4-29[a]. NUFT-Simulated and Measured Temperatures Compared along Borehole 80 at (a) 175, (b) 365, (c) 730, (d) 1,096, (e) 1,500, and (f) 2,005 Days	7-12[a]
7.4-30[a]. NUFT-Simulated and Measured Temperature Histories Compared at (a) Borehole 133: Sensor 23, (b) Borehole 134: Sensor 8, (c) Borehole 137: Sensor 23, and (d) Borehole 137: Sensor 53.....	7-14[a]
7.4-31[a]. NUFT-Simulated and Measured Temperature Histories Compared at (a) Borehole 144: Sensor 21, (b) Borehole 144: Sensor 51, (c) Borehole 168: Sensor 20, and (d) Borehole 168: Sensor 50.....	7-15[a]
7.4-32[a]. NUFT-Simulated and Measured Temperature Histories Compared at (a) Borehole 79: Sensor 29, (b) Borehole 79: Sensor 34, (c) Borehole 80: Sensor 48, and (d) Borehole 80: Sensor 53.....	7-16[a]
7.4-33[a]. NUFT-Simulated and Measured Liquid-Phase Saturations in the Matrix Compared along Borehole 66 at (a) 877 Days, (b) 1,242 Days, (c) 1,510 Days, and (d) 1,917 Days.....	7-18[a]

FIGURES (Continued)

	Page
7.4-34[a]. NUFT-Simulated and Measured Liquid-Phase Saturations in the Matrix Compared along Borehole 67 at (a) 200 Days, (b) 350 Days, (c) 877 Days, and (d) 1,917 Days.....	7-19[a]
7.4-35[a]. NUFT-Simulated and Measured Liquid-Phase Saturations in the Matrix Compared along Borehole 68 at (a) 877 Days, (b) 1,242 Days, (c) 1,510 Days, and (d) 1,917 Days.....	7-20[a]
7.4-36[a]. NUFT-Simulated and Measured Liquid-Phase Saturations in the Matrix Compared along Borehole 79 at (a) 877 Days, (b) 1,242 Days, (c) 1,510 Days, and (d) 1,917 Days.....	7-21[a]
7.4-37[a]. NUFT-Simulated and Measured Liquid-Phase Saturations in the Matrix Compared along Borehole 80 at (a) 877 Days, (b) 1,242 Days, (c) 1,510 Days, and (d) 1,917 Days.....	7-22[a]
7.8-1[a]. Thermal-Hydrologic Conditions Predicted by the MSTHM and 3-D Pillar-Scale TH Model Compared along the Drift, Including (a) Peak Waste Package Temperature and (b) Time When Boiling Ceases on the Waste Package	7-26[a]
7.8-2[a]. Thermal-Hydrologic Conditions Predicted by the MSTHM and 3-D Pillar-Scale TH Model Compared at the Repository Center and Edge for the pwr1-1 Waste Package, Including Waste Package (a) Temperature and (b) Relative Humidity, and Liquid-Phase Saturation at the (c) Drift Wall and in the (d) Invert.....	7-27[a]
7.8-3[a]. Thermal-Hydrologic Conditions Predicted by the MSTHM and 3-D Pillar-Scale TH Model Compared at the Repository Center and Edge for the dhlw-11 Waste Package, Including Waste Package (a) Temperature and (b) Relative Humidity, and Liquid-Phase Saturation at the (c) Drift Wall and in the (d) Invert.....	7-28[a]
7.8-4[a]. Thermal-Hydrologic Conditions Predicted by the MSTHM and 3-D Pillar-Scale TH Model Compared at the Repository Center and Edge for the pwr2-1 Waste Package, Including Waste Package (a) Temperature and (b) Relative Humidity, and Liquid-Phase Saturation at the (c) Drift Wall and in the (d) Invert.....	7-29[a]
7.8-5[a]. Thermal-Hydrologic Conditions Predicted by the MSTHM and 3-D Pillar-Scale TH Model Compared at the Repository Center and Edge for the bwr1-1 Waste Package, Including Waste Package (a) Temperature and (b) Relative Humidity, and Liquid-Phase Saturation at the (c) Drift Wall and in the (d) Invert.....	7-30[a]
7.8-6[a]. Thermal-Hydrologic Conditions Predicted by the MSTHM and 3-D Pillar-Scale TH Model Compared at the Repository Center and Edge for the bwr2-1 Waste Package, Including Waste Package (a) Temperature and (b) Relative Humidity, and Liquid-Phase Saturation at the (c) Drift Wall and in the (d) Invert.....	7-31[a]

FIGURES (Continued)

	Page
7.8-7[a]. Thermal-Hydrologic Conditions Predicted by the MSTHM and 3-D Pillar-Scale TH Model Compared at the Repository Center and Edge for the dhlw-s1 Waste Package, Including Waste Package (a) Temperature and (b) Relative Humidity, and Liquid-Phase Saturation at the (c) Drift Wall and in the (d) Invert.....	7-32[a]
7.8-8[a]. Thermal-Hydrologic Conditions Predicted by the MSTHM and 3-D Pillar-Scale TH Model Compared at the Repository Center and Edge for the pwr1-2 Waste Package, Including Waste Package (a) Temperature and (b) Relative Humidity, and Liquid-Phase Saturation at the (c) Drift Wall and in the (d) Invert.....	7-33[a]
7.8-9[a]. Thermal-Hydrologic Conditions Predicted by the MSTHM and 3-D Pillar-Scale TH Model Compared at the Repository Center and Edge for the pwr1-3 Waste Package, Including Waste Package (a) Temperature and (b) Relative Humidity, and Liquid-Phase Saturation at the (c) Drift Wall and in the (d) Invert.....	7-34[a]
8.5-1[a]. CCDF for Peak Waste Package Temperature for the P10 Percolation Flux/Host-Rock Thermal Conductivity Case.....	8-12[a]
8.5-2[a]. CCDF for the Time When Boiling Ceases on the Waste Package for the P10 Percolation Flux/Host-Rock Thermal Conductivity Case	8-13[a]
I-1[a]. Plot of In-Drift Effective Thermal Conductivity between the Drip Shield and Drift Wall as a Function of Temperature Difference	I-6[a]
VIII-1[a]. Color Plot of the Five Percolation Bins within the Heated Footprint of the Heated Repository Footprint in the SMT Submodel Mesh Overlain on the UZ Flow Model Grid	VIII-4[a]
X-1[a]. Comparison of the Developed Water Retention Relationship for the Invert Ballast Materials and the Relationship Provided to the MSTHM	X-9[a]
X-2[a]. Hydraulic Conductivity as a Function of Capillary Pressure for Residual Saturations of 0.15 (black curve) and 0.01 (dashed red curve) When Water Density is 987.88 kg/m^3 and Dynamic Viscosity is $5.46 \times 10^{-4} \text{ kg/m}\cdot\text{s}$	X-13[a]
XI-1[a]. Range of Effective K_{th} Calculated for Rubble with Dry Particles	XI-5[a]
XI-2[a]. Range of Effective K_{th} Calculated for Rubble with Wet Particles.....	XI-6[a]

INTENTIONALLY LEFT BLANK

TABLES

	Page
3-1[a].	Qualified/Baseline Software Used.....3-1[a]
4-1[a].	Summary of Direct Input Data and Information Required by the MSTHM.....4-2[a]
4-2[a].	Summary of Emplacement Panels and Drifts Represented in the SMT Submodel for the Layout4-8[a]
4-3[a].	Listing of the Input Data and Their Sources for the LTBM-2 Material4-8[a]
5.4-1[a].	Summary of Waste Package Types in the Repository Inventory and in the MSTHM.....5-5[a]
6.2-5[a].	Summary of Repository-Wide-Averaged Percolation Flux for the Four Climate States6-17[a]
6.2-6[a].	Summary of Waste Packages Included in the MSTHM Calculations6-22[a]
6.2-7[a].	Repository-Averaged Thicknesses for the Generic Thermal-Hydrologic Stratigraphy Used in the LDTH Submodels6-24[a]
6.3-47[a].	Relationship between the Modeled Uncertainty Cases (blue background) and the Uncertainty Cases Not Directly Modeled (green background), with the Identity of the Surrogate Case Show in Red.....6-35[a]
6.3-48[a].	Relationship between the Modeled Uncertainty Cases (blue background) and the Uncertainty Cases Not Directly Modeled (green background), with the Names of the Five Uncertainty Cases Not Directly Modeled Shown in Red.....6-35[a]
6.3-49[a].	Peak Drift Wall and Waste Package Temperatures Summarized for the Seven Modeled Uncertainty Cases6-41[a]
6.3-50[a].	Time When Boiling Ceases at the Drift Wall Summarized for the Seven Modeled Uncertainty Cases6-41[a]
6.3-51[a].	Maximum Lateral Extent of the Boiling-Point Isotherm (96°C) Measured from the Drift Centerline, Summarized for the Seven Modeled Uncertainty Cases6-43[a]
6.5-2[a].	FEPs Addressed by This Report6-66[a]
7.4-4[a].	Summary of Thermocouple Boreholes Used to Compare Field-Measured Temperatures with NUFT-Simulated Temperatures7-3[a]
7.4-5[a].	Coordinates of Thermocouple Sensors Used in Figures 7.4-30[a], 7.4-31[a], and 7.4-32[a]7-13[a]
7.4-6[a].	Summary of Boreholes Used to Compare Field-Measured Saturations with NUFT-Simulated Saturations.....7-17[a]
8-1[a].	Data Tracking Numbers Associated with the Output Produced by This Addendum.....8-1[a]
IV-1[a].	Interpolation of Thermal Diffusivity and Thermal Conductivity Outlined for Stainless Steel Type 316IV-8[a]
IV-2[a].	Interpolation of Thermal Diffusivity and Thermal Conductivity Outlined for TitaniumIV-9[a]
IV-3a[a].	Specific Heat Capacity, Thermal Conductivity (dry and wet), and Bulk Density for the GFM2000 UnitsIV-13[a]
IV-3b[a].	Thermal Properties for the UZ Model Layers.....IV-15[a]

TABLES (Continued)

	Page
IV-4[a]. Matrix and Fracture Properties for the Drift-Scale Calibrated Property Set for the 30th Percentile Infiltration Map	IV-17[a]
IV-5[a]. Fracture Frequency and Fracture-to-Matrix Interface Area.....	IV-18[a]
VI-1[a]. Value of the Coefficient <i>C</i> from Equation VI-8[a] Calculated for Different Values of Emissivity at the Drift Wall.....	VI-3[a]
X-1[a]. Intergranular Porosity, Intergranular Residual Water Content, and Intergranular Residual Water Saturation for the LTBM-2 Crushed Tuff	X-7[a]
X-2[a]. Description of the Spreadsheets in Workbook <i>arya_original data interpretation 4 17Jul07.xls</i> , Located in Output DTN: MO0703PAHYTHRM.000	X-8[a]
X-3[a]. Description of the Spreadsheets in Workbook <i>Van Genuchten Properties 17Jul07.xls</i>	X-8[a]
X-4[a]. Best-Fit van Genuchten Parameters for the LTBM-2 Material	X-8[a]
X-5[a]. Thermal Conductivity (W/m-K) for a Single-Sized Particle Medium as a Function of Particle Size, Porosity, and Temperature	X-11[a]
X-6[a]. Unsaturated Hydraulic Conductivity as a Function of Moisture Potential	X-12[a]
XI-1[a]. Parameter Ranges for Calculation of Effective K_{th} for the MSTHM	XI-4[a]

ACRONYMS AND ABBREVIATIONS

AML	areal mass loading (mass of spent nuclear fuel and high-level waste per unit area of heated repository footprint MTU/acre)
BSC	Bechtel SAIC Company
BWR	boiling water reactor (in reference to a waste package type)
CCDF	complementary cumulative distribution function
CDSP	codisposal (in reference to a waste package type)
CR	Condition Report
CSNF	commercial spent nuclear fuel (in reference to a waste package type)
DDT	Discrete-heat-source, Drift-scale, Thermal-conduction submodel of the MSTHM (a three-dimensional NUFT submodel)
DHLW	defense high-level (radioactive) waste (in reference to a waste package type)
DIRS	Document Input Reference System
DKM	dual-permeability model
DMTH	Discrete-heat-source, Mountain-scale, Thermal-Hydrologic model (result of the MSTHM)
DOE	U.S. Department of Energy
DST	Drift Scale Test
DTN	data tracking number
EBS	Engineered Barrier System
FEPs	features, events, and processes
HD	Heated Drift
HLW	high-level (radioactive) waste (in reference to a waste package type)
LA	license application
LDTH	Line-averaged-heat-source, Drift-scale, Thermal-Hydrologic submodel of the MSTHM; this submodel is a two-dimensional NUFT submodel
LLNL	Lawrence Livermore National Laboratory
LMTH	Line-averaged-heat-source, Mountain-scale, Thermal-Hydrologic model (an intermediate result of the MSTHM)
LTBM	laboratory tunnel boring machine (in reference to LTBM-2 material)
MSTHM	multiscale thermohydrologic model
MTU	metric tons of uranium (measure of mass of radioactive waste, which is also a measure of the thermal power loading)
NRC	U.S. Nuclear Regulatory Commission

ACRONYMS AND ABBREVIATIONS (Continued)

PWR	pressurized water reactor (in reference to a waste package type)
RH	relative humidity
RIT	Regulatory Integration Team
SDT	Smeared-heat-source, Drift-scale, Thermal-conduction submodel (a one-dimensional NUFT submodel)
SMT	Smeared-heat-source, Mountain-scale, Thermal-conduction submodel (this submodel is a three-dimensional NUFT submodel)
SNF	spent nuclear fuel (in reference to a waste package type)
SZ	saturated zone
TAD	transporation, aging, and disposal (canister)
TH	thermal-hydrologic
TSPA	total system performance assessment
TWP	technical work plan
UZ	unsaturated zone
WAPDEG	waste package degradation (analysis)
YMP	Yucca Mountain Project
YMRP	<i>Yucca Mountain Review Plan, Final Report</i>
3-D	three-dimensional

1[a]. PURPOSE

The purpose of this addendum is to predict thermal-hydrologic (TH) conditions using updated parameters and modeling techniques for repository simulation in total system performance assessment (TSPA), with appropriate consideration of parameter uncertainty and spatial variability. The purpose is unchanged from the parent report.

This addendum documents a recalculation of the multiscale thermohydrologic model (MSTHM) to achieve the following:

- Address Condition Reports (CRs) 6521 and 6543 by implementing the corrected discrete-heat-source, drift-scale, thermal conduction (DDT) submodel thermal inputs and corrected software (see Section 8.5[a] for more information).
- Use new hydrologic and thermal properties for the invert ballast to address CR-5154 (note that this CR is considered completed by the Corrective Action Program).
- Address other CRs: 6730, 7191, 7892, 7969, 9740, 10733, and 10846 (see Section 8.5[a] for more information).
- Simulate waste emplacement in the entire layout (with contingency drifts), where the total amount of emplaced waste represented this way may exceed the statutory maximum. This analysis does not imply any changes from the licensing requirements of 10 CFR Part 63 or with the Nuclear Waste Policy Act of 1982, as amended (DOE 2002 [DIRS 180715]).
- Implement new percolation flux estimates from the unsaturated zone (UZ) flow model (SNL 2007 [DIRS 175177]), which uses the new MASSIF infiltration model (DTN: SN0704T0502206.047 [DIRS 181200]), while applying percolation flux values from grid blocks in the UZ flow model to MSTHM locations, without interpolation.
- Use new calibrated hydrologic properties (also from the UZ flow model).
- Generate TH predictions out to 1,000,000 years, to represent the period of geologic stability specified in the proposed rule at 10 CFR Part 63 (70 FR 53313 [DIRS 178394]).
- Implement updated design dimensions (as of the start of MSTHM calculations) for waste packages, drip shields, and the invert.
- Implement new heat generation histories for waste packages, associated with the transportation, aging, and disposal (TAD) canister (the average drift-load is unchanged).
- Implement design changes (as of the start of MSTHM calculations) in the repository layout.
- Simplify specification of rock properties for far-field (non-host) units in the thermal-hydrologic line-averaged-heat-source, drift-scale, thermal-hydrologic (LDTH)

submodels. This implements part of the “generic LDTH submodel” approach planned in *Technical Work Plan for: Additional Multiscale Thermohydrologic Modeling* (BSC 2006 [DIRS 178297]) as discussed below.

- Extend the lower boundaries of the smeared-heat-source, drift-scale, thermal-conduction (SDT) and LDTH submodel domains to 1 km below the water table to better estimate repository temperature at late time (after 5,000 years).
- Revise the seismic drift-collapse cases to conform to model changes listed above.
- Update the comparison of TH model simulations with Drift Scale Test (DST) data.
- Develop, qualify, and use the software NUFT V4.0 (see Section 3.1.1.9[a] and Table 3-1[a]) to acquire the results presented in this addendum.

CR-6730 has been addressed through changes to the software code reformat_EXT_to_TSPA V2.0 (see Section 3.1.1.10[a] and Table 3-1[a]) to allow selection of waste packages according to various temperature bins (i.e., percentiles) for TSPA sensitivity studies. Running the software to generate additional temperature bins for TSPA is not included in this addendum.

This addendum was prepared in accordance with the technical work plan (TWP) (BSC 2006 [DIRS 178297]). Several deviations from the TWP were implemented as a result of minor re-scoping of the work. These deviations are as follows:

- **Model Changes** – Implementation of the generic LDTH submodel approach was limited to: (1) simplification of the thermal and hydrologic properties for non-host rock units in the LDTH submodels, and (2) use of only two host rock units/types for lithophysal and non-lithophysal host-rock units. Changes to baselined software were not required. In addition, the LDTH and SDT submodels were extended to 1 km below the water table, with new host-rock hydrologic property values applied, and were deployed at each of the 560 UZ flow model columns within the heated repository footprint. These improvements allowed the stratigraphic information and updated percolation flux values for the heated repository footprint to be taken directly from the UZ flow model output without spatial interpolation (SNL 2007 [DIRS 175177]). These are the only changes in the multiscale model from that documented in the parent report.

Justification: The decision not to implement the features of the “generic LDTH submodel” approach reduced technical and schedule risk, without affecting model completeness, representativeness, precision, or accuracy because the modeling approach used in preparation of this addendum is nearly identical to the parent report. Those features of the “generic LDTH submodel” approach that were retained in the new calculations are submodel improvements that are not central to the multiscale abstraction methodology. The fact that the abstraction methodology is unchanged is evident because no changes were made when implementing the software MSTHAC V7.0 (see Section 3.1.1.3[a] and Table 3-1[a]).

- **Validation Task 1** – Not all validation and testing activities are repeated; rather the original validation (see Section 7 of the parent report) and particularly the three-drift validation problem (Section 7.5[a]) are retained. A new post-development validation exercise (Section 7.8[a]) is added to this addendum where the multiscale methodology is applied and compared to a new three-dimensional (3-D) pillar-scale TH simulation of a single repository drift. In addition, a set of confidence-building simulations performed during development of the model changes for this addendum is included. These simulations address the simplification of thermal and hydrologic properties for the non-host rock units as well as new lithophysal and non-lithophysal property sets to represent the four host-rock units: Tptpul, Tptpmn, Tptpll, and Tptpln.

Justification: The multiscale abstraction methodology applied in this addendum is the same as in the parent report; therefore, the validation documented previously remains applicable. As stated above, the model changes implemented in this addendum are not central to the methodology, which is evident because no software changes were made. Notwithstanding these points, a new validation exercise is added (Section 7.8[a]) that parallels the previous exercise (Section 7.5[a]) and implements the new model changes, but is now conducted at the full pillar scale. Finally, the simulations performed during model development provide appropriate confidence that the submodel changes improve the established abstraction methodology.

- **Validation Task 2** – A fully three-dimensional TH simulation of the DST is performed (Section 7.4.6[a]), supplementing the previous one (Section 7.4 of the parent report) The purpose is to evaluate the updated thermal and hydrologic properties used to represent the host rock.

Justification: Validation Task 2 is required to verify the validity of the LDTH model with updated thermal-hydrologic properties.

- **Other Deviations** – The average thermal line load used in the parent report was not changed in the calculations documented in this addendum, although it is mentioned in the TWP (BSC 2006 [DIRS 178297], Section 1.2.5) as a change. In addition, the temporally and spatially variable ventilation efficiency is retained from the parent report in this addendum, although it is mentioned in the TWP as a change.

Justification: The average load was deliberately preserved, even though new thermal output histories for individual waste packages were developed. This was to ensure thermal loading conditions equal to those used in other two-dimensional coupled-process simulations, for example those in *Mountain-Scale Coupled Processes (TH/THC/THM) Models* (BSC 2005 [DIRS 174101]). The development of new thermal output for individual packages, to include changes resulting from use of TAD canisters, is documented in *Initial Radionuclides Inventory* (SNL 2007 [DIRS 180472]) and in DTN: MO0702PASTREAM.001 [DIRS 179925]. The fixed ventilation efficiency was a feature of the “generic LDTH submodel” approach previously under development. It was not needed in the MSTHM calculations documented in this addendum because the LDTH submodels were assigned to specific locations for which spatially and temporally dependent ventilation efficiency data (available in the parent report) are again calculated

in this addendum for use in TSPA. The same sources of parameter uncertainty are represented, except that lumped property values are developed for far-field non-host-rock units (this change was addressed by the simulations undertaken during model development discussed in Validation Task 2). Design features of the Engineered Barrier System (EBS) are represented in the MSTHM the same as they were previously, although a few parameters were updated (e.g., waste package dimensions).

As stated in the footnote of Table 1-1 of the parent report, the invert relative humidity is calculated by TSPA, using the MathCad spreadsheet described in Appendix XV of the parent report, based on the MSTHM-predicted temperature and liquid-phase saturation in the invert.

The features, events, and processes (FEPs) (see Table 6.5-1 of the parent report) and the criteria from *Yucca Mountain Review Plan, Final Report* (YMRP) (NRC 2003 [DIRS 163274]) addressed by the MSTHM are unchanged from those identified in the TWP (BSC 2006 [DIRS 178297], Section 2.1.4). However, two additional FEPs, as noted in Table 6.5-2[a], are addressed in this addendum.

2[a]. QUALITY ASSURANCE

This addendum was prepared in accordance with *Technical Work Plan for: Additional Multiscale Thermohydrologic Modeling* (BSC 2006 [DIRS 178297]) and SCI-PRO-006, *Models*.

As discussed in the TWP (BSC 2006 [DIRS 178297]), the initial planning of the analysis presented herein was originally intended for a revision of the parent report. However, it was later decided to present the analysis in an addendum to the parent report. This is a deviation from the planning done in the TWP.

Planning and preparation of this addendum was initiated under the Bechtel SAIC Company (BSC) Quality Assurance Program. Therefore, forms and associated documentation prepared prior to October 2, 2006, the date this work transitioned to the Lead Laboratory, were completed in accordance with BSC procedures. Forms and associated documentation executed on or after October 2, 2006, were prepared in accordance with Lead Laboratory procedures.

INTENTIONALLY LEFT BLANK

3[a]. USE OF SOFTWARE

3.1[a] SOFTWARE

Software utilized by the MSTHM process model in this addendum is listed here along with qualification status. No other software will be developed except for items defined as exempt in accordance with IM-PRO-003, *Software Management*.

A complete list of the qualified software and the associated software tracking number is given in Table 3-1[a].

Table 3-1[a]. Qualified/Baseline Software Used

Software Name and Version	DIRS Number	Software Tracking Number	Platform Used
RADPRO v4.0	164273	10204-4.0-00	SunOS 5.8
XTOOL v10.1	148638	10208-10.1-00	SunOS 5.6.1
MSTHAC v7.0	164274	10419-7.0-00	SunOS 5.8
readsUnits v1.0	164542	10602-1.0-00	SunOS 5.5.1
YMESS v1.54	163894	10172-1.54-00	SunOS 5.8
boundary_conditions v1.0	164275	11042-1.0-00	SunOS 5.8
heatgen_ventTable_emplace v1.0	164276	11039-1.0-00	SunOS 5.8
rme6 v1.2	163892	10617-1.2-00	SunOS 5.8
reformat_EXT_to_TSPA v2.0	180261	11061-2.0-00	SunOS 5.8
NUFT v3.0s	164541	10088-3.0s-02	SunOS 5.8
NUFT v4.0	180382	11228-4.0-00	Sun OS 5.8
extractBlocks_EXT v1.0	164281	11040-1.0-00	Sun OS 5.8

NOTE: DIRS = Document Input Reference System.

3.1.1[a] Qualified Software

3.1.1.1[a] RADPRO v4.0

RADPRO v4.0 is baselined as qualified software per IM-PRO-003, and was obtained from Software Configuration Management and run on a Sun workstation with a SunOS 5.8 (Solaris 8) operating system. RADPRO v4.0 was selected because it calculates the radiative heat transfer coefficients in the emplacement drift. Its use was consistent with its intended use and within the documented validation range of the software. Because this software is only used to conduct simple arithmetic functions, it is not applicable to identify validation ranges or limitations of use.

3.1.1.2[a] XTOOL v10.1

XTOOL v10.1 is baselined as a qualified software routine per IM-PRO-003, and was obtained from Software Configuration Management and run on a Sun workstation with a SunOS 5.6.1 operating system. XTOOL v10.1 is used to generate graphical representations of the results given in the NUFT and MSTHAC v7.0 time-history files (which are files with the suffix: *.ext). XTOOL v10.1 is the only appropriate software for this task. Because this software is only used

to generate graphical displays of data, it is not applicable to identify validation ranges or limitations of use.

3.1.1.3[a] MSTHAC v7.0

MSTHAC v7.0 is baselined as qualified software per IM-PRO-003, and was obtained from Software Configuration Management and run on a Sun workstation with a SunOS 5.8 (Solaris 8) operating system. MSTHAC v7.0 integrates the results of NUFT submodel calculations to predict the multiscale thermal-hydrologic conditions in the emplacement drifts and adjoining host rock throughout the repository area. MSTHAC v7.0 is the only appropriate software for this task. Because MSTHAC integrates the results of NUFT submodel calculations, its validation range is the same as that described for NUFT.

3.1.1.4[a] readsUnits v1.0

Software routine readsUnits v1.0 is baselined as qualified software per IM-PRO-003, and was obtained from Software Configuration Management and run on a Sun workstation with a SunOS 5.5.1 operating system. This code reads YMESH-generated data describing a stratigraphic column and generates comment lines for NUFT input files that summarize the thicknesses of each of the hydrostratigraphic units (also called UZ model layers) in that column. Software routine readsUnits v1.0 is the only appropriate software for this task. Because this software is only used to generate comment lines in the NUFT input files, it does not influence any model predictions. Therefore, it is not applicable to identify validation ranges or limitations of use.

3.1.1.5[a] YMESH v1.54

YMESH v1.54 is baselined as qualified software per IM-PRO-003, and was obtained from Software Configuration Management and run on a Sun workstation with a SunOS 5.8 (Solaris 8) operating system. YMESH v1.54 is used to generate the thicknesses of the hydrostratigraphic units (also called the UZ model layers) in the various MSTHM submodels based upon the grids from *Development of Numerical Grids for UZ Flow and Transport Modeling* (BSC 2004 [DIRS 169855]). YMESH v1.54 is the only appropriate software for this task. Because this software is only used to generate numerical grids on the basis of geometric relationships, it is not applicable to identify validation ranges or limitations of use.

3.1.1.6[a] boundary_conditions v1.0

The software routine boundary_conditions v1.0 is baselined as qualified software per IM-PRO-003, and was obtained from Software Configuration Management and run on a Sun workstation with a SunOS 5.8 (Solaris 8) operating system. The purpose of this routine is to generate upper and lower boundary conditions for the LDTH, smeared-heat-source, mountain-scale, thermal-conduction (SMT), and SDT submodels of the MSTHM, as well as for other models such as the 3-D TH model for the DST. The software routine boundary_conditions v1.0 is the only appropriate software for this task. Because this software is only used to conduct simple interpolations of data, it is not applicable to identify validation ranges or limitations of use.

3.1.1.7[a] heatgen_ventTable_emplace v1.0

The software routine `heatgen_ventTable_emplace v1.0` is baselined as qualified software per IM-PRO-003, and was obtained from Software Configuration Management and run on a Sun workstation with a SunOS 5.8 (Solaris 8) operating system. The software routine `heatgen_ventTable_emplace v1.0` modifies a heat-generation-rate-versus-time table in two ways. First, it can “age” the heat-generation table by adding a specified number of years to the time entries. Second, it can account for the heat-removal efficiency of ventilation by multiplying the heat-generation-rate values by a specified fraction during the specified ventilation period. The software routine `heatgen_ventTable_emplace v1.0` can also incorporate the dependence of the heat-removal efficiency table on distance (along the emplacement drift) from the ventilation inlet. The software routine `heatgen_ventTable_emplace v1.0` is the only appropriate software for this task. Because this software is only used to conduct simple arithmetic functions, it is not applicable to identify validation ranges or limitations of use.

3.1.1.8[a] rme6 v1.2

The software routine `rme6 v1.2` is baselined as qualified software per IM-PRO-003, and was obtained from Software Configuration Management and run on a Sun workstation with a SunOS 5.8 (Solaris 8) operating system. This code converts the grid from *Development of Numerical Grids for UZ Flow and Transport Modeling* (BSC 2004 [DIRS 169855]) to a format that is readable by YMESH v1.54. The software routine `rme6 v1.2` is the only appropriate software for this task. Because this software is only used to reformat input data for YMESH v1.54, it is not applicable to identify validation ranges or limitations of use.

3.1.1.9[a] NUFT v3.0s and 4.0

NUFT v3.0s and 4.0 are qualified software codes and are used to conduct all of the submodel calculations required by the MSTHM. NUFT v3.0s was run on Sun workstations with the Sun OS 5.8 operating system. NUFT v4.0 was run on the Lawrence Livermore National Laboratory (LLNL) uP supercomputer using operating system AIX5.3CSM1.5, the LLNL Thunder supercomputer using operating system AIX5.2PSSP3.5, and the LLNL Snowbert supercomputer using the CHAOS3.1 operating system. NUFT was selected because it solves the governing equations of the mathematical model, is supported by a suite of special-purpose software that completes implementation of the MSTHM, and imposes no limitations on outputs. As discussed below, the use of NUFT v4.0 for the submodel calculations was within the documented validation range of the software. Therefore, the use of this software was consistent with its intended use.

NUFT is a general-purpose code for simulating mass and heat transport in fractured porous media. Because NUFT is based on the conservation of mass and energy, it is valid for any such calculation, provided the mass- and heat-transport parameters are used within their validation ranges. In other words, what limits the range of validation of NUFT are the mass- and heat-transport-phenomena-related parameters (or constitutive properties), such as thermal conductivity, which affects heat conduction, and permeability, which affects gas- and liquid-phase flow. Thus, if thermal conductivity and permeability are applicable for the range of predicted temperatures, the software (NUFT) is valid for this range. The validation range and

limitation of applicability of NUFT is determined by the validation studies conducted in conjunction with the Drift Scale Test. Note that NUFT version 4.0 was used prior to qualification. The executable file (documented in Appendix XVI[a]) did not change from the preliminary version used to conduct the modeling to the qualified/baselined version.

3.1.1.10[a] reformat_EXT_to_TSPA v2.0

The software routine `reformat_EXT_to_TSPA v2.0` is baselined as qualified software per IM-PRO-003 and was obtained from Software Configuration Management and run on a Sun workstation with a SunOS 5.8 (Solaris 8) operating system. The purpose of `reformat_EXT_to_TSPA v2.0` is to post-process the micro-abstraction data produced by MSTHAC V7.0 (see Appendix VII of the parent report for more details). The processing includes finding the typical waste package and location from a set of locations forming a bin and writing an output file in a format specified by the TSPA organization. The software routine `reformat_EXT_to_TSPA v2.0` is the only appropriate software for this task. Because this software is only used to reformat MSTHM output data, it is not applicable to identify validation ranges or limitations of use.

3.1.1.11[a] extractBlocks_EXT v1.0

The software routine `extractBlocks_EXT v1.0` is baselined as qualified software per IM-PRO-003 and was obtained from Software Configuration Management and run on a Sun workstation with a SunOS 5.8 (Solaris 8) operating system. The purpose of `extractBlocks_EXT` is to determine the effective thermal conductivity for the gridblocks in the drift cavity of an LDTH submodel based on a correlation accounting for the influence of natural convection. The software routine `extractBlocks_EXT v1.0` is the only appropriate software for this task. Because this software is only used to conduct simple arithmetic functions, it is not applicable to identify validation ranges or limitations of use.

3.1.2[a] Exempt Software

Commercial off-the-shelf software (in accordance with IM-PRO-003) was used in the creation of tables and figures shown in this document as well as some data processing. This software was run on a Sun workstation with a SunOS 5.8 (Solaris 8) operating system, except Excel 2003, which was run on Microsoft Windows 2000 and 2003 operating systems.

The following discusses the use of this software on the SunOS 5.8 (Solaris 8) operating system. Figures presented in this report were prepared using MatLab v6.1.0450 release 12.1. The figures can be divided into the following types: line plots showing time histories, contour plots showing the variation in some property at a particular point in time for a cross-sectional area of interest, plots showing material properties for the repository plan view, and schematic drawings showing repository design parameters.

Numerical results from the use of commercial off-the-shelf software in this report are not dependent on the software used. The documentation of each such use includes sufficient detail to allow an independent reviewer to reproduce or verify the results by visual inspection or hand calculation. Some MatLab scripts and UNIX C-Shells were used to process input and output files and to extract and format data for plotting and presentation.

4[a]. INPUTS

Updated direct inputs needed by the MSTHM process model to obtain the parameters and data tracking numbers (DTNs) identified in Tables 4-1[a] and 4-3[a] are detailed in this section. Note that the direct input data in Tables 4-1[a] through 4-3[a] contain only the direct inputs that have changed since the parent report. Refer to Sections 4 and 4.1 of the parent report for the remaining direct inputs, which have not changed.

4.1[a] PARAMETERS/DATA

Many design inputs have been updated in this addendum, including waste emplacement in designated contingency areas, which accommodates more than 70,000 metric tons of heavy metal as emplaced waste. Including the contingency areas enables TSPA to address all potential locations for waste package emplacement. Waste package thermal output has also been updated to accommodate the waste package length changes associated with TAD canister implementation, while preserving the same 1.45 kW/m average line load and decay at emplacement used for previous versions of the MSTHM. These engineering design inputs have been consolidated into four technical reports (SNL 2007 [DIRS 179466]; SNL 2007 [DIRS 179354]; SNL 2007 [DIRS 179394]; SNL 2007 [DIRS 179567]), all of which are cited as direct input in Table 4-1[a].

Besides engineering design information, the two most important parameters of the MSTHM are percolation flux and host-rock thermal conductivity. The MSTHM uses percolation fields from the unsaturated zone flow model, as updated to incorporate new infiltration maps (i.e., 10th, 30th, 50th, and 90th percentile infiltration maps).

Mean thermal conductivity values for each host-rock unit are the global mean values for each unit from *Thermal Conductivity of the Potential Repository Horizon* (BSC 2004 [DIRS 169854]). However, a new approach to develop estimates for reasonable lower- and upper-bound thermal conductivity values for the lithophysal and non-lithophysal host-rock units has been developed (see Section 6.2.13.3[a]).

Data used to develop the MSTHM are not used to validate the model.

Table 4-1[a]. Summary of Direct Input Data and Information Required by the MSTHM

Model Input	Value	Source
Design Information		
Repository emplacement-drift layout (elevations and end-point coordinates for each emplacement drift)	See Document	SNL 2007 [DIRS 179466], Table 4-1
Drift spacing	81 m	SNL 2007 [DIRS 179466], Table 4-1
End-to-end waste package spacing	0.1 m	SNL 2007 [DIRS 179466], Table 4-1
Drift diameter	5.5 m	SNL 2007 [DIRS 179354], Section 4.1.2, Figure 4-1
Invert height from bottom of drift	0.806 m	Source was the same as used for previous MSTHM calculations, but will be reconciled with the value of 1.321 m (4'-4") from SNL 2007 [DIRS 179354], Table 4-1 (see Section 6.3.19[a] for details)
TAD waste package inner-vessel thickness (21-PWR and 44-BWR)	0.0508 m	SNL 2007 [DIRS 179394], Table 4-3
TAD waste package outer-barrier thickness (21-PWR and 44-BWR)	0.0254 m	SNL 2007 [DIRS 179394], Table 4-3
Nominal quantity of 21-PWR waste packages in LA-design inventory	4,586	DTN: MO0702PASTREAM.001 [DIRS 179925], file: <i>DTN-Inventory-Rev00a.xls</i> , tab: "Unit Cell"
Nominal quantity of 44-BWR (TAD) waste packages in LA-design inventory	3,037	DTN: MO0702PASTREAM.001 [DIRS 179925], file: <i>DTN-Inventory-Rev00a.xls</i> , tab: "Unit Cell"
5 DHLW/DOE SNF-LONG waste package inner-vessel thickness	0.0508 m	SNL 2007 [DIRS 179567], Table 4-9
5 DHLW/DOE SNF-LONG waste package outer-barrier thickness	0.0254 m	SNL 2007 [DIRS 179567], Table 4-9
Nominal quantity of 5 DHLW/DOE SNF-LONG waste packages in LA-design inventory	1,940	DTN: MO0702PASTREAM.001 [DIRS 179925], file: <i>DTN-Inventory-Rev00a.xls</i> , tab: "Unit Cell"
5 DHLW/DOE SNF-SHORT waste package inner-vessel thickness	0.0508 m	SNL 2007 [DIRS 179567], Table 4-8
5 DHLW/DOE SNF-SHORT waste package outer-barrier thickness	0.0254 m	SNL 2007 [DIRS 179567], Table 4-8
Nominal quantity of 5 DHLW/DOE SNF-SHORT waste packages in LA-design inventory	1,257	DTN: MO0702PASTREAM.001 [DIRS 179925], file: <i>DTN-Inventory-Rev00a.xls</i> , tab: "Unit Cell"
Drip shield thickness (plate-1 or plate-2)	0.015 m	SNL 2007 [DIRS 179354]
Intersection of drip shield plate-1 with drip shield plate-2 from base/top of invert	1,891 mm	SNL 2007 [DIRS 179354]
Total nominal quantity of waste packages in LA-design inventory	11,629	DTN: MO0702PASTREAM.001 [DIRS 179925], file: <i>DTN-Inventory-Rev00a.xls</i> , tab: "Unit Cell"
Nominal weight of drip shield	5,000 kg	SNL 2007 [DIRS 179354], Table 4-1

Table 4-1[a]. Summary of Input Data and Information Required by the MSTHM (Continued)

Model Input	Value	Source
Properties of the Engineered System		
Invert Thermal and Hydrologic Properties		
Intragranular permeability (calibrated parameters from one-dimensional inversion of saturation and water-potential data for 30% infiltration case – tsw35)	$1.11 \times 10^{-17} \text{ m}^2$	DTN: LB0610UZDSCP30.001 [DIRS 179180], file: <i>Calibrated Parameter_R113_30%.doc</i>
Intragranular porosity, tsw35 unit (tswM5 unit; calibrated parameters from one-dimensional inversion of saturation and water-potential data for 30% infiltration case)	0.131	DTN: LB0208UZDSCPMI.002 [DIRS 161243], file: <i>drift-scale calibrated properties for mean infiltration2.xls</i> , worksheet: "Drift-scale Cal. Hydro Props"
Intragranular porosity, tsw34 unit (tswM4 unit; calibrated parameters from one-dimensional inversion of saturation and water-potential data for 30% infiltration case)	0.111	DTN: LB0208UZDSCPMI.002 [DIRS 161243], file: <i>drift-scale calibrated properties for mean infiltration2.xls</i> , worksheet: "Drift-scale Cal. Hydro Props"
Intragranular van Genuchten α (calibrated parameters from one-dimensional inversion of saturation and water-potential data for 30% infiltration case – tsw35 (tswM5 unit))	$3.38 \times 10^{-6} \text{ Pa}^{-1}$	DTN: LB0610UZDSCP30.001 [DIRS 179180], file: <i>Calibrated Parameter_R113_30%.doc</i>
Intragranular van Genuchten m, tsw35 unit (tswM5 unit; matrix continuum for mean infiltration-flux property set)	0.216	DTN: LB0610UZDSCP30.001 [DIRS 179180], file: <i>Calibrated Parameter_R113_30%.doc</i>
Intragranular residual saturation, tsw35 unit (tswM5 unit; calibrated parameters from one-dimensional inversion of saturation and water-potential data for 30% infiltration case)	0.12	DTN: LB0208UZDSCPMI.002 [DIRS 161243], file: <i>drift-scale calibrated properties for mean infiltration2.xls</i> , worksheet: "Drift-scale Cal. Hydro Props"
Intragranular residual saturation, tsw34 unit (tswM4 unit; for estimating intergranular properties of the invert ballast)	0.19	DTN: LB0208UZDSCPMI.002 [DIRS 161243], file: <i>drift-scale calibrated properties for mean infiltration2.xls</i> , worksheet: "Drift-scale Cal. Hydro Props"
Bulk density of invert	1,530 kg/m ³ (applied to LDTH submodels)	DTN: SN0404T0503102.011 [DIRS 169129], file: <i>ReadMe Summary.doc</i> , Table 7-10; taking the value of solid density for the Tptpl unit (1,980 kg/m ³), and determining bulk density using the fracture porosity (0.0096) from DTN: LB0208UZDSCPMI.002 [DIRS 161243], and invert intergranular porosity (0.22), from Appendix X[a]

Table 4-1[a]. Summary of Input Data and Information Required by the MSTHM (Continued)

Model Input	Value	Source
Bulk density of invert	1,270 kg/m ³ (applied to DDT submodels)	DTN: GS020183351030.001 [DIRS 163107], file: zz_sep_262417.txt, Table S02025_001, rows 321 through 370; see full explanation in Section 6.2.13.2[a].
Specific heat of invert	930 J/kg·K	DTN: SN0307T0510902.003 [DIRS 164196], file: rock_grain_heat_capacity (edited).xls, worksheet: "Cp grain 25-325," column: Y Cp Rock Grain 25-325C round(cell,2); applied value for the Tptpl unit
Mass density of the internal cylinder of the 21-PWR AP waste package (TAD)	3,495 kg/m ³	SNL 2007 [DIRS 179567], Table 4-1
Mass density of the internal cylinder of the 44-BWR waste package (TAD)	3,342 kg/m ³	SNL 2007 [DIRS 179567], Table 4-1
Mass density of the internal cylinder of the 5 DHLW/DOE SNF-SHORT waste package	2,175 kg/m ³	SNL 2007 [DIRS 179567], Table 4-1
Mass density of the internal cylinder of the 5 DHLW/DOE SNF-LONG waste package	2,302 kg/m ³	SNL 2007 [DIRS 179567], Table 4-1
Specific heat of the internal cylinder of the 21-PWR AP waste package (TAD)	378.0 J/kg·K	SNL 2007 [DIRS 179567], Table 4-1
Specific heat of the internal cylinder of the 44-BWR waste package (TAD)	395.0 J/kg·K	SNL 2007 [DIRS 179567], Table 4-1
Specific heat of the internal cylinder of the 5 DHLW/DOE SNF-SHORT waste package	718.0 J/kg·K	SNL 2007 [DIRS 179567], Table 4-1
Specific heat of the internal cylinder of the 5 DHLW/DOE SNF-LONG waste package	731.0 J/kg·K	SNL 2007 [DIRS 179567], Table 4-1
Drift Wall Ground Support Thermal Emissivity		
Emissivity Stainless Steel Type 316 (Bernold-style surface plates)	Range of 0.57 to 0.66 for 450°F to 1,600°F, and 0.28 for 75°F; 0.44 is the actual input value; see Section 6.2.13.6[a]	McAdams 1954 [DIRS 161435], p.475 (see Section 6.2.13.6[a] and Appendix V[a] for details)

Table 4-1[a]. Summary of Input Data and Information Required by the MSTHM (Continued)

Model Input	Value	Source
Properties of the Natural System		
Hydrologic Properties of Unsaturated-Zone Model Layers: Parameters		
Matrix and fracture properties of UZ model layers	See DTN (values used are from tsw34 and tsw35)	DTN: LB0610UZDSCP30.001 [DIRS 179180], file: <i>Calibrated Parameter_R113_30%.doc</i>
Matrix porosity, matrix residual saturation, fracture porosity, and fracture residual saturation	See DTN (values used are from tsw34 (tswM4) and tsw35 (tswM5))	DTN: LB0208UZDSCPMI.002 [DIRS 161243], file: <i>drift-scale calibrated properties for mean infiltration2.xls</i> , worksheet: "Drift-scale Cal. Hydro Props"
Fracture frequency and fracture-matrix interfacial area of UZ model layers	See DTN (values used are from tsw34 and tsw35)	DTN: LB0205REVUZPRP.001 [DIRS 159525], file: <i>FRACTURE PROPERTY.xls</i> , worksheet: "Table 1. Fracture Properties"
Bulk Thermal Properties of the Unsaturated-Zone Model Layers: Parameters		
Thermal conductivity and bulk density of the GFM2000 layers of the nonrepository layers	See DTN	DTN: SN0303T0503102.008 [DIRS 162401], file: <i>NonrepositoryThermalConductivityModel031403.xls</i> , worksheet: "Sheet 1"
Thermal conductivity of the repository horizon GFM2000 layers	See DTN	DTN: SN0404T0503102.011 [DIRS 169129], files: <i>tptpl1.zip, tptpl2.zip, tptpl3.zip, tptpln1.zip, tptpln2.zip, tptpln3.zip, tptpmn1.zip, tptpmn2.zip, tptpmn3.zip, tptpul1.zip, tptpul2.zip, and tptpul3.zip</i>
Bulk density of host-rock units of GFM2000 layers	See DTN (values used are for Tptpul, Tptpmn, Tptpl1, and Tptpln)	DTN: SN0404T0503102.011 [DIRS 169129], file: <i>ReadMe Summary.doc</i> , Table 7-10
Specific heat capacity of the mineralogic model layers	See DTN	DTN: SN0307T0510902.003 [DIRS 164196], File: <i>rock_grain_heat_capacity (edited).xls</i> , Worksheet: "Cp grain 25-325," Column: Y Cp Rock Grain 25-325C round(cell,2)
Distribution of Percolation Flux Below PTn Unit: Parameters		
Percolation flux from PTn/TSw interface for 10th, 30th, 50th and 90th percentiles of flux, for monsoonal climate	Files: <i>ptn_bot_flux_10%.xls</i> <i>ptn_bot_flux_30%.xls</i> <i>ptn_bot_flux_50%.xls</i> <i>ptn_bot_flux_90%.xls</i>	DTN: LB0701MOPTNTSW.001 [DIRS 179156]

Table 4-1[a]. Summary of Input Data and Information Required by the MSTHM (Continued)

Model Input	Value	Source
Percolation flux from PTn/TSw interface for 10th, 30th, 50th and 90th percentiles of flux, for glacial-transition climate	Files: ptn_bot_flux_10%_gt.xls ptn_bot_flux_30%_gt.xls ptn_bot_flux_50%gt.xls ptn_bot_flux_90%_gt.xls	DTN: LB0701GTPTNTSW.001 [DIRS 179153]
Percolation flux from PTn/TSw interface for 10th, 30th, 50th and 90th percentiles of flux, for present-day climate	Files: ptn_bot_flux_10%_pd.xls ptn_bot_flux_30%_pd.xls ptn_bot_flux_50%pd.xls ptn_bot_flux_90%_pd.xls	DTN: LB0612PDPTNTSW.001 [DIRS 179150]
Percolation flux from PTn/TSw interface for 10th, 30th, 50th and 90th percentiles of flux, for post-10,000-year climate	Files: ptn_bot_q_pd1_10k.xls ptn_bot_q_pd2_10k.xls ptn_bot_q_pd3_10k.xls ptn_bot_q_pd4_10k.xls	DTN: LB0702UZPTN10K.002 [DIRS 179332]
Weighting factors for Infiltration maps using the uncertainty (glue) method	File: summary.xls	DTN: LB0701PAWFNFM.001 [DIRS 179283]
Waste Package Heat-Generation and Ventilation Heat-Removal Efficiency: Design Information		
Heat-generation rate history for entire repository	See DTN	DTN: MO0702PASTREAM.001 [DIRS 179925], file: DTN-Inventory-Rev00A.xls, tab: "Decay Curves"
Average initial heat-generation rate per meter	1.45 kW/m	DTN: MO0702PASTREAM.001 [DIRS 179925], file: DTN-Inventory-Rev00A.xls, tab: "Decay Curves"
Ventilation period duration	50 years after emplacement	SNL 2007 [DIRS 179466], Table 4-2
Duration of waste package emplacement	23 years	SNL 2007 [DIRS 179466], Table 4-2
Heat-generation rates for each of the waste package types	See DTN	DTN: MO0702PASTREAM.001 [DIRS 179925], file: DTN-Inventory-Rev00A.xls, tab: "Decay Curves"
Ventilation heat-removal efficiency as a function of time and distance from the inlet of the emplacement drift	See DTN	DTN: MO0701VENTCALC.000 [DIRS 179085] ^a
TAD waste package overall length	5.8501 m	SNL 2007 [DIRS 179394], Table 4-3; DTN: MO0702PASTREAM.001 [DIRS 179925]

Table 4-1[a]. Summary of Input Data and Information Required by the MSTHM (Continued)

Model Input	Value	Source
TAD waste package overall diameter	1.963 m	SNL 2007 [DIRS 179394], Table 4-3
TAD waste package inner vessel diameter	1.8212 m	SNL 2007 [DIRS 179394], Table 4-3
Weight (loaded mass) of TAD waste package	73,500 kg	SNL 2007 [DIRS 179394], Table 4-3
5 DHLW/DOE SNF-LONG waste package overall length	5.3039 m	SNL 2007 [DIRS 179567], Table 4-9
5 DHLW/DOE SNF-LONG waste package overall diameter	2.1260 m	SNL 2007 [DIRS 179567], Table 4-9
5 DHLW/DOE SNF-LONG waste package inner vessel diameter	1.9845 m	SNL 2007 [DIRS 179567], Table 4-9
Weight (loaded mass) of 5 DHLW/DOE SNF-LONG waste package	59,600 kg ^c	SNL 2007 [DIRS 179567], Table 4-9
5 DHLW/DOE SNF-SHORT waste package overall length	3.6974 m	SNL 2007 [DIRS 179567], Table 4-8
5 DHLW/DOE SNF-SHORT waste package overall diameter	2.1260 m	SNL 2007 [DIRS 179567], Table 4-8
5 DHLW/DOE SNF-SHORT waste package inner vessel diameter	1.9845 m	SNL 2007 [DIRS 179567], Table 4-8
Weight (loaded mass) of 5 DHLW/DOE SNF-SHORT waste package	48,700 kg ^c	SNL 2007 [DIRS 179567], Table 4-8
Drip shield length	5.805 m	SNL 2007 [DIRS 179354], Table 4-2
Drip shield width	2.535 m ^b	SNL 2007 [DIRS 179354], Table 4-2

^a For the first 50 years (all that are used in the MSTHM), there are differences in the data set out in the ninth decimal between Base Case Ventilation Efficiency Results.xls (DTN: MO0701VENTCALC.000 [DIRS 179085]) and ventData.dat (Output DTN: LL0704PA003MST.022) due to regeneration and manipulation of this file in preparation for MSTHM calculations. These differences in no way impact the model results.

^b The value used in the LDTH and DDT submodel is 2.533 m, which differs insignificantly from the input value of 2.535 m.

^c Within the 0% to 5% tolerance level of the unloaded waste package mass.

NOTE: BWR = boiling water reactor; DOE = U.S. Department of Energy; LA = license application; PWR = pressurized water reactor; SNF = spent nuclear fuel.

Table 4-2[a]. Summary of Emplacement Panels and Drifts Represented in the SMT Submodel for the Layout

Panel	Number of Drifts	Drift Length (m)
1 (central)	6	3,392
2 (south)	27	18,876
3W (north-central)	26	15,246
3E (northeast)	19	11,040
4 (northwest)	30	16,719
TOTAL:	108	65,273

Source: DTN: MO0702PASTREAM.001 [DIRS 179925], file: *DTN-Inventory-Rev00a.xls*, tab: "Unit Cell."

Table 4-3[a] contains the inputs used in Appendix X[a] to calculate the hydrologic properties of the invert. These inputs are used in the calculations presented in Output DTN: MO0703PAHYTHRM.000.

Table 4-3[a]. Listing of the Input Data and Their Sources for the LTBM-2 Material

Input Data Name	Average Value	Minimum Value	Maximum Value	Sources
Intergranular porosity	0.22	0.18	0.31	See Table X-1[a]
Intergranular void ratio	0.29	0.22	0.46	Calculated: Void Ratio = Porosity / (1-Porosity)
Specific gravity (g/cm ³) [same as particle density (kg/m ³)]	2.550 [2,550]	2.520 [2,520]	2.580 [2,580]	SNL 2007 [DIRS 179354], Table 4-1
Bulk density (lb/ft ³)[(kg/m ³)]	115 [1,842]	110 [1,762]	120 [1,922]	SNL 2007 [DIRS 179354], Table 4-1
Capillary retention scaling parameter, α (dimensionless)*	1.285	N/A	N/A	Arya et al. 1999 [DIRS 176802], Figure 5 (Sand)
Surface tension of water (N/m) (at an ambient temperature of 25°C)*	7.20E-02	N/A	N/A	Incropera and DeWitt 1996 [DIRS 108184], Table A.6
Density of water (kg/m ³) (at an ambient temperature of 25°C)*	1,000	N/A	N/A	Incropera and DeWitt 1996 [DIRS 108184], Table A.6
Acceleration due to gravity (m/sec ²)*	9.81	N/A	N/A	Incropera and DeWitt 1996 [DIRS 108184], Back Cover
Beta (β)	1	N/A	N/A	Kunii and Smith 1960 [DIRS 153166], p. 72
Gamma (γ)	0.667	N/A	N/A	Kunii and Smith 1960 [DIRS 153166], p. 72

* Constant value used in the analysis.

NOTE: The designation "LTBM" in "LTBM-2 Material" denotes material produced using a laboratory tunnel boring machine.

4.1.1[a] Qualification for Intended Use of Outside Sources

The outside sources from Arya et al. (1999 [DIRS 176802]), McAdams (1954 [DIRS 161435]), Kunii and Smith (1960 [DIRS 153166]) and Incropera and DeWitt (1996 [DIRS 108184]) were not used as direct inputs in the parent report. The sources from Arya et al. (1999 [DIRS 176802]), McAdams (1954 [DIRS 161435]) and Kunii and Smith (1960 [DIRS 153166])

are qualified here for intended use below in Sections 4.1.1.1[a], 4.1.1.2[a], and 4.1.1.3[a] in accordance with SCI-PRO-006 and SCI-PRO-001. With regard to the source from Incropera and DeWitt (1996 [DIRS 108184]), the values used (see Table 4-3[a]) are data accepted widely by the scientific community. Also, this source is widely used as an engineering/scientific textbook and thus considered to be “Established Fact” per Attachment I of SCI-PRO-004, *Managing Technical Product Inputs*.

Qualification of External Source Data—The sections below present planning and documentation for the data qualification of unqualified external source data used as direct input only to this report. Data qualification is performed in accordance with SCI-PRO-006.

Data for Qualification—There are three external sources of data used as direct input to this addendum:

1. The capillary retention scaling parameter from Arya et al. (1999 [DIRS 176802]), as discussed in Section 4.1.1.1[a] and Table 4-3[a] of this addendum.
2. The emissivity of stainless steel from McAdams (1954 [DIRS 161435]), as discussed in Section 4.1.1.2[a] and Table 4-1[a] of this addendum.
3. The β and γ parameters from Kunii and Smith (1960 [DIRS 153166], p. 72) that are implemented in the calculations presented in Appendix X[a], as discussed in Section 4.1.1.3[a] and Table 4-3[a] of this addendum.

Method of Qualification Selected—The method for qualification of all the external sources of data is the “technical assessment method.” The rationale for using this method is that all three of the qualification approaches for technical assessment (SCI-PRO-001, Attachment 3) of external source data are appropriate for consideration. Other qualification methods are not considered because they require information not available through the original source (i.e., scientific journal or publication). Qualification process attributes used in the technical assessment of each external source are selected from the list provided in Attachment 4 of SCI-PRO-001. Attributes used specifically as data qualification attributes in this addendum are:

1. The extent to which the data demonstrate the properties of interest (e.g., physical, chemical, geologic, mechanical).
2. Prior uses of the data and associated verification processes.
3. Data must be demonstrated to be reliable as judged by the experience of the originators and reputation of the originating organization.
4. Data must be sufficiently extensive to cover the context of this application.

4.1.1.1[a] Technical Assessment of External Data from Arya et al. 1999 [DIRS 176802]

The following criteria were used to assess the external data:

- Data must appropriately demonstrate properties of interest.
- Data must be sufficiently extensive to cover the context of this application.
- Data must be demonstrated to be reliable as judged by the experience of the originators and reputation of the originating organization.

The referenced source for the capillary retention scaling parameter in Table 4-3[a] is the article “Characterization and Measurement of the Hydraulic Properties of Unsaturated Porous Media,” presented at the *Proceedings of the International Workshop on Characterization and Measurement of the Hydraulic Properties of Unsaturated Porous Media* (Arya et al. 1999 [DIRS 176802]) held at the U.S. Salinity Laboratory in Riverside, California. This reference is justified for intended use based on the reliability of data source as per SCI-PRO-006. The conference proceedings were edited by the well-known soil scientists M. Th. van Genuchten and F. J. Leij. This parameter value, developed for sand, is qualified for its use in this report to represent the LTBM-2 material (Appendix X[a]), based on the fact that the data appropriately demonstrates the properties of interest to this addendum, the data is sufficiently extensive and covers the context of this application, and the reliability of the data source and the qualification of the organization publishing the data. It should also be noted that there is a relative insensitivity of water retention curves to this parameter.

Based on the assessment made above, data from Arya et al. (1999 [DIRS 176802]) are qualified for use as direct input to this addendum.

4.1.1.2[a] Technical Assessment of External Data from McAdams 1954 [DIRS 161435]

The following criteria were used to assess the external data:

- Data must appropriately demonstrate properties of interest.
- Data must be sufficiently extensive to cover the context of this application.
- Data must be demonstrated to be reliable as judged by the experience of the originators and reputation of the originating organization.
- Prior uses of the data and associated verification process.

The emissivity of stainless steel from McAdams (1954 [DIRS 161435]) is qualified for the intended use in this addendum because it is specific to the material, and thus the data appropriately demonstrate the properties of interest. This data also sufficiently cover the context of the application of use in this model because modeling of thermal-hydrologic response in the repository drifts has limited sensitivity to uncertainty in this value. Temperature differences for radiant heat transfer are proportional to the fourth root of the waste package thermal power. As discussed in the parent report (Section 6.2.13.6), when peak temperatures occur at the drift wall,

variations in drift wall emissivity result in small variations in drip shield temperature. These variations in temperature are small compared to the influence of host-rock thermal conductivity uncertainty at the repository horizon during the preclosure period. Thus, although there is uncertainty as to the condition of the stainless steel surfaces in the repository, which affects their emissivity, the corresponding uncertainty in calculated temperature differences is small. Note also that this monograph by McAdams (1954 [DIRS 161435]) is a prominent work in heat transfer and is listed in the McGraw-Hill Series in Chemical Engineering. The monograph was sponsored by the Committee on Heat Transmission of the National Research Council. This monograph has been extensively used throughout the Yucca Mountain Project (YMP) as a direct input and is currently a source in over ten controlled YMP products. Thus, these data have demonstrated to be reliable as judged by the experience of the numerous YMP originators that have used the data. Based on the assessment made above, data from McAdams (1954 [DIRS 161435]) are qualified for use as direct input to this report.

4.1.1.3[a] Technical Assessment of External Data from Kunii and Smith 1960 [DIRS 153166]

The following criteria were used to assess the external data:

- Data must appropriately demonstrate properties of interest.
- Data must be sufficiently extensive to cover the context of this application.
- Data must be demonstrated to be reliable as judged by the experience of the originators and reputation of the originating organization.
- Prior uses of the data and associated verification process.

The β and γ parameters from Kunii and Smith (1960 [DIRS 153166], p. 72) are qualified for the intended use in this addendum because they are specific to aggregate materials as represented in the estimation scheme, and thus the data appropriately demonstrate the properties of interest. The data are published in the peer-reviewed scientific journal *American Institute of Chemical Engineers Journal*, which has been in publication since 1955. These data have also been used in other project reports (e.g., BSC 2004 [DIRS 170033]) using the same parameters as inputs. The parameters from Kunii and Smith (1960 [DIRS 153166]) are implemented in the calculations presented in Appendix X[a] and Table 4-3[a]. The relationship presented by Kunii and Smith (1960 [DIRS 153166]) requires two parameters. The β parameter is expressed as the ratio of the characteristic length between two neighboring solid particles divided by the particle diameter. As stated by Kunii and Smith (1960 [DIRS 153166]), the value will range from 0.9 to 1.0 for almost all packed beds. A value of 1.0 is selected for analysis assuming loose or open packing appropriate for collapsed rubble. The γ parameter is expressed as the ratio of the effective thickness of the fluid film adjacent to the surface of two solid particles divided by particle diameter. This ratio equals 0.67 (Kunii and Smith 1960 [DIRS 153166], p. 72). Based on the assessment made above, data from Kunii and Smith (1960 [DIRS 153166]) are qualified for use as direct input to this report.

4.2[a] YUCCA MOUNTAIN REVIEW PLAN ACCEPTANCE CRITERIA

The MSTHM report predicts results that directly pertain to quantity of water contacting the engineered barriers and waste forms as described in *Yucca Mountain Review Plan, Final Report* (YMRP) (NRC 2003 [DIRS 163274], Section 2.2.1.3.3.3). The YMRP acceptance criteria for this category are:

4.2.1[a] Acceptance Criterion 1 – System Description and Model Integration Are Adequate

- (1) Total system performance assessment adequately incorporates important design features, physical phenomena, and couplings, and uses consistent and appropriate assumptions throughout the quantity and chemistry of water contacting engineered barriers and waste forms abstraction process.
- (2) The abstraction of the quantity and chemistry of water contacting engineered barriers and waste forms uses assumptions, technical bases, data, and models, that are appropriate and consistent with other related U.S. Department of Energy abstractions.
- (3) Important design features, such as waste package design and material selection, backfill, drip shield, ground support, thermal loading strategy, and degradation processes, are adequate to determine the initial and boundary conditions for calculations of the quantity and chemistry of water contacting engineered barriers and waste forms.
- (4) Spatial and temporal abstractions appropriately address physical couplings (thermal-hydrologic-mechanical-chemical).
- (5) Sufficient technical bases and justification are provided for total system performance assessment assumptions and approximations for modeling coupled thermal-hydrologic-mechanical-chemical effects on seepage and flow, the waste package chemical environment, and the chemical environment for radionuclide release. The effects of distribution of flow on the amount of water contacting the engineered barriers and waste forms are consistently addressed, in all relevant abstractions.
- (6) The expected ranges of environmental conditions within the waste package emplacement drifts, inside the breached waste packages, and contacting the waste forms and their evolution with time are identified.
- (7) The model abstraction for quantity and chemistry of water contacting engineered barriers and waste forms is consistent with the detailed information on engineered barrier design and other engineered features.
- (8) Adequate technical bases are provided, including activities such as independent modeling, laboratory or field data, or sensitivity studies, for inclusion of any thermal-hydrologic-mechanical-chemical couplings and features, events, and processes.

- (9) Performance-affecting processes that have been observed in thermal-hydrologic tests and experiments are included into the performance assessment.
- (12) Guidance in NUREG-1297 and NUREG-1298 (Altman et al. 1988 [DIRS 103597]; Altman et al. 1988 [DIRS 103750]), or other acceptable approaches, is followed.

4.2.2[a] Acceptance Criterion 2 – Data Are Sufficient for Model Justification

- (1) Geological, hydrological, and geochemical values used in the license application are adequately justified. Adequate description of how the data were used, interpreted, and appropriately synthesized into the parameters is provided.
- (2) Sufficient data were collected on the characteristics of the natural system and engineered materials to establish initial and boundary conditions for conceptual models of thermal-hydrological-mechanical-chemical coupled processes, that affect seepage and flow and the engineered barrier chemical environment.
- (3) Thermal-hydrologic tests were designed and conducted with the explicit objectives of observing thermal-hydrologic processes for the temperature ranges expected for repository conditions and making measurements for mathematical models. Data are sufficient to verify that thermal-hydrologic conceptual models address important thermal-hydrologic phenomena.
- (4) Sufficient information to formulate the conceptual approach(es) for analyzing water contact with the drip shield, engineered barriers, and waste forms is provided.

4.2.3[a] Acceptance Criterion 3 – Data Uncertainty Is Characterized and Propagated through the Model Abstraction

- (1) Models use parameter values, assumed ranges, probability distributions, and bounding assumptions that are technically defensible, reasonably account for uncertainties and variabilities, and do not result in an under-representation of the risk estimate.
- (2) Parameter values, assumed ranges, probability distributions, and bounding assumptions used in the total system performance assessment calculations of quantity and chemistry of water contacting engineered barriers and waste forms are technically defensible and reasonable, based on data from the Yucca Mountain region (e.g., results from large block and drift-scale heater and niche tests), and a combination of techniques that may include laboratory experiments, field measurements, natural analog research, and process-level modeling studies.
- (3) Input values used in the total system performance assessment calculations of quantity and chemistry of water contacting engineered barriers (e.g., drip shield and waste package) are consistent with the initial and boundary conditions and the assumptions of the conceptual models and design concepts for the Yucca Mountain site. Correlations between input values are appropriately established in the U.S. Department of Energy total system performance assessment. Parameters used to

define initial conditions, boundary conditions, and computational domain in sensitivity analyses involving coupled thermal-hydrologic-mechanical-chemical effects on seepage and flow, the waste package chemical environment, and the chemical environment for radionuclide release, are consistent with available data. Reasonable or conservative ranges of parameters or functional relations are established.

- (4) Adequate representation of uncertainties in the characteristics of the natural system and engineered materials is provided in parameter development for conceptual models, process-level models, and alternative conceptual models. The U.S. Department of Energy may constrain these uncertainties using sensitivity analyses or conservative limits. For example, the U.S. Department of Energy demonstrates how parameters used to describe flow through the engineered barrier system bound the effects of backfill and excavation-induced changes.

4.2.4[a] Acceptance Criterion 4 – Model Uncertainty Is Characterized and Propagated through the Model Abstraction

- (1) Alternative modeling approaches of features, events, and processes are considered and are consistent with available data and current scientific understanding, and the results and limitations are appropriately considered in the abstraction.
- (2) Alternative modeling approaches are considered and the selected modeling approach is consistent with available data and current scientific understanding. A description that includes a discussion of alternative modeling approaches not considered in the final analysis and the limitations and uncertainties of the chosen model is provided.
- (3) Consideration of conceptual-model uncertainty is consistent with available site characterization data, laboratory experiments, field measurements, natural analog information and process-level modeling studies; and the treatment of conceptual-model uncertainty does not result in an under-representation of the risk estimate.
- (4) Adequate consideration is given to effects of thermal-hydrologic-mechanical-chemical coupled processes in the assessment of alternative conceptual models.
- (5) If the U.S. Department of Energy uses an equivalent continuum model for the total system performance assessment abstraction, the models produce conservative estimates of the effects of coupled thermal-hydrologic-mechanical-chemical processes on calculated compliance with the postclosure public health and environmental standards.

4.2.5[a] Acceptance Criterion 5 – Model Abstraction Output Is Supported by Objective Comparisons

- (1) The models implemented in this total system performance assessment abstraction provide results consistent with output from detailed process-level models and/or empirical observations (laboratory and field testing and/or natural analogs).

- (3) Accepted and well-documented procedures are used to construct and test the numerical models that simulate coupled thermal-hydrologic-mechanical-chemical effects on seepage and flow, engineered barrier chemical environment, and the chemical environment for radionuclide release. Analytical and numerical models are appropriately supported. Abstracted model results are compared with different mathematical models, to judge robustness of results.

The above stated criteria are also presented in *Technical Work Plan for: Additional Multiscale Thermohydrologic Modeling* (BSC 2006 [DIRS 178297], Section 3.3).

INTENTIONALLY LEFT BLANK

5[a]. ASSUMPTIONS

5.1[a] BOUNDARY CONDITIONS

5.1.1[a] Ground-Surface Relative Humidity

Applicable to this addendum, with no changes required.

5.1.2[a] Ambient Percolation Flux above Repository Horizon

Applicable to this addendum, with no changes required.

5.1.3[a] Barometric Pressure Fluctuations at the Ground Surface

Applicable to this addendum, with no changes required.

5.1.4[a] Timing of Climate Change Influence on Percolation Flux above Repository

Applicable to this addendum, with no changes required. Note that the addition of a post-10,000-year climate state, which is discussed in Section 6.2.12.4[a], involves the application of the proposed 10 CFR Part 63 (70 FR 53313 [DIRS 178394]), and is therefore not subject to any assumptions.

5.1.5[a] Water Table Rise

Applicable to this addendum, with no changes required.

5.2[a] HEAT FLOW PROCESSES

5.2.1[a] Mountain-Scale Heat Flow

Applicable to this addendum, with no changes required.

5.2.2[a] Drift-Scale Heat Flow

Applicable to this addendum, with no changes required.

5.2.3[a] Waste Package Emplacement

Applicable to this addendum, with no changes required.

5.3[a] MATERIAL PROPERTIES

5.3.1[a] Hydrologic Properties

5.3.1.1[a] Permeability of the Drip Shield and Waste Package for the MSTHM

Applicable to this addendum, with no changes required.

5.3.1.2[a] Hydrologic Properties of the Intragranular Porosity in the Invert Materials

Applicable to this addendum, with no changes required.

5.3.1.3[a] Hydrologic Properties for the Concrete Invert in the Drift Scale Test

Applicable to this addendum, with no changes required.

5.3.1.4[a] Fracture Permeability of the Host Rock in the Wing-Heater Array of the Drift Scale Test

Applicable to this addendum, with no changes required.

5.3.1.5[a] Permeability of the Bulkhead in the Drift Scale Test

Applicable to this addendum, with no changes required.

5.3.1.6[a] Permeability of the Bulkhead in the Three-Dimensional Monolithic Thermal-Hydrologic Model Used in the MSTHM Validation Test Case

Applicable to this addendum, with no changes required.

5.3.1.7[a] Pseudo Permeability of the Gas-Filled Cavities inside the Emplacement Drifts in the LDTH Submodels

Applicable to this addendum, with no changes required.

5.3.1.8[a] Permeability of the Intergranular Porosity of the Invert Materials

Applicable to this addendum, with no changes required.

5.3.1.9[a] Tortuosity Factor for Binary Gas-Phase Diffusion

Applicable to this addendum, with no changes required.

5.3.1.10[a] Permeability of Host Rock at Emplacement Drift Wall

Applicable to this addendum, with no changes required.

5.3.1.11[a] Residual Saturation of the Intergranular Porosity of the Crushed Tuff in the Invert

Assumption: The residual saturation of the intergranular porosity of the invert is assumed to be the same as that of the fractures (0.01) of the Tptpl host-rock unit. This assumption is used in the LDTH submodels (Section 6.2.16[a]) and in the properties of the invert (Section 6.2.13.2[a]).

Rationale: As discussed in Section 6.3.14[a] and shown in Figure 6.3-72[a], thermal-hydrologic conditions in the invert are insensitive to the residual saturation of the intergranular porosity of the crushed tuff in the invert, over a wide range of residual saturation values: 0.01 to 0.15.

Confirmation Status: On the basis of the rationale given above, this assumption is justified and does not require further confirmation.

Use in the Model: This assumption is used in Sections 6.2.13.2[a] and 6.2.16[a].

5.3.2[a] Thermal Properties

5.3.2.1[a] Thermal Conductivity in SDT, DDT, and SMT Submodels

Applicable to this addendum, with no changes required.

5.3.2.2[a] SMT Submodel Saturated-Zone Thermal Properties

Applicable to this addendum, with no changes required.

5.3.2.3[a] Thermal Conductivity and Mass Density for the Dual-Permeability Model

Applicable to this addendum, with no changes required.

5.3.2.4[a] Thermal Properties of the Lumped Drip Shield/Waste Package Heat Source in the LDTH Submodels

Applicable to this addendum, with no changes required.

5.3.2.5[a] Thermal Properties for the Concrete Invert in the Drift Scale Test

Applicable to this addendum, with no changes required.

5.3.2.6[a] Thermal Conductivity and Thickness of the Bulkhead in the Drift Scale Test

Applicable to this addendum, with no changes required.

5.3.2.7[a] Emissivity of Emplacement Drift Wall

Not applicable to this addendum.

5.4[a] WASTE PACKAGE MODELING

5.4.1[a] Average Waste Package Diameter and Location above Invert

Applicable to this addendum, with the following changes required:

Assumption: The waste package outer diameter is 2.0085 m, which is an approximately weighted averaged value, based on the unit cell of the DDT submodel (Section 6.2.8[a]). This value is taken as the average diameter for the waste packages emplaced over the entire repository. The location of the average waste package centerline above the invert surface is taken to be 1.218 m, which is an approximately interpolated value based on the values for the respective waste packages in the unit cell of the DDT submodel. This waste package location

above the invert is used across the entire repository. This information is used only in the DDT submodels (Section 6.2.8[a]).

Rationale: This assumption only influences two aspects of the MSTHM: (1) the temperature difference between the waste package and drip shield and (2) the waste package-to-waste package variation of this temperature difference. This temperature difference depends primarily on the waste package heat output. As is indicated in Table 4-1[a], the range in waste package diameter is small, from 1.963 m for the TAD PWR and BWR waste packages to 2.126 m for the 5 DHLW/DOE SNF-LONG and 5 DHLW/DOE SNF-SHORT waste packages. This small range in waste package diameter has an insignificant influence on temperature difference between the waste package and drip shield. Similarly, the small range in waste package location above the invert has an insignificant influence on temperature difference between the waste package and drip shield.

Confirmation Status: On the basis of the rationale given above, this assumption is justified and does not require further confirmation.

Use in the Model: This assumption is used in Sections 6.2.8[a], 6.2.17[a], 6.3[a], and 7.5[a].

5.4.2[a] Waste Package Sequence along Drifts

Applicable to this addendum, with the following changes required:

Assumption: The waste package sequence shown in Table 6.2-6[a] is assumed to be applicable over all emplacement drifts. Thus, this sequence is assumed to be representative of waste package-to-waste package heat output variability throughout the entire repository. The use of this sequence is equivalent to assuming that defense high-level waste (DHLW) waste packages, which produce much less heat than commercial spent nuclear fuel (CSNF) waste packages, will not be grouped together. In other words, DHLW waste packages will always be placed adjacent to CSNF waste packages.

Rationale: Table 5.4-1[a] lists the nominal number of waste packages for the repository inventory. Table 5.4-1[a] also lists the waste packages of the assumed sequence in the MSTHM calculations. The waste packages in the assumed sequence in the MSTHM cover 93.04% of the total inventory. Moreover, the percentages of each of the respective waste package types in the MSTHM are similar to the corresponding percentages in the repository inventory. Therefore, the waste package sequence assumed in all of the MSTHM calculations is representative of the inventory of waste packages in the repository.

Confirmation Status: On the basis of the rationale given above, this assumption is justified and does not require further confirmation.

Use in the Model: This assumption is used in Section 6.2.17[a].

Table 5.4-1[a]. Summary of Waste Package Types in the Repository Inventory and in the MSTHM

Waste Package Type	Nominal Number in Inventory ^a	Nominal Percentage of Inventory (%)	Number Represented in MSTHM ^b	Percentage of Waste Packages Represented in MSTHM (%)
21-PWR TAD	4,586	39.44 42.38 ^c	3	42.86
44-BWR TAD	3,037	26.12 28.07 ^c	2	28.57
5 DHLW/DOE SNF-LONG	1,940	16.68 17.93 ^c	1	14.29
5 DHLW/DOE SNF-SHORT	1,257	10.81 11.62 ^c	1	14.29
Total Number of 21-PWR TAD, 44-BWR TAD, 5 DHLW/DOE SNF-LONG, 5 DHLW/DOE SNF-SHORT	10,820	93.04 100.0 ^c	7	100
Total Inventory	11,629	100	7	100

^a Source: DTN: MO0702PASTREAM.001 [DIRS 179925], file: *DTN-Inventory-Rev00.xls*, tab: "Unit Cell."

^b See Figure 6.2-2[a] and Table 6.2-6[a].

^c Percentage of 21-PWR AP, 44-BWR AP, 5 DHLW/DOE SNF LONG and DHLW/DOE SNF SHORT only.

5.5[a] RELATIVE HUMIDITY IN EMPLACEMENT DRIFTS

Applicable to this addendum, with no changes required.

5.6[a] CONDENSATE DRAINAGE AROUND EMPLACEMENT DRIFTS

Applicable to this addendum, with no changes required.

5.7[a] GAS- AND LIQUID-PHASE FLOW IN THE LONGITUDINAL DIRECTION ALONG EMPLACEMENT DRIFTS (THE COLD-TRAP EFFECT)

Applicable to this addendum, with no changes required.

5.8[a] PROPERTIES OF HOST-ROCK RUBBLE FOR LOW-PROBABILITY-SEISMIC COLLAPSED-DRIFT SCENARIO

5.8.1[a] Bulk Density of Host-Rock Rubble

Not applicable to this addendum.

INTENTIONALLY LEFT BLANK

6[a]. MODEL DISCUSSION

Applicable to this addendum, with no changes required.

6.1[a] YUCCA MOUNTAIN THERMOHYDROLOGY CONCEPTUAL MODEL

Applicable to this addendum, with no changes required.

6.2[a] THE MULTISCALE THERMOHYDROLOGIC MODELING APPROACH

6.2.1[a] Overview of the MSTHM

Applicable to this addendum, with no changes required.

6.2.2[a] Incorporating the Unsaturated Zone Hydrology Model in the MSTHM

Applicable to this addendum, with no changes required.

6.2.3[a] Governing Equations for Unsaturated Zone Thermohydrology

Applicable to this addendum, with no changes required.

6.2.4[a] MSTHM Calculation Sequence

Applicable to this addendum, with updates to the current MSTHM implementation discussed in Section 6.2.12[a].

6.2.5[a] SMT Submodels

Applicable to this addendum, with updates to the current SMT submodel discussed in Section 6.2.14[a].

6.2.6[a] LDTH Submodels

Applicable to this addendum, with updates to the current LDTH submodels discussed in Section 6.2.16[a].

6.2.7[a] SDT Submodels

Applicable to this addendum, with updates to the current SDT submodels discussed in Section 6.2.15[a].

6.2.8[a] DDT Submodels

Applicable to this addendum, with updates to the current DDT submodels discussed in Section 6.2.17[a].

6.2.9[a] SMT and SDT Submodels for the Low-Probability-Seismic Collapsed-Drift Scenario

Applicable to this addendum, with no changes required.

6.2.10[a] LDTH Submodels for the Low-Probability-Seismic Collapsed-Drift Scenario

Applicable to this addendum, with updates to the current LDTH submodels discussed in Section 6.2.18[a].

6.2.11[a] DDT Submodels for the Low-Probability-Seismic Collapsed-Drift Scenario

Applicable to this addendum, with updates to the current DDT submodels discussed in Section 6.2.19[a].

6.2.12[a] Modifications to MSTHM Implementation for TSPA

The MSTHM methodology is similar to the previous version of the model described in Section 6.2.4 of the parent report. A primary difference is that the number of LDTH/SDT submodel pairs has been increased from 108 to 560, which corresponds to the number of UZ flow model grid columns documented in *Development of Numerical Grids for UZ Flow and Transport Modeling* (BSC 2004 [DIRS 169855]), either fully or partially occurring within the emplacement region of the repository footprint (herein referred to as the repository footprint or heated repository footprint). As shown in Figure 6.2-19[a], the current MSTHM implementation assumes that the heated repository footprint includes all of the contingency drifts in the southern portion of Panel 2, whereas the previous implementation did not include the contingency drifts. There is one LDTH/SDT submodel pair corresponding to each of the UZ flow model grid columns within the heated repository footprint. This approach directly utilizes 100% of the percolation flux values generated by the UZ flow model within the heated repository footprint, whereas the previous implementation of the MSTHM did not directly use all of those values. Unlike the previous implementation of the MSTHM, wherein 2,874 interpolated “virtual” LDTH and SDT submodels were generated between the 108 “real” LDTH/SDT submodel locations, the current implementation does not utilize any interpolation between the 560 LDTH/SDT submodel locations for mapping out 3264 “virtual” LDTH submodels. The current MSTHM calculations are calculated for 1,000,000 years, including the present-day (0- to 600-year) climate, the monsoonal (600- to 2,000-year) climate, the glacial-transition (2,000- to 10,000-year) climate, and the post-10,000-year (10,000- to 1,000,000-year) climate, while the previous implementation was for 20,000 years, including the present-day (0- to 600-year), monsoonal (600- to 2,000-year), and glacial-transition (2,000- to 20,000-year) climates.

As discussed above, the most important revision to the MSTHM implementation is the use of LDTH submodels at each of the 560 UZ flow model columns. This revision provides for the full use of the repository-scale stratigraphic information and direct utilization of the percolation flux data of the UZ flow model in the LDTH submodels. This alleviates the need to interpolate the “virtual” LDTH submodels between the “real” LDTH submodels. As discussed in Section 6.2.4 of the parent report, the 108 real LDTH submodels were used to interpolate the virtual LDTH submodels for each of the 2,874 SMT submodel gridblocks within the heated repository footprint. In the current implementation of the MSTHM, the 560 LDTH submodels are mapped

onto the 3,264 SMT submodel gridblocks within the heated repository footprint, thereby creating the 3,264 virtual LDTH submodels. It is important to note that this mapping does not involve any interpolation.

The current MSTHM implementation includes additional information that is supplied to TSPA. For each of the waste package degradation (WAPDEG) analysis and TSPA files, information is included in the header of the respective files, including:

1. Times when boiling ceases on the drift wall, drip shield, waste package, and in the invert are given for that particular waste package and location.
2. Minimum and maximum times when boiling ceases on the drift wall and on the waste packages are given for the entire drift in which that waste package resides.
3. Average percolation flux is given for the drift in which a waste package resides for the present-day, monsoonal, glacial-transition, and post-10,000-year climates.

6.2.12.1[a] Binning MSTHM Results for TSPA

The EBS thermal-hydrological environment submodel of TSPA implements the MSTHM results in the TSPA model. The MSTHM subdivides the repository footprint into 3,264 subdomains. Each of the 3,264 subdomains is of equal area, 81 m wide by 20 m long, where the length component is along the emplacement drift axis. For each of the thermal conductivity (K_{th})/percolation flux scenarios, the MSTHM calculates time-dependent thermohydrology variables: temperature and relative humidity for six representative CSNF waste packages and two representative codisposal (CDSP) waste packages, and their respective drip shields, at each subdomain location. In addition, the MSTHM calculates time-dependent values for average drift wall temperature, duration of boiling at the drift wall, invert temperature, invert saturation, and invert liquid flux at each of the 3,264 subdomains.

Before any information could be provided from the MSTHM to downstream TSPA submodels, two sets of analyses were performed. First, the percolation flux values for each of the 3,264 MSTHM subdomain locations were used to group the locations into five repository percolation subregions, as discussed below.

The values of percolation flux for each subdomain location were sorted in ascending order and then grouped based on the five percolation quantile ranges: 0 to 0.05, 0.05 to 0.3, 0.3 to 0.7, 0.7 to 0.95, and 0.95 to 1.0. These quantiles are consistent with the approach used for previous performance assessments, which is a reasonable approach for representing the discrete distribution of flux values using the number of ranges (five) selected for TSPA (see Appendix VIII[a]). Each subdomain location and associated model results were designated as belonging to the appropriate percolation subregion. The 30th percentile, glacial-transition climate, percolation flux at the base of the PTn geologic unit was used to determine the five subregions (see Figure VIII-1[a]). This approach is similar to the approach used in previous performance assessments (see Appendix VIII of the parent report), with a small difference being the use of the 30th percentile case rather than the “mean” case used in the parent report. The subregion assignments determined for the 30th percentile glacial-transition map were applied to all four percolation flux cases and to all four climate states.

The second analysis involved determining a single “representative” CSNF waste package and a single “representative” CDSP waste package for the radionuclide inventory in the waste packages in each percolation subregion, for each K_{th} /percolation flux case. The representative waste packages are intended for use in the part of the TSPA model that simulates degradation of the waste form and transport of radionuclides, for nominal, seismic, and igneous calculations. Selection of the representative waste packages reduces the computational effort for TSPA, while representing spatial variability in repository conditions that control radionuclide release (principally percolation flux). The determination of the repository subregions and the selection of the representative waste packages are summarized as follows.

The MSTHM abstraction produces two sets of outputs that are indexed by waste type and percolation subregion. One set contains the comprehensive MSTHM results for each of the eight possible waste package types, at each subdomain location, for each percolation subregion. The MSTHM results in the first set are reported at each subdomain location for six CSNF waste packages and two CDSP waste packages. This information is intended for use in the TSPA waste package and drip shield degradation model component, the drift-seepage component, and the drift wall condensation component. The histories in this set are compiled in lookup tables that give parameter values at discrete time steps.

The second set contains the MSTHM results for the selected representative CSNF and CDSP waste packages for each percolation subregion. The MSTHM results reported include average drip shield and waste package temperature and relative humidity histories; average drift wall temperature history; and average invert temperature, relative humidity, liquid flux, and saturation histories.

The representative CSNF and CDSP waste packages in each percolation subregion are selected by first compiling the peak waste package temperature and duration of boiling at the waste package for every waste package of each type and percolation subregion. The two measures, the peak waste package temperature and the duration of boiling at the waste package, are sorted from low to high, and the percentile calculated for every waste package of each type. The percentiles are converted to deviations from the median, and then a composite score is computed by combining the sum of the squared deviations, for each waste package. For each waste package type and subregion, the representative waste package has the score closest to zero (see discussion in Appendix VIII[a]). Selection of waste packages with median thermal characteristics within each subregion is an appropriate model simplification for representing environmental conditions for radionuclide release and transport behaviors that occur at late times, after substantial cooling of the EBS.

After the process described above is completed, temperature and relative humidity for each representative waste package and associated drip shield, average drift wall temperature, average invert temperature, average invert saturation, and average invert flux (all as a function of time) are stored in a file set that is used directly in TSPA. This file is used by the EBS thermohydrology environment submodel to provide representative thermohydrology responses for each subregion. The information for representative waste packages is intended for use in TSPA as input to the EBS chemical environment component, the EBS flow component, the waste form degradation and mobilization model component, and the EBS transport component.

The histories in this set are compiled in lookup tables that give parameter values at discrete time steps.

6.2.12.2[a] Changes to the Percolation Flux/Host-Rock Thermal Conductivity Cases from Past Performance Assessments for the Current TSPA

Previous implementations of the MSTHM in the parent report developed results for five percolation flux/host-rock thermal conductivity cases. The current implementation develops seven cases, which accomplish two objectives: (1) percolation flux and K_{th} are sampled over their full ranges of variation; and (2) calculated results together represent a substantial portion of the overall likelihood of percolation flux/ K_{th} combinations. The current implementation covers four percentiles of percolation flux at the repository horizon (10th, 30th, 50th, and 90th) using the mean K_{th} for all host-rock units, plus a “low/low” scenario (10th percentile percolation flux with low K_{th}), a “low/high” case (10th percolation flux with high K_{th}), and a “high/high” case (90th percolation flux with high K_{th}). Implementation in TSPA also requires assigning surrogate cases (set of results) for the cases that were not calculated: the 30th percentile, low- and high-host-rock thermal conductivity cases, the 50th percentile low- and high-host-rock thermal conductivity cases, and the 90th percentile low-host-rock thermal conductivity case. The process of selecting the best surrogate case is described in Section 6.2.12.3[a] and in Output DTN: LL0703PA053MST.021.

6.2.12.3[a] Treatment of Parameter Uncertainty

As discussed in Section 6.3.2 of the parent report, the two most important uncertain input parameters influencing TH conditions across the repository are percolation flux and host-rock thermal conductivity. These factors are addressed with four different percolation flux cases, described in Section 6.2.16[a], and low, mean, and high host-rock thermal conductivity cases, described in Section 6.2.13.3[a], resulting in a total of twelve uncertainty cases. Of these twelve cases, seven are directly modeled with the MSTHM (Table 6.3-47[a]), representing 78% of the total uncertainty. To represent a given uncertainty case not directly modeled with the MSTHM, a process was developed to identify the surrogate case (from among the seven modeled cases) that best approximates TH behavior for that case (Output DTN: LL0703PA053MST.021). The objective was to identify the case that is closest with respect to the time when boiling ceases on the drift wall. A complementary cumulative distribution function (CCDF) is plotted for each of the seven modeled cases. A “synthetic” CCDF is developed for each of the five unmodeled uncertainty cases, using a boiling-duration ratio approach (see file *Readme.pdf* of Output DTN: LL0703PA053MST.021 for more details). The synthetic CCDFs are compared with those of the seven modeled cases, using several approaches. The selected surrogates are shown in Table 6.3-47[a]. It was found that the selected surrogate cases for six of the seven cases were always the best choice, regardless of the method applied to choosing the surrogate. For one of the cases (P90L), the surrogate was the best choice in two of three approaches that were applied. Further details of this surrogate selection process are given in Section 6.3.15[a] and in Output DTN: LL0703PA053MST.021.

6.2.12.4[a] Changes Required in the MSTHM Implementation for the Current TSPA for a One-Million-Year Performance Assessment Period

Past performance assessments used a performance assessment period of 10,000 years. The current TSPA extends to 1 million years, resulting in an additional post-10,000-year climate state with unique percolation flux conditions corresponding to the 10th, 30th, 50th, and 90th percentile conditions described in Section 6.3.15[a].

To calculate post-10,000-year thermal-hydrologic conditions, four percolation fields were developed corresponding to quartiles of the range of average infiltration (log uniform distribution from 13 to 64 mm/yr) as identified in the proposed 10 CFR Part 63 (70 FR 53313 [DIRS 178394]). The quartile approach was used in lieu of post-10,000-year flux values from the UZ flow model report (SNL 2007 [DIRS 175177]) (which were unavailable at the time this analysis was initiated) to expedite the MSTHM calculations. This approximation is justified because the post-10,000-year thermal-hydrologic responses are insensitive to percolation flux. Whereas boiling-period duration and peak temperature conditions do depend on percolation flux, those conditions occur much earlier than 10,000 years. Subsequent temperature and humidity changes will be small, and are caused by gradual cooling dominated by thermal conduction and decaying waste heat output.

Center values were determined for each quartile, and the pre-10,000-year percolation field with average repository flux (i.e., area-weighted average of the 560 columns of the UZ flow model; SNL 2007 [DIRS 175177]) in which the closest value to each center value was identified. The selected percolation field was then rescaled (by a factor) so that its average matched that of the selected center value, and the resulting field was used to define post-10,000-year flux at each of the 3,264 MSTHM subdomain locations. This procedure was repeated for the 10th, 30th, 50th, and 90th percentile conditions. The files developed using this procedure are archived with the other inputs in the DTNs listed in the notes of Table 6.3-47[a] and in Figures 6.3-71[a] and 6.3-72[a]. Further discussion of the procedure is provided in Sections 6.2.16[a] and 6.3.15[a].

The TSPA architecture requires that percolation flux values (including post-10,000-year values) from the UZ flow model (SNL 2007 [DIRS 175177]) be available in the MSTHM files. Therefore, the MSTHM results were further post-processed to replace the post-10,000-year flux values used in the MSTHM calculation with the corresponding values for each case from the UZ flow model (SNL 2007 [DIRS 175177]). The original MSTHM results calculated with post-10,000-year fluxes developed from quartiles of the distribution from the proposed rule 10 CFR Part 63 (70 FR 53313 [DIRS 178394]) are listed in Section 6.3.15[a] as DTNs containing “intermediate results.” The files containing substituted values for post-10,000-year fluxes, but otherwise containing the original MSTHM results, are listed in Section 6.3.15[a] as outputs to be used as inputs to TSPA (see Figure 6.3-73[a]).

For the five surrogates for non-calculated cases that are described in Section 6.3.15[a], complete sets of surrogate output files are provided in five DTNs (Table 6.3-47[a]). These are based on the surrogate, calculated MSTHM results, which were further post-processed to replace the post-10,000-year flux values used in the MSTHM calculation with the corresponding values for each case from the UZ flow model (SNL 2007 [DIRS 175177]). These substituted, surrogate

files are also listed in Section 6.3.15[a] as outputs to be used as inputs to TSPA (see Figure 6.3-75[a]).

6.2.13[a] Overview of Model Input Revisions

The revisions to the model inputs include (1) natural-system hydrologic properties, (2) invert hydrologic and thermal properties, (3) host-rock thermal conductivity, (4) nonrepository-unit thermal properties used in the LDTH and DDT submodels, (5) drift rubble thermal conductivity, (6) influence of Bernold-style surface sheets on drift wall emissivity, and (7) repository layout and in-drift dimensions. These revisions are described in Sections 6.2.13.1[a] through 6.2.13.7[a].

6.2.13.1[a] Natural System Hydrologic Properties

The LDTH submodels apply the drift-scale calibrated property set for the 30th percentile infiltration map (DTN: LB0610UZDSCP30.001 [DIRS 179180]). In Section 6.3.14, both the 30th percentile and 10th percentile (DTN: LB0610UZDSCP10.001 [DIRS 180502]) were evaluated, and it was found that near-field and in-drift TH behavior are insensitive to the choice of property set. The 30th percentile property set was chosen because the 30th percentile percolation fluxes are closer to the median values and are judged to best represent (among the 10th, 30th, 50th, and 90th percentile property sets) the range of percolation fluxes used in TSPA. Section 6.2.16[a] describes how the data in DTN: LB0610UZDSCP30.001 [DIRS 179180] are applied to the LDTH submodel stratigraphy.

6.2.13.2[a] Invert Hydrologic and Thermal Properties

The revisions to the intergranular hydrologic and thermal properties of the invert are described in Appendix X[a]. The intragranular properties of the invert apply the matrix properties of the Tptpll unit from the drift-scale calibrated property set for the 30th percentile infiltration map (DTN: LB0610UZDSCP30.001 [DIRS 179180]), which is the property set that is applied to the host-rock units. The Tptpll unit is chosen because it is the predominant host-rock unit over the heated repository footprint. The revisions to the intergranular hydrologic and thermal properties are minor compared to those used in the parent report. As discussed in Section 5.3.1.11[a], the residual saturation of the intergranular porosity of the crushed tuff in the invert is assumed to be the same (0.01) as that of the fractures of the Tptpll host-rock unit. As demonstrated in Section 6.3.14[a], thermal-hydrologic conditions in the invert are insensitive to the residual saturation of the crushed tuff in the invert over a wide range of values: 0.01 to 0.15.

The DDT submodels use the same invert bulk density ($1,270 \text{ kg/m}^3$) used in the parent report, from DTN: GS020183351030.001 [DIRS 163107], while the LDTH submodels use an updated value ($1,530 \text{ kg/m}^3$), which is from DTN: SN0404T0503102.011 [DIRS 169129], adjusted for the updated invert intergranular porosity of 0.22. Because heat flow changes so slowly in the model, heat storage effects on temperature are negligible, and thus difference in invert bulk density has no significant impact on in-drift and near-field temperature histories.

6.2.13.3[a] Host-Rock Thermal Conductivity

Revised values of mean wet and dry host-rock thermal conductivity were developed in Output DTN: MO0612MEANTHER.000 using DTN: SN0404T0503102.011 [DIRS 169129]. The revised mean thermal conductivity values were developed using the data for all 50 realizations in DTN: SN0404T0503102.011 [DIRS 169129], and for all 23,392 geographic locations in that model (i.e., the ensemble). Accordingly, harmonic mean values (over the vertical dimension) were generated for each of the 50 realizations times 23,392 geographic locations. These harmonic means were arithmetically averaged for all $50 \times 23,392$ harmonic averages. This process is repeated for the four host-rock units, which are the UZ flow model units: tsw33, tsw34, tsw35, and tsw36. As is shown in Table 6-5 of *Development of Numerical Grids for UZ Flow and Transport Modeling* (BSC 2004 [DIRS 169855]), the tsw34 model unit consist of the Tptpmn unit, the tsw35 model unit consists of the Tptpll unit, and the tsw36 model unit consists of the Tptpln unit. Also shown in Table 6-5 of *Development of Numerical Grids for UZ Flow and Transport Modeling* (BSC 2004 [DIRS 169855]), the tsw33 model unit consists of the Tptrl, Tptf, and Tptpul GFM2000 lithostratigraphic units. In DTN: SN0303T0503102.008 [DIRS 162401] (file: *NonrepositoryThermalConductivityModel 031403.xls*, worksheet 1), the Tptrl and Tptf units have the same values of dry and wet thermal conductivity (1.30 and 1.81 W/m-K, respectively). The assumption is made that half of the tsw33 model unit consists of the Tptpul unit and half consists of the Tptrl and Tptf units. The wet and dry mean thermal conductivity values for the tsw33 model units are computed by taking the harmonic mean of the Tptpul-unit values, generated in Output DTN: MO0612MEANTHER.000, and the Tptrl/Tptf-unit values, which results in wet and dry thermal conductivity values of 1.22 and 1.78 W/m-K, respectively, for the tsw33 model unit.

Low (10-percentile) and high (90-percentile) values of wet and dry host-rock thermal conductivity were developed from the same $50 \times 23,392$ harmonic averages by ranking the harmonic means for the entire population of 50 realizations and 23,392 geographic locations and picking the 10- and 90-percentile values (addressed in Output DTN: LL0703PA026MST.013). The thermal-conductivity analyses in Output DTN: LL0703PA026MST.013 use repository-averaged generic LDTH submodels described in Section 6.2.20[a]. Because there are no uncertainty data for the Tptrl and Tptf units, the 10- and 90-percentile values of wet and dry thermal conductivity for the Tptpul unit are assigned to the entire tsw33 model unit.

The weighting factors for the high, mean, and low host-rock thermal-conductivity (K_{th}) cases are determined to be 0.34, 0.37, and 0.29, respectively (Output DTN: LL0703PA026MST.013), which provides a reasonable representation of host-rock thermal-conductivity uncertainty. The weighting factors are determined using the moment matching method for the mean, m , and variance, var , for the peak temperature and the boiling duration plus the constraint that the weighting factors sum up to 1. Thus, the respective weighting factors are determined by solving the following set of five equations:

First and second moments for peak temperature (PT) equations:

$$m^{PT} = w_0 p_0^{PT} + w_{10} p_{10}^{PT} + w_{50} p_{50}^{PT} + w_{90} p_{90}^{PT} + w_{100} p_{100}^{PT}$$

$$var^{PT} = w_0 (m^{PT} - p_0^{PT})^2 + w_{10} (m^{PT} - p_{10}^{PT})^2 + w_{50} (m^{PT} - p_{50}^{PT})^2 + w_{90} (m^{PT} - p_{90}^{PT})^2 + w_{100} (m^{PT} - p_{100}^{PT})^2$$

First and second moments for boiling duration (BD) equations:

$$m^{BD} = w_0 p_0^{BD} + w_{10} p_{10}^{BD} + w_{50} p_{50}^{BD} + w_{90} p_{90}^{BD} + w_{100} p_{100}^{BD}$$

$$var^{BD} = w_0 (m^{BD} - p_0^{BD})^2 + w_{10} (m^{BD} - p_{10}^{BD})^2 + w_{50} (m^{BD} - p_{50}^{BD})^2 + w_{90} (m^{BD} - p_{90}^{BD})^2 + w_{100} (m^{BD} - p_{100}^{BD})^2$$

Constraint on weighting factors:

$$1 = w_0 + w_{10} + w_{50} + w_{90} + w_{100}$$

where p_0 , p_{10} , p_{50} , p_{90} , and p_{100} are the 0th, 10th, 50th, 90th and 100th percentiles of either peak temperature or boiling duration, respectively. The extra two percentiles, p_0 and p_{100} , correspond respectively to the minimum and maximum of either peak temperature or boiling duration. These two end-percentile numbers enable us to force any tailing (asymmetry) of the probability density function and to ensure that the system of equation is well posed. Once unknown weighting factors w_0 , w_{10} , w_{50} , w_{90} and w_{100} are determined by solving the five stated equations, w_0 and w_{10} are combined to determine the weighting factor for the low- K_{th} case, while w_{90} and w_{100} are combined to determine the weighting factor for the high- K_{th} case, and w_{50} is applied as the weighting factor for the mean- K_{th} case for host-rock thermal conductivity.

6.2.13.4[a] Nonrepository-Unit Thermal Properties for LDTH and DDT Submodels

For the LDTH submodels (Section 6.2.16[a]) and DDT submodels (Section 6.2.17[a]), the thermal properties of the nonrepository units are appropriately averaged in order to facilitate computational efficiency without affecting the accuracy of the results. Because the nonrepository units are far enough removed from the emplacement drifts, heat flow within those units occurs primarily as one-dimensional heat conduction in the LDTH and DDT submodels. The nonrepository units, above and below the repository horizon, function as a series of resistors to one-dimensional vertical heat conduction. Therefore, the effective lumped thermal conductivity is appropriately calculated using the thickness-weighted harmonic mean of the upper and lower nonrepository units, respectively. The other thermal properties, specific heat capacity and bulk density (the latter being determined by the solid mass density and porosity), result in the volumetric heat capacity. The effective lumped volumetric heat capacity is appropriately calculated using thickness-weighted arithmetic averaging.

For thermal conductivity, a harmonic mean is calculated at each of the 560 UZ flow model columns in the heated repository footprint. The harmonic mean values are arithmetically averaged over the 560 UZ flow model columns, with an area weighting factor for each of the 560 UZ flow model columns. The area weighting factor is the number of heated SMT submodel gridblocks in that column divided by 3,264, which is the total number of heated SMT submodel

gridblocks in the repository footprint. For all other thermal properties, such as bulk density and heat capacity, the respective thermal properties are arithmetically averaged, weighted by the thickness of each of the respective units. As with the thermal conductivity, these values are arithmetically averaged over the 560 UZ flow model columns, with an area weighting factor for each of the 560 UZ flow model columns. Details of this averaging process are found in Output DTN: LL0704PA003MST.022.

6.2.13.5[a] Drift-Rubble Thermal Conductivity

A temperature-dependent drift-rubble thermal conductivity is used in the collapsed-drift case. Wet and dry thermal conductivity values are developed for the LDTH submodels, while the DDT submodel uses the wet thermal conductivity values for the reasons discussed below. The development of the temperature-dependent drift-rubble thermal conductivity is described in Appendix XI[a].

For heat flow in the rock, the SDT, SMT, and DDT submodels only represent thermal conduction, and cannot represent the influence of liquid-phase saturation changes on thermal conductivity. As is justified in Section 5.3.2.1 of the parent report, it is reasonable to use the wet thermal conductivity in the thermal-conduction (SDT, SMT, and DDT) submodels. As is discussed in Section 6.2.8 of the parent report, the DDT submodel is only used to determine waste package-to-waste package variability in temperature, compared to line-averaged heat-source conditions along the drift. As discussed in Section 6.2.6 of the parent report, the LDTH submodel predicts temperature rise (and resulting hydrologic effects) resulting from line-averaged heat-source conditions. The LDTH submodel also addresses the influence of rubble dry out on temperature rise. A comparison of Figures XI-1[a] and XI-2[a], which plot effective thermal conductivity for dry and wet rubble particles, respectively, reveals that the influence of temperature is much stronger than the influence of liquid-phase saturation. Moreover, the influence of parametric uncertainty, as captured by the low and high rubble thermal conductivity cases, is much stronger than the influence of liquid-phase saturation. Because the DDT submodels implement a temperature-dependent effective rubble thermal conductivity, as well as a range of effective thermal conductivity, shown in Figure XI-2[a], they adequately represent waste package-to-waste package variability in temperature. Accordingly, waste package-to-waste package variability in temperature is reasonably represented in the MSTHM calculations for the collapsed-drift case.

6.2.13.6[a] Influence of Bernold-Type Surface Sheets on Drift Wall Emissivity

The influence of the Bernold-style surface sheets (Michel 1999 [DIRS 163054]) on emissivity is included in both the LDTH and DDT submodels, using the software RADPRO v4.0, described in Section 3.1.3 of the parent report, and by modifying the value of drift wall emissivity (from the value applicable to a rock surface) in the respective RADPRO input file as follows. The Bernold-style sheets are made of Stainless Steel Type 316, which has an emissivity of 0.28 at 75°F (24°C) and 0.57 at 450°F (232°C) (McAdams 1954 [DIRS 161435], p. 475). Interpolating to 140°C, which is a typical peak drift wall temperature, results in an emissivity of 0.44. This is not the final value of emissivity in the RADPRO input file. As described in Appendix VI[a], an effective emissivity is calculated using Equation VI-8[a]. An emissivity value of 0.44 could be considered too small in light of the potential impact of dust on the surface

of the Bernold-style sheets. However, the thermal contact resistance between the Bernold-style surface sheets and drift wall will increase the temperature difference between the drift wall and the drip shield, which will lower the effective emissivity of the drift wall. Therefore, an emissivity value of 0.44 is reasonable, even with the presence of dust. As discussed in Appendix VI[a], because radiant heat transfer temperature differences are proportional to the fourth root of the emissivity (for constant waste package heat flux), temperature rise in the drift is weakly dependent on emissivity. Consequently, when peak temperatures occur at the drift wall, variations in drift wall emissivity result in small variations in drip shield temperature. These temperature uncertainties due to emissivity uncertainty are small compared to the influence of host-rock thermal conductivity uncertainty at the repository horizon during the preclosure period.

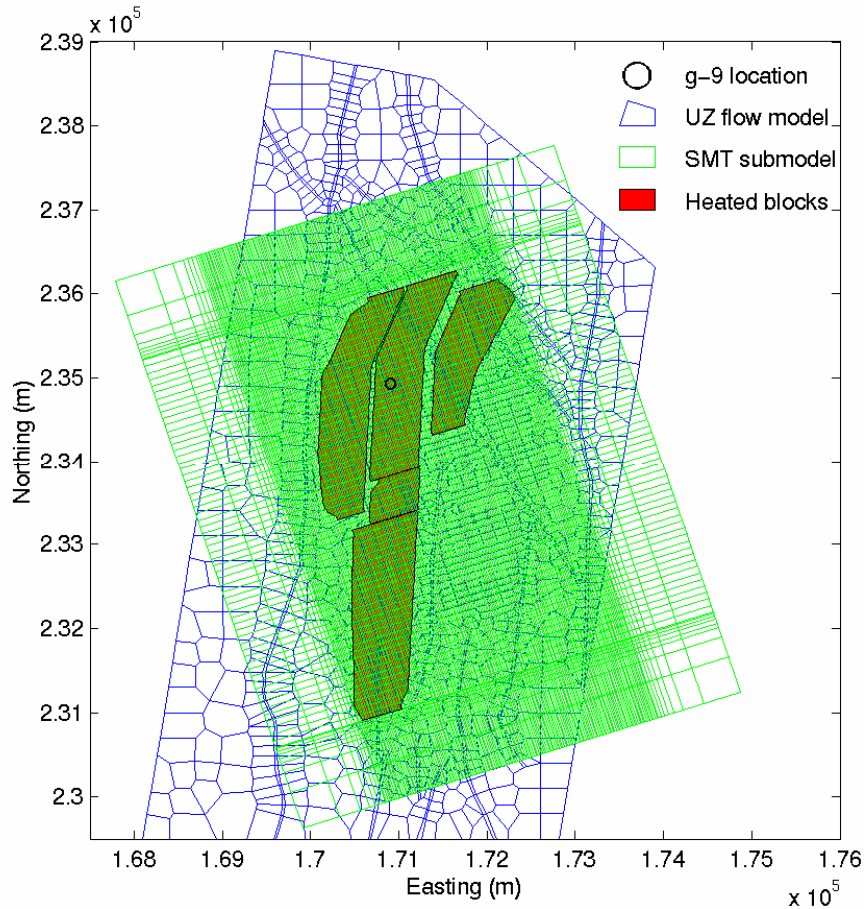
6.2.13.7[a] Repository Layout and In-Drift Dimensions

An updated repository layout (SNL 2007 [DIRS 179466]) is implemented in the current MSTHM. The updated layout has slightly different drift end-point coordinates than the layout used in the previous MSTHM implementation, described in the parent report. The updated layout implemented in the current MSTHM also includes all contingency drifts (see Figure 6.2-19[a]), whereas the previous MSTHM implementation did not include these drifts.

6.2.14[a] Current SMT Submodel

The current SMT submodel (Figure 6.2-13[a]) represents the updated repository layout (SNL 2007 [DIRS 179466]), which has been slightly revised since the previous MSTHM implementation described in Section 6.2.4 of the parent report. The SMT submodel represents heating from each of the 108 emplacement drifts, which includes all contingency drifts in the southernmost portion of Panel 2 (see Figure 6.2-18[a]). The thermal conductivity values of the host-rock units were updated as described in Section 6.2.13.3[a]. Minor revisions were made to a few of the specific heat capacity values for the lower nonrepository units to address minor discrepancies described in the footnote of Table IV-3a of the parent report. These minor revisions in specific heat capacity were also incorporated in the current SDT, DDT, and LDTH submodels.

Of the 560 UZ flow model (SNL 2007 [DIRS 175177]) columns that occur within the heated repository footprint, 39 correspond to fault zones. For fault zones, the UZ flow model uses lumped fault-zone units. For example, the entire TSw sequence is lumped into one unit. As is described in Appendix IV[a], the thermal property values for a given lumped fault-zone unit are determined by the straight arithmetic average for all units residing within that unit. This averaging is utilized in both the current SMT and SDT submodels. Because the fault zones are relatively narrow and occupy a small fraction of the repository footprint (<2% as shown in Table 6.3-3 of the parent report), the averaging of thermal properties within the fault zones has an insignificant impact on mountain-scale heat flow. For reasons discussed in Section 6.2.16[a], this averaging approach is not applied to the current LDTH submodels.



Source: DTN: LB03023DKMGRID.001 [DIRS 162354] and Output DTN: LL0702PA013MST.068.

NOTE: SMT submodel mesh shown as green mesh; UZ flow model mesh shown as blue mesh (SNL 2007 [DIRS 175177]). The heated repository footprint is shaded in red lines and outlined in black, as discussed in SNL 2007 [DIRS 179466].

Figure 6.2-13[a]. SMT Submodel Mesh and UZ Flow Model Mesh, Together with Heated Repository Footprint Represented by the SMT Submodel

As described in Section 6.2.5 of the parent report, the SMT submodel represents heat flow in the upper 1,000 m of the saturated zone (SZ), with a fixed boundary temperature 1,000 m below the water table. The thermal properties of the SZ are determined using a straight arithmetic average of the respective values in each of the 14 model units that intersect the water table over the SMT submodel domain. The SZ thermal property values in the current SMT submodel are also applied in the current SDT submodels (see Section 6.2.15[a]).

6.2.15[a] Current SDT Submodels

An SDT submodel (Figure 6.2-14[a]) is included in each of the 560 UZ flow model (SNL 2007 [DIRS 175177]) grid columns that occur within the heated repository footprint, which results in a total of 560 SDT submodel locations. The current SDT submodels use the same stratigraphic representation and vertical discretization as that of the current SMT submodel at each of the respective 560 SDT submodel locations, which are the same as the 560 LDTH submodel

locations. As with the current SMT submodel, the current SDT submodel includes the upper 1,000 m of the saturated zone, whereas in previous MSTHM implementations, the SDT submodels had a constant-temperature boundary at the water table.

<p style="text-align: center;">Ground Surface Fixed boundary temperature</p>
<p style="text-align: center;">TCw-PTn-UpperTSw Discrete tcw11-tsw33 thermal properties</p>
<p style="text-align: center;">Tptpul (tsw33) tsw33 thermal properties</p>
<p style="text-align: center;">Tptpmn (tsw34) tsw34 thermal properties</p>
<p style="text-align: center;">Tptpll (tsw35) tsw35 thermal properties</p>
<p style="text-align: center;">Tptpln (tsw36,tsw37) tsw36 thermal properties</p>
<p style="text-align: center;">LowerTSw-CHnz/v-PP-BF-TR Discrete tsw38-tr2 thermal properties</p>
<p style="text-align: center;">Water Table Averaged thermal properties of UZ units intersecting water table Saturated Zone</p>
<p style="text-align: center;">Lower Boundary Fixed boundary temperature 1,000 m below water table</p>

Figure 6.2-14[a]. Schematic of the Stratigraphic Representation in the SDT Submodel

The SZ thermal properties in the current SDT submodels are the same as those of the current SMT submodel (see Section 6.2.14[a]). The current SDT submodels have a specified fixed boundary temperature 1,000 m below the water table. The lower boundary temperatures are extrapolated from those of the UZ flow model (DTN: LB991201233129.001 [DIRS 146894]), using the software routine boundary_conditions v1.0, described in Section 3.1.8 of the parent report. This software routine is also used to generate the fixed upper boundary temperature at the ground surface. Unlike the previous MSTHM implementation, the current SDT submodel is used to generate a temperature history at the water table, which is used as a time-dependent

lower boundary temperature for the corresponding LDTH submodel. Prior to repository closure, each of the 560 SDT submodels has a unique local time-dependent heat-removal efficiency due to ventilation, which is the same as that applied to the corresponding LDTH submodel, and which is determined using `heatgen_ventTable_emplace v1.0`, described in Section 3.1.9 of the parent report, and the heat-removal-efficiency table given in DTN: MO0701VENTCALC.000 [DIRS 179085]. The heat-removal-efficiency table in DTN: MO0701VENTCALC.000 [DIRS 179085] is determined with a thermal model that accounts for the movement of ventilation air along emplacement drifts from the inlet side of the drift to the outlet side of the drift. Locations closer to the inlet side of the drift receive more of the ventilation cooling effect than locations further removed from the inlet. The software `heatgen_ventTable_emplace v1.0` interpolates local values of heat-removal efficiency from the source DTN, based on the distance of that location from the emplacement drift inlet.

6.2.16[a] Current LDTH Submodels

An LDTH submodel (Figure 6.2-15[a]) is included in each of the 560 UZ flow model grid columns that occur within the heated repository footprint, which results in a total of 560 LDTH submodel locations. The LDTH submodels incorporate the same vertical stratigraphy of the host-rock sequence and repository elevation as in the corresponding SDT submodel, and as in the corresponding location of the SMT submodel. The LDTH submodel also incorporates the same elevations for the ground surface and water table as in the corresponding SDT submodel, and as in the corresponding location of the SMT submodel.

As shown in Figure 6.2-15[a] and described in Section 6.2.13.4[a], for the non-host-rock (i.e., nonrepository) units, the LDTH submodel utilizes “lumped” units wherein the thermal properties have been averaged for the respective units contained within that unit. The nonrepository units lying above the Tptpul host-rock unit (tsw33 model unit) are averaged into the lumped unit called uz1. The nonrepository units lying below the Tptpln host-rock (tsw36 and tsw37 model units) are averaged into the lumped unit called uz2. The averaging approach is described and justified in Section 6.2.13.4[a]. The combining of tsw36 and tsw37 into one unit is justified because both units have the same thermal and hydrologic properties. Note also that the current DDT submodel (Section 6.2.17[a]) utilizes the same representation of nonrepository unit thermal properties, with the only distinction being that the DDT submodel only utilizes the wet value of thermal conductivity. Note, finally, that the LDTH, SDT, DDT, and SMT submodels utilize the same thermal property values for the host-rock units, with the only distinction being that the LDTH submodels utilize both wet and dry thermal conductivity values, while the SDT submodels (Section 6.2.15[a]), SMT submodels (Section 6.2.14[a]), and DDT submodels (Section 6.2.17[a]) only utilize the wet thermal conductivity values. For heat flow in the rock, the SDT, SMT, and DDT submodels only represent thermal conduction, and cannot represent the influence of liquid-phase saturation changes on thermal conductivity. As is justified in Section 5.3.2.1 of the parent report, it is reasonable to use the wet thermal conductivity in the thermal-conduction (SDT, SMT, and DDT) submodels.

<p style="text-align: center;">Ground Surface Fixed boundary temperature, liquid-phase saturation, gas-phase pressure, and air-mass fraction</p>
<p style="text-align: center;">UZ1 tsw35 hydrologic properties Averaged tcw11-tsw32 thermal properties</p>
<p style="text-align: center;">Ttpul (tsw33) tsw35 hydrologic properties tsw33 thermal properties</p>
<p style="text-align: center;">Ttpmn (tsw34) tsw34 hydrologic properties tsw34 thermal properties</p>
<p style="text-align: center;">Ttpll (tsw35) tsw35 hydrologic properties tsw35 thermal properties</p>
<p style="text-align: center;">Ttpln (tsw36 and tsw37) tsw34 hydrologic properties tsw36 thermal properties</p>
<p style="text-align: center;">UZ2 tsw34 hydrologic properties Averaged tsw38-tr2 thermal properties</p>
<p style="text-align: center;">Water Table Fixed boundary liquid-phase saturation, gas-phase pressure, and air-mass fraction; time-dependent boundary temperature from corresponding SDT submodel</p>

Figure 6.2-15[a]. Schematic of the Stratigraphic Representation in the LDTH Submodel

As is justified in Section 6.3.14[a], the two lithophysal units (Ttpul and Ttpll) can be represented using a common representation of the hydrologic properties, which are those of the Ttpll unit taken from the drift-scale calibrated property set for the 30th percentile infiltration map (DTN: LB0610UZDSCP30.001 [DIRS 179180]). Similarly, the two nonlithophysal units (Ttpmn and Ttpln) can be represented using a common representation of the hydrologic properties, which are those of the Ttpmn unit taken from DTN: LB0610UZDSCP30.001 [DIRS 179180]. As demonstrated in Section 6.3.14[a], with respect to the influence of hydrologic properties on near-field and in-drift thermal-hydrologic behavior, the properties of the near-field are dominant. In other words, the hydrologic properties of the far-field units have an insignificant influence on near field and in-drift thermal-hydrologic behavior. Consequently, it was decided to assign the hydrologic properties of the Ttpul and Ttpll units to the uz1 unit and to assign the properties of the Ttpmn and Ttpln units to the uz2 unit (Figure 6.2-15[a]). These

simplifications to the distribution of thermal and hydrologic properties are justified in a sensitivity analysis in Section 6.3.14[a].

Of the 560 UZ flow model (SNL 2007 [DIRS 175177]) columns that occur within the heated repository footprint, 39 correspond to fault zones. For fault zones, the UZ flow model represents entire sequences of units as a lumped fault-zone unit. For example, the entire TSw sequence is lumped into one unit. However, there are no hydrologic property sets for the lumped fault-zone units that correspond to the drift-scale calibrated property set for the 30th percentile infiltration map (DTN: LB0610UZDSCP30.001 [DIRS 179180]). There are two plausible ways to address this situation, with one involving lumping of the hydrologic and thermal properties for the TSw sequence using DTN: LB0610UZDSCP30.001 [DIRS 179180], and the other involving the use of the stratigraphy from the closest available UZ flow model non-fault-zone column. Note that lumping of the hydrologic and thermal properties of the entire TSw sequence involves averaging information that is not specific to the host-rock units themselves. A key objective of the suite of MSTHM cases is to reasonably quantify the impact of host-rock thermal conductivity uncertainty, which cannot be reasonably implemented if nonrepository units are lumped together with host-rock (i.e., repository) units. Therefore, it was decided that the most reasonable approach would be to build the meshes for the LDTH submodels residing within each of the 39 fault-zone columns with the use of the closest available non-fault-zone stratigraphy. Thus, fault zones are not discretely represented with different properties from the rest of the host rock. However, because each of the LDTH submodels within fault zones use the percolation flux values that pertain to that particular UZ flow model fault-zone column, the influence of the fault zones on percolation flux is fully and discretely represented.

As discussed in Appendix I of the parent report, the ground-surface boundary temperature, gas-phase pressure, and air-mass fraction are fixed, based on DTN: LB991201233129.001 [DIRS 146894], using software routine boundary_conditions v1.0, described in Section 3.1.8 of the parent report. Using the same software and DTN, the gas-phase pressure and liquid-phase saturation are fixed at the water table. A distinction from the parent report is that a time-dependent water-table boundary temperature is taken from the corresponding SDT submodel (Section 6.2.15[a]).

Percolation flux is obtained for 10-, 30-, 50-, and 90-percentile infiltration maps for the present-day, monsoonal, and glacial-transition climates from DTNs: LB0612PDPTNTSW.001 [DIRS 179150], LB0701MOPTNTSW.001 [DIRS 179156], and LB0701GTPTNTSW.001 [DIRS 179153], respectively. The abbreviations for these cases are P10, P30, P50, and P90. The current MSTHM utilizes the percolation flux values that pertain to the 560 UZ flow model columns residing within the heated repository footprint.

Post-10,000-year percolation flux distributions accommodate the log-uniform distribution between 13 and 64 mm/yr specified in the proposed changes to U.S. Nuclear Regulatory Commission (NRC) regulation 10 CFR Part 63 (70 FR 53313 [DIRS 178394]). The NRC's log-uniform distribution is divided into four equal quartiles (0.125, 0.375, 0.625, and 0.875). The percolation fluxes corresponding to the mid-point of each of these quartiles are determined, resulting in 15.9, 23.6, 35.2, and 52.4 mm/yr, respectively (Table 6.2-5[a]). These values are applied as the repository-wide-averaged post-10,000-year percolation flux values for the P10, P30, P50, and P90 cases, respectively. Percolation flux distributions for the post-10,000-year

climate are obtained using a scaling procedure and the repository-wide-averaged post-10,000-year percolation fluxes of 15.9, 23.6, 35.2, and 52.4 mm/yr for the P10, P30, P50, and P90 cases, respectively. Repository-wide-averaged percolation fluxes are determined for the glacial transition climate for the four percolation cases (Table 6.2-5[a]) using area weighting factors for each of the 560 UZ flow model columns (Output DTN: LL0704PA003MST.022, file: *chimneyWeights.dat*). The area weighting factor for a given UZ flow model column is determined by the number of heated SMT submodel gridblocks within that column, divided by 3,264, which is the total number of heated SMT submodel gridblocks within the repository footprint. The scaling factor for a given percolation flux case is determined by dividing the repository-wide-averaged post-10,000-year percolation flux (e.g., 15.9 mm/yr for the P10 case) by the repository-wide-averaged glacial-transition percolation flux (e.g., 12.2 mm/yr for the P10 case). The post-10,000-year percolation fluxes for each of the UZ flow model columns are obtained by multiplying the glacial-transition percolation flux for that column by the scaling factor for that percolation flux case (e.g., P10). This procedure is repeated for the P10, P30, P50, and P90 cases. This approach is justified because it results in repository-wide-averaged post-10,000-year percolation fluxes that are consistent with the values specified in the proposed changes to 10 CFR Part 63 (70 FR 53313 [DIRS 178394]). Moreover, the influence of post-10,000-year percolation flux on thermal-hydrologic behavior is limited to a small effect on temperature. The period of repository-heat-affected hydrological conditions occurs within the first two thousand years (see Figure 6.3-4 of the parent report).

Table 6.2-5[a]. Summary of Repository-Wide-Averaged Percolation Flux for the Four Climate States

Percolation Flux Case	Repository-Wide-Averaged Percolation Flux (mm/yr)			
	Present-Day	Monsoonal	Glacial-Transition	Post-10,000-Year
P10	4.1	7.8	12.2	15.9
P30	10.2	16.1	26.3	23.6
P50	14.6	19.5	36.2	35.2
P90	34.1	92.4	69.7	52.4

Source: Output DTN: LL0705PA038MST.030.

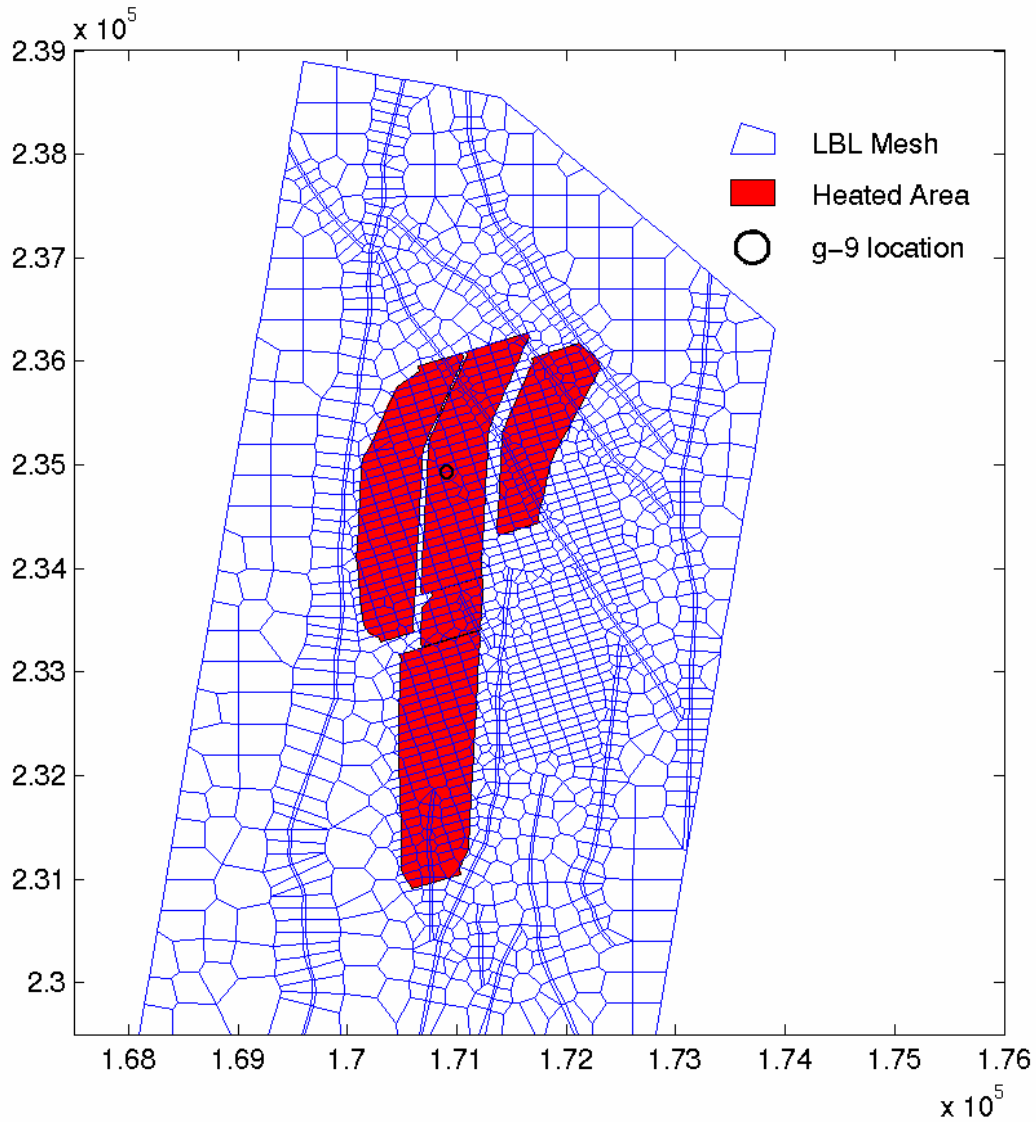
Three (low, mean, and high) host-rock thermal conductivity uncertainty cases are addressed, using the host-rock thermal conductivity values described in Section 6.2.13.3[a]. As discussed in Section 6.2.12.3[a], to address the combination of percolation flux and host-rock thermal conductivity uncertainty, seven cases are run, four with mean host-rock thermal conductivity (P10, P30, P50, and P90), and three other cases (P10L, P10H, and P90H, where L and H stand for low and high thermal conductivity, respectively). These seven cases were chosen to (1) cover the entire range of percolation flux uncertainty addressed by the UZ flow model for the mean host-rock thermal conductivity case, (2) cover the entire range of host-rock thermal conductivity uncertainty for the P10 case (which is the highest probability percolation flux case; see Table 6.3-47[a]), and (3) cover the extremes of combined percolation flux/host-rock thermal conductivity uncertainty. As discussed in Section 6.2.12.3[a], these seven cases address 78% of combined percolation flux/host-rock thermal conductivity uncertainty. The other five cases are addressed with the use of surrogate cases, as described in Sections 6.2.12.3[a] and 6.3.15[a]. As described in Section 6.2.13.6[a], the influence on emissivity of the Bernold-style surface ground-support sheets, which are rock-bolted to the drift wall, is included.

6.2.17[a] Current DDT Submodels

As is discussed in Section 6.2.8 of the parent report, the DDT submodel is only used to determine waste package-to-waste package variability in temperature, compared to line-averaged heat-source conditions along the drift. The DDT submodel (Figure 6.2-16[a]) is similar to the version in the parent report, with the following revisions. The vertical stratigraphy is the same as the LDTH submodel at the g_9 UZ flow model column, which is close to the repository center in drift P3W-13 (Figure 6.2-17[a]). The ground-surface boundary temperature is fixed to be the same as that of the LDTH submodel for the g_9 UZ flow model column. As discussed in Section 6.2.8 of the parent report, the water-table boundary temperature is fixed, based on DTN: LB991201233129.001 [DIRS 146894] using software routine boundary_conditions v1.0, described in Section 3.1.8 of the parent report. As described in Section 6.2.13.6[a], the influence on emissivity of the Bernold-style surface sheets, which are rock-bolted to the drift wall, is included.

<p style="text-align: center;">Ground Surface Fixed boundary temperature</p>
<p style="text-align: center;">UZ1 Averaged tcw11-tsw32 thermal properties</p>
<p style="text-align: center;">Tptpul (tsw33) tsw33 thermal properties</p>
<p style="text-align: center;">Tptpmn (tsw34) tsw34 thermal properties</p>
<p style="text-align: center;">Tptpll (tsw35) tsw35 thermal properties</p>
<p style="text-align: center;">Tptpln (tsw36, tsw37) tsw36 thermal properties</p>
<p style="text-align: center;">UZ2 Averaged tsw38-tr2 thermal properties</p>
<p style="text-align: center;">Water Table Fixed boundary temperature</p>

Figure 6.2-16[a]. Schematic of the Stratigraphic Representation in the DDT Submodel

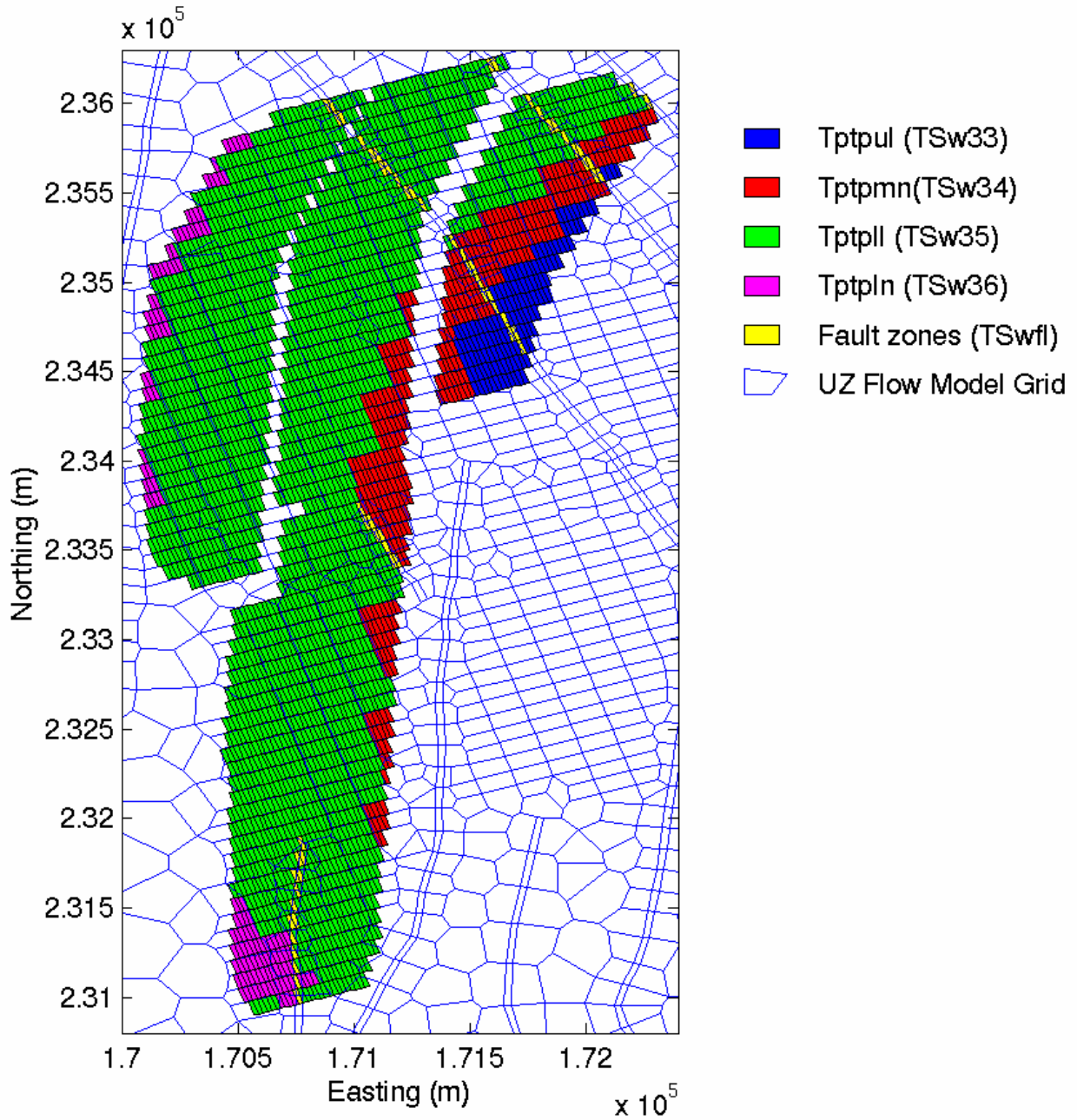


Source: DTN: LB03023DKMGRID.001 [DIRS 162354]; SNL 2007 [DIRS 179466]; Output DTN: LL0702PA013MST.068.

NOTE: Heated repository footprint shown as red fill (SNL 2007 [DIRS 179466]); UZ flow model grid shown as blue mesh (SNL 2007 [DIRS 175177]).

Figure 6.2-17[a]. Heated Repository Footprint of the SMT Submodel Mesh, Overlain on the UZ Flow Model Mesh and Showing the g_9 Location

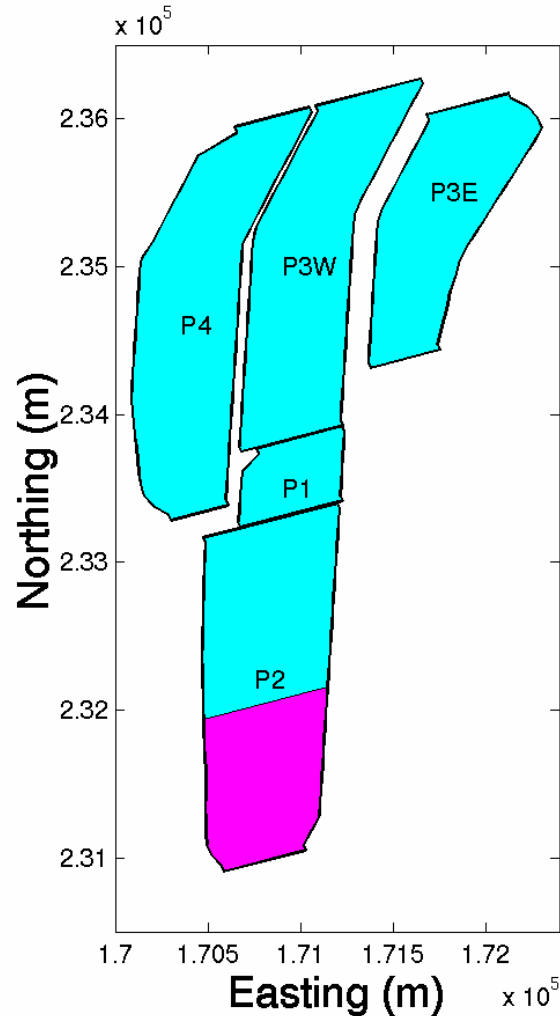
The stratigraphic units through which the repository is carved are shown in Figure 6.2-18[a] and they include Tptpul, Tptpmn, Tptpll, Tptpln, and fault zones. These are overlain on the UZ flow model grid in the plane of the repository.



Source: DTN: LB03023DKMGRID.001 [DIRS 162354] and Output DTN: LL0702PA013MST.068.

NOTE: UZ flow model grid shown as blue mesh (SNL 2007 [DIRS 175177]).

Figure 6.2-18[a]. Distribution of the Host-Rock Units Within the Heated Repository Footprint of the SMT Submodel Mesh Overlain on the UZ Flow Model Grid



Source: Output DTN: LL0702PA013MST.068.

NOTE: Contingency drifts (SNL 2007 [DIRS 179466]) shown in purple.

Figure 6.2-19[a]. Heated Repository Footprint of the SMT-Submodel Mesh, Showing Panel Numbers and Contingency Drifts at the South End

The heat-generation histories (Table 6.2-6[a]) of the eight waste package types in the DDT submodels, which include six full waste packages and two half waste packages, are based on information in DTN: MO0702PASTREAM.001 [DIRS 179925]. The time-dependent ventilation heat-removal efficiency for the DDT submodel, which is slightly different from that used in the parent report, is based on an area-weighted average for the 560 LDTH/SDT submodel locations. The area weight is based on the number of heated SMT submodel gridblocks within each of the 560 respective UZ flow model gridblock columns. The previous DDT submodel used the time-dependent ventilation heat-removal efficiency specific to the g_9 UZ flow model LDTH/SDT submodel location (Figure 6.2-17[a]). The repository-wide-average heat-removal efficiency is used because the DDT submodel is applied to the entire repository area. Waste package dimensions used in the DDT submodel, which are slightly different from those used in the parent report, are from DTN: MO0702PASTREAM.001 [DIRS 179925], and from *Total*

System Performance Assessment Data Input Package for Requirements Analysis for TAD Canister and Related Waste Package Overpack Physical Attributes Basis for Performance Assessment (SNL 2007 [DIRS 179394]) and *Total System Performance Assessment Data Input Package for Requirements Analysis for DOE SNF/HLW and Navy SNF Waste Package Overpack Physical Attributes Basis for Performance Assessment* (SNL 2007 [DIRS 179567]). The small differences are seen by comparing Table 6.3-13 of the parent report and Table 6.2-6[a].

Table 6.2-6[a]. Summary of Waste Packages Included in the MSTHM Calculations

Waste Package Name in MSTHM	Waste Package type	Length in Model (m)	Initial Heat-Generation Rate (kW)	Notes (based on MSTHM output temperatures and heat output)
pwr1-1	21-PWR AP CSNF <i>½ 21-PWR AP</i>	2.92505	6.086 ^a	Half waste package in model; coolest PWR waste package in sequence, but “average” PWR waste package with respect to heat output
dhlw-l1	5 DHLW/DOE SNF-LONG <i>5-HLW LONG</i>	5.2280 ^b	0.407	Coolest waste package in sequence with the lowest heat output
pwr2-1	21-PWR AP CSNF <i>21-PWR AP (HOT)</i>	5.8501	12.660	“Average” PWR waste package in sequence with respect to temperatures, but highest heat output in sequence
bwr1-1	44-BWR CSNF <i>44-BWR AP</i>	5.8501	7.704	Hottest BWR waste package in sequence, but “average” BWR waste package with respect to heat output
bwr2-1	44-BWR CSNF <i>44-BWR AP ADJUSTED</i>	5.8501	7.704	“Oldest” BWR waste package in sequence
dhlw-s1	5 DHLW/DOE SNF-SHORT <i>5-HLW SHORT</i>	3.6814 ^c	3.620	Hottest DHLW waste package in sequence
pwr1-2	21-PWR AP CSNF <i>21-PWR AP</i>	5.8501	12.170	Average PWR waste package with respect to heat output
pwr1-3	21-PWR CSNF <i>½ 21-PWR AP</i>	2.92505	6.086 ^a	Half waste package in model; “hottest” waste package in sequence, but average PWR waste package with respect to heat output
Total		38.860 ^d	56.437	Initial heat output of 1.45 kW/m

Source: DTN: MO0702PASTREAM.001 [DIRS 179925]; SNL 2007 [DIRS 179394]; SNL 2007 [DIRS 179567].

^a These values represent the heat-generation rate for a half waste package.

^b This value differs slightly from that (5.3039 m) of source (SNL 2007 [DIRS 179567], Table 4-9). The small difference of 0.076 m has a negligible influence on local temperature deviations, relative to line-averaged temperature conditions. In the context of the MSTHM methodology, the primary function of the DDT submodel is to determine local temperature deviations relative to line-averaged conditions. Therefore, the small difference in length for the dhlw-l1 waste package has an insignificant influence on MSTHM-predicted TH conditions.

^c This value differs slightly from that (3.6974 m) of source (SNL 2007 [DIRS 179567], Table 4-8). The small difference of 0.016 m has a negligible influence on local temperature deviations, relative to line-averaged temperature conditions. In the context of the MSTHM methodology, the primary function of the DDT submodel is to determine local temperature deviations relative to line-averaged conditions. Therefore, the small difference in length for the dhlw-l1 waste package has an insignificant influence on MSTHM-predicted TH conditions.

^d Includes 10-cm gap between waste packages.

NOTE: HLW = high-level (radioactive) waste. *Adjusted* 44-BWR waste package has a heat output history that enables the line-averaged heat load to correspond more closely with that used in the LDTH, SDT, and SMT submodels.

6.2.18[a] Current LDTH Submodels for the Low-Probability-Seismic Collapsed-Drift Case

The current LDTH submodels for the low-probability-seismic collapsed-drift case only differ from those described in Section 6.2.10 of the parent report in two respects. First, the nominal LDTH submodel, upon which these collapsed-drift LDTH submodels are based has been updated, as discussed in Section 6.2.16[a]. Second, the thermal properties of the rubble have been updated, as described in Section 6.2.13.5[a] and Appendix XI[a].

As discussed in Section 6.2.10.3 of the parent report, the van Genuchten alpha parameter for the fracture continuum of the rubble is 0.01 Pa^{-1} , which is consistent with Assumption 6 in Section 5 of *Drift-Scale Coupled Processes (DST and TH Seepage) Models* (BSC 2005 [DIRS 172232]). The value of the van Genuchten “*m*” parameter is 0.633 for the rubble fracture continuum, which is the same as that of the fractures in the drift-scale calibrated property set for the 30th percentile infiltration map (DTN: LB0610UZDSCP30.001 [DIRS 179180]). Note that the fracture van Genuchten alpha varies from 4.99×10^{-3} to $2.08 \times 10^{-5} \text{ Pa}^{-1}$ in DTN: LB0610UZDSCP30.001 [DIRS 179180]. Because the van Genuchten alpha value of 0.01 Pa^{-1} for the fracture continuum of the rubble is within a factor of two of the upper range of the fracture alpha values from DTN: LB0610UZDSCP30.001 [DIRS 179180], it is reasonable to apply the value of van Genuchten “*m*” parameter from the same DTN to the rubble. Note also that the van Genuchten “*m*” parameter is 0.633 for all fractures in an earlier drift-scale hydrologic property set (DTN: LB0208UZDSCPMI.002 [DIRS 161243]).

6.2.19[a] Current DDT Submodels for the Low-Probability-Seismic Collapsed-Drift Case

The current DDT submodels for the low-probability-seismic collapsed-drift case only differ from those described in Section 6.2.11 of the parent report in two respects. First, the nominal DDT submodel, upon which the collapsed-drift DDT submodels are based, has been updated as discussed in Section 6.2.17[a]. Second, the thermal properties of the rubble have been updated, as described in Section 6.2.13.5[a] and Appendix XI[a].

6.2.20[a] Repository-Averaged Generic LDTH Submodels

As described in Section 6.2.16[a], the current LDTH submodels utilize a generic thermal-hydrologic stratigraphy that consists of the four host-rock units (tsw33, tsw34, tsw35, and tsw36), an upper nonrepository unit called uz1, and a lower nonrepository unit called uz2 (Figure 6.2-15[a]). The LDTH-submodel calculations associated with the thermal conductivity analyses described in Section 6.2.13.3[a] and contained in Output DTN: LL0703PA026MST.013 utilize generic LDTH submodels implementing unit thicknesses close to the repository-averaged values (Table 6.2-7[a]).

Table 6.2-7[a]. Repository-Averaged Thicknesses for the Generic Thermal-Hydrologic Stratigraphy Used in the LDTH Submodels

Generic Thermal-Hydrologic Unit	Unit Thickness (m)	
	Repository Averaged ^a	As Applied to Repository-Averaged Generic LDTH Submodel ^b
uz1	169.6171	171.0
tsw33	77.4857	78.0
tsw34	33.9107	34.0
tsw35	100.5237	102.0
tsw36	37.6211	45.0
uz2	197.8750	207.0
Total	617.0333	637.0

^a Output DTN: LL0705PA038MST.030.

^b Values applied in the LDTH submodels of Output DTN: LL0703PA026MST.013.

6.2.21[a] Direction of Ventilation Implemented in LDTH and SDT Submodels

As described in Section 8.5.8[a], the ventilation direction was reversed for Panels 2 and 4 due to a change in nomenclature for these panels. Despite the reversal in ventilation direction for Panels 2 and 4, differences in peak temperature and boiling duration between the corrected and uncorrected cases are well within the ranges of parametric uncertainty. For the median waste package, the range in peak temperature arising from parametric uncertainty is on the order of 30°C (Figure 6.3-77[a] and Table 6.3-49[a]), while the impact of the reversed ventilation direction is on the order of 1°C (Figure 8.5-1[a]). The range in median waste package boiling duration for the entire model is on the order of 500 years (Figure 6.3-78[a] and Table 6.3-50[a]), while the impact of the reversed ventilation direction is on the order of 1 year (Figure 8.5-2[a]). Therefore, the influence of the reversed ventilation direction is insignificant.

6.3[a] MSTHM RESULTS

6.3.1[a] TSPA-LA Base Case

Updated MSTHM results for the TSPA base case are described in Section 6.3.16[a].

6.3.2[a] Parameter-Uncertainty Sensitivity Analyses

Applicable to this addendum, with the current MSTHM parameter sensitivity analyses described in Section 6.3.16[a].

6.3.3[a] Mass Flux in the Invert

Applicable to this addendum, with no changes required. Although the current model uses revised invert properties (see Section 6.2.13.2[a]), this section is still applicable as a qualitative analysis of mass balance in the invert.

6.3.4[a] Combined Influences of Percolation Flux and Host-Rock Thermal Conductivity Uncertainty on the TSPA-LA Base Case

Applicable to this addendum, with the current analyses of the combined influences of percolation flux and host-rock thermal conductivity uncertainty described in Section 6.3.16[a].

6.3.5[a] Summary of the Range of Thermal-Hydrologic Conditions for the TSPA-LA Base Case

Applicable to this addendum, with the current summary of the range of thermal-hydrologic conditions described in Section 6.3.16[a].

6.3.6[a] Relationship between Relative Humidity on the Waste Package and Drip Shield and Temperature on the Drift Wall

Applicable to this addendum, with no changes required. Although the current model has been updated, this section is still applicable as a qualitative analysis of the relationship between relative humidity on the waste package and drip shield and temperature on the drift wall.

6.3.7[a] Influence of a Low-Probability-Seismic Collapsed-Drift Scenario on In-Drift Thermal-Hydrologic Conditions

Applicable to this addendum, with the current MSTHM analyses of the influence of drift collapse described in Section 6.3.17[a].

6.3.8[a] Comparison of Results for the TSPA-LA Base Case with Those for the FY01 Supplemental Science and Performance Analyses (SSPA)

Applicable to this addendum, with no changes required, except to note that the TSPA-LA base case has been updated as part of this addendum.

6.3.9[a] Influence of Host-Rock Hydrologic-Property Variability and Uncertainty

Applicable to this addendum, with no changes required.

6.3.10[a] Influence of Pseudo-Permeability on In-Drift Temperature and Relative Humidity

Applicable to this addendum, with no changes required.

6.3.11[a] Influence of Invert Hydrologic-Property Variability and Uncertainty

Applicable to this addendum, with no changes required.

6.3.12[a] Influence of Ventilation Heat-Removal Efficiency Uncertainty

Applicable to this addendum, with no changes required.

6.3.13[a] Relationship between Temperature and Relative Humidity on Waste Packages

Applicable to this addendum, with no changes required.

6.3.14[a] Sensitivity Analysis of the Influence of the Simplified Thermal-Hydrologic Stratigraphy in the Current LDTH Submodels

As described in Sections 6.2.13.4[a] and 6.2.16[a], the current LDTH submodels implement a simplified thermal-hydrologic stratigraphy, compared to the LDTH submodels used in the previous version of the MSTHM (Section 6.2.6 of the parent report). As described in Section 6.2.13.4[a], the thermal property stratigraphy is simplified by averaging the thermal properties of the nonrepository (i.e., non-host-rock) units lying above and below the host-rock units. As shown in Figure 6.2-15[a], the upper and lower averaged (or “lumped”) units are called uz1 and uz2, respectively. As described in Section 6.2.16[a] and as shown in Figure 6.2-15[a], the hydrologic stratigraphy is simplified by applying the hydrologic properties of the Tptpll (tsw35) unit to both of the lithophysal units—Tptpul (tsw33) and Tptpll (tsw35)—and by applying the hydrologic properties of the Tptpmn (tsw34) unit to both of the nonlithophysal units—Tptpmn (tsw34) and Tptpln (tsw36). As shown in Figure 6.2-15[a], further simplifications to the hydrologic stratigraphy are made by applying the Tptpll (tsw35) hydrologic properties to not only the Tptpul (tsw33), but to the overlying uz1 unit as well, and by applying the Tptpmn (tsw34) hydrologic properties to not only the Tptpln (tsw36), but to the underlying uz2 unit as well.

To justify the reasonableness of the simplifications to the thermal and hydrologic stratigraphy, a sensitivity study is conducted with the LDTH submodel for the P10 percolation flux case at the g_9 location (Figure 6.2-17[a]), which is close to the repository center. The P10 percolation flux case at this location is representative of a typical location in the center of the repository for the following reasons. It is within the predominant host-rock unit, which is the Tptpll (tsw35) unit, close to the center of the repository area. Moreover, the local P10 percolation flux values, which are 3.6, 6.8, 13.6, and 17.8 mm/yr for the present-day, monsoonal, glacial-transition, and post-10,000-year climates, respectively, are close to the repository-wide averages (4.1, 7.8, 12.2, and 15.9 mm/yr) for the P10 percolation flux case (see Table 6.2-5[a]). A four-way comparison is made for the following cases:

1. **Full thermal-hydrologic stratigraphy:** The thermal and hydrologic properties of all 39 UZ flow model units are discretely represented, just as was done in the parent report.
2. **Full thermal, lumped hydrologic stratigraphy:** The thermal properties of all 39 UZ flow model units are discretely represented, while the hydrologic stratigraphy utilizes only the Tptpmn (tsw34) and Tptpll (tsw35) hydrologic properties, as described above and in Section 6.2-16[a].

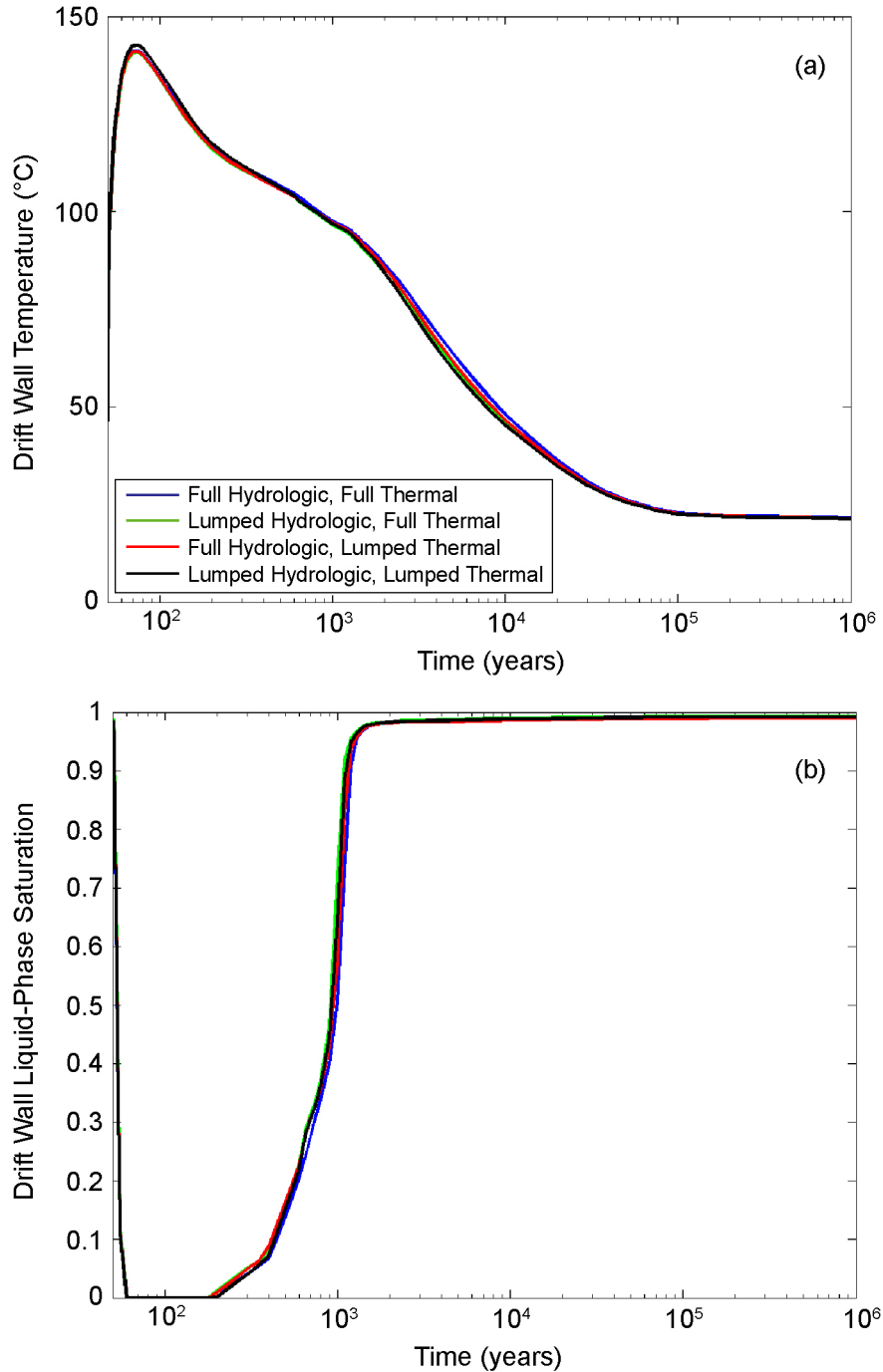
3. **Full hydrologic, lumped thermal stratigraphy:** The hydrologic properties of all 39 UZ flow model units are discretely represented, while the thermal stratigraphy employs the lumped uz1 and uz2 units described above and in Sections 6.2.13.4[a] and 6.2.16[a].
4. **Lumped thermal, lumped hydrologic stratigraphy:** The hydrologic and thermal properties are lumped as described above and in Sections 6.2.13.4[a] and 6.2.16[a].

As is done for the current LDTH submodels, all four of these cases use the drift-scale calibrated property set for the 30th percentile infiltration map (DTN: LB0610UZDSCP30.001 [DIRS 179180]). The thermal properties are the same as those used in the parent report, except that the thermal conductivity values are updated for the four host-rock units: Tptpul (tsw33), Tptpmn (tsw34), Tptpll (tsw35), and Tptpln (tsw36), as discussed in Section 6.2.13.3[a].

As shown in Figure 6.3-70[a], the drift wall temperature and liquid-phase saturation histories are nearly the same for these four cases. Therefore, thermal-hydrologic conditions in the drift are insensitive to the lumping of thermal properties in the nonrepository units and insensitive to the use of only the hydrologic properties of the Tptpmn and Tptpll units for the entire unsaturated zone, as discussed in Section 6.2.16[a]. This comparison validates the reasonableness of the simplified thermal-hydrologic stratigraphy implemented in the current LDTH submodels, as described in Section 6.2-16[a].

In addition to assessing the influence of the simplified thermal-hydrologic stratigraphy on the current MSTHM results, it is useful to assess the influence of host-rock hydrologic properties. In addition to the drift-scale calibrated property set for the 30th percentile infiltration map (DTN: LB0610UZDSCP30.001 [DIRS 179180]), the drift-scale calibrated property set for the 10th percentile infiltration map (DTN: LB0610UZDSCP10.001 [DIRS 180502]) is also available. This comparison is made using the same LDTH submodel used to compare the influence of the simplified thermal-hydrologic stratigraphy on TH behavior. Figure 6.3-71[a] clearly shows that drift wall temperature and liquid-phase saturation are insensitive to the choice of hydrologic property set. Accordingly, near-field and in-drift TH behavior are insensitive to the choice of hydrologic property set.

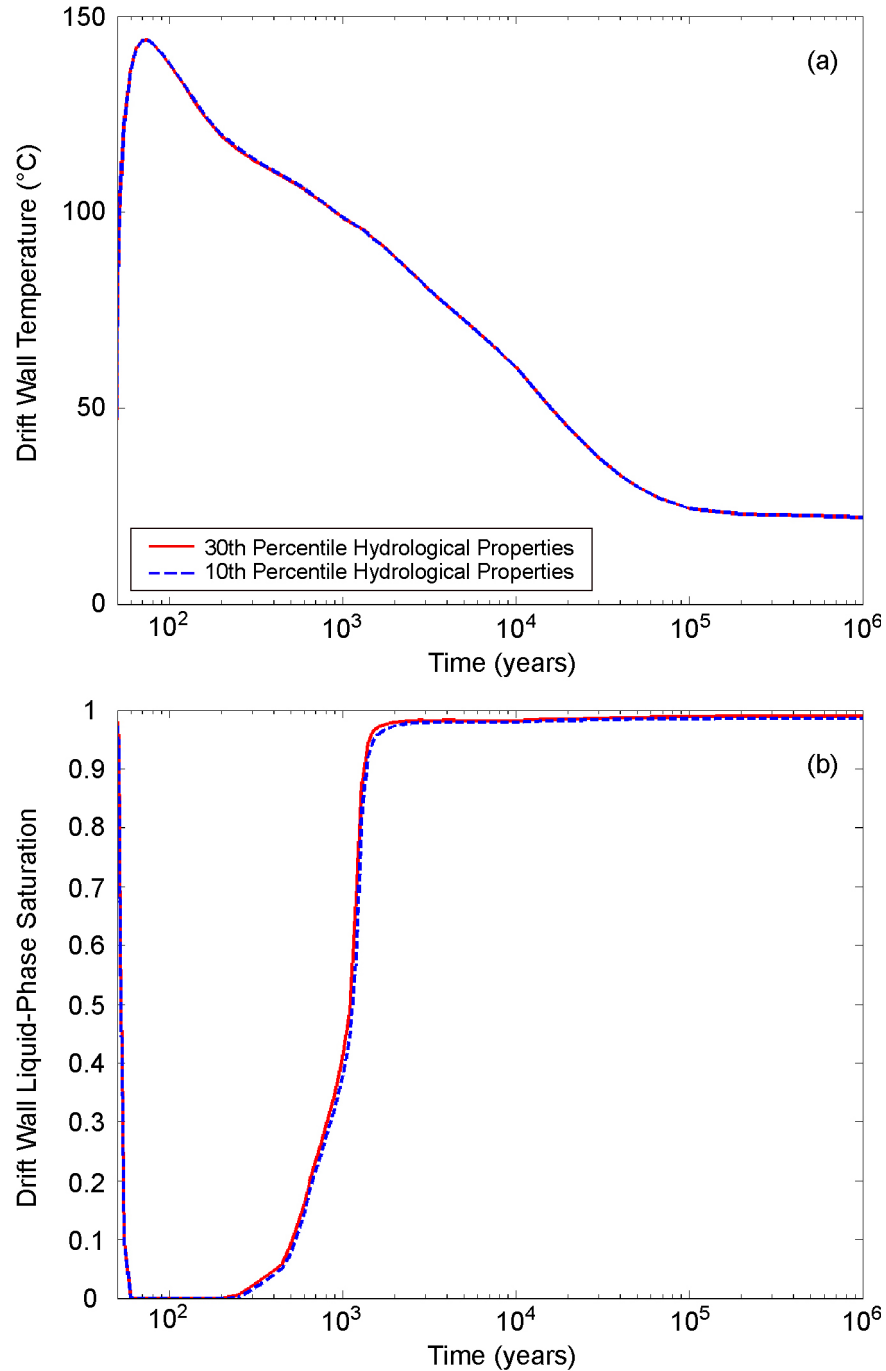
It should be noted that this sensitivity analysis is designed to test the effect of lumping thermal and hydrologic variables on the temperature and saturation in the geologic units. It can be directly inferred that because lumping had negligible impacts on drift wall temperatures and saturations, it has even smaller effects on waste package temperatures and relative humidities (because these parameters are not physically impacted by the lumped parameters). Recall that the only parameters changed in these model runs are host rock thermal and hydrologic variables and no changes are made to the waste form or in-drift characteristics.



Source: Output DTN: LL0705PA032MST.028.

NOTE: Temperature and matrix liquid-phase saturation histories are calculated by the LDTH submodel (Section 6.2.16[a]) for an areal mass loading (AML) of 55 metric tons of uranium (MTU) per acre and for a location close to the center of the repository (the g_9 location shown in Figure 6.2-17[a]) for the P10 case. Four cases are considered: (1) full thermal-hydrologic stratigraphy for 39 model units, (2) full thermal, lumped hydrologic stratigraphy, (3) full hydrologic, lumped thermal stratigraphy, and (4) lumped thermal, lumped hydrologic stratigraphy.

Figure 6.3-70[a]. Drift Wall Temperature (a) and Liquid-Phase Saturation (b) at the Repository Center for Different Representations of Thermal-Hydrologic Stratigraphy

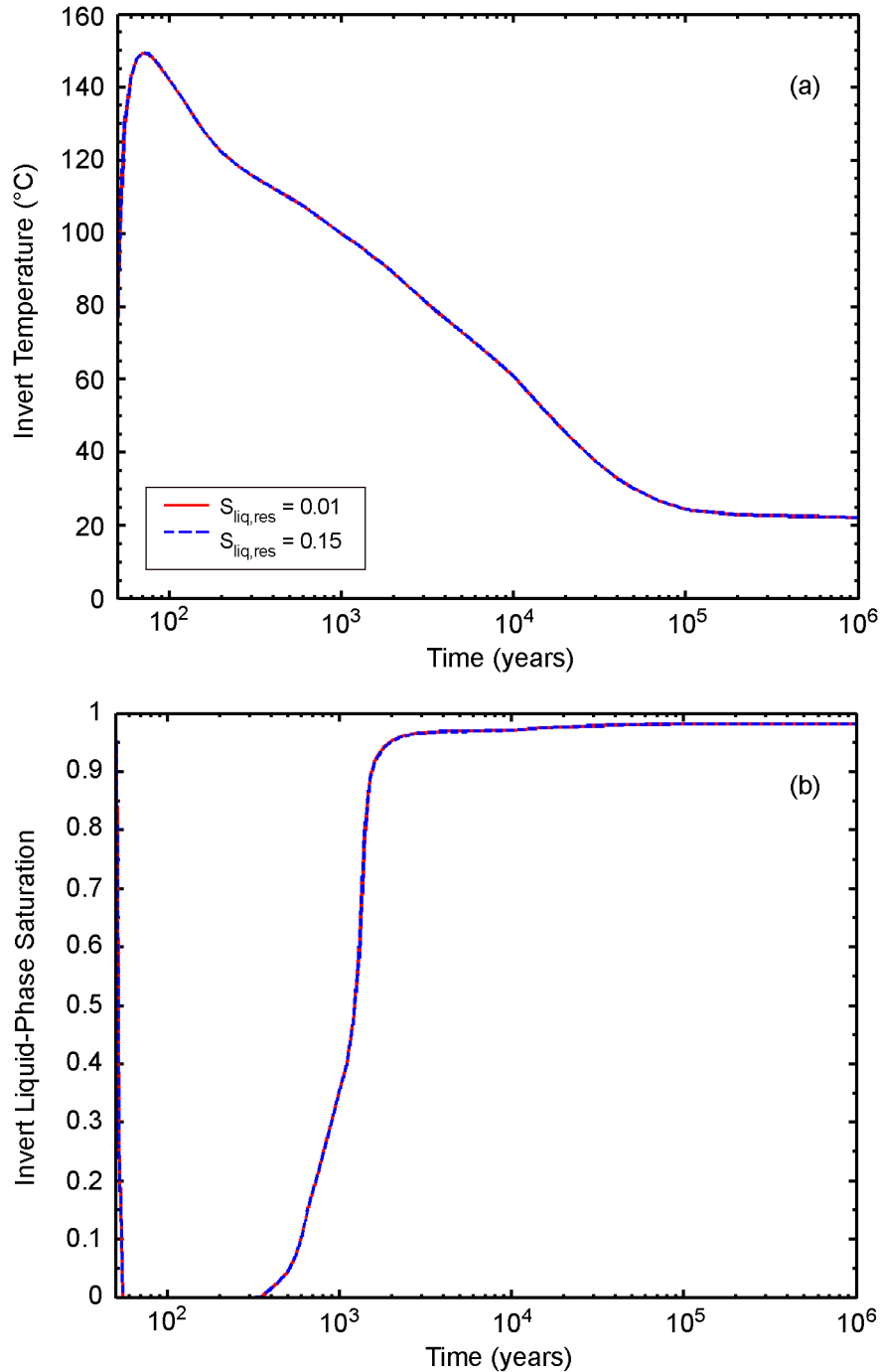


Source: Output DTN: LL0705PA032MST.028.

NOTE: Temperature and matrix liquid-phase saturation histories are calculated by the LDTH submodel (Section 6.2.16[a]) for an AML of 55 MTU/acre and for a location close to the center of the repository (the g_9 location shown in Figure 6.2-17[a]) for the P10 case. Two cases are considered: (1) with the drift-scale calibrated property set for the 30th percentile map (DTN: LB0610UZDSCP30.001 [DIRS 179180]), and (2) with the drift-scale calibrated property set for the 10th percentile map (DTN: LB0610UZDSCP10.001 [DIRS 180502]).

Figure 6.3-71[a]. Drift Wall Temperature (a) and Liquid-Phase Saturation (b) at the Repository Center Using the 30th and 10th Percentile Hydrologic Property Sets

In addition to assessing the influence of the simplified thermal-hydrologic stratigraphy on the current MSTHM results, it is useful to assess the influence of the residual saturation of the intergranular porosity of the crushed tuff in the invert. As discussed in Section 5.3.1.11[a], the residual saturation of the intergranular porosity of the invert is assumed to be the same as that of the fractures (0.01) of the Ttp11 host-rock unit. The same LDTH submodel that is used in the sensitivity analysis of the simplified thermal-hydrologic stratigraphy is used to compare the influence of two values of residual saturation of the intergranular porosity, including a value of 0.01 and a value of 0.15, which is a relatively large value that is similar to the value of residual saturation of the matrix continuum in the host-rock units. For example, the residual saturation is 0.12 for the matrix continuum of the Ttp11 unit (DTN: LB0208UZDSCPMI.002 [DIRS 161243]). The drift-scale calibrated property set for the 30th percentile infiltration map (DTN: LB0610UZDSCP30.001 [DIRS 179180]) is used for this comparison. Figure 6.3-72[a] clearly shows that temperature and liquid-phase saturation of the intragranular porosity of the crushed tuff in the invert are insensitive to whether the residual intergranular saturation is either 0.01 or 0.15. Note that the value of liquid-phase saturation in the invert provided to TSPA is that of the intragranular porosity. Therefore, the invert liquid-phase saturation provided to TSPA is unaffected by the choice of residual saturation in the intergranular porosity of the crushed tuff in the invert.



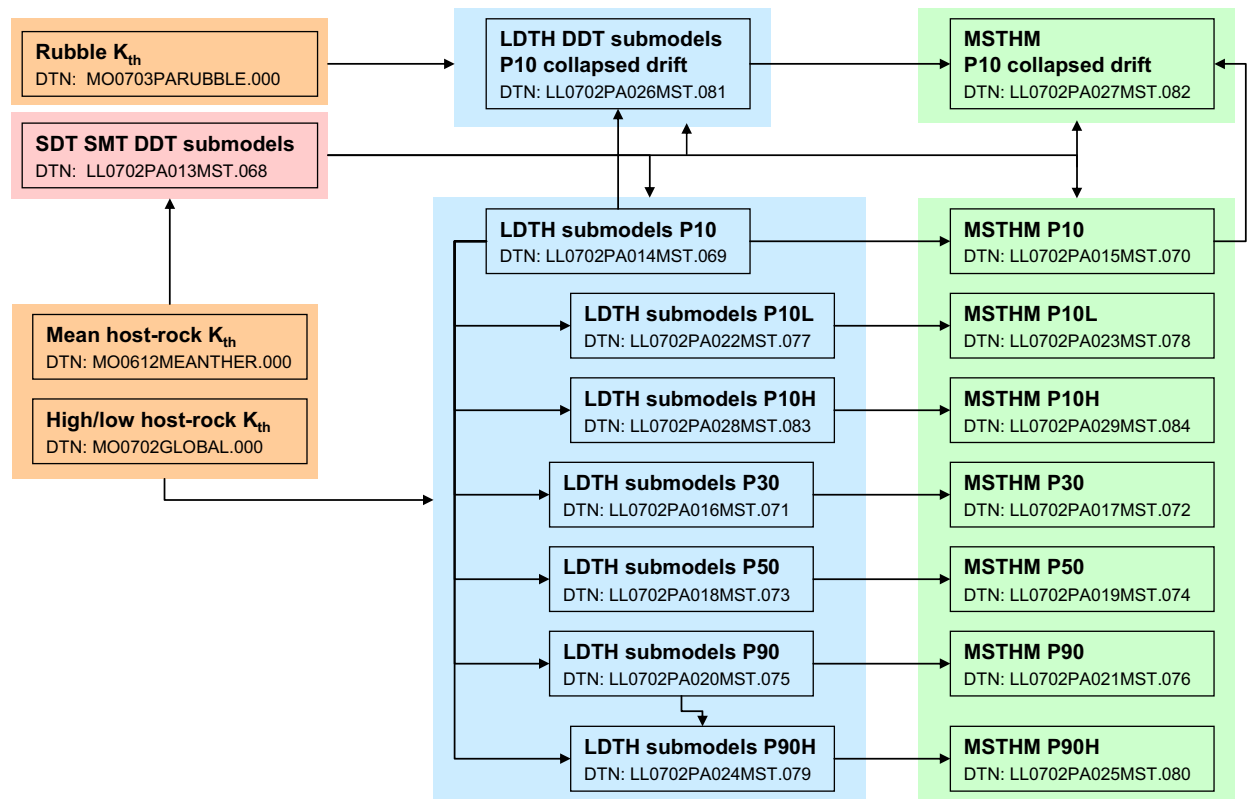
Source: Output DTN: LL0705PA032MST.028.

NOTE: Temperature and intragranular-porosity liquid-phase saturation histories are calculated by the LDTH submodel (Section 6.2.16[a]) for an AML of 55 MTU/acre and for a location close to the center of the repository (the g_9 location shown in Figure 6.2-17[a]) for the P10 case. These cases use the drift-scale calibrated property set for the 30th percentile map (DTN: LB0610UZDSCP30.001 [DIRS 179180]). Two cases of residual saturation of the intergranular porosity of the crushed tuff in the invert are considered, with residual saturation values of 0.01 and 0.15.

Figure 6.3-72[a]. Invert Temperature (a) and Liquid-Phase Saturation of the Intragranular Porosity of the Crushed Tuff in the Invert (b) at the Repository Center

6.3.15[a] Data Flow between Current MSTHM DTNs

Figure 6.3-73[a] shows the data flow between Output DTNs generated by the MSTHM to generate seven uncertainty cases for TSPA, as well as for the MSTHM collapsed-drift case. The Output DTNs fall under four general categories: (1) thermal conductivity values, (2) SDT, SMT, and DDT submodels, (3) LDTH submodels, and (4) MSTHM feeds to TSPA. Details of the relationships between the data files in the Output DTNs shown in Figure 6.3-73[a] are provided in the respective ReadMe files of those Output DTNs. The TSPA roadmap is depicted in Figures 6.3-73[a] through 6.3-75[a].

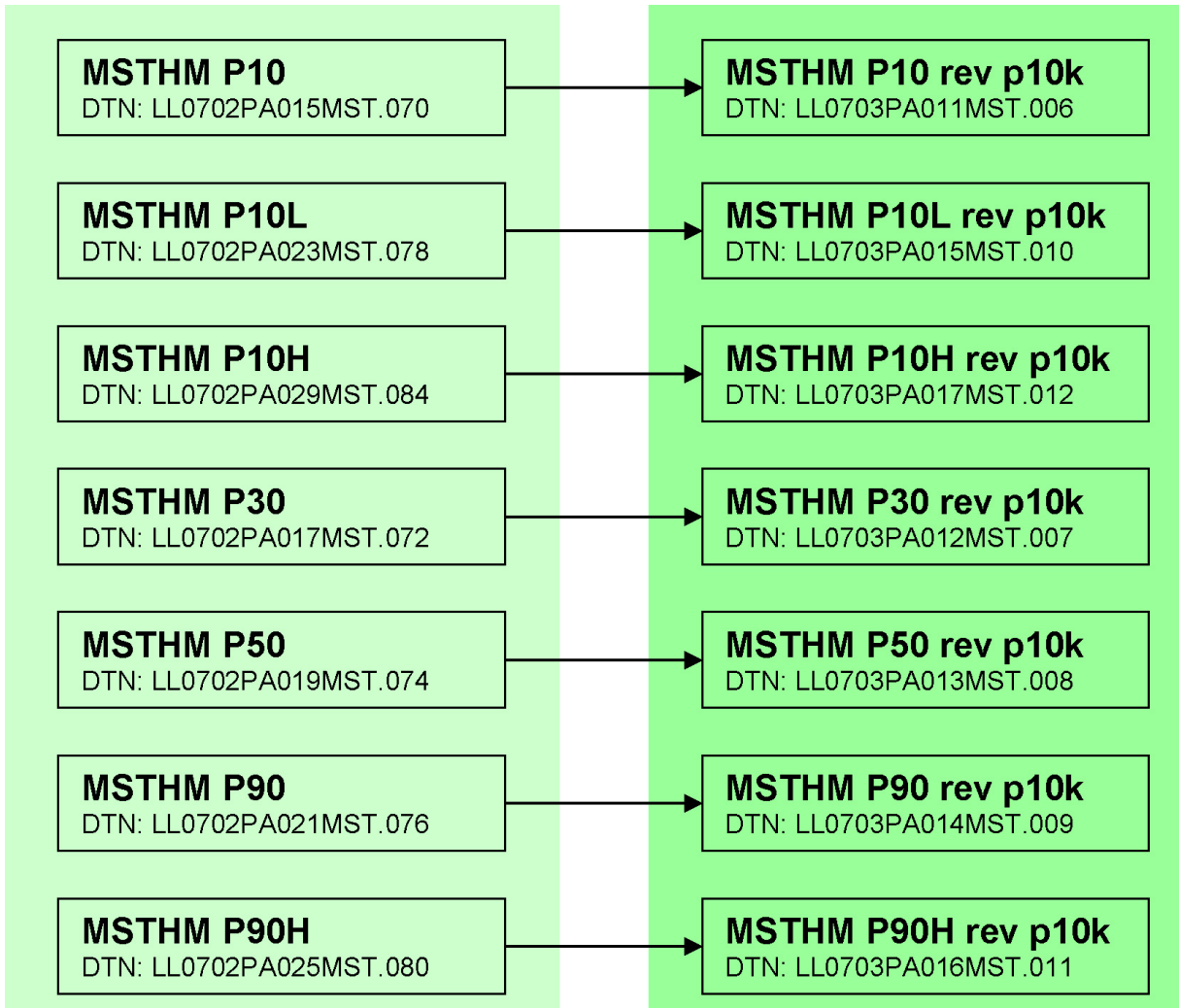


NOTE: Output DTN: LL0702PA027MST.082 is a direct feed to TSPA, with all other DTNs being intermediate DTNs.

Figure 6.3-73[a]. Data Flow between the Output DTNs Generated by the MSTHM, Showing the Relationship between the Submodel Output DTNs and the MSTHM Output DTNs

The MSTHM Output DTNs for the seven uncertainty cases in Figure 6.3-73[a] all have the actual post-10,000-year percolation fluxes that were directly employed in the LDTH submodels used to generate those results. As described in Section 6.2-16[a], those post-10,000-year percolation fluxes were generated by a scaling procedure. After the MSTHM calculations in Figure 6.3-73[a] were conducted, the post-10,000-year percolation fluxes from the UZ flow model became available (DTN: LB0702UZPTN10K.002 [DIRS 179332]). For the purpose of seepage analyses, TSPA requires the post-10,000-year percolation fluxes generated by the UZ flow model to be available in the MSTHM DTNs. Figure 6.3-74[a] shows the process of creating the DTNs that provide TSPA with the UZ flow model-calculated post-10,000-year percolation fluxes. The MSTHM Output DTNs for the seven uncertainty cases (shown in Figure 6.3-73[a]) are modified by replacing the scaled post-10,000-year percolation fluxes with post-10,000-year percolation fluxes from the UZ flow model (DTN: LB0702UZPTN10K.002 [DIRS 179332]). Figure 6.3-74[a] shows the relationship between the MSTHM DTNs with the scaled post-10,000-year percolation fluxes and those from the UZ flow model (DTN: LB0702UZPTN10K.002 [DIRS 179332]).

Table 6.3-47[a] shows the seven uncertainty cases that were modeled with the MSTHM, as well as the five cases not directly modeled with the MSTHM. Table 6.3-47[a] also gives the weights for all twelve cases, which is the product of the percolation flux weights and the host-rock thermal conductivity weights. Based on Output DTN: LL0703PA053MST.021, surrogate cases were selected for each of the five uncertainty cases that were not directly modeled. Table 6.3-48[a] shows the effective weights for each of the seven modeled uncertainty cases, which is the sum of the weight for that particular case, plus the weight(s) of the unmodeled uncertainty case(s) for which that case is a surrogate. Thus, to generate one of the five unmodeled uncertainty cases, it requires two output DTNs, with one containing the surrogate TH data and the other containing the percolation flux data required for that DTN. Figure 6.3-75[a] shows the relationship between these respective output DTNs. The top file on the left is the surrogate output DTN and the bottom file is the output DTN containing the appropriate percolation flux data.



NOTE: The output DTNs shown on the right are direct feeds to TSPA, with intermediate DTNs shown on the left. Modified post-10,000-year values are taken from DTN: LB0702UZPTN10K.002 [DIRS 179332].

Figure 6.3-74[a]. Data Flow between the Output DTNs Generated by the MSTHM, Showing the Relationship between the Output DTNs with the Scaled Post-10,000-Year Percolation Flux Values and the DTNs with the Modified Post-10,000-Year Values

Table 6.3-47[a]. Relationship between the Modeled Uncertainty Cases (blue background) and the Uncertainty Cases Not Directly Modeled (green background), with the Identity of the Surrogate Case Show in Red

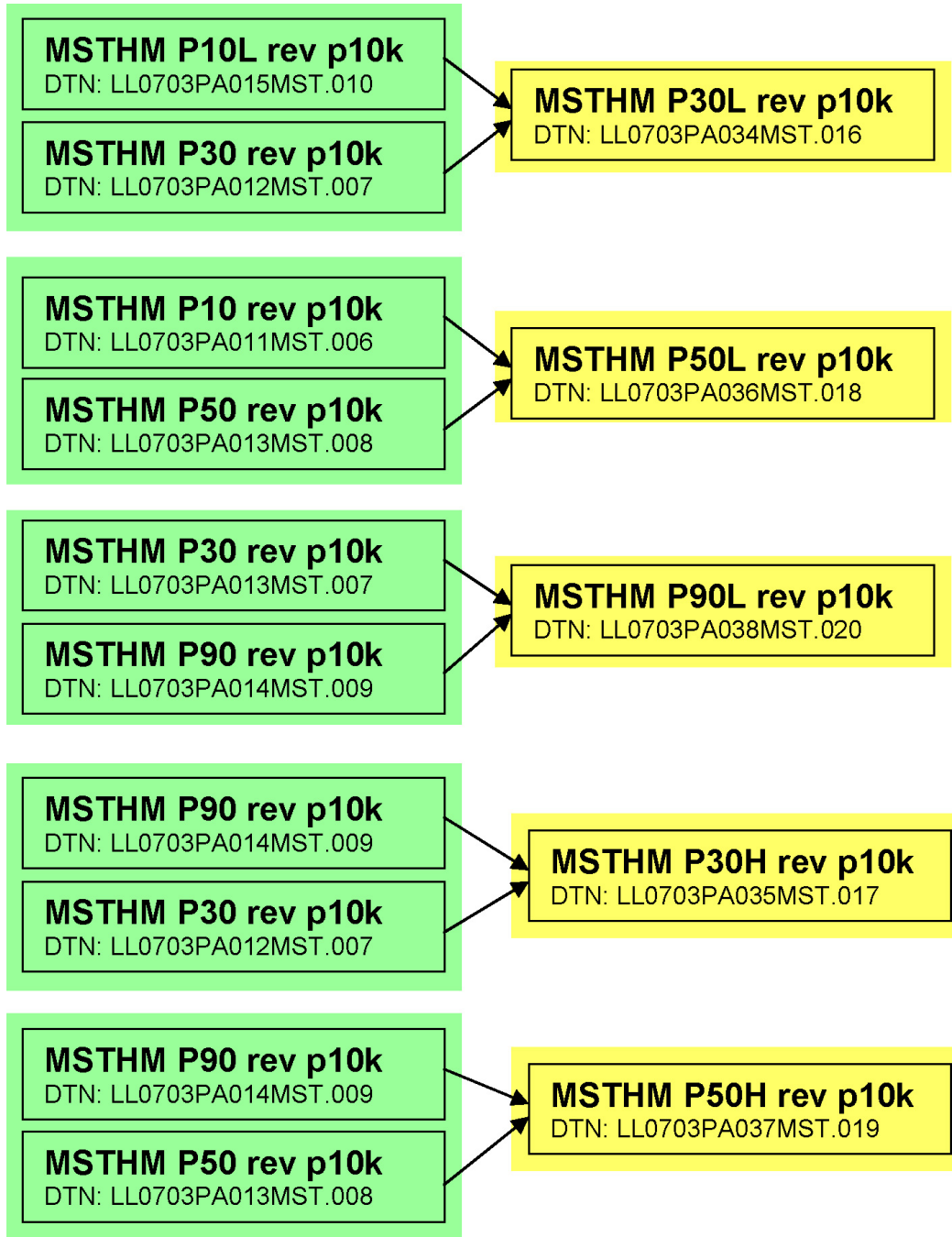
		Percolation Flux Uncertainty			
		P10	P30	P50	P90
Host-Rock Thermal Conductivity Uncertainty		0.6191 ^a	0.1568 ^a	0.1645 ^a	0.0596 ^a
	H 0.34 ^b	P10H 0.2105 ^c	P90 ^d 0.0533 ^c	P90 ^d 0.0559 ^c	P90H 0.0203 ^c
	M 0.37 ^b	P10 0.2291 ^c	P30 0.0580 ^c	P50 0.0609 ^c	P90 0.0220 ^c
	L 0.29 ^b	P10L 0.1795 ^c	P10L ^d 0.0455 ^c	P10 ^d 0.0477 ^c	P30 ^d 0.0173 ^c

- ^a Weights are obtained from DTN: LB0701PAWFINFM.001 [DIRS 179283].
- ^b Weights are obtained from Output DTN: LL0703PA026MST.013.
- ^c This denotes the weight of that case, which is the product of the percolation flux weight and the host-rock thermal conductivity weight.
- ^d Denotes a surrogate case from which the TH results are obtained (see Output DTN: LL0703PA053MST.021).

Table 6.3-48[a]. Relationship between the Modeled Uncertainty Cases (blue background) and the Uncertainty Cases Not Directly Modeled (green background), with the Names of the Five Uncertainty Cases Not Directly Modeled Shown in Red

		Percolation Flux Uncertainty			
		P10	P30	P50	P90
Host-Rock Thermal Conductivity Uncertainty		0.6191	0.1568	0.1645	0.0596
	H 0.34	P10H 0.2105 ^a 0.2105 ^b	P90 0.0533 ^a 0.0000 ^b	P90 0.0559 ^a 0.0000 ^b	P90H 0.0203 ^a 0.0203 ^b
	M 0.37	P10 0.2291 ^a 0.2768 ^b	P30 0.0580 ^a 0.0753 ^b	P50 0.0609 ^a 0.0609 ^b	P90 0.0220 ^a 0.1312 ^b
	L 0.29	P10L 0.1795 ^a 0.2250 ^b	P30L 0.0455 ^a 0.0000 ^b	P50L 0.0477 ^a 0.0000 ^b	P90L 0.0173 ^a 0.0000 ^b

- ^a This denotes the weight of that case, which is the product of the percolation flux weight and the host-rock thermal conductivity weight.
- ^b Sum of that case's own weight plus the weights of the cases for which that case is a surrogate.



NOTE: The output DTNs shown on the right are direct feeds to TSPA. For output DTNs shown on left, see Figure 6.3-74[a].

Figure 6.3-75[a]. Data Flow between the Output DTNs Generated by the MSTHM, Showing How the Surrogate Cases Flow into the Five Uncertainty Cases That Were Not Directly Modeled

6.3.16[a] Current MSTHM Results for the TSPA Base Case

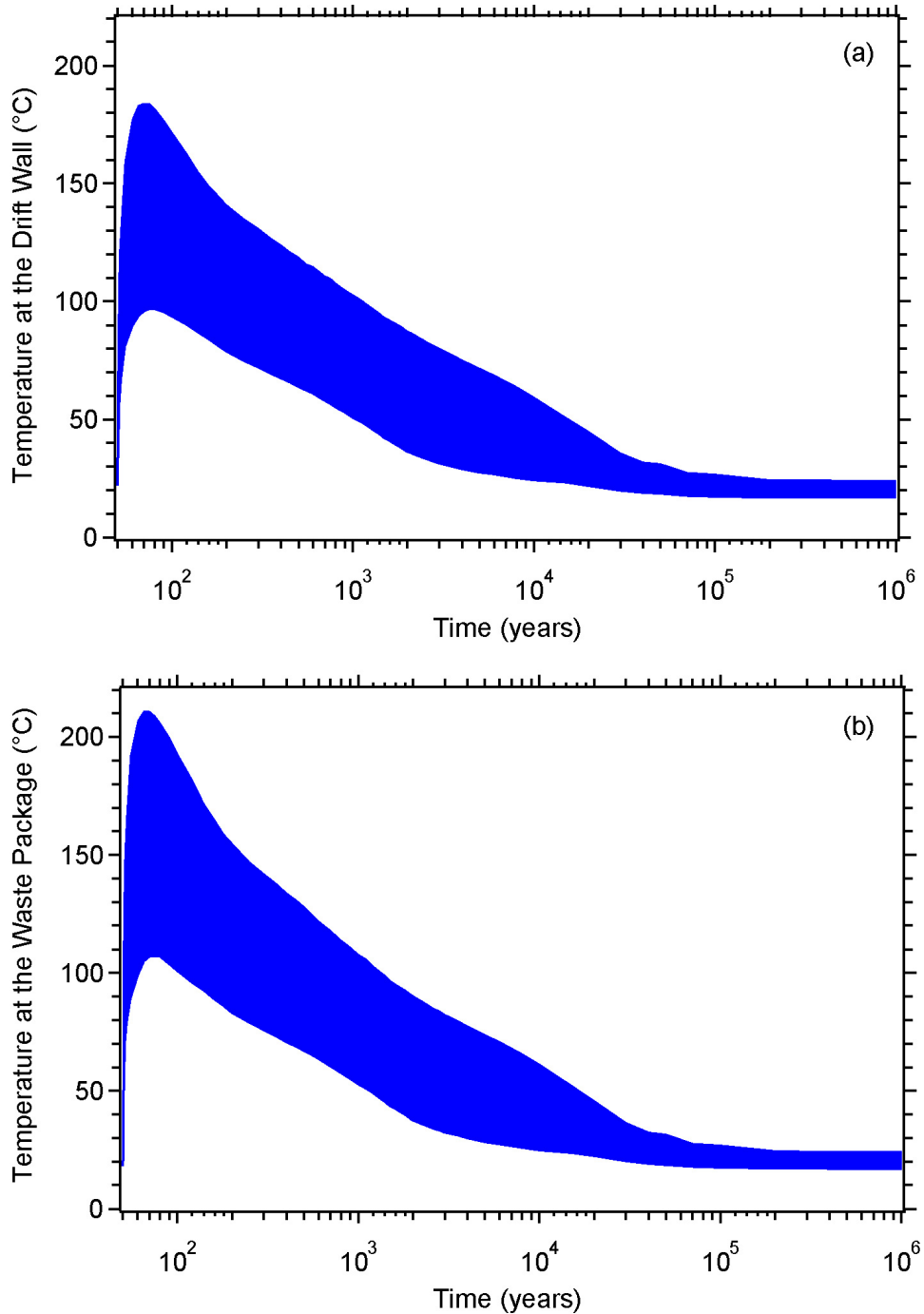
As discussed in Section 6.3.2 of the parent report, the two most significant sources of parametric uncertainty for the output of the MSTHM are host-rock thermal conductivity and percolation flux. Percolation flux uncertainty is addressed with four cases: P10, P30, P50, and P90 (Table 6.3-48[a]). Host-rock thermal conductivity uncertainty is addressed by three cases: low (L), mean (M), and high (H), as shown in Table 6.3-48[a]. Of the twelve possible uncertainty cases, seven are directly modeled with the MSTHM, and five are represented with the use of surrogates, as discussed in Sections 6.2.12.3[a] and 6.3.15[a].

Figure 6.3-76[a] plots the entire range of drift wall and waste package temperature histories arising from parametric uncertainty. Because the seven modeled uncertainty cases include the P10L case (which results in the driest, hottest conditions) and the P90H case (which results in the wettest, coolest conditions), Figure 6.3-76[a] envelopes all possible temperatures arising from parametric uncertainty of the key sources: percolation flux and host-rock thermal conductivity.

Figure 6.3-77[a] gives the CCDF of peak drift wall and waste package temperature for the seven modeled uncertainty cases, as well as for the ensemble of cases. Table 6.3-49[a] summarizes the range of peak temperature conditions for those cases. The ensemble of peak temperatures includes all of the peak temperature values from the seven modeled uncertainty cases and weights them according to the weighting factors listed in Table 6.3-48[a]. Thus, because the weight factors in Table 6.3-48[a] include the weight factors of the unmodeled uncertainty cases, the ensemble is representative of all twelve uncertainty cases. Note that the median peak temperatures of the ensemble are similar to those of the P90 case.

Figure 6.3-78[a] gives the CCDF of the time when boiling ceases on the drift wall and waste package for the seven modeled uncertainty cases. Table 6.3-50[a] summarizes the values from Figure 6.3-78[a]. Note that the median value for the ensemble is between that of the P10H and P90 cases.

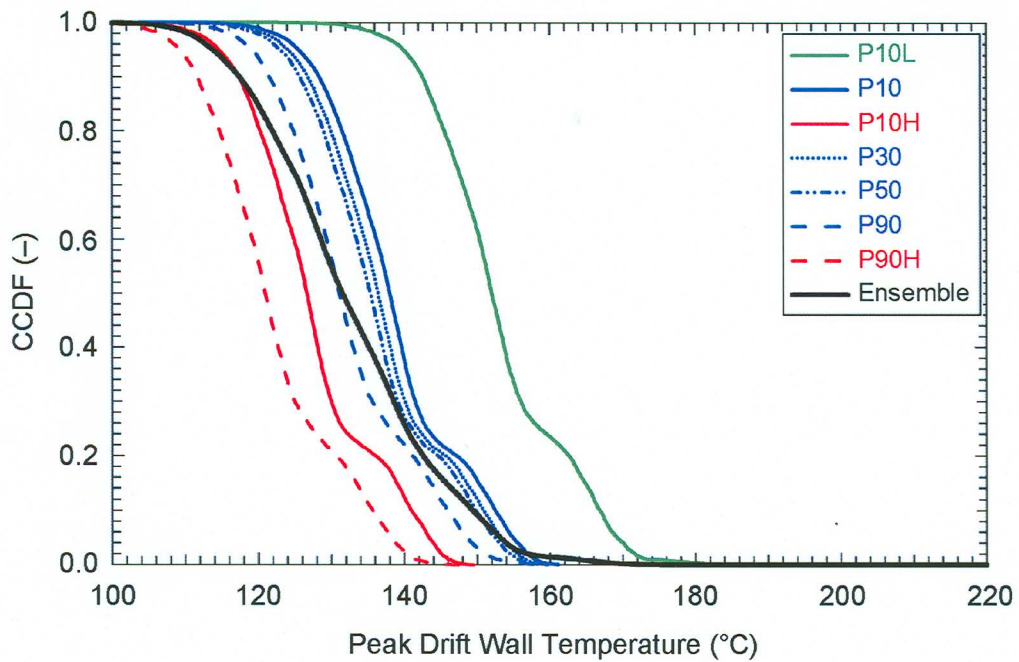
Figure 6.3-79[a] gives the CCDF of the maximum lateral extent of the boiling-point isotherm (96°C) for the seven modeled uncertainty cases. Table 6.3-51[a] summarizes the values from Figure 6.3-79[a]. Note that the median value for the ensemble is between that of the P30 and P50 cases.



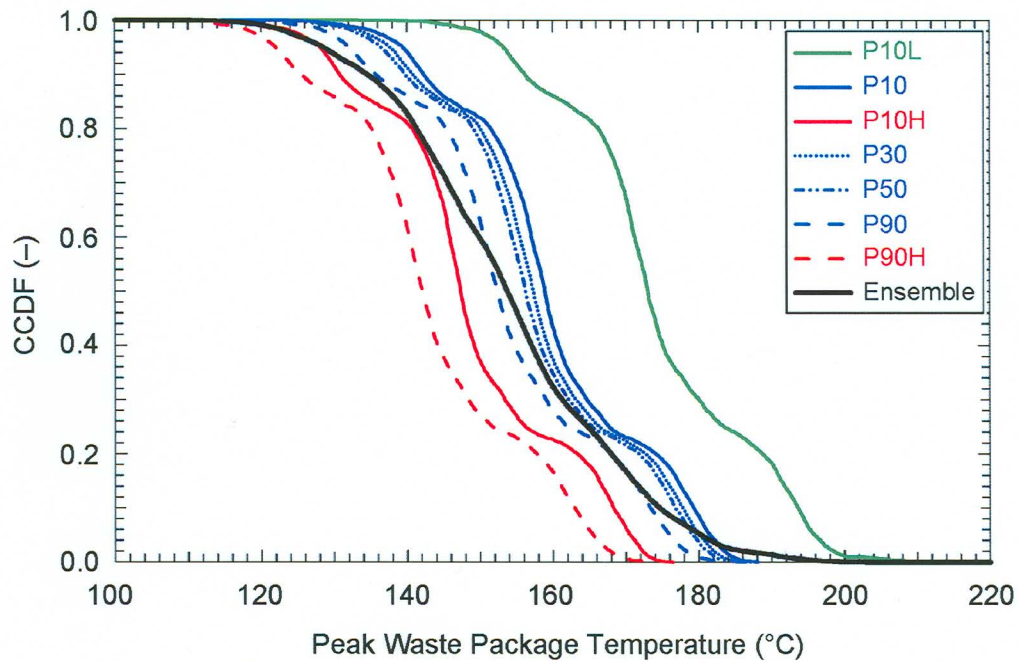
Source: Output DTNs: LL0702PA015MST.070, LL0702PA017MST.072, LL0702PA019MST.074, LL0702PA021MST.076, LL0702PA023MST.078, LL0702PA025MST.080, and LL0702PA029MST.084.

NOTE: The areas shown in blue represent “horsetail plots” of 182,784 temperature histories, which is the product of eight waste package types, 3,264 locations across the repository, and seven uncertainty cases. The minimum and maximum values represent either a minimum or maximum value for all 182,784 histories at any point in time.

Figure 6.3-76[a]. Range in (a) Drift Wall Temperature and (b) Waste Package Temperature for the Range of Parametric Uncertainty Addressed by the MSTHM



EVA
8/29/07

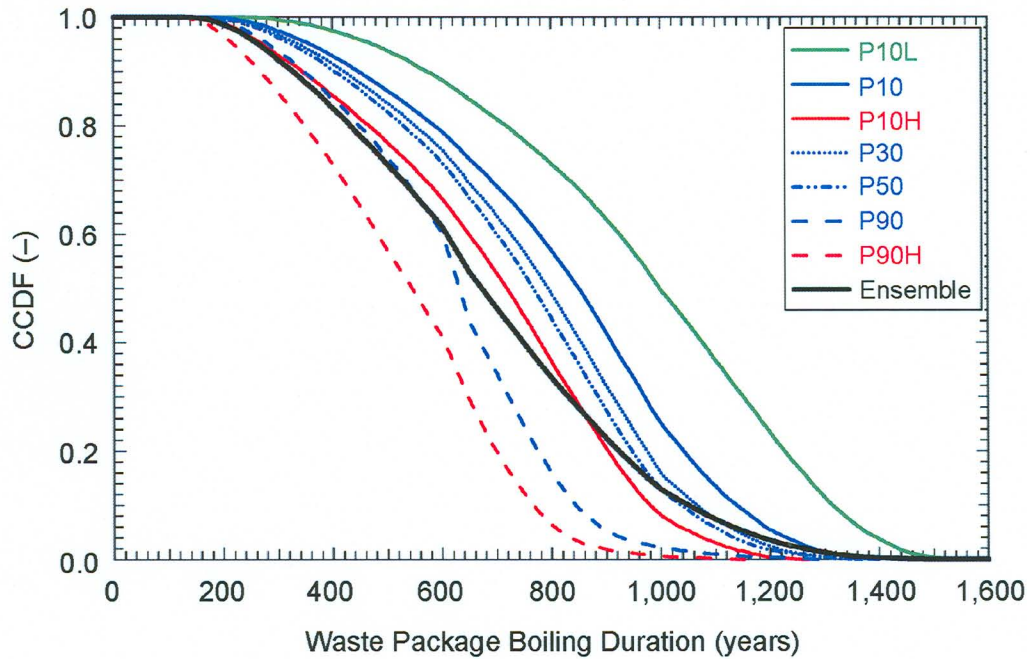
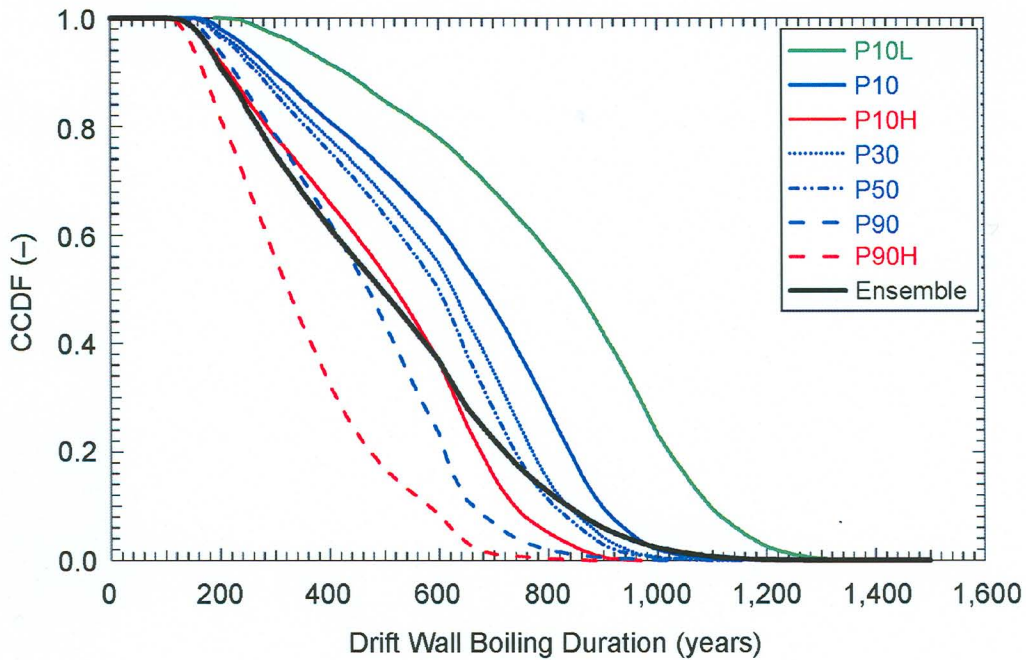


Source: Output DTNs: LL0702PA015MST.070, LL0702PA017MST.072, LL0702PA019MST.074, LL0702PA021MST.076, LL0702PA023MST.078, LL0702PA025MST.080, and LL0702PA029MST.084.

NOTE: Each of the seven CCDF plots represents 26,112 values, which is the product of eight different waste package types at 3,264 locations across the repository. These are the maximum temperature values corresponding to the 182,784 temperature histories in Figure 6.3-76[a]. The ensemble is based on all of the data from the seven cases, weighted using the weights from Table 6.3-48[a].

Figure 6.3-77[a]. CCDF for (a) Peak Drift Wall Temperature and (b) Peak Waste Package Temperature for the Range of Parametric Uncertainty Addressed by the MSTHM

EVA
8/29/07



Source: Output DTNs: LL0702PA015MST.070, LL0702PA017MST.072, LL0702PA019MST.074, LL0702PA021MST.076, LL0702PA023MST.078, LL0702PA025MST.080, and LL0702PA029MST.084.

NOTE: Each of the seven CCDF plots represents 26,112 values, which is the product of eight different waste package types at 3,264 locations across the repository. These are the times when boiling ceases corresponding to the 182,784 temperature histories in Figure 6.3-76[a]. The ensemble is based on all of the data from the seven cases, weighted using the weights from Table 6.3-48[a].

Figure 6.3-78[a]. CCDF for the Time When Boiling Ceases on the (a) Drift Wall and (b) Waste Package for the Range of Parametric Uncertainty Addressed by the MSTHM

Table 6.3-49[a]. Peak Drift Wall and Waste Package Temperatures Summarized for the Seven Modeled Uncertainty Cases

Infiltration Flux, Host-Rock Thermal Conductivity Case	Peak Drift Wall Temperature (°C)			Peak Waste Package Temperature (°C)		
	Coollest	Median	Hottest	Coollest	Median	Hottest
P10L (low K_{th})	120.5	152.0	184.3	131.6	173.0	211.0
P10 (mean K_{th})	111.3	138.0	161.2	122.3	158.9	188.1
P10H (high K_{th})	102.7	126.7	149.5	113.6	147.2	176.5
P30 (mean K_{th})	109.2	136.4	160.5	120.1	157.3	187.3
P50 (mean K_{th})	107.8	135.4	159.6	118.8	156.3	186.4
P90 (mean K_{th})	103.8	131.1	159.6	114.6	152.4	186.4
P90H (high K_{th})	96.9	121.0	147.4	107.5	142.1	174.7
Ensemble ^a	96.9	137.4	184.3	107.5	158.2	211.0

Source: Output DTNs: LL0702PA015MST.070, LL0702PA017MST.072, LL0702PA019MST.074, LL0702PA021MST.076, LL0702PA023MST.078, LL0702PA025MST.080, and LL0702PA029MST.084.

^a The ensemble is based on all of the data from the seven cases, weighted using the weights from Table 6.3-48[a].

NOTE: These cases cover the range of percolation flux and host-rock thermal conductivity uncertainty addressed in this report. This table is based on data plotted in Figure 6.3-76[a].

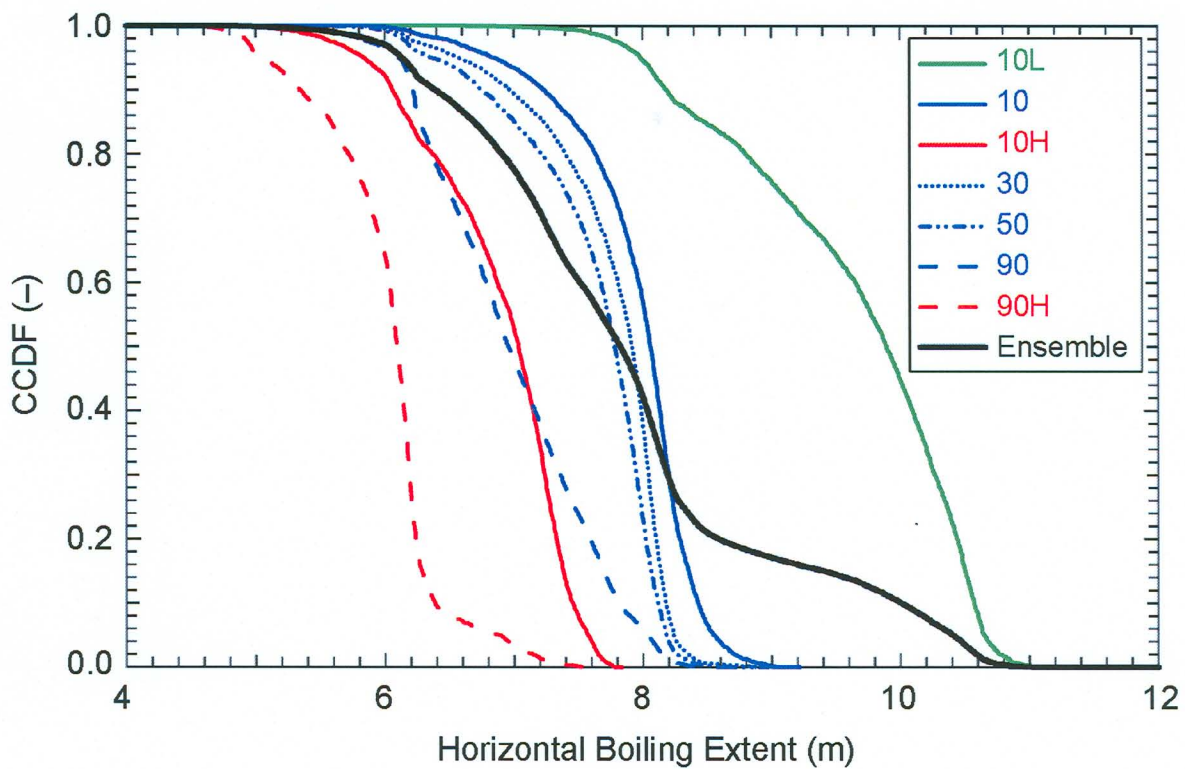
Table 6.3-50[a]. Time When Boiling Ceases at the Drift Wall Summarized for the Seven Modeled Uncertainty Cases

Infiltration Flux, Host-Rock Thermal Conductivity Case	Time When Boiling at the Drift Wall Ceases (years)						
	Shortest	10 Percentile	30 Percentile	Median	70 Percentile	90 Percentile	Longest
P10L (low K_{th})	189.2	428.3	683.3	853.1	966.8	1096.1	1345.1
P10 (mean K_{th})	148.5	298.9	521.6	677.5	789.3	897.7	1153.3
P10H (high K_{th})	115.2	216.9	369.4	520.1	628.6	737.9	968.9
P30 (mean K_{th})	139.0	280.7	476.6	625.6	722.6	835.9	1129.3
P50 (mean K_{th})	134.0	268.1	449.3	599.0	689.0	811.1	1114.4
P90 (mean K_{th})	116.3	227.4	353.3	470.4	564.7	662.2	1030.7
P90H (high K_{th})	87.3	170.4	246.9	324.1	412.7	581.2	900.8
Ensemble ^a	87.3	266.8	459.0	614.8	748.3	937.5	1345.1

Source: Output DTNs: LL0702PA015MST.070, LL0702PA017MST.072, LL0702PA019MST.074, LL0702PA021MST.076, LL0702PA023MST.078, LL0702PA025MST.080, and LL0702PA029MST.084.

^a The ensemble is based on all of the data from the seven cases, weighted using the weights from Table 6.3-48[a].

NOTE: These cases cover the range of percolation flux and host-rock thermal conductivity uncertainty addressed in this report. This table is based on data plotted in Figure 6.3-78a[a].



Source: Output DTNs: LL0702PA015MST.070, LL0702PA017MST.072, LL0702PA019MST.074, LL0702PA021MST.076, LL0702PA023MST.078, LL0702PA025MST.080, and LL0702PA029MST.084.

NOTE: Each of the seven CCDF plots represents 26,112 values, which is the product of eight different waste package types at 3,264 locations across the repository. These are the maximum lateral extents of boiling corresponding to the 182,784 temperature histories in Figure 6.3-76[a]. The ensemble is based on all of the data from the seven cases, weighted using the weights from Table 6.3-48[a].

Figure 6.3-79[a]. CCDF of the Maximum Lateral Extent of the Boiling-Point Isotherm (96°C) from the Drift Centerline for the Range of Parametric Uncertainty Addressed by the MSTHM

Table 6.3-51[a]. Maximum Lateral Extent of the Boiling-Point Isotherm (96 °C) Measured from the Drift Centerline, Summarized for the Seven Modeled Uncertainty Cases

Infiltration-Flux, Host-Rock Thermal Conductivity Case	Maximum Lateral Extent of Boiling ($T > 96^{\circ}\text{C}$) (m)						
	Least	10 Percentile	30 Percentile	Median	70 Percentile	90 Percentile	Greatest
P10L (low K_{th})	6.62	8.19	9.25	9.89	10.27	10.57	11.12
P10 (mean K_{th})	5.86	7.24	7.84	8.06	8.20	8.43	9.21
P10H (high K_{th})	5.00	6.06	6.68	7.03	7.24	7.45	7.83
P30 (mean K_{th})	5.64	6.97	7.65	7.91	8.04	8.18	9.18
P50 (mean K_{th})	5.46	6.75	7.51	7.78	7.95	8.12	8.94
P90 (mean K_{th})	4.97	6.22	6.59	6.95	7.36	7.82	8.66
P90H (high K_{th})	4.38	5.34	5.92	6.09	6.19	6.38	7.69
Ensemble ^a	4.38	6.39	7.23	7.82	8.19	10.01	11.12

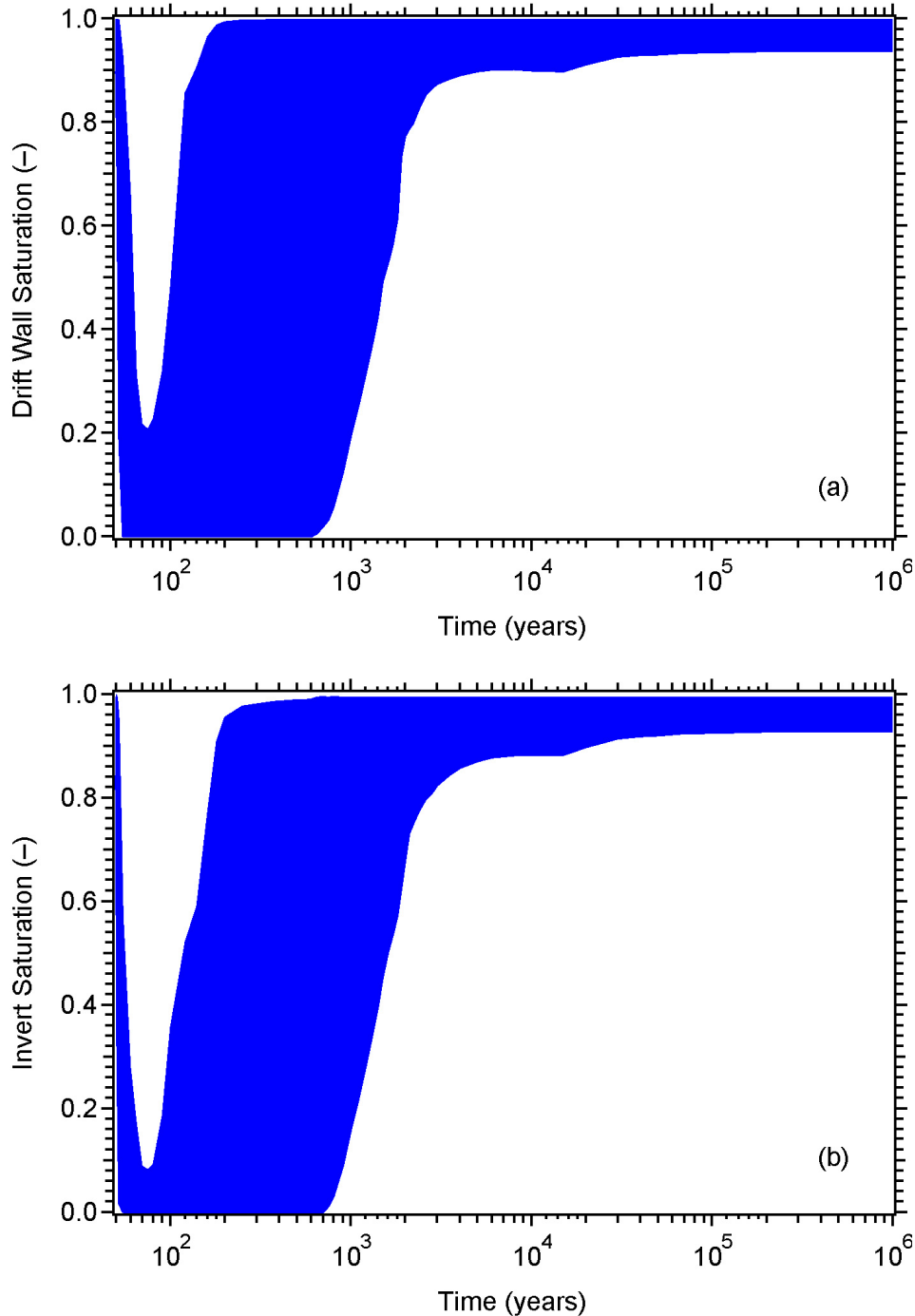
Source: Output DTNs: LL0702PA015MST.070, LL0702PA017MST.072, LL0702PA019MST.074, LL0702PA021MST.076, LL0702PA023MST.078, LL0702PA025MST.080, and LL0702PA029MST.084.

^a The ensemble is based on all of the data from the seven cases, weighted using the weights from Table 6.3-48[a].

NOTE: These cases cover the range of percolation flux and host-rock thermal conductivity uncertainty addressed in this report. This table is based on data plotted in Figure 6.3-79[a].

Figure 6.3-80[a] plots the entire range of drift wall and invert liquid-phase saturation histories arising from parametric uncertainty. Because the seven modeled uncertainty cases include the P10L case (which results in the driest, hottest conditions) and the P90H case (which results in the wettest, coolest conditions), Figure 6.3-80[a] envelopes all possible drift wall and invert liquid-phase saturation values arising from parametric uncertainty of the key sources: percolation flux and host-rock thermal conductivity.

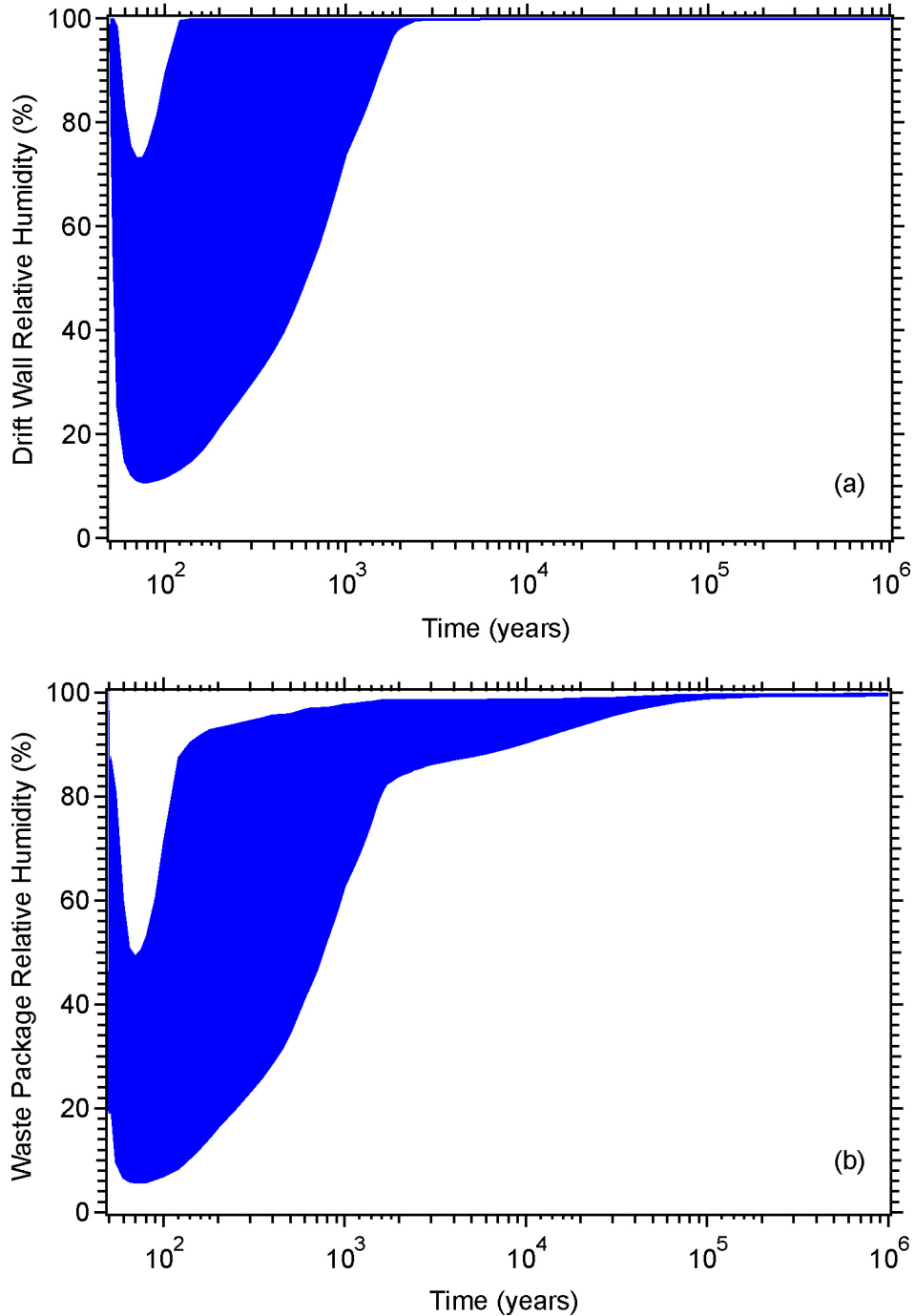
Figure 6.3-81[a] plots the entire range of drift wall and waste package relative-humidity histories arising from parametric uncertainty. Because the seven modeled uncertainty cases include the P10L case (which results in the driest, hottest conditions) and the P90H case (which results in the wettest, coolest conditions), Figure 6.3-81[a] envelopes all possible drift wall and waste package relative-humidity values arising from parametric uncertainty of the key sources: percolation flux and host-rock thermal conductivity.



Source: Output DTNs: LL0702PA015MST.070, LL0702PA017MST.072, LL0702PA019MST.074, LL0702PA021MST.076, LL0702PA023MST.078, LL0702PA025MST.080, and LL0702PA029MST.084.

NOTE: The areas shown in blue represent "horsetail plots" of 182,784 liquid-phase saturation histories, which is the product of eight waste package types, 3,264 locations across the repository, and seven uncertainty cases. The minimum and maximum values represent either a minimum or maximum value for all 182,784 histories at any point in time. The liquid-phase saturation pertains to the matrix continuum in the host rock at the drift wall and in the intragranular porosity of the crushed tuff in the invert.

Figure 6.3-80[a]. Range in (a) Drift Wall and (b) Invert Liquid-Phase Saturation for the Range of Parametric Uncertainty Addressed by the MSTHM



Source: Output DTNs: LL0702PA015MST.070, LL0702PA017MST.072, LL0702PA019MST.074, LL0702PA021MST.076, LL0702PA023MST.078, LL0702PA025MST.080, and LL0702PA029MST.084.

NOTE: The areas shown in blue represent “horsetail plots” of 182,784 relative-humidity histories, which is the product of eight waste package types, 3,264 locations across the repository, and seven uncertainty cases. The minimum and maximum values represent either a minimum or maximum value for all 182,784 histories at any point in time.

Figure 6.3-81[a]. Range in (a) Drift Wall and (b) Waste Package Relative Humidity for the Range of Parametric Uncertainty Addressed by the MSTHM

6.3.17[a] Current MSTHM Results for the Low-Probability-Seismic Collapsed-Drift Case

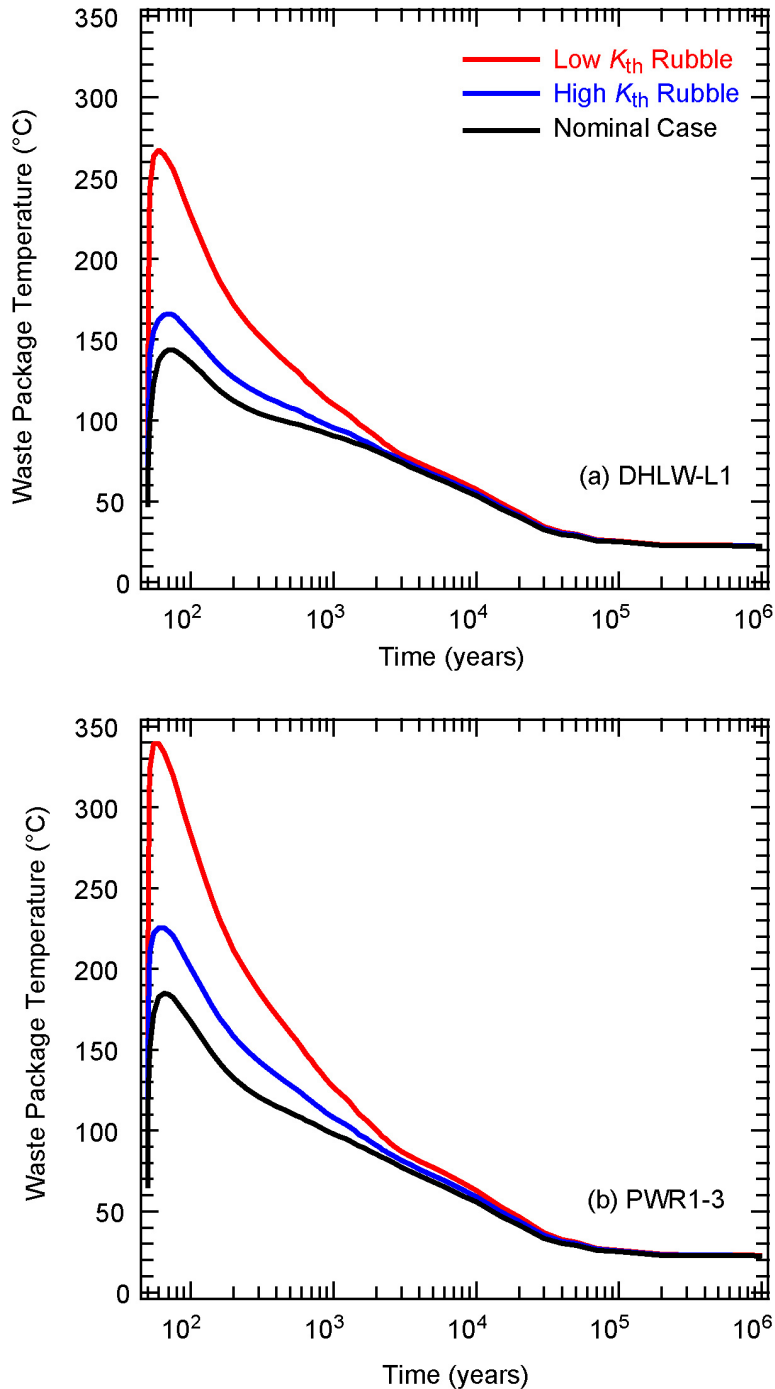
The low-probability-seismic collapsed-drift case is considered for the P10 percolation flux case at the g_9 location (see Figure 6.2-17[a]), which is a typical location at the center of the repository. The P10 percolation flux case at this location is representative of a typical location in the center of the repository for the following reasons. It is within the predominant host-rock unit, which is the Tptpl (tsw35) unit, close to the center of the repository area. Moreover, the local P10 percolation flux values, which are 3.6, 6.8, 13.6, and 17.8 mm/yr for the present-day, monsoonal, glacial-transition, and post-10,000-year climates, respectively, are close to the repository-wide averages (4.1, 7.8, 12.2, and 15.9 mm/yr) for the P10 percolation flux case (see Table 6.2-5[a]).

Sections 6.2.9, 6.2.10, and 6.2.11 of the parent report describe the changes to the MSTHM submodels that are required to model the influence of drift collapse. Although a full MSTHM calculation involves submodels located at 560 locations spread across the entire repository, it is only necessary to conduct an MSTHM calculation at a single repository location for the purpose of analyzing the influence of drift collapse on in-drift thermal-hydrologic conditions. The reasoning for this is that the purpose of this section is to generate tables of “deltas,” which are the differences between the thermal-hydrologic results for the case with drift collapse and those for the intact (nominal) case with no drift collapse. The differences between the collapsed-drift case and the corresponding intact-drift case depend primarily on the thermal conductivity of the rubble and are relatively insensitive to the host-rock properties and local percolation flux. The rationale for this approach is described in greater detail in Section 6.3.7.1 of the parent report. Because of this lack of sensitivity to conditions outside of the drift, these calculated differences (or deltas) can then be applied to the MSTHM results of the seven nominal cases with no drift collapse, described in Section 6.3-16[a].

The differences (deltas) are determined for the eight different waste packages addressed by the MSTHM. The deltas are calculated by subtracting nominal (uncollapsed) temperature histories from (collapsed) histories such as those shown in Figure 6.3-82[a]. These time-dependent delta histories can be applied at any point during a TSPA simulation when drift collapse occurs, and for all simulation time thereafter. This is a close approximation to the thermal effect of drift collapse because: (1) the collapse rubble forms from rock that has already been heated, and (2) near-field temperatures will actually respond relatively quickly (compared with TSPA time-stepping intervals) when drift collapse occurs. The low-probability-seismic scenario causes severe shaking that fails the host rock (breaking it into blocks of rubble) out to a diameter of 11 m. This scenario is shown in *Drift Degradation Analysis* (BSC 2004 [DIRS 166107], Figure 139f). The result of this is a host-rock rubble zone that extends from the outer surface of the drip shield out to the “modified” drift wall, which is the interface between host rock rubble and intact host rock. A schematic of this case is given in Figure 6.4-16 of *Abstraction of Drift Seepage* (SNL 2007 [DIRS 181244]). The key uncertainty influencing in-drift thermal-hydrologic conditions is the effective thermal conductivity K_{th} of the host-rock rubble (Section 6.2.13.5[a] and Appendix XI[a]). Two K_{th} cases are considered to address this uncertainty: (1) high- K_{th} case and (2) low- K_{th} case. On the basis of the discussion in Section 6.2.10.3 of the parent report, the high- and low- K_{th} cases are assigned the same probability (of 50%).

Figures 6.3-82[a], 6.3-83[a], and 6.3-84[a] show the influence of drift collapse, out to a diameter of 11 m, on in-drift thermal-hydrologic conditions for the coolest and hottest waste packages, which are the dhlw-11 and pwr1-3 waste packages listed in Table 6.2-6[a], respectively. Figure 6.3-82[a] shows the range in drip shield and waste package temperature increase caused by drift collapse, compared to the nominal (intact drift) case. Figure 6.3-83[a] shows the range in drip shield and waste package relative humidity reduction caused by drift collapse, compared to the nominal case. Figure 6.3-84[a] shows the range in ~~drip shield and~~ invert liquid-phase saturation reduction caused by drift collapse, compared to the nominal case. *ELW 8/29/07*

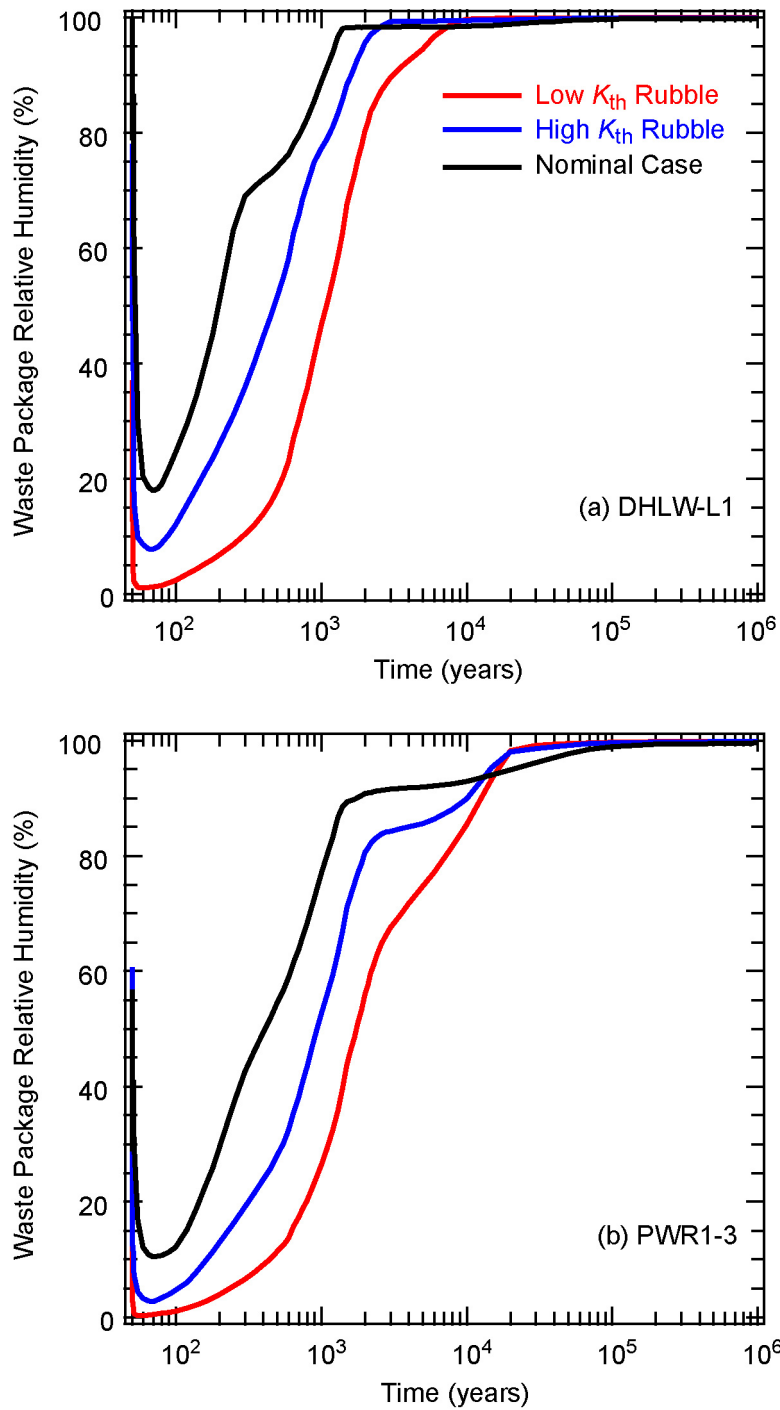
Figures 6.3-85[a] and 6.3-86[a] show the time-varying waste packages temperatures for DHLW and CSNF, respectively. Various percentiles illustrate the range of temperatures of the packages within a collapsed drift including the 1st, 5th, 10th, 50th, 90th, 95th, and 99th percentiles. Figure 6.3-87[a] illustrates the peak waste package temperature CCDFs for all DHLW and CSNF waste packages subject to high and low rubble K_{th} .



Source: Output DTN: LL0702PA027MST.082.

NOTE: These calculations pertain to the g_9 location (see Figure 6.2.17[a]), close to the repository center. The dhlw-l1 and pwr1-3 waste packages are the coolest and hottest waste packages of the eight different waste packages represented by the MSTHM.

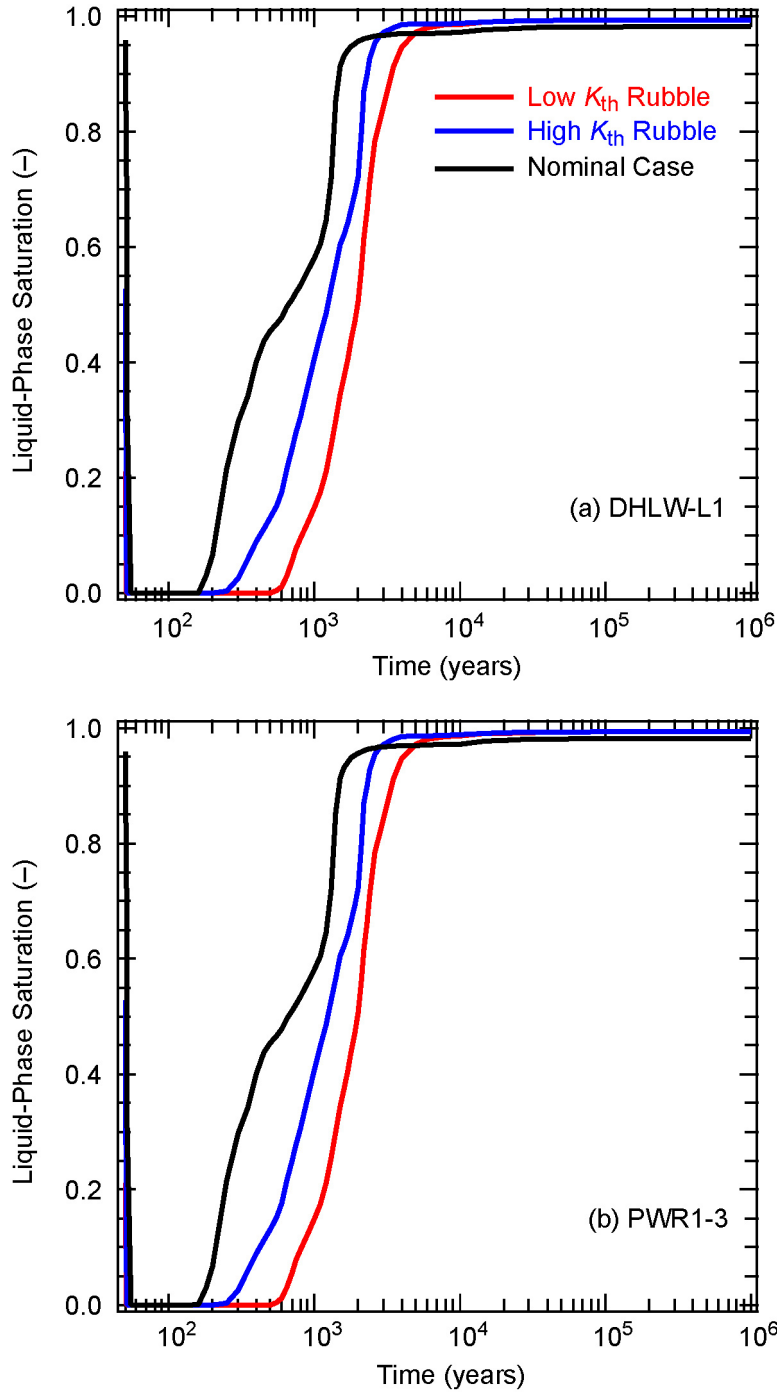
Figure 6.3-82[a]. Waste Package Temperature History for the (a) DHLW/DOE SNF-Long (dhlw-l1) Waste Package and the (b) 21-PWR AP CSNF (pwr1-3) Waste Package for the Nominal (Intact Drift) Case and Low and High Rubble Thermal Conductivity Collapsed-Drift Cases



Source: Output DTN: LL0702PA027MST.082.

NOTE: These calculations pertain to the g_9 location (see Figure 6.2.17[a]), close to the repository center. The dhlw-l1 and pwr1-3 waste packages are the coolest and hottest waste packages of the eight different waste packages represented by the MSTHM.

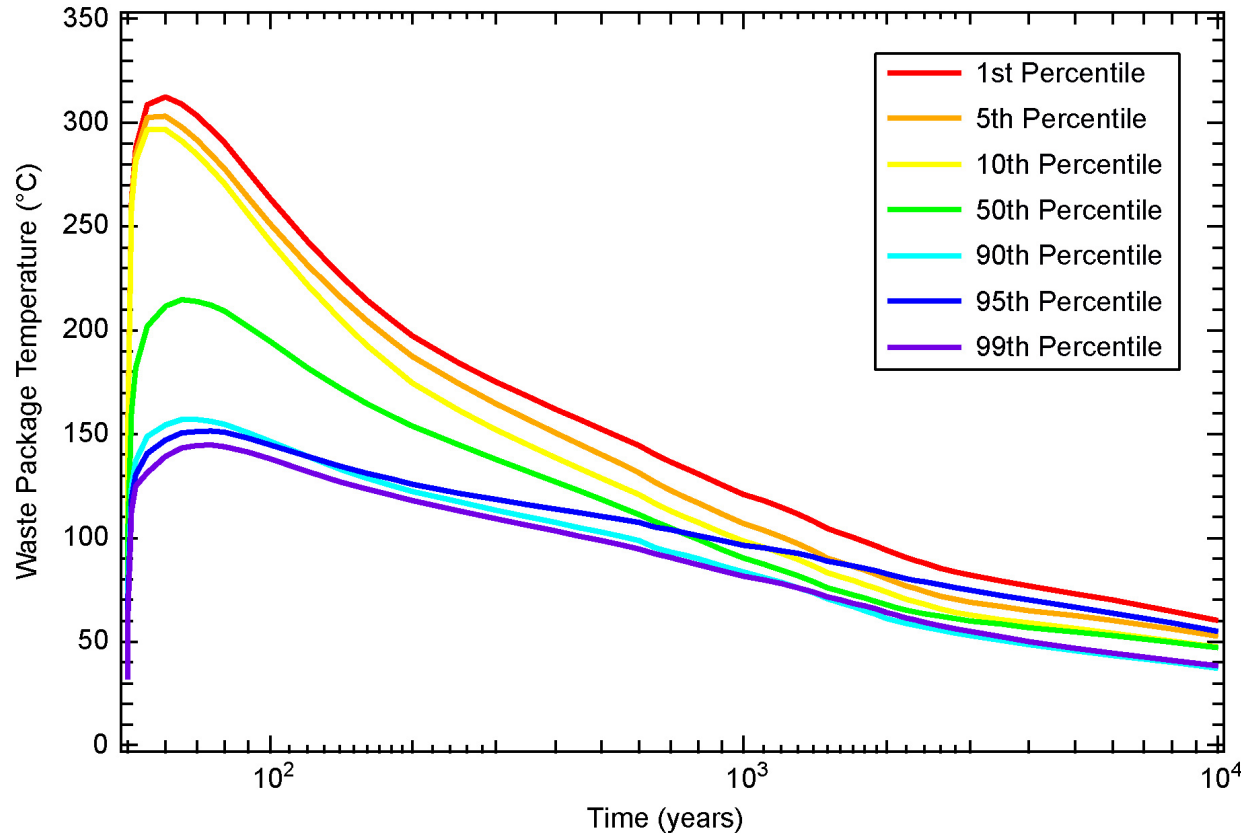
Figure 6.3-83[a]. Waste Package Relative Humidity History for the (a) DHLW/DOE SNF-Long (dhlw-l1) Waste Package and the (b) 21-PWR AP CSNF (pwr1-3) Waste Package for the Nominal (Intact Drift) Case and Low and High Rubble Thermal Conductivity Collapsed-Drift Cases



Source: Output DTN: LL0702PA027MST.082.

NOTE: These calculations pertain to the g_9 location (see Figure 6.2-17[a]), close to the repository center. The dhlw-l1 and pwr1-3 waste packages are the coolest and hottest waste packages of the eight different waste packages represented by the MSTHM.

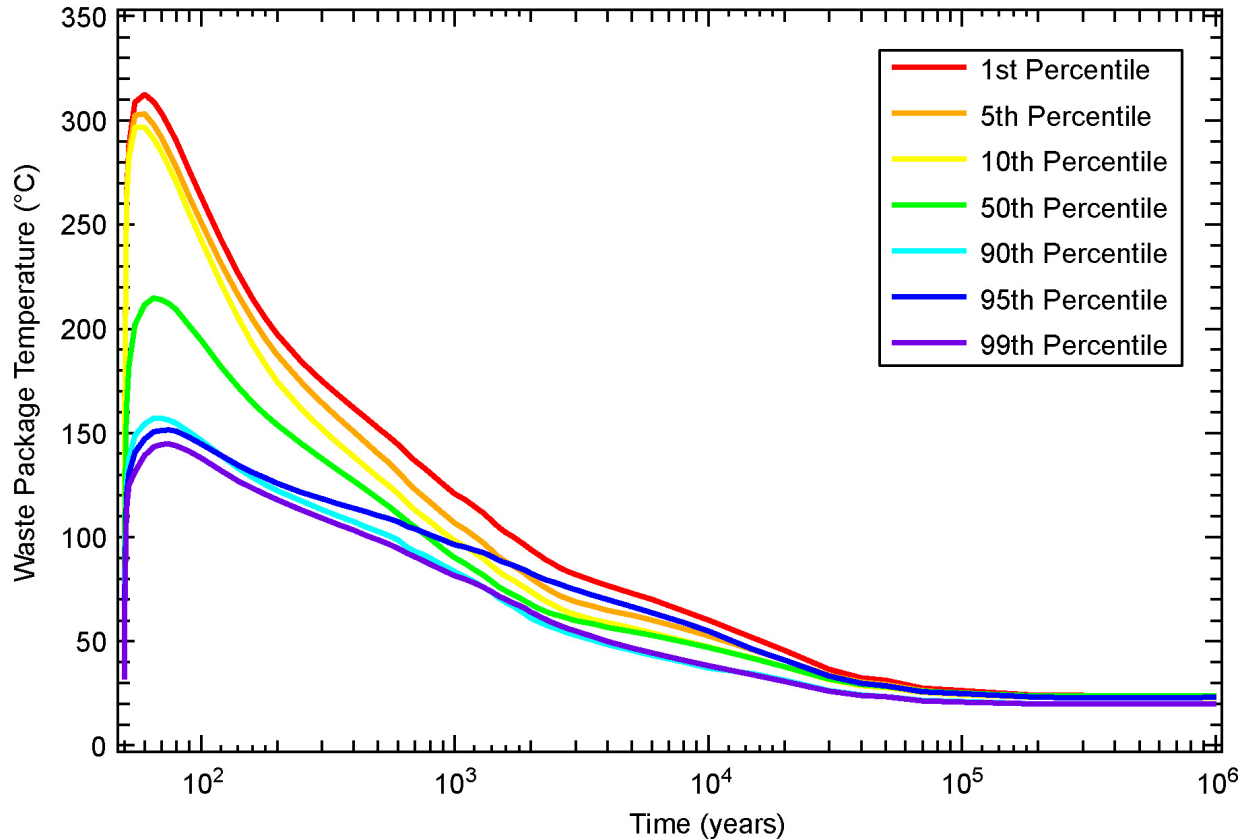
Figure 6.3-84[a]. Invert Liquid-Phase Saturation History for the Intragranular Porosity for the (a) DHLW/DOE SNF-Long (dhlw-l1) Waste Package and the (b) 21-PWR AP CSNF (pwr1-3) Waste Package for the Nominal (Intact Drift) Case and Low and High Rubble Thermal Conductivity Collapsed-Drift Cases



Source: Output DTNs: LL0702PA015MST.070, LL0702PA017MST.072, LL0702PA019MST.074, LL0702PA021MST.076, LL0702PA023MST.078, LL0702PA025MST.080, LL0702PA029MST.084, and LL0702PA027MST.082. The seven waste package temperature history files are in DTN: MO0707TH2D3DDC.000 [DIRS 182472].

NOTE: The "deltas" for DHLW waste package temperature for the low and high rubble thermal conductivity cases from DTN: LL0702PA027MST.082 are added to the DHLW waste package temperatures from DTNs: LL0702PA015MST.070, LL0702PA017MST.072, LL0702PA019MST.074, LL0702PA021MST.076, LL0702PA023MST.078, LL0702PA025MST.080, and LL0702PA029MST.084, resulting in 91,392 DHLW waste package temperature histories, which are then ranked according to peak DHLW waste package temperature. The 1st, 5th, 10th, 50th, 90th, 95th, and 99th percentile DHLW waste package temperature histories are selected and plotted.

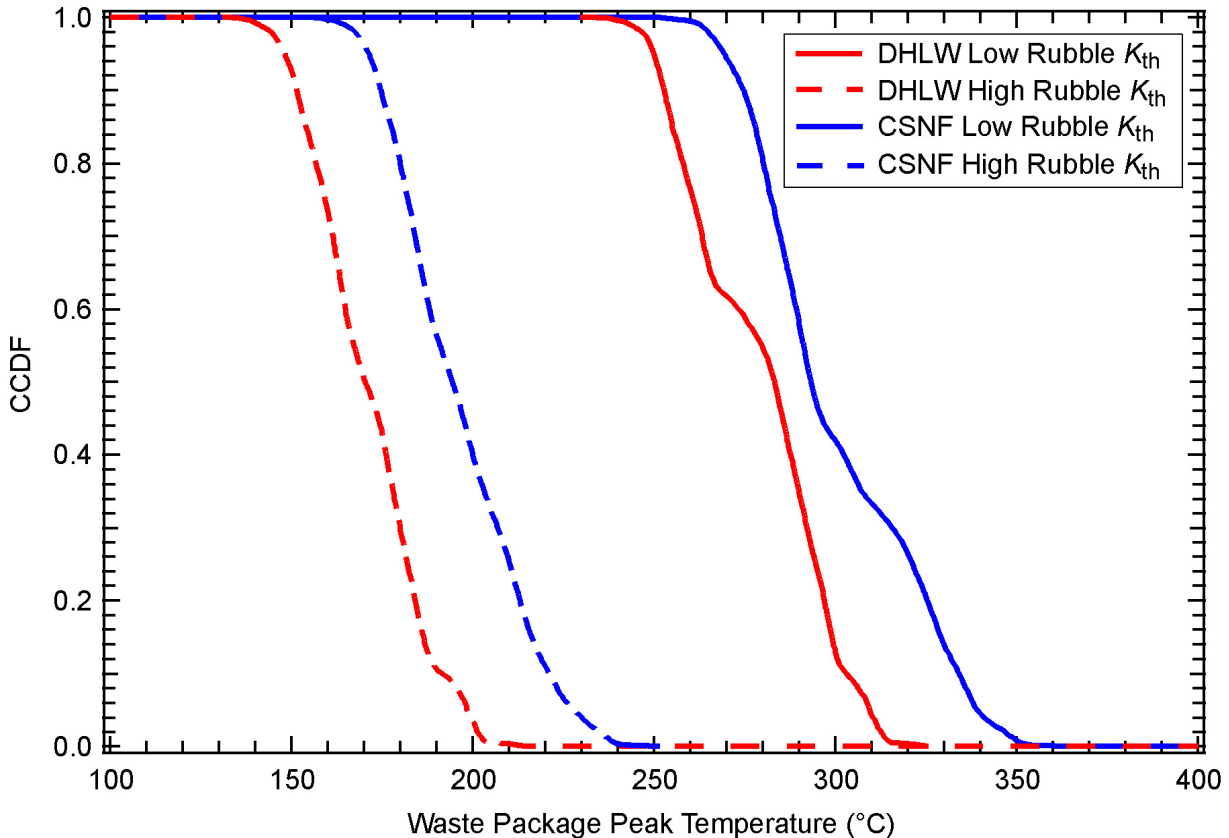
Figure 6.3-85[a]. Waste Package Temperature Histories and Corresponding Percentiles Showing Ranges for the DHLW/DOE SNF-Long (dhlw-l1) Waste Packages for the Collapsed-Drift Case



Source: Output DTNs: LL0702PA015MST.070, LL0702PA017MST.072, LL0702PA019MST.074, LL0702PA021MST.076, LL0702PA023MST.078, LL0702PA025MST.080, LL0702PA029MST.084, and LL0702PA027MST.082. The seven waste package temperature history files are in DTN: MO0707TH2D3DDC.000 [DIRS 182472].

NOTE: The “deltas” for CSNF waste package temperature for the low and high rubble thermal conductivity cases from DTN: LL0702PA027MST.082 are added to the CSNF waste package temperatures from DTNs: LL0702PA015MST.070, LL0702PA017MST.072, LL0702PA019MST.074, LL0702PA021MST.076, LL0702PA023MST.078, LL0702PA025MST.080, and LL0702PA029MST.084, resulting in 274,176 CSNF waste package temperature histories, which are then ranked according to peak CSNF waste package temperature. The 1st, 5th, 10th, 50th, 90th, 95th, and 99th percentile CSNF waste package temperature histories are selected and plotted.

Figure 6.3-86[a]. Waste Package Temperature Histories and Corresponding Percentiles Showing Ranges for the 21-PWR AP CSNF (pwr1-3) Waste Packages for the Collapsed-Drift Case



Source: Output DTNs: LL0702PA015MST.070, LL0702PA017MST.072, LL0702PA019MST.074, LL0702PA021MST.076, LL0702PA023MST.078, LL0702PA025MST.080, LL0702PA029MST.084, and LL0702PA027MST.082. The four CCDF files are in DTN: MO0707TH2D3DDC.000 [DIRS 182472].

NOTE: The peak waste package temperatures for the DHLW waste packages correspond to the 91,392 DHLW waste package temperature histories used to select the DHLW waste package temperature histories plotted in Figure 6.3-85[a]. The peak waste package temperatures for the CSNF waste packages correspond to the 274,176 CSNF waste package temperature histories used to select the CSNF waste package temperature histories plotted in Figure 6.3-86[a]. The weights used in CCDF calculations are: P10 (0.2768), P10L (0.2250), P10H (0.2105), P30 (0.0753), P50 (0.0609), P90 (0.1312), and P90H (0.0203).

Figure 6.3-87[a]. CCDFs for Peak Waste Package Temperatures for CSNF and DHLW Waste Packages for Collapsed-Drift Cases Subject to Low and High Rubble K_{th}

6.3.18[a] Analysis of In-Drift Vapor Flow and Condensation Using the Three-Dimensional Pillar-Scale Thermal-Hydrologic Model

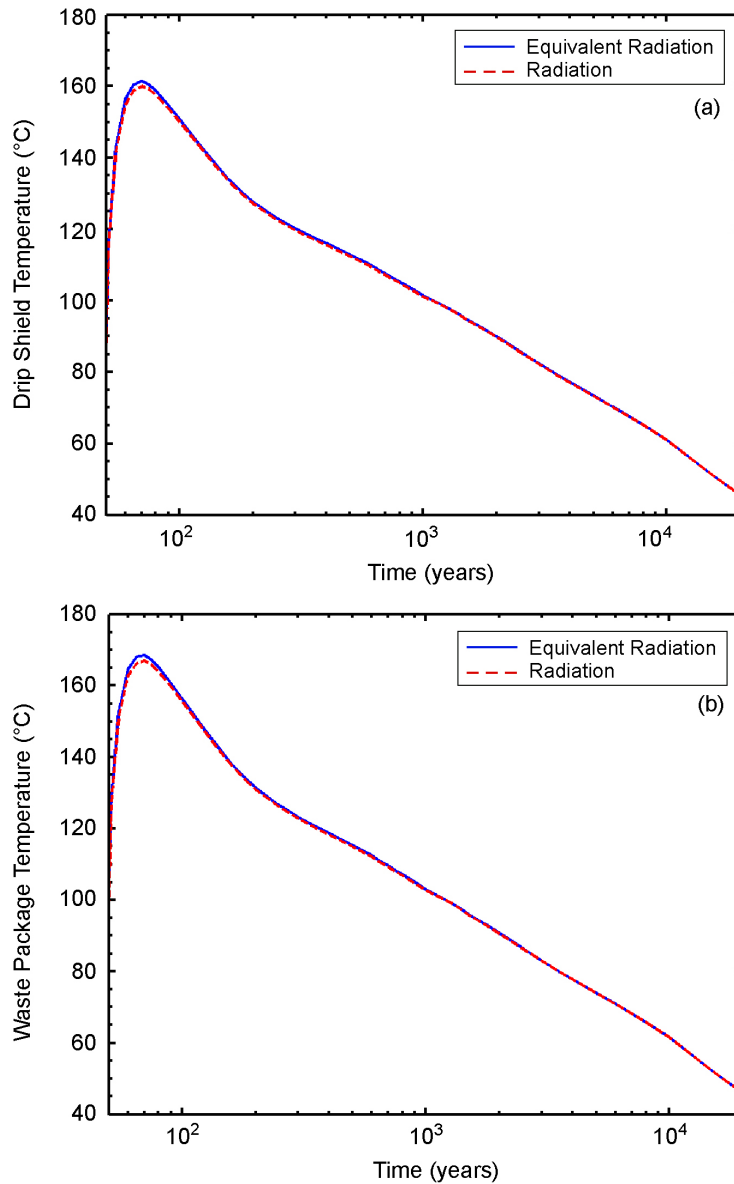
As discussed in Section 5.7 of the parent report, the MSTHM does not represent longitudinal vapor flow, and the resulting condensation, along the emplacement drift. It is demonstrated in Section 7.8[a] that the assumption that in-drift longitudinal vapor flow has an insignificant influence on the MSTHM output parameters provided to TSPA. The 3-D pillar-scale TH model, which represents a full-scale emplacement drift (Section 7.8[a]), includes the influence of vapor flow and condensation along the drift. The 3-D pillar-scale TH model uses the same qualified data sources and design information, such as waste package dimensions, discussed in Section 4.1[a] and listed in Table 4-1[a]. Thus, all inputs implemented in the MSTHM calculations that support the TSPA are also applied to the 3-D pillar-scale TH model. Moreover,

in a model confidence-building exercise discussed in Section 7.8[a], differences in TH parameters predicted by the 3-D pillar-scale TH model and the MSTHM are shown to be insignificant. Therefore, the 3-D pillar-scale TH model generates TH output parameters that are qualified for use by TSPA.

In addition to model validation (Section 7.8[a]), the 3-D pillar scale TH model also provides information for use by the condensation model (SNL 2007 [DIRS 181648], Section 6.2[a]), to bound the occurrence and rate of drift wall condensation during Stage 2 (when some waste package locations are still at temperatures above boiling). The needed output parameters are vapor flow and condensation along the emplacement drift (see Output DTN: LL0705PA032MST.028). Data from that output DTN are generated for a wide range of percolation flux, including the P10 and P90 percolation flux cases (Section 6.2.16[a]). These calculations were conducted for the P10 and P90 cases for a typical location in the repository, which is the g₉ UZ flow model grid column location (Figure 6.2-17[a]). The local P10 percolation flux values for the g₉ location are 3.6, 6.8, 13.6, and 17.8 mm/yr for the present-day, monsoonal, glacial-transition, and post-10,000-year climates, respectively (Output DTN: LL0702PA014MST.069). The local P90 percolation flux values for the g₉ location are 26.8, 75.4, 59.3, and 44.6 mm/yr for the present-day, monsoonal, glacial-transition, and post-10,000-year climates, respectively (Output DTN: LL0702PA018MST.075). To bound the uncertainty in the influence of turbulent natural-convective mixing of water vapor and air in the drift, the 3-D pillar-scale TH model calculations were conducted for a range of gas-phase dispersion coefficient factors: 200, 1,000, 2,000, and 10,000 in the emplacement drift. For the P10 case, a dispersion-coefficient factor of 100,000 was also considered. Note that a dispersion-coefficient factor of 1,000 was used in the model confidence-building test case (Section 7.8[a]). The gas-phase dispersion coefficient factor is a multiplier applied to the nominal binary gas-phase diffusion coefficient for an open system, which is determined by the NUFT code as a function of temperature.

As discussed in Section 7.8[a], the 3-D pillar-scale TH model represents in-drift heat transfer by radiation and natural convection using a calibrated “equivalent” thermal conductivity versus time relationship. A special LDTH model, which discretely represents the drip shield and waste package, is used for this purpose. Because this model has the same cross-sectional geometry as the 3-D DDT submodel (see Section 6.2.17[a]), and produces “target” results, it is called the “target” 2-D DDTH model. The target model represents thermal radiation between the drip shield and drift wall and between the waste package and drip shield, and uses the effective thermal conductivity for air, representing the influence of natural convection, on the basis of correlations from the FLUENT code thermal model in *In-Drift Natural Convection and Condensation* (SNL 2007 [DIRS 181648], Appendix J). The corresponding 2-D DDTH model with the calibrated effective (equivalent) thermal conductivity is called the “calibration” model. Figure 6.3-88[a] compares temperature histories, both on the drip shield and waste package, predicted by the target and calibration models. The agreement in temperature histories demonstrates the effective (equivalent) thermal conductivity to be a good approximation of in-drift thermal radiation and convection, which is used in the 3-D pillar-scale TH models (Sections 6.3.18[a]) and 7.8 [a]). Details of the target and calibration models are in Output DTN: LL0705PA032MST.028.

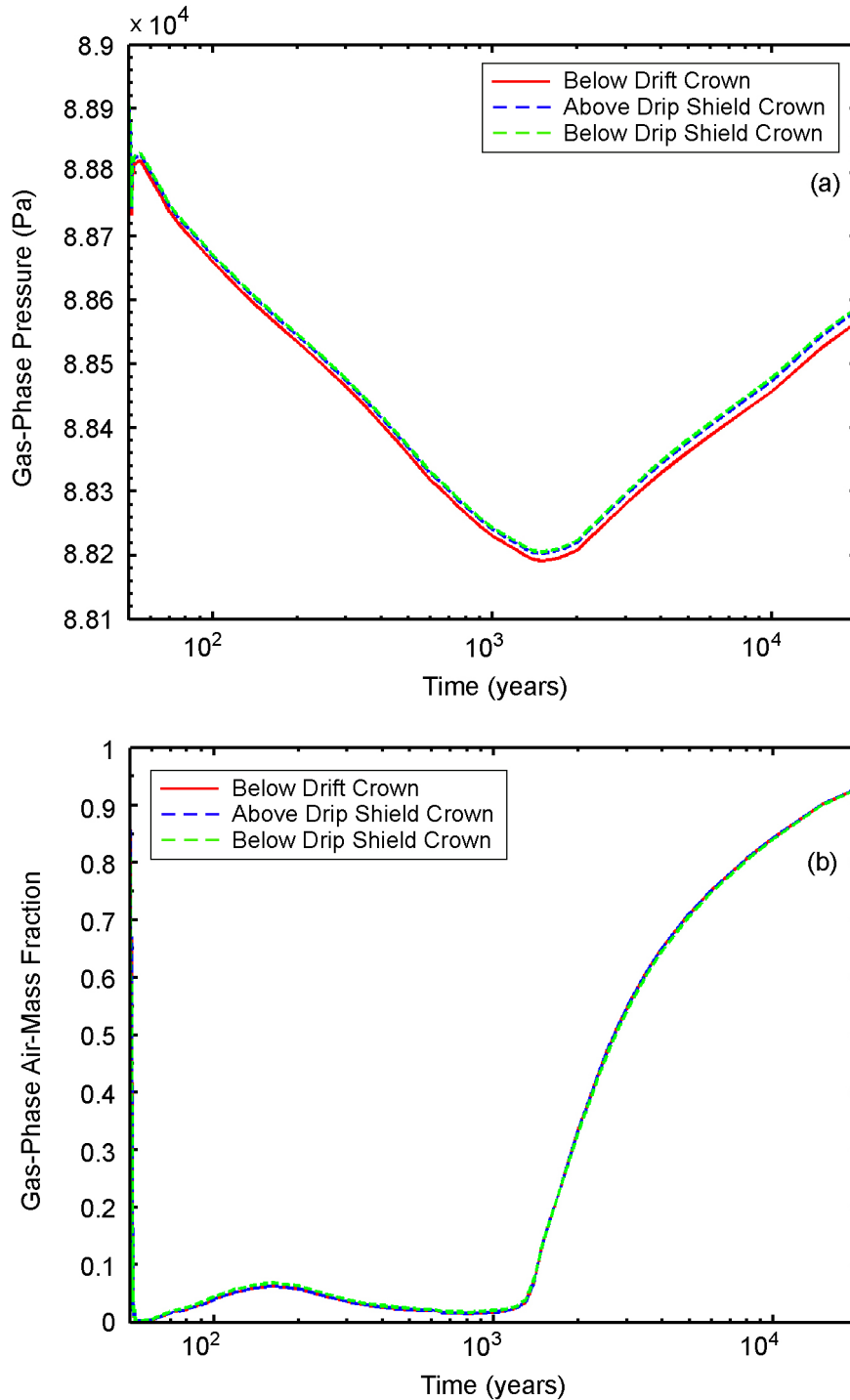
Figure 6.3-89[a] plots gas-phase pressure, P_g , and air-mass fraction, X_{air} , histories at three locations in the drift: (1) beneath the drift crown, (2) above the drip shield crown, and (3) beneath the drip shield crown. Because P_g and X_{air} control partial pressure of water vapor, P_v , (or absolute humidity), this demonstrates that absolute humidity is well mixed within the drift, both outside and inside the drip shield.



Source: Output DTN: LL0705PA032MST.028.

NOTE: These 2-D DDTH-model calculations pertain to the g_9 location (see Figure 6.2-17[a]), close to the repository center. The 2-D DDTH submodel is different from the standard LDTH submodel in that it discretely represents the drip shield and waste package, while the standard LDTH submodel does not. These two cases differ in that one represents in-drift thermal radiation explicitly, while the other uses a calibrated (equivalent) in-drift thermal conductivity to represent in-drift thermal radiation.

Figure 6.3-88[a]. Temperature on the Drip Shield (a) and Waste Package (b) at the Repository Center for Different Representations of In-Drift Thermal Radiation



Source: Output DTN: LL0705PA032MST.028.

NOTE: These 2-D DDTH-model calculations pertain to the g_9 location (see Figure 6.2-17[a]), close to the repository center. The 2-D DDTH submodel is different from the standard LDTH submodel in that it discretely represents the drip shield and waste package, while the standard LDTH submodel does not. This model uses the calibrated “equivalent” in-drift thermal-conductivity relationship to represent thermal radiation.

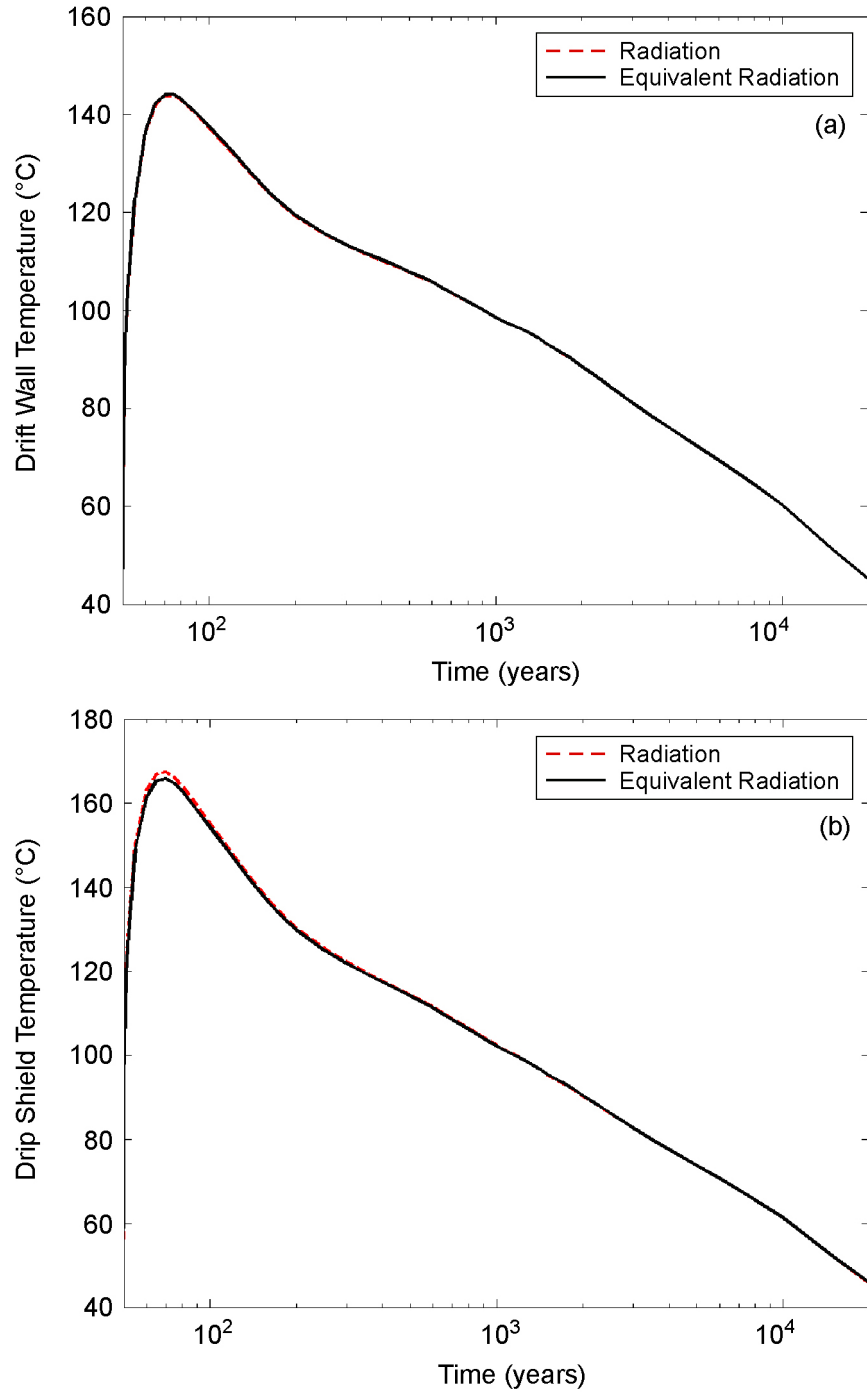
Figure 6.3-89[a]. Gas-Phase Pressure (a) and Air Mass Fraction (b) beneath the Drift Crown, above the Drip Shield Crown, and below the Drip Shield Crown at the Repository Center

The foregoing discussion pertains to axial vapor transport effects on thermal hydrology in uncollapsed drifts. The effects of vapor transport in collapsed drifts are discussed in *Features, Events, and Processes for the Total System Performance Assessment* (SNL 2007 [DIRS 179476], FEP 1.2.03.02.0D).

6.3.19[a] Influence of Invert Depth on Thermal-Hydrologic Conditions

The MSTHM calculations supporting TSPA use a value for invert depth (i.e., height from bottom of the drift) of 0.806 m, while *Total System Performance Assessment Data Input Package for Requirements Analysis for EBS In-Drift Configuration* (SNL 2007 [DIRS 179354]) gives a value of 4 ft 4 in. (1.32 m). The purpose of this section is to conduct a sensitivity analysis of the influence of invert depth on predicted in-drift TH conditions with the use of the LDTH submodel (Section 6.2.16). The sensitivity study is conducted for the P10 percolation flux/host-rock thermal conductivity case at the g_9 location (Figure 6.2-17[a]), which is close to the repository center. This is the same case and location used in other sensitivity analyses (see Sections 6.3.14 and 6.3.17) in this report. To conduct the sensitivity analysis, an effective in-drift thermal conductivity was used to represent the influence of in-drift thermal radiation. Note that this is the same effective in-drift thermal conductivity used in the 3-D pillar-scale TH model (Sections 6.3.18[a] and 7.8[a]). Figures 6.3-90[a] through 6.3-93[a], which compare TH conditions calculated with an LDTH submodel with explicitly represented in-drift thermal radiation with those calculated with the LDTH submodel using the effective in-drift thermal conductivity, clearly demonstrate that the use of the effective in-drift thermal conductivity results in almost identical in-drift TH conditions. Differences between these two cases are insignificant compared to the range of TH conditions arising from parametric uncertainty.

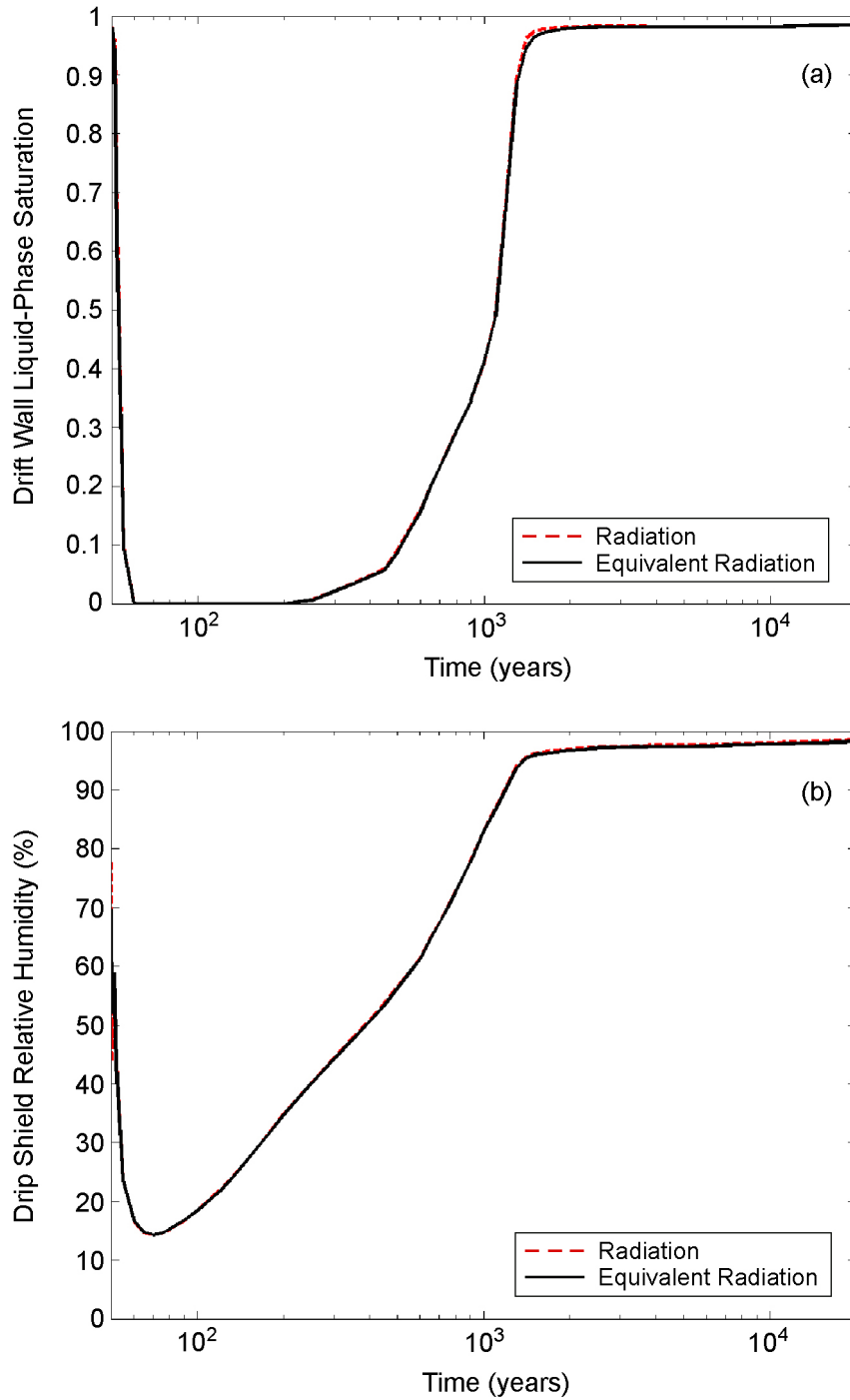
Figures 6.3-94[a] through 6.3-97[a], which compare TH conditions calculated with the LDTH submodel with the base case value of invert depth (0.806 m) with an LDTH submodel with a revised invert depth of 1.32 m, demonstrate a very weak influence of invert depth. Only the drip shield temperature shows more than indiscernible differences. Peak drip shield temperature is 6.0°C higher for the case with the revised invert depth than for the base case. However, as discussed in Appendix VI[a], the drift wall emissivity (0.44) applied to the base case is lower than the average value (0.83) from DTN: MO0109EBSAEQST.009 [DIRS 156696] (file: *s01143_001_002.pdf*). If an emissivity value of 0.83 were used, rather than 0.44, this would reduce the peak drip shield temperature by 3.0°C. Had the larger values of drift wall emissivity (0.83) and invert depth (1.32 m) been applied to the LDTH submodel, the net result would be the calculated peak drip shield temperature being about 3°C higher than that calculated by the base-case LDTH submodel. A difference in peak drip shield temperature of 3°C is insignificant compared to the influence of parametric uncertainty addressed in the MSTHM, as shown in Figures 6.3-76[a] and 6.3-77[a] and in Table 6.3-49[a]. It should be noted that waste package temperatures closely track drip shield temperatures, and thus any conclusions regarding drip shield temperatures apply to the waste packages as well.



Source: Output DTN: LL0705PA038MST.030.

NOTE: These LDTH submodel calculations pertain to the g_9 location (see Figure 6.2-17[a]), close to the repository center. These two cases differ in that one represents in-drift thermal radiation explicitly, while the other uses an equivalent in-drift thermal conductivity to represent in-drift thermal radiation.

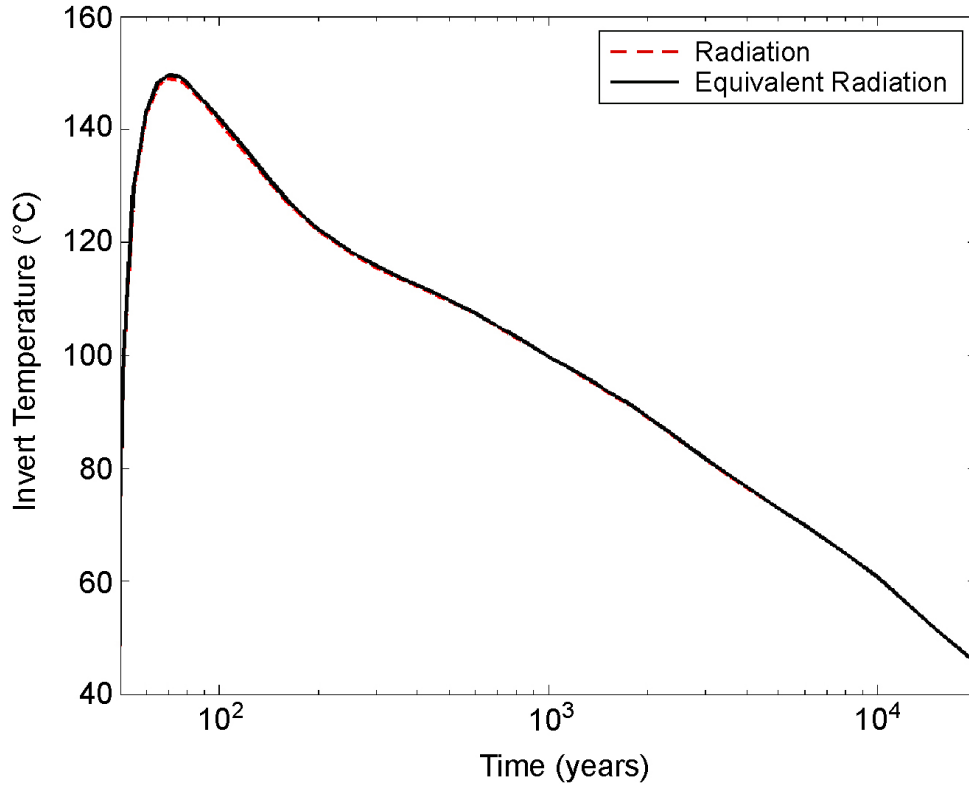
Figure 6.3-90[a]. Temperature on the Drift Wall (a) and Drip Shield (b) at the Repository Center for Different Representations of In-Drift Thermal Radiation



Source: Output DTN: LL0705PA038MST.030.

NOTE: These LDTH submodel calculations pertain to the g_9 location (see Figure 6.2-17[a]), close to the repository center. These two cases differ in that one represents in-drift thermal radiation explicitly, while the other uses an equivalent in-drift thermal conductivity to represent in-drift thermal radiation. The drift wall liquid-phase saturation pertains to the matrix continuum.

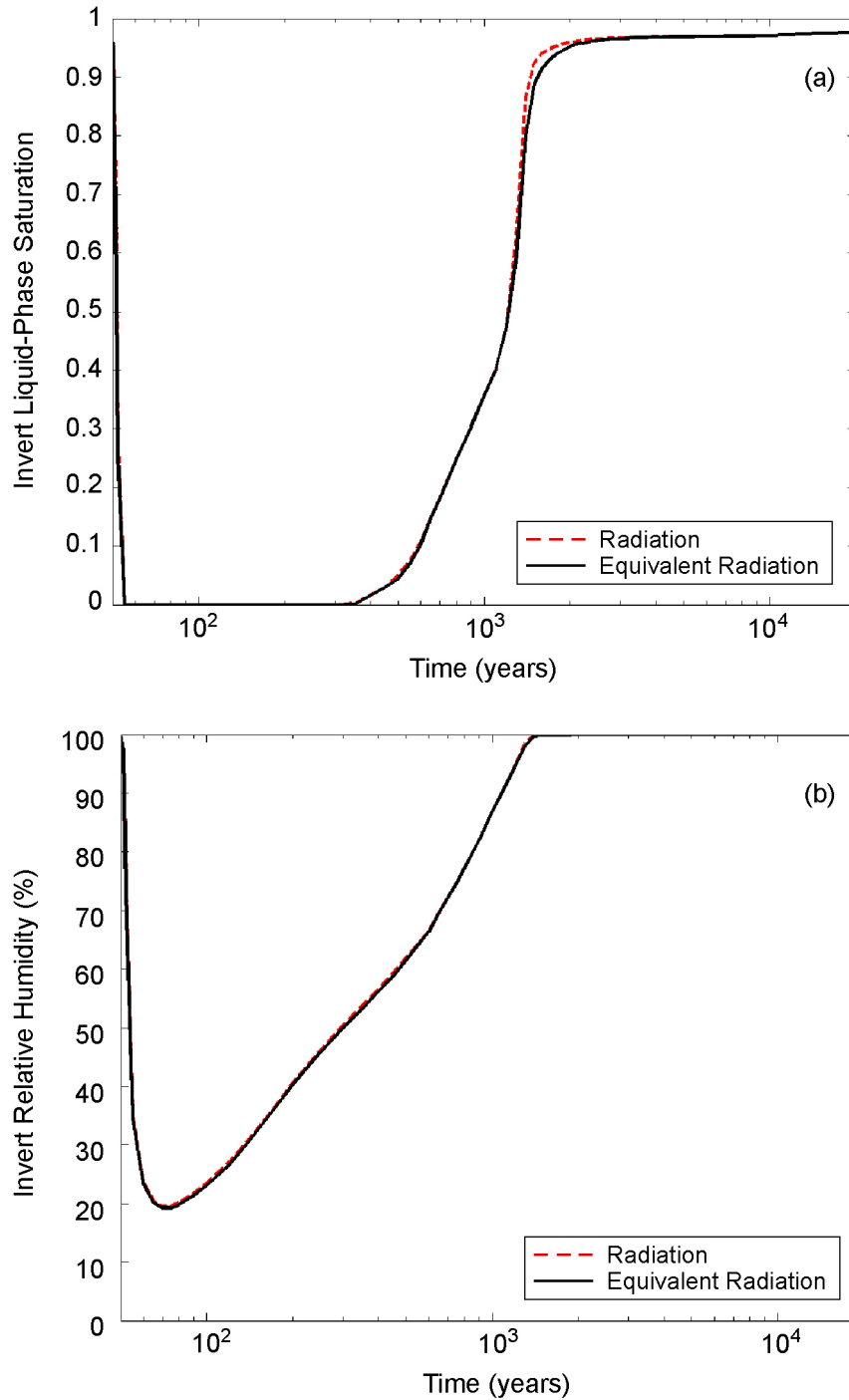
Figure 6.3-91[a]. Drift Wall Liquid-Phase Saturation (a) and Drip Shield Relative Humidity (b) at the Repository Center for Different Representations of In-Drift Thermal Radiation



Source: Output DTN: LL0705PA038MST.030.

NOTE: These LDTH submodel calculations pertain to the g_9 location (see Figure 6.2-17[a]), close to the repository center. These two cases differ in that one represents in-drift thermal radiation explicitly, while the other uses an equivalent in-drift thermal conductivity to represent in-drift thermal radiation.

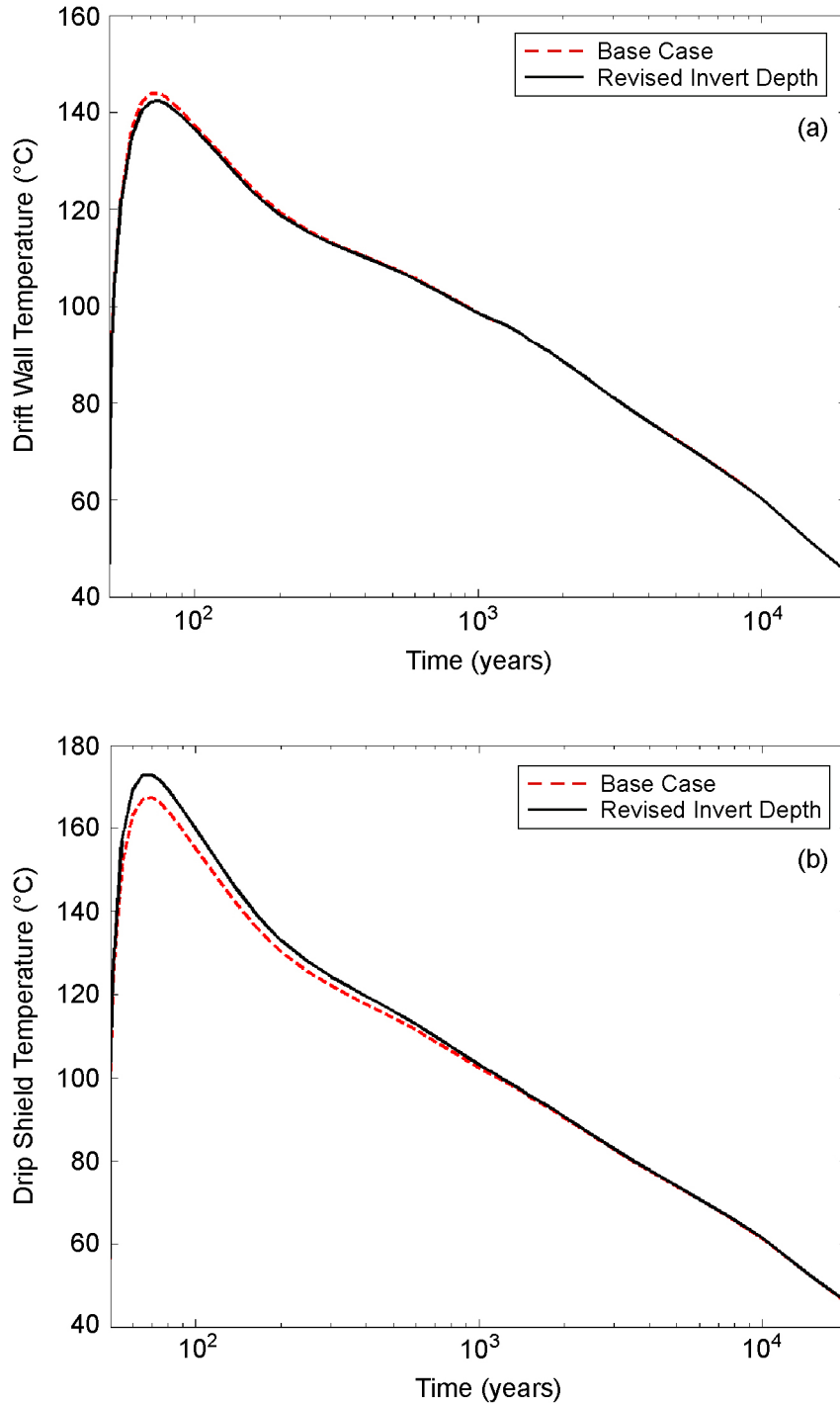
Figure 6.3-92[a]. Invert Temperature at the Repository Center for Different Representations of In-Drift Thermal Radiation



Source: Output DTN: LL0705PA038MST.030.

NOTE: These LDTH submodel calculations pertain to the g_9 location (see Figure 6.2-17[a]), close to the repository center. These two cases differ in that one represents in-drift thermal radiation explicitly, while the other uses an equivalent in-drift thermal conductivity to represent in-drift thermal radiation. The invert liquid-phase saturation pertains to the intragranular porosity.

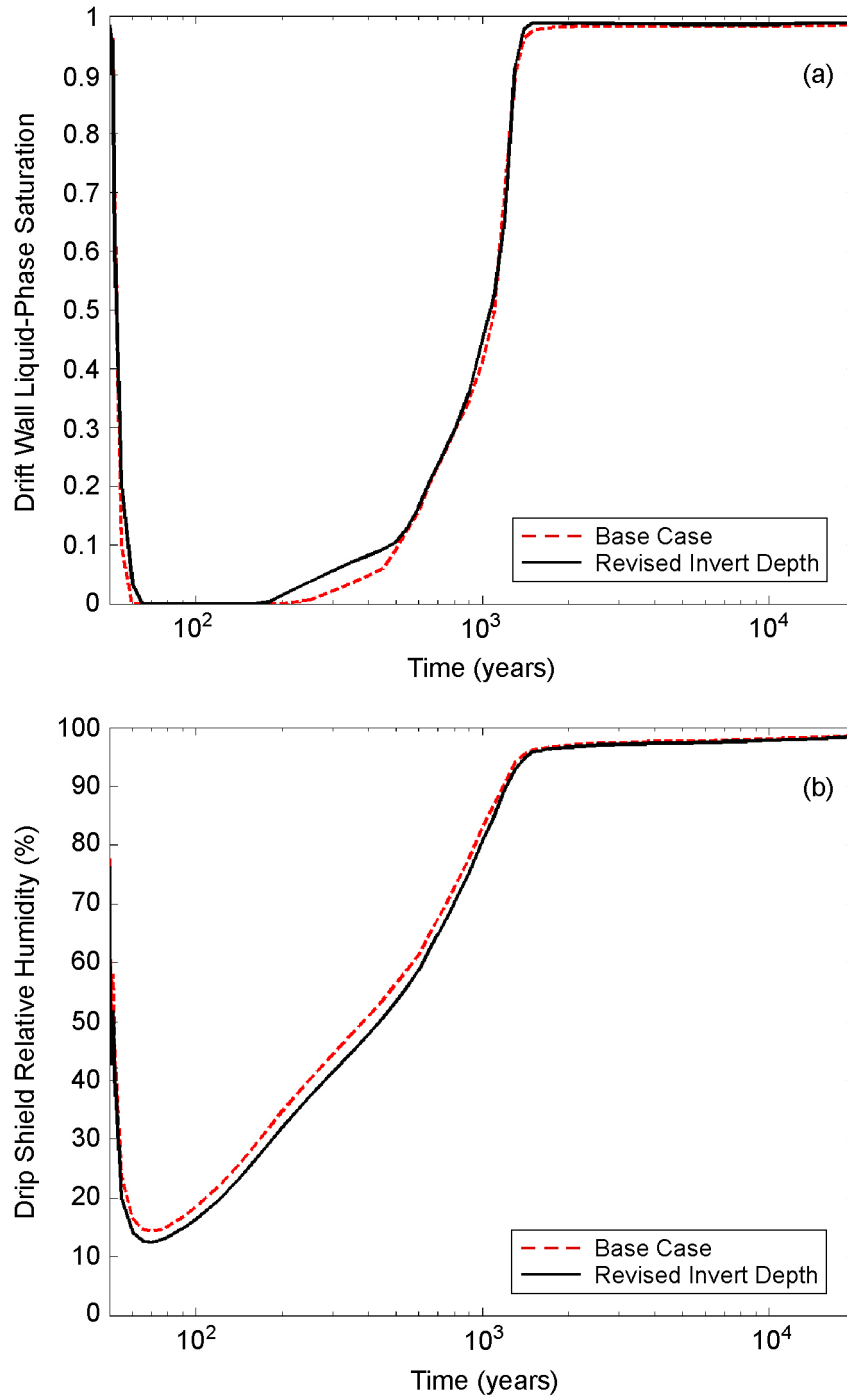
Figure 6.3-93[a]. Invert Liquid-Phase Saturation (a) and Relative Humidity (b) at the Repository Center for Different Representations of In-Drift Thermal Radiation



Source: Output DTN: LL0705PA038MST.030.

NOTE: These LDTH submodel calculations pertain to the g_9 location (see Figure 6.2-17[a]), close to the repository center for two cases of invert depth. The base case has an invert depth of 0.806 m, while the other case has a revised invert depth of 1.32 m.

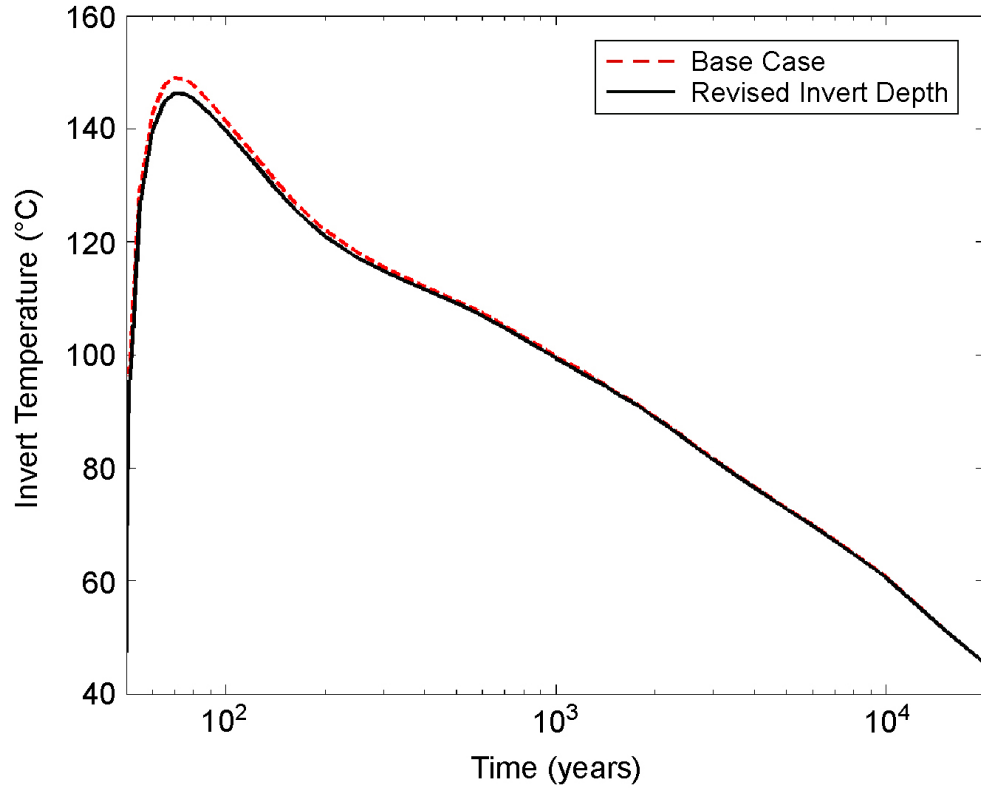
Figure 6.3-94[a]. Temperature on the Drift Wall (a) and Drip Shield (b) at the Repository Center for the Base Case with an Invert Depth of 0.806 m and a Case with an Updated Invert Depth of 1.32 m



Source: Output DTN: LL0705PA038MST.030.

NOTE: These LDTH submodel calculations pertain to the g_9 location (see Figure 6.2-17[a]), close to the repository center for two cases of invert depth. The base case has an invert depth of 0.806 m, while the other case has a revised invert depth of 1.32 m. The drift wall liquid-phase saturation pertains to the matrix continuum.

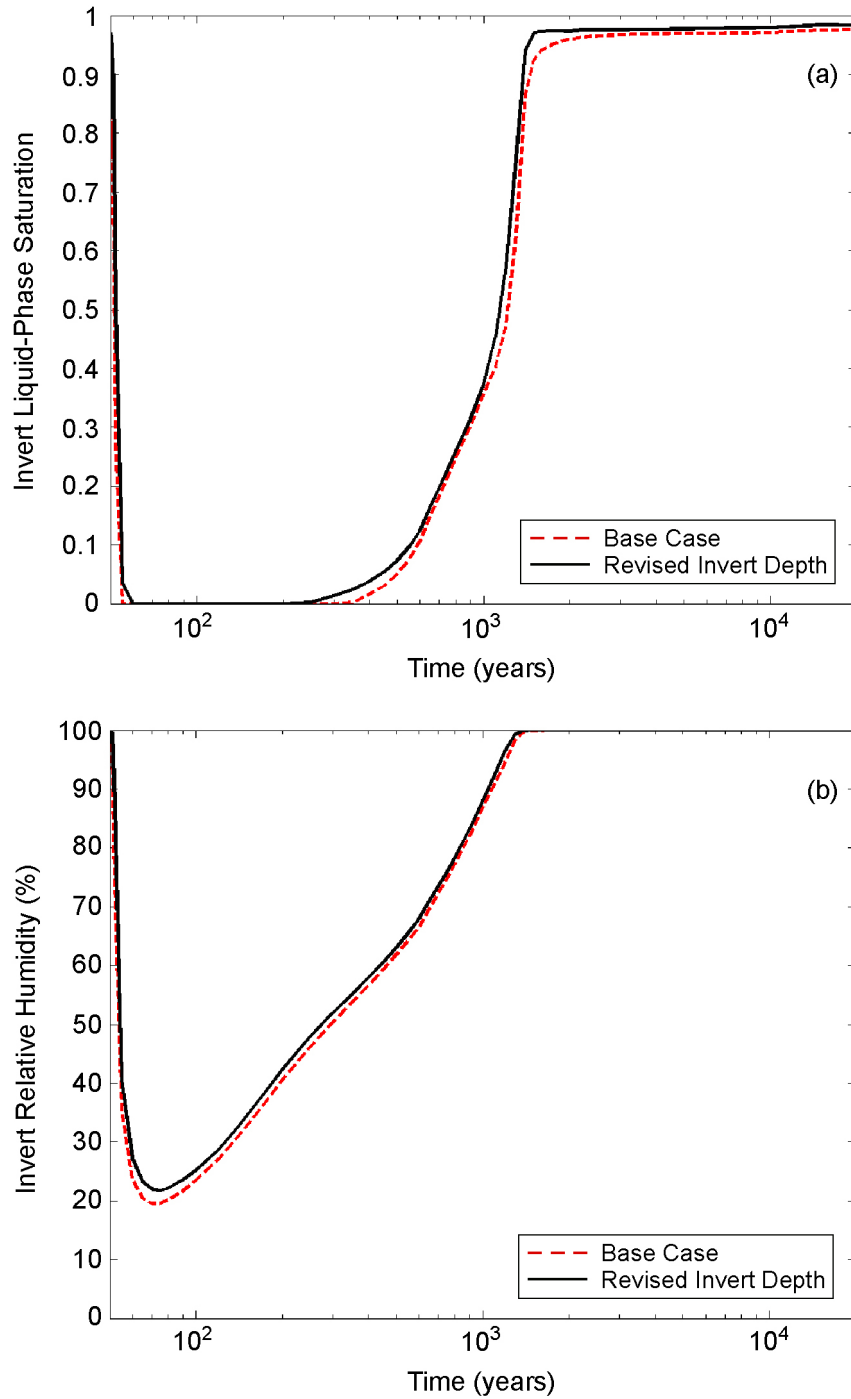
Figure 6.3-95[a]. Drift Wall Liquid-Phase Saturation (a) and Drip Shield Relative Humidity (b) at the Repository Center for the Base Case with an Invert Depth of 0.806 m and a Case with an Updated Invert Depth of 1.32 m



Source: Output DTN: LL0705PA038MST.030.

NOTE: These LDTH submodel calculations pertain to the g_9 location (see Figure 6.2-17[a]), close to the repository center for two cases of invert depth. The base case has an invert depth of 0.806 m, while the other case has a revised invert depth of 1.32 m.

Figure 6.3-96[a]. Invert Temperature at the Repository Center for the Base Case with an Invert Depth of 0.806 m and a Case with an Updated Invert Depth of 1.32 m



Source: Output DTN: LL0705PA038MST.030.

NOTE: These LDTH submodel calculations pertain to the g_9 location (see Figure 6.2-17[a]), close to the repository center for two cases of invert depth. The base case has an invert depth of 0.806 m, while the other case has a revised invert depth of 1.32 m. The invert liquid-phase saturation pertains to the intragranular porosity.

Figure 6.3-97[a]. Invert Liquid-Phase Saturation (a) and Relative Humidity (b) at the Repository Center for the Base Case with an Invert Depth of 0.806 m and a Case with an Updated Invert Depth of 1.32 m

6.4[a] COMPARISON AGAINST AN ALTERNATIVE CONCEPTUAL MODEL

Applicable to this addendum, with no changes required.

6.5[a] FEPS

Applicable to this addendum, with the following additions.

Table 6.5-2[a]. FEPS Addressed by This Report

FEP	Name	Section Where Disposition Is Addressed
2.2.07.10.0A	Condensation zone forms around drifts	6.3.18[a] and 7.8[a]
2.2.10.10.0A	Two-phase buoyant flow/heat pipes	6.3.16[a]

7[a]. MODEL VALIDATION

SCI-PRO-006 requires that TSPA model components be validated for their intended purpose and stated limitations, and to the level of confidence required by a component's relative importance to the performance of the repository. Section 1[a] of this addendum and Section 1 of the parent report provide the intended use of the MSTHM and the model limitations.

The governing technical work plan (TWP) (BSC 2006 [DIRS 178297]) identifies Level I as the appropriate level of validation for the MSTHM. The appropriateness of Level I is based on the relative importance of the model results to TSPA dose.

7.1[a] CONFIDENCE BUILDING DURING MODEL DEVELOPMENT TO ESTABLISH SCIENTIFIC BASIS AND ACCURACY FOR INTENDED USE

Applicable to this addendum, with no changes required.

7.2[a] CONFIDENCE BUILDING AFTER MODEL DEVELOPMENT TO SUPPORT THE SCIENTIFIC BASIS OF THE MODEL

Applicable to this addendum, with one update as follows.

- **Comparison of the MSTHM results against a 3-D pillar-scale TH model**—Using a pillar-scale model-confidence-building test case, the MSTHM output parameters provided to TSPA are shown to be in good agreement with those of the 3-D TH model.

7.3[a] COMPARISON OF NUFT THERMAL-HYDROLOGIC MODEL AGAINST THE LARGE BLOCK TEST

Applicable to this addendum, with no changes required.

7.4[a] VALIDATION OF THE LDTH SUBMODEL USING THE DRIFT SCALE TEST

Applicable to this addendum, with no changes required.

7.4.1[a] Design and Geometry of the DST

Applicable to this addendum, with no changes required.

7.4.2[a] Description of Three-Dimensional Thermal-Hydrologic Model of the DST

Applicable to this addendum, with no changes required.

7.4.2.1[a] Wing-Heater Arrays

Applicable to this addendum, with no changes required.

7.4.2.2[a] Bulkhead

Applicable to this addendum, with no changes required.

7.4.2.3[a] Initial and Boundary Conditions

Applicable to this addendum, with no changes required.

7.4.3[a] Comparison of Simulated and Field-Measured Temperatures

Applicable to this addendum, with no changes required.

7.4.4[a] Comparison of Simulated and Field-Measured Liquid-Phase Saturations in the Matrix

Applicable to this addendum, with no changes required.

7.4.5[a] Summary of Model Validation Using DST Data

Applicable to this addendum, with updates discussed in Section 7.4.7[a].

7.4.6[a] Updated Comparison of Simulated and Field-Measured Temperatures

The 3-D thermal-hydrologic (TH) model “base case” of the Drift Scale Test (DST) is rerun using the updated thermal and hydrologic properties used in the current MSTHM calculations supporting TSPA (Section 6.3.16[a]). As described in Section 7.4.2 of the parent report, the base case represents the bulkhead as being thermally insulated and permeable, thereby being leaky to gas flow. The sealed bulkhead case represents the bulkhead as being thermally insulated and impermeable, thereby allowing no gas flow across it. The updated 3-D DST TH model applies the drift-scale calibrated property set for the 30th percentile infiltration map (DTN: LB0610UZDSCP30.001 [DIRS 179180]), as well as the mean host-rock thermal conductivity values from Output DTN: MO0612MEANTHER.000. A percolation flux of 13.9 mm/yr is used, which corresponds to the DST location, and to the P10 percolation flux case, which is from DTN: LB0612PDPTNTSW.001 [DIRS 179156].

The simulated temperatures are compared, at various times, with the field-measured temperatures for many of the boreholes for which the comparison was made in Section 7.4.3 of the parent report. The similarity in locations is seen by comparing Table 7.4-4 with Table 7.4-1 of the parent report. Figures 7.4-21[a] through 7.4-25[a] compare the simulated and field-measured temperatures for six vertically oriented boreholes. Figures 7.4-26[a] and 7.4-27[a] compare the simulated and field-measured temperatures for two laterally oriented boreholes. Figures 7.4-28[a] and 7.4-29[a] compare the simulated and field-measured temperatures for two longitudinally oriented boreholes. Included in these figures are the simulated temperatures for the previous base case, which are reported in Section 7.4.3 of the parent report. Comparing the current base case with the previous base case, and comparing both cases against the field-measured temperatures, the following observations can be made:

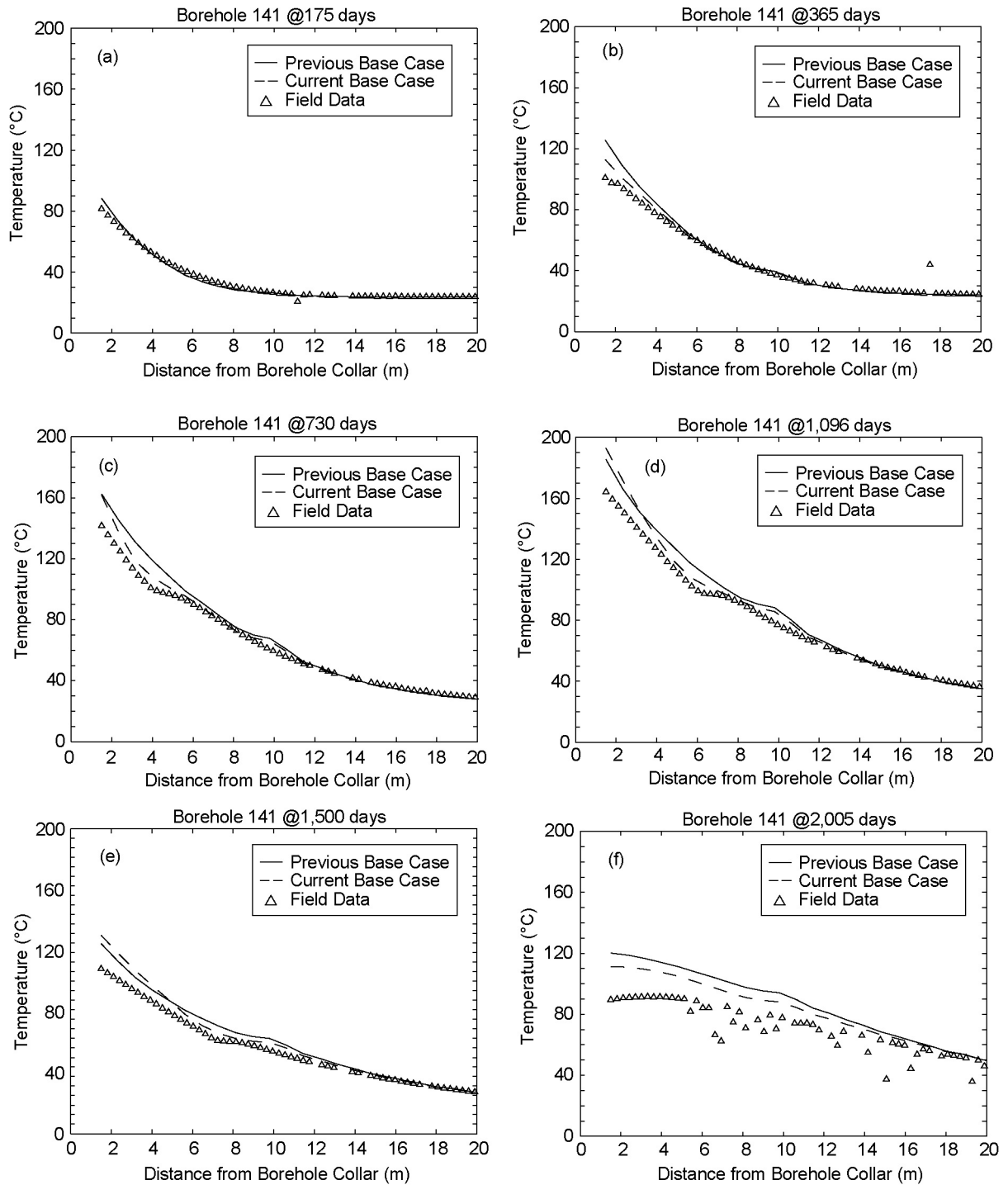
- Where field-measured temperatures are at or above the boiling point (96°C), the current base case predicts lower temperatures than the previous base case.

- Where field-measured temperatures are at or above the boiling point (96°C), the current base case predicts temperatures that are in better agreement with the field-measure temperatures than are predicted by the previous base case.
- Where field-measured temperatures are close to the boiling point (96°C), the current base case predicts a more pronounced “temperature plateau,” which is in better agreement with field-measured temperatures, than is predicted by the previous base case.
- Where field-measured temperatures are below the boiling point (96°C), the current and previous base cases predict similar temperatures that are in good agreement with the field-measured temperatures.

Table 7.4-4[a]. Summary of Thermocouple Boreholes Used to Compare Field-Measured Temperatures with NUFT-Simulated Temperatures

Borehole Number	Figure	Orientation	Collar X Coordinate (lateral)	Collar Y Coordinate (longitudinal)	Collar Z Coordinate (vertical)
141	7.4-21[a]	Vertical below HD (-Z)	0.764	11.893	-1.637
158	7.4-22[a]	Vertical above HD (+Z)	0.757	22.847	2.565
168	7.4-23[a]	Vertical above HD (+Z)	-0.071	31.952	2.451
169	7.4-24[a]	Vertical below HD (-Z)	-0.003	32.007	-1.629
170	7.4-25[a]	Vertical above HD (+Z)	0.751	39.306	2.488
143	7.4-26[a]	Lateral (+X)	2.665	11.890	-0.008
164	7.4-27[a]	Lateral (-X)	2.489	22.869	0.016
79	7.4-28[a]	Longitudinal (+Y)	9.460	-11.022	3.752
80	7.4-29[a]	Longitudinal (+Y)	-9.486	-11.059	3.228

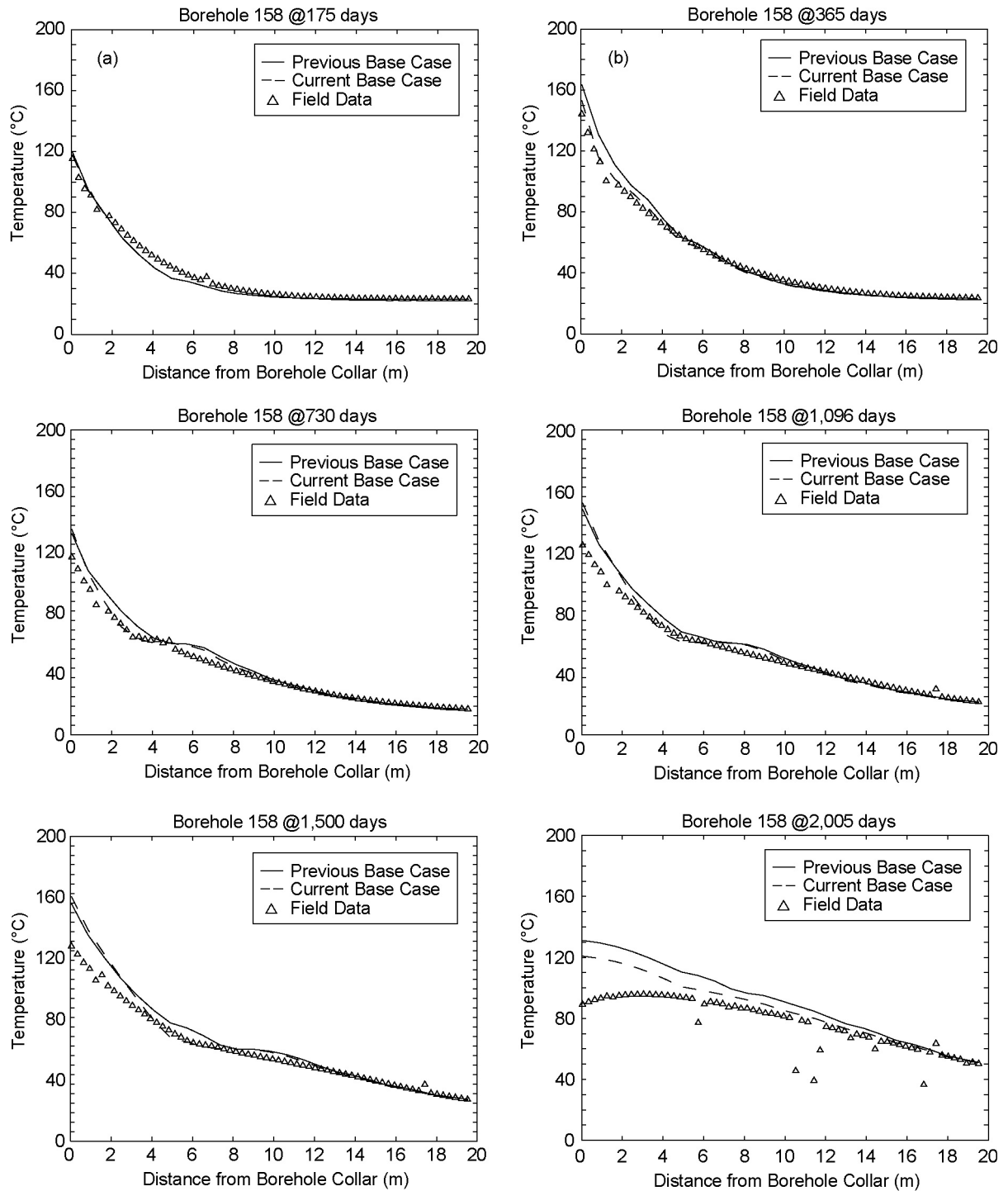
NOTE: HD = Heated Drift. The indicated orientation is relative to the Heated Drift. The source of the coordinates is given in Table 4-1 of CRWMS M&O 1998 [DIRS 111115] (collar coordinates used).



Source: Output DTN: LL0705PA032MST.028; see Table 4.4-2 of the parent report for field data DTNs.

NOTE: The NUFT simulations are for the two indicated cases. The “current base case” uses the updated thermal and hydrologic properties used in the current MSTHM calculations supporting TSPA. The “previous base case” is the base case from Section 7.4.3 of the parent report.

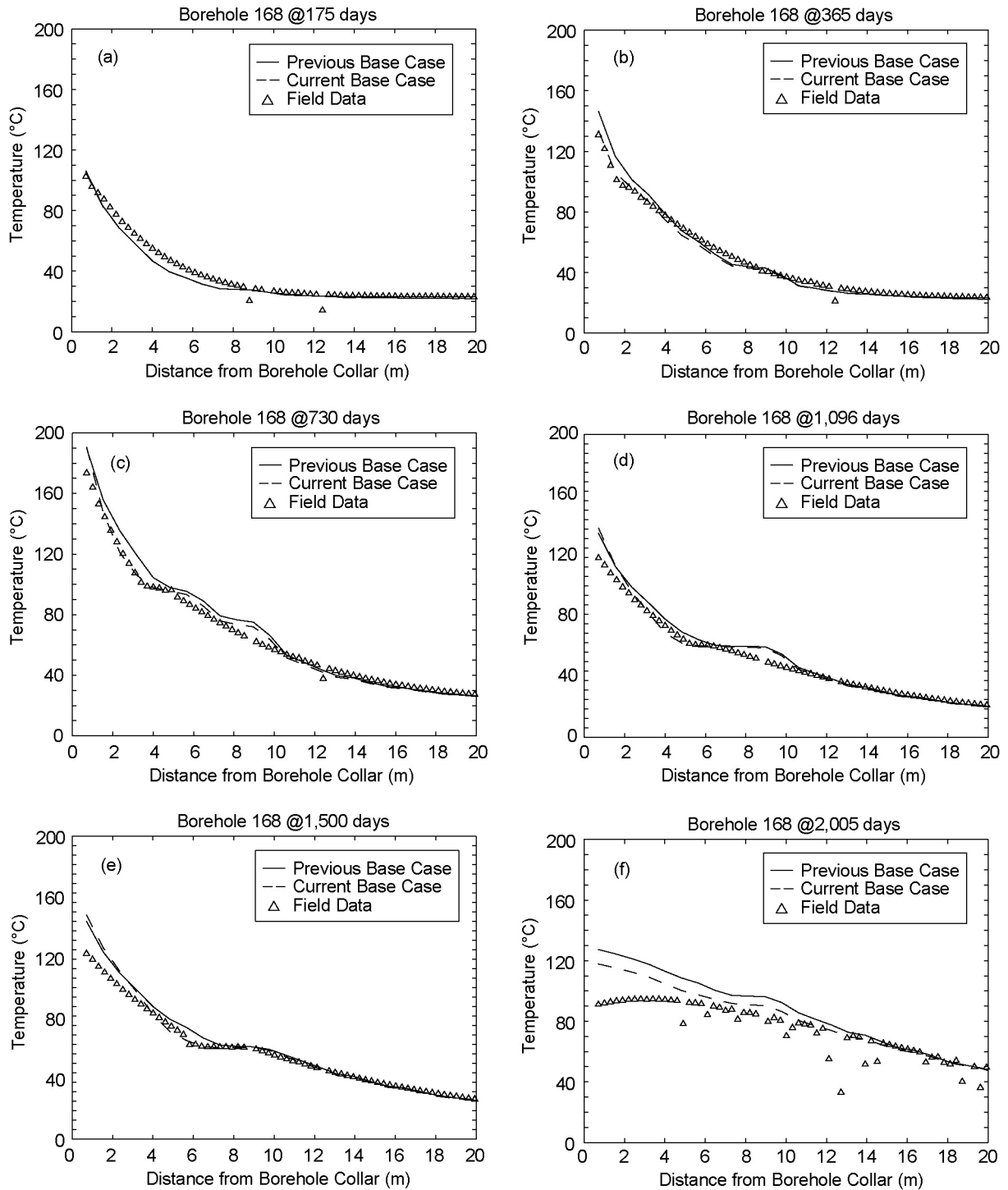
Figure 7.4-21[a]. NUFT-Simulated and Measured Temperatures Compared along Borehole 141 at (a) 175, (b) 365, (c) 730, (d) 1,096, (e) 1,500, and (f) 2,005 Days



Source: Output DTN: LL0705PA032MST.028; see Table 4.4-2 of the parent report for field data DTNs.

NOTE: The NUFT simulations are for the two indicated cases. The “current base case” uses the updated thermal and hydrologic properties used in the current MSTHM calculations supporting TSPA. The “previous base case” is the base case from Section 7.4.3 of the parent report.

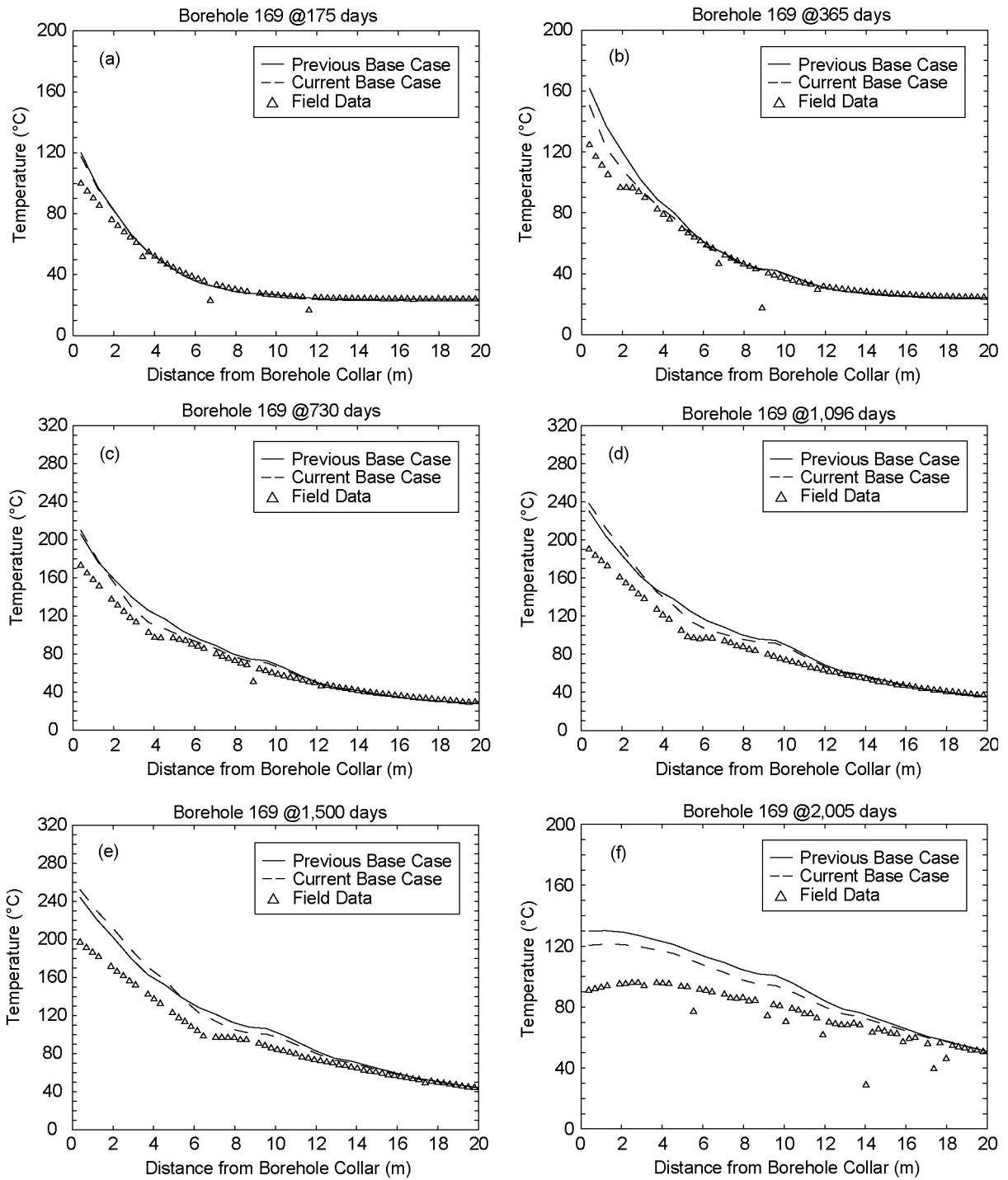
Figure 7.4-22[a]. NUFT-Simulated and Measured Temperatures Compared along Borehole 158 at (a) 175, (b) 365, (c) 730, (d) 1,096, (e) 1,500, and (f) 2,005 Days



Source: Output DTN: LL0705PA032MST.028; see Table 4.4-2 of the parent report for field data DTNs.

NOTE: The NUFT simulations are for the two indicated cases. The “current base case” uses the updated thermal and hydrologic properties used in the current MSTHM calculations supporting TSPA. The “previous base case” is the base case from Section 7.4.3 of the parent report.

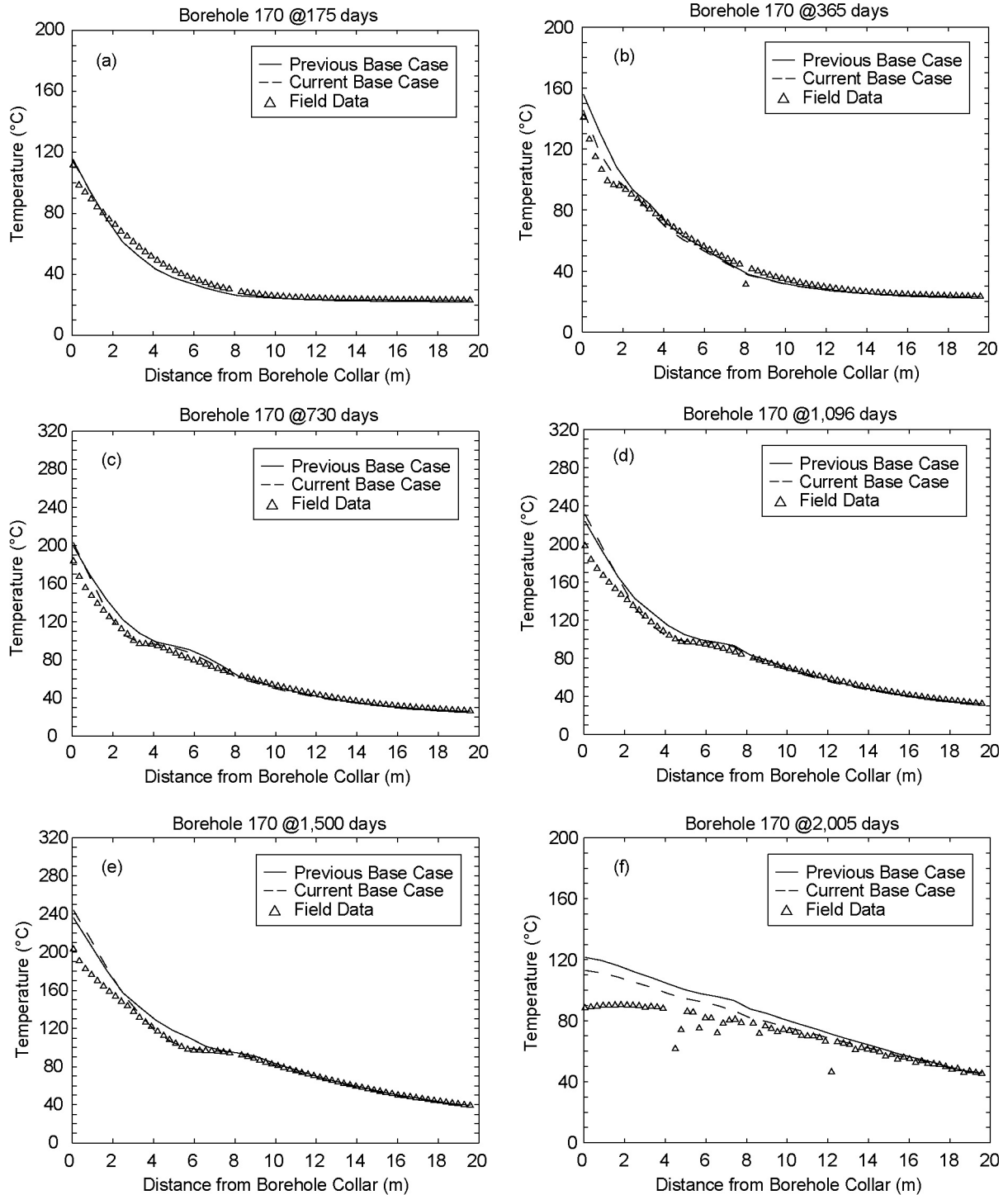
Figure 7.4-23[a]. NUFT-Simulated and Measured Temperatures Compared along Borehole 168 at (a) 175, (b) 365, (c) 730, (d) 1,096, (e) 1,500, and (f) 2,005 Days



Source: Output DTN: LL0705PA032MST.028; see Table 4.4-2 of the parent report for field data DTNs.

NOTE: The NUFT simulations are for the two indicated cases. The “current base case” uses the updated thermal and hydrologic properties used in the current MSTHM calculations supporting TSPA. The “previous base case” is the base case from Section 7.4.3 of the parent report.

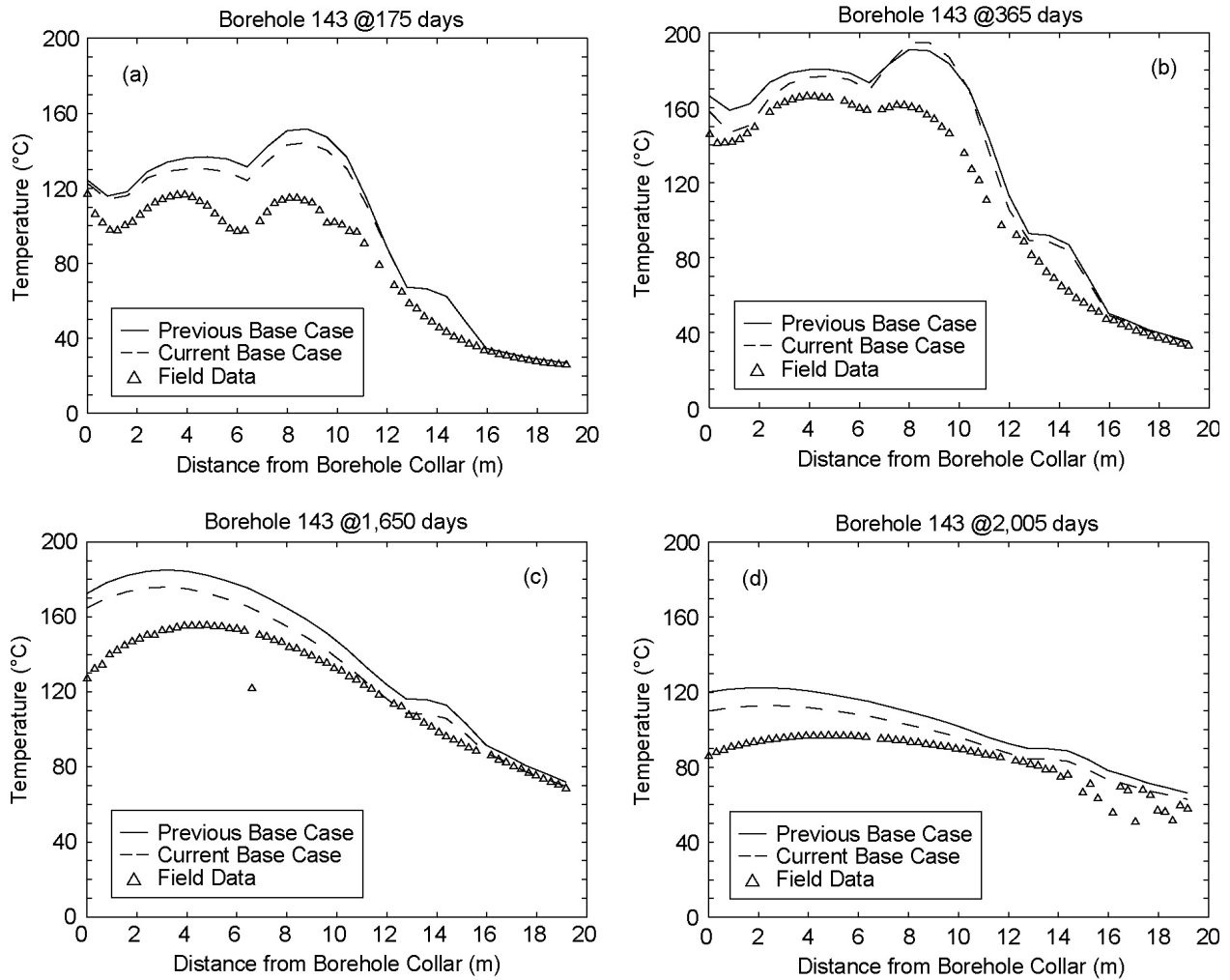
Figure 7.4-24[a]. NUFT-Simulated and Measured Temperatures Compared along Borehole 169 at (a) 175, (b) 365, (c) 730, (d) 1,096, (e) 1,500, and (f) 2,005 Days



Source: Output DTN: LL0705PA032MST.028; see Table 4.4-2 of the parent report for field data DTNs.

NOTE: The NUFT simulations are for the two indicated cases. The “current base case” uses the updated thermal and hydrologic properties used in the current MSTHM calculations supporting TSPA. The “previous base case” is the base case from Section 7.4.3 of the parent report.

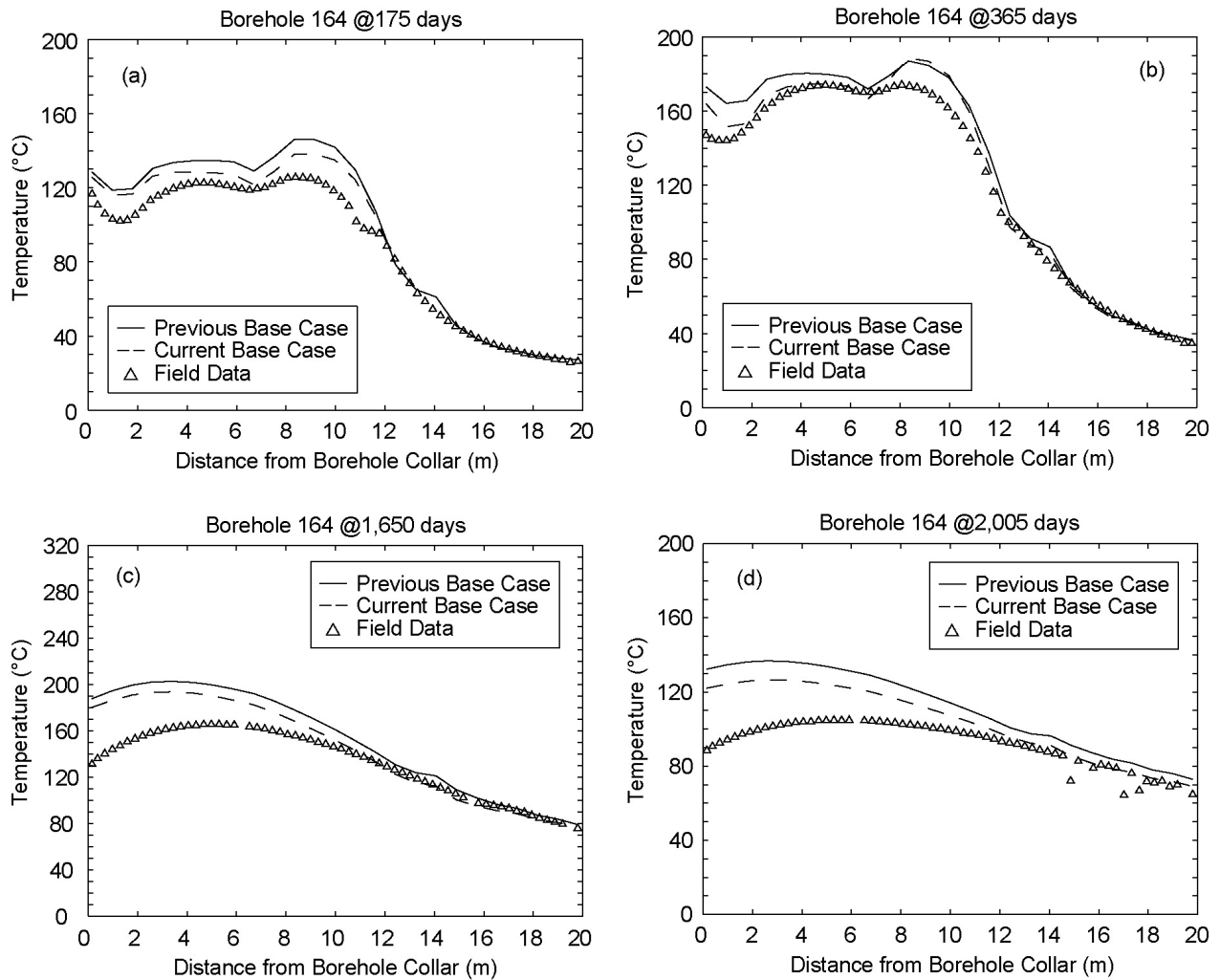
Figure 7.4-25[a]. NUFT-Simulated and Measured Temperatures Compared along Borehole 170 at (a) 175, (b) 365, (c) 730, (d) 1,096, (e) 1,500, and (f) 2,005 Days



Source: Output DTN: LL0705PA032MST.028; see Table 4.4-2 of the parent report for field data DTNs.

NOTE: The NUFT simulations are for the two indicated cases. The “current base case” uses the updated thermal and hydrologic properties used in the current MSTHM calculations supporting TSPA. The “previous base case” is the base case from Section 7.4.3 of the parent report.

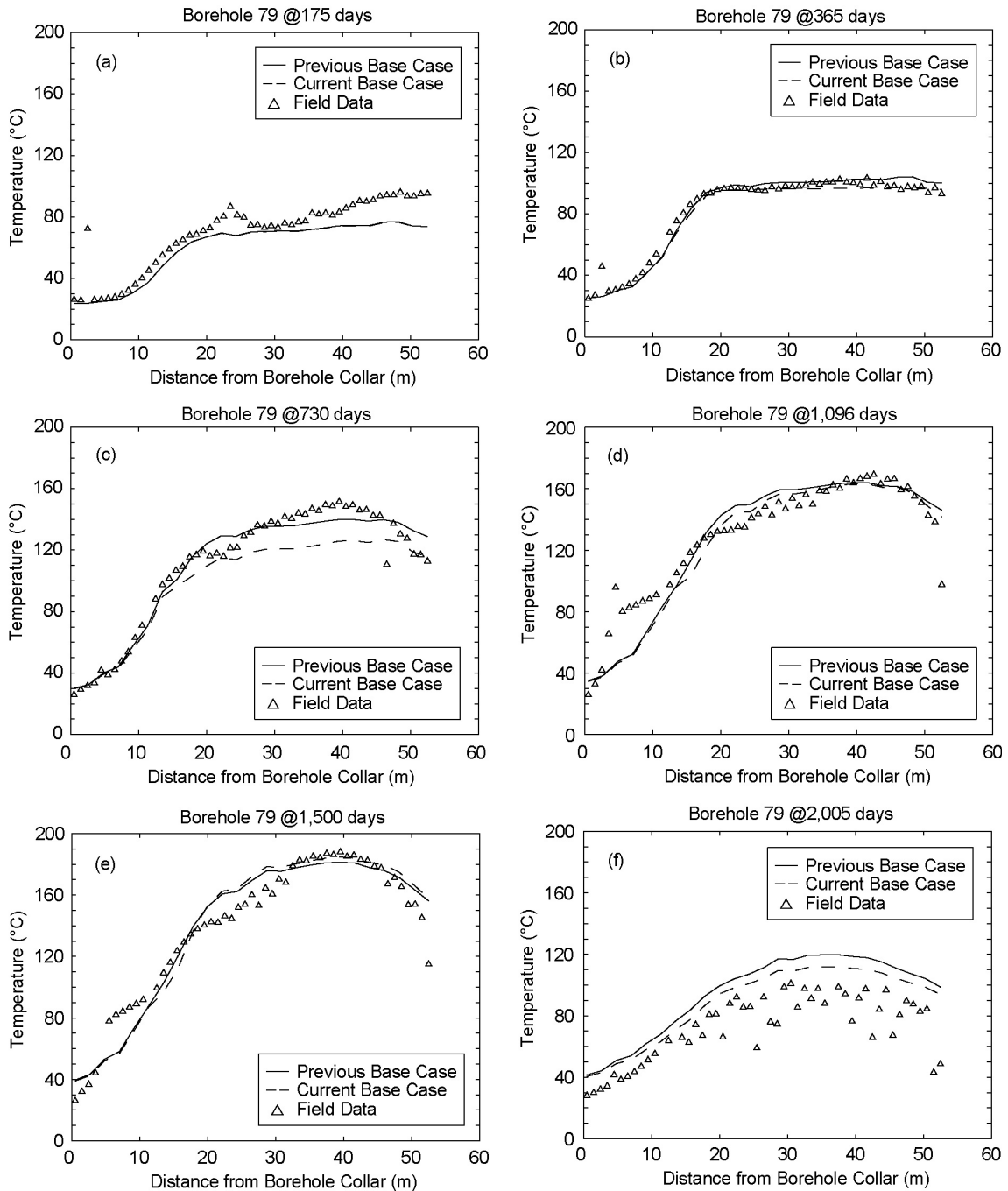
Figure 7.4-26[a]. NUFT-Simulated and Measured Temperatures Compared along Borehole 143 at (a) 175, (b) 365, (c) 1,650, and (d) 2,005 Days



Source: Output DTN: LL0705PA032MST.028; see Table 4.4-2 of the parent report for field data DTNs.

NOTE: The NUFT simulations are for the two indicated cases. The “current base case” uses the updated thermal and hydrologic properties used in the current MSTHM calculations supporting TSPA. The “previous base case” is the base case from Section 7.4.3 of the parent report.

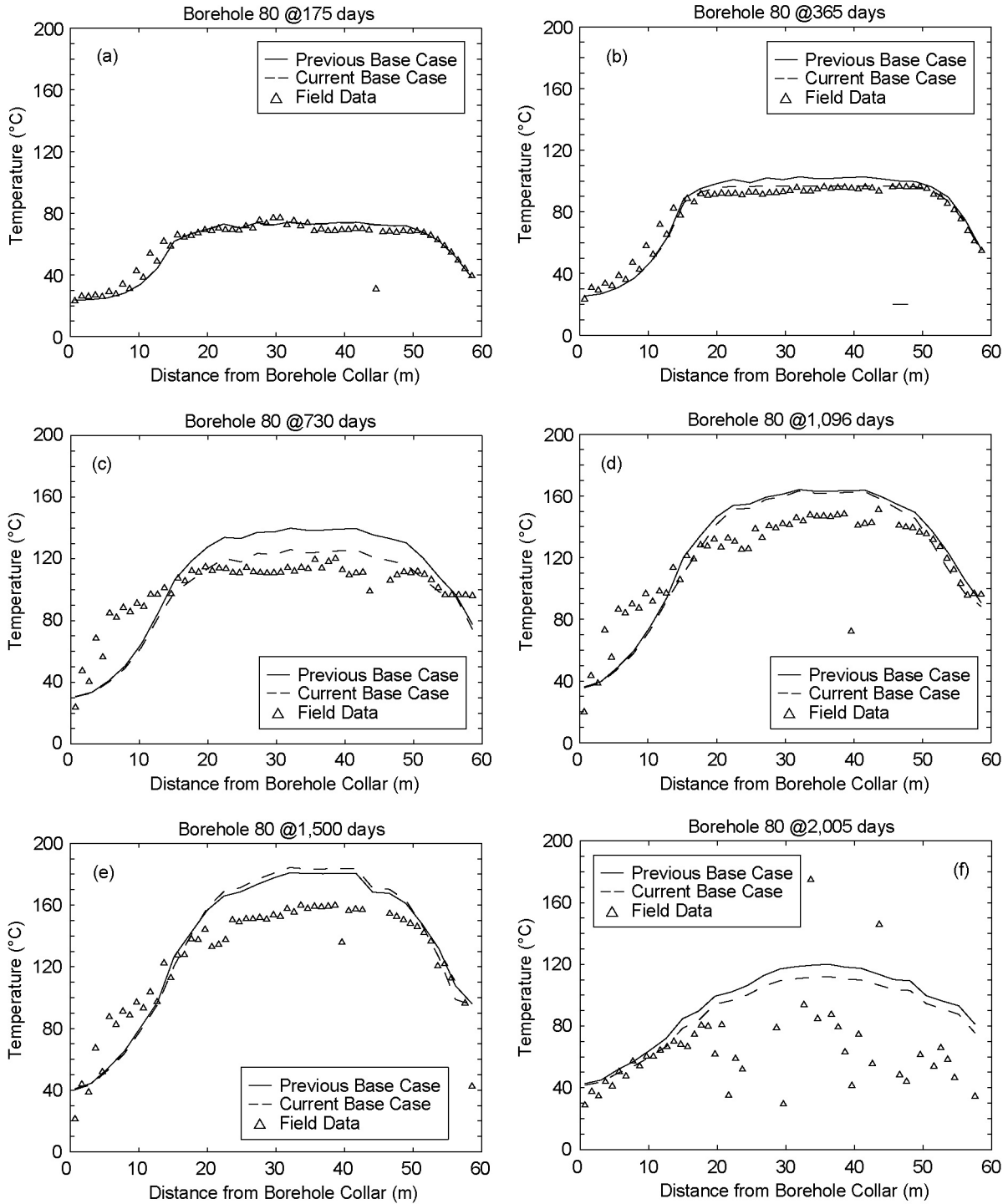
Figure 7.4-27[a]. NUFT-Simulated and Measured Temperatures Compared along Borehole 164 at (a) 175, (b) 365, (c) 1,650, and (d) 2,005 Days



Source: Output DTN: LL0705PA032MST.028; see Table 4.4-2 of the parent report for field data DTNs.

NOTE: The NUFT simulations are for the two indicated cases. The “current base case” uses the updated thermal and hydrologic properties used in the current MSTHM calculations supporting TSPA. The “previous base case” is the base case from Section 7.4.3 of the parent report.

Figure 7.4-28[a]. NUFT-Simulated and Measured Temperatures Compared along Borehole 79 at (a) 175, (b) 365, (c) 730, (d) 1,096, (e) 1,500, and (f) 2,005 Days



Source: Output DTN: LL0705PA032MST.028; see Table 4.4-2 of the parent report for field data DTNs.

NOTE: The NUFT simulations are for the two indicated cases. The “current base case” uses the updated thermal and hydrologic properties used in the current MSTHM calculations supporting TSPA. The “previous base case” is the base case from Section 7.4.3 of the parent report.

Figure 7.4-29[a]. NUFT-Simulated and Measured Temperatures Compared along Borehole 80 at (a) 175, (b) 365, (c) 730, (d) 1,096, (e) 1,500, and (f) 2,005 Days

Table 7.4-5[a] lists the borehole sensor locations where the simulated and field-measured temperature histories are compared. Figures 7.4-30[a] through 7.4-32[a] compare the simulated and field-measured temperature histories at various locations. The simulated temperature histories are applicable to the current base case. A comparison of Figures 7.4-30[a] through 7.4-32[a] with Figures 7.4-13 through 7.4-15 of the parent report results in the following observations:

- Where field-measured temperatures are at or above the boiling point (96°C), the simulated temperatures for the current base case are in better agreement with field-measured temperatures.
- Where field-measured temperatures are close to the boiling point (96°C), the simulated temperatures for the current base case provide a better approximate temperature plateau than the previous base case.
- Where field-measured temperatures are below the boiling point (96°C), the simulated temperatures for the current and previous base cases are in good agreement with the field-measured temperatures.

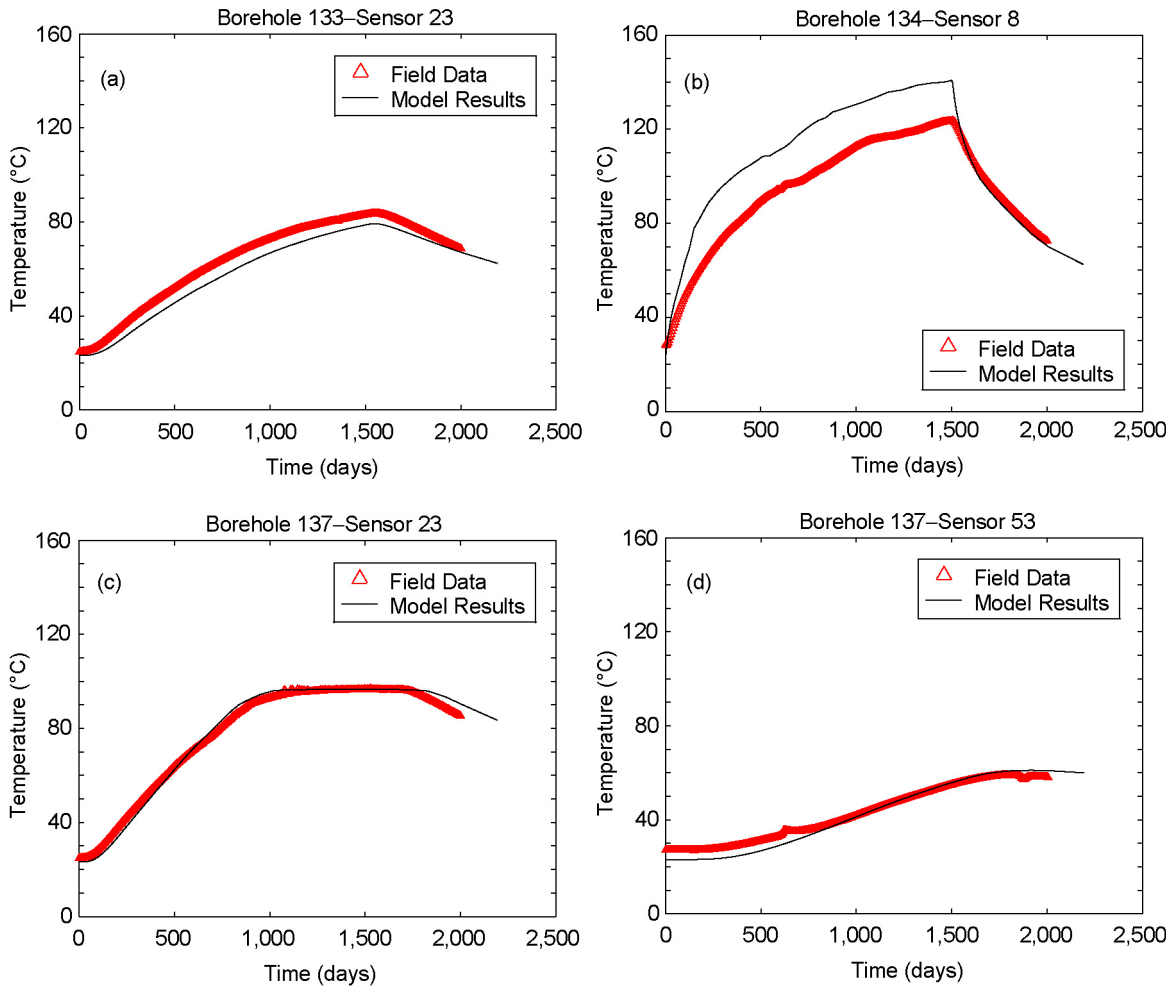
The primary cause of the better agreement between simulated and field-measured temperatures for the current base case is the larger matrix permeability in the Tptpmn (tsw34), which is the host-rock unit in which the DST occurs. The larger matrix permeability imposes less resistance to vapor flow out of the matrix and into the fracture, which results in less throttling of vaporization within the boiling zone. With a smaller increase in gas-phase pressure in the matrix, boiling can occur at temperatures closer to the nominal boiling point (96°C). The influence of reduced resistance to vapor flow is manifested by the more distinct “temperature plateau.”

Table 7.4-5[a]. Coordinates of Thermocouple Sensors Used in Figures 7.4-30[a], 7.4-31[a], and 7.4-32[a]

Borehole	Sensor	Figure	X Coordinate (lateral)	Y Coordinate (longitudinal)	Z Coordinate (vertical)
133	23	7.4-30[a]	0.79	2.77	9.12
134	8	7.4-30[a]	0.73	2.74	-3.13
137	23	7.4-30[a]	0.81	11.89	8.9
137	53	7.4-30[a]	0.86	11.86	17.88
144	21	7.4-31[a]	6.31	11.96	6.27
144	51	7.4-31[a]	12.66	12.02	12.63
168	20	7.4-31[a]	0.15	31.96	8.86
168	50	7.4-31[a]	0.27	31.97	17.87
79	29	7.4-32[a]	9.46	10.48	3.37
79	34	7.4-32[a]	9.46	15.48	3.29
80	48	7.4-32[a]	-9.81	35.54	3.18
80	53	7.4-32[a]	-9.85	40.53	3.17

Source: CRWMS M&O 1998 [DIRS 111115].

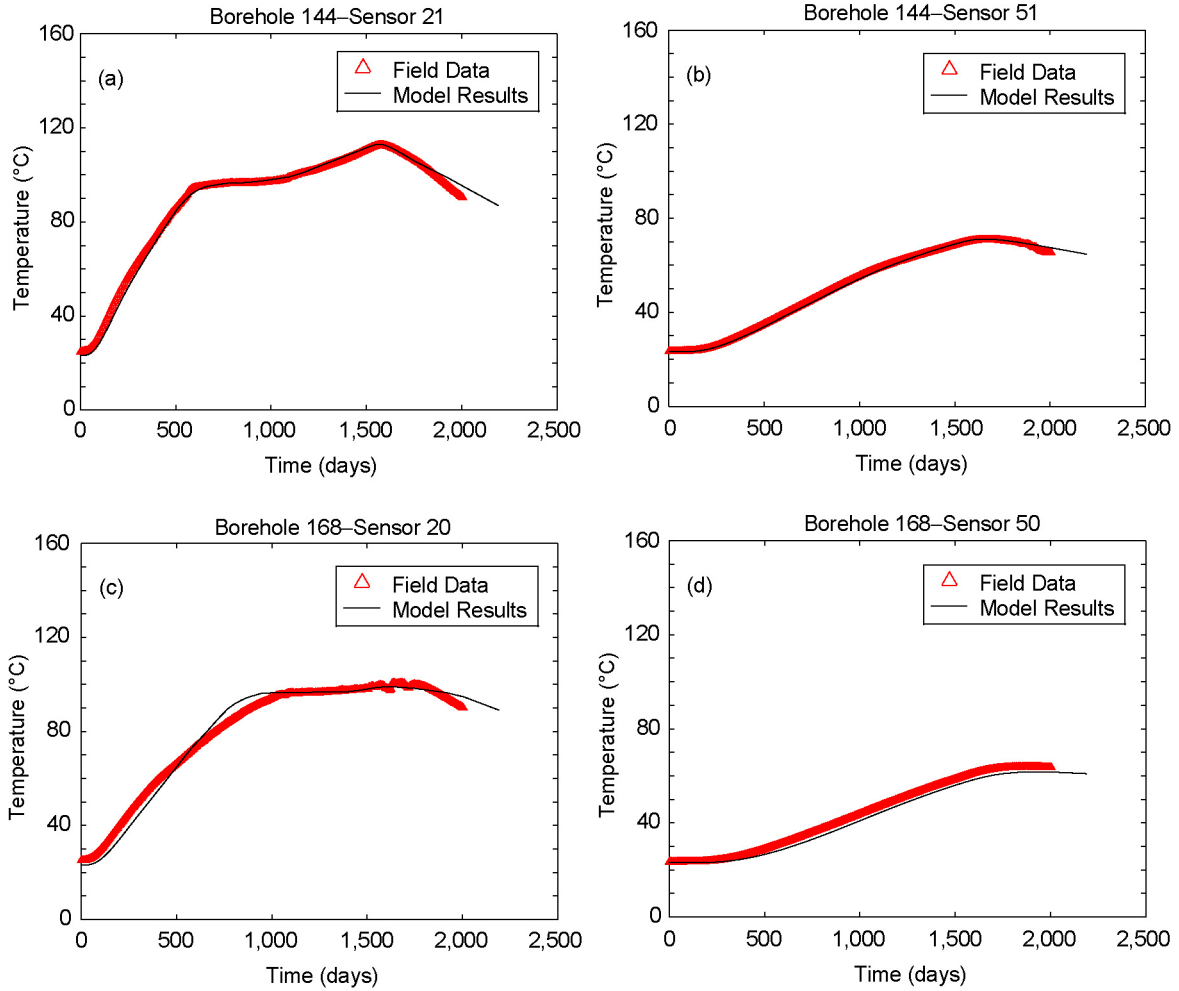
NOTE: The source of the coordinates is given in the top of Table 4.4-2 of the parent report.



Source: Output DTN: LL0705PA032MST.028; see Table 4.4-2 of the parent report for field data DTNs.

NOTE: The NUFT simulation is for the current base case, which uses the updated thermal and hydrologic properties used in the current MSTHM calculations supporting TSPA.

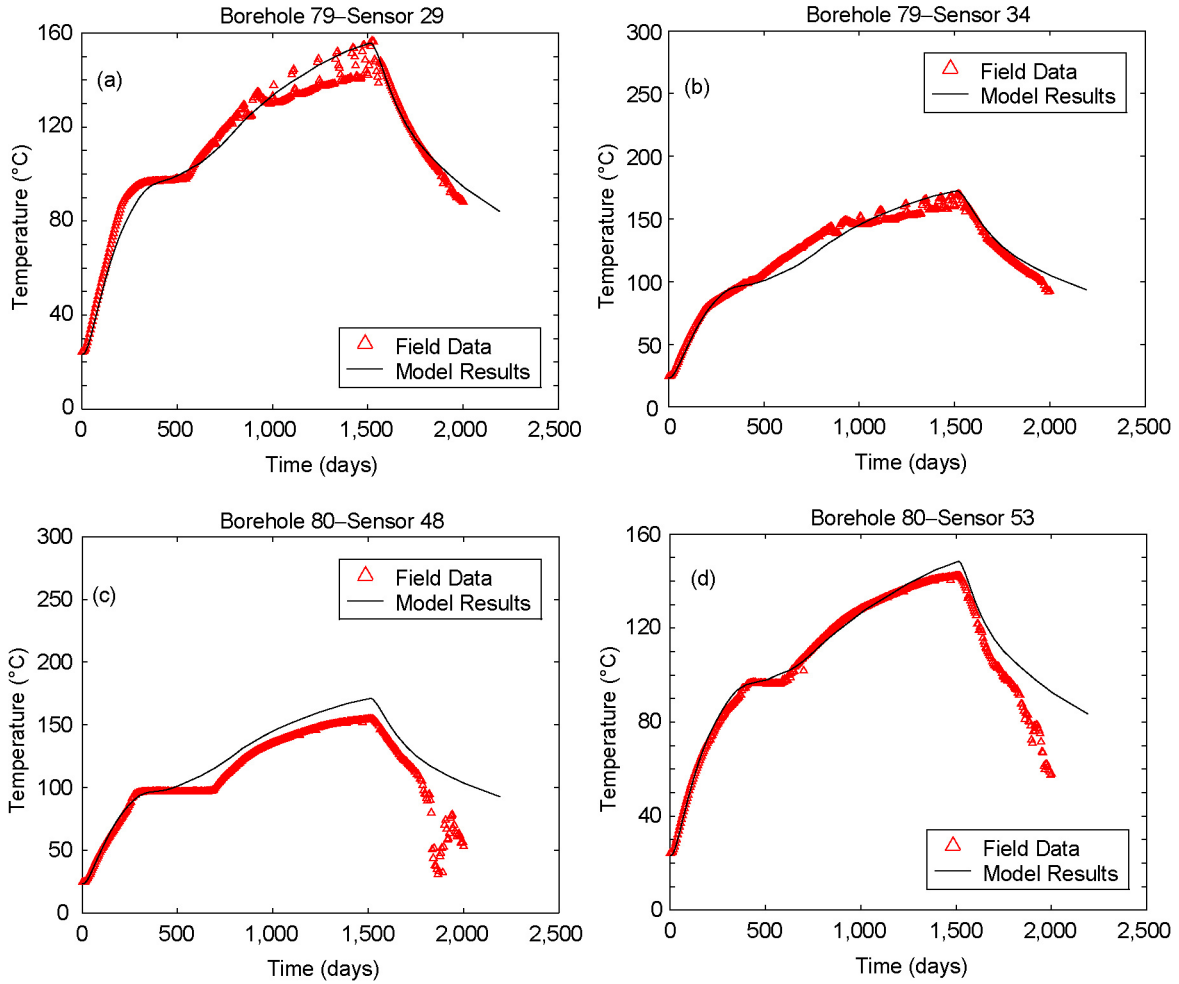
Figure 7.4-30[a]. NUFT-Simulated and Measured Temperature Histories Compared at (a) Borehole 133: Sensor 23, (b) Borehole 134: Sensor 8, (c) Borehole 137: Sensor 23, and (d) Borehole 137: Sensor 53



Source: Output DTN: LL0705PA032MST.028; see Table 4.4-2 of the parent report for field data DTNs.

NOTE: The NUFT simulation is for the current base case, which uses the updated thermal and hydrologic properties used in the current MSTHM calculations supporting TSPA.

Figure 7.4-31[a]. NUFT-Simulated and Measured Temperature Histories Compared at (a) Borehole 144: Sensor 21, (b) Borehole 144: Sensor 51, (c) Borehole 168: Sensor 20, and (d) Borehole 168: Sensor 50



Source: Output DTN: LL0705PA032MST.028; see Table 4.4-2 of the parent report for field data DTNs.

NOTE: The NUFT simulation is for the current base case, which uses the updated thermal and hydrologic properties used in the current MSTHM calculations supporting TSPA.

Figure 7.4-32[a]. NUFT-Simulated and Measured Temperature Histories Compared at (a) Borehole 79: Sensor 29, (b) Borehole 79: Sensor 34, (c) Borehole 80: Sensor 48, and (d) Borehole 80: Sensor 53

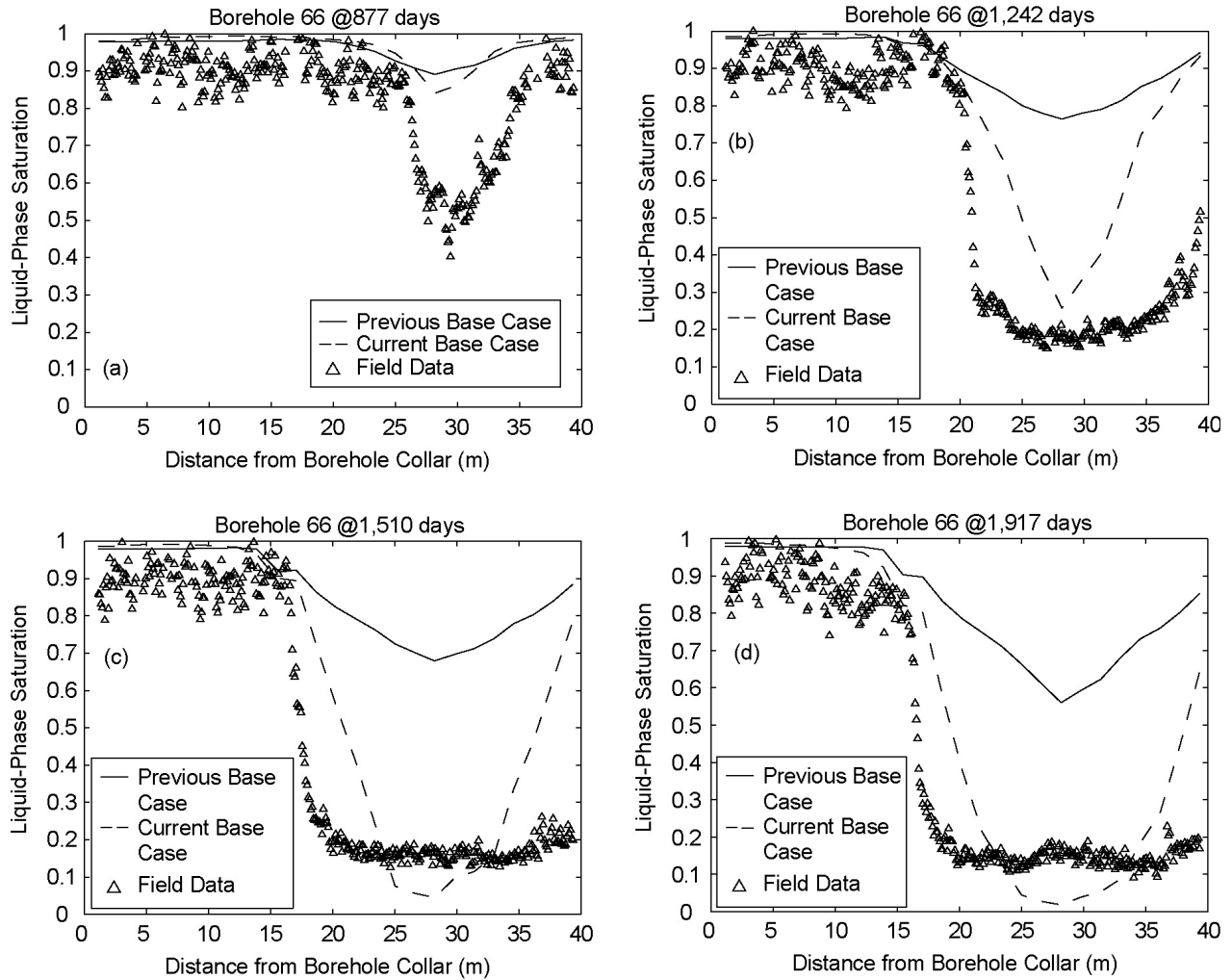
7.4.7[a] Updated Comparison of Simulated and Field-Measured Liquid-Phase Saturations in the Matrix

Table 7.4-6[a] lists the borehole sensor locations where the simulated and field-measured temperature histories are compared. Figures 7.4-33[a] through 7.4-37[a] compare field-measured and simulated liquid-phase saturations for both the current base case and previous base case. The current base case consistently predicts drier conditions than predicted by the previous base case. Rock dryout is predicted to start earlier with the current base case than with the previous base case. In most of the comparisons with the field-measured liquid-phase saturation, the current base case predicts liquid-phase saturations that are in better agreement with the field-measured liquid-phase saturations than predicted by the previous base case. The primary cause of the better agreement for the current base case is the larger matrix permeability in the Tptpmn (tsw34), which is the host-rock unit in which the DST was conducted. The larger matrix permeability imposes less resistance to vapor flow out of the matrix and into the fracture, which results in less throttling of vaporization within the boiling zone. The influence of reduced resistance to vapor flow is manifested by a more distinct “temperature plateau.”

Table 7.4-6[a]. Summary of Boreholes Used to Compare Field-Measured Saturations with NUFT-Simulated Saturations

Borehole Number	Figure	Orientation	Collar Coordinates			End Coordinates		
			x	y	z	x	y	z
66	7.4-33[a]	Lateral (+X)	-29.118	26.506	5.999	10.682	26.580	6.890
67	7.4-34[a]	Lateral (+X-Z)	-28.974	26.489	5.222	8.262	25.877	-7.953
68	7.4-35[a]	Lateral (+X-Z)	-29.116	26.550	4.588	6.847	26.856	-12.272
79	7.4-36[a]	Longitudinal (+Y)	9.460	-11.022	3.752	9.459	48.478	2.706
80	7.4-37[a]	Longitudinal (+Y)	-9.486	-11.059	3.228	-9.903	48.570	3.162

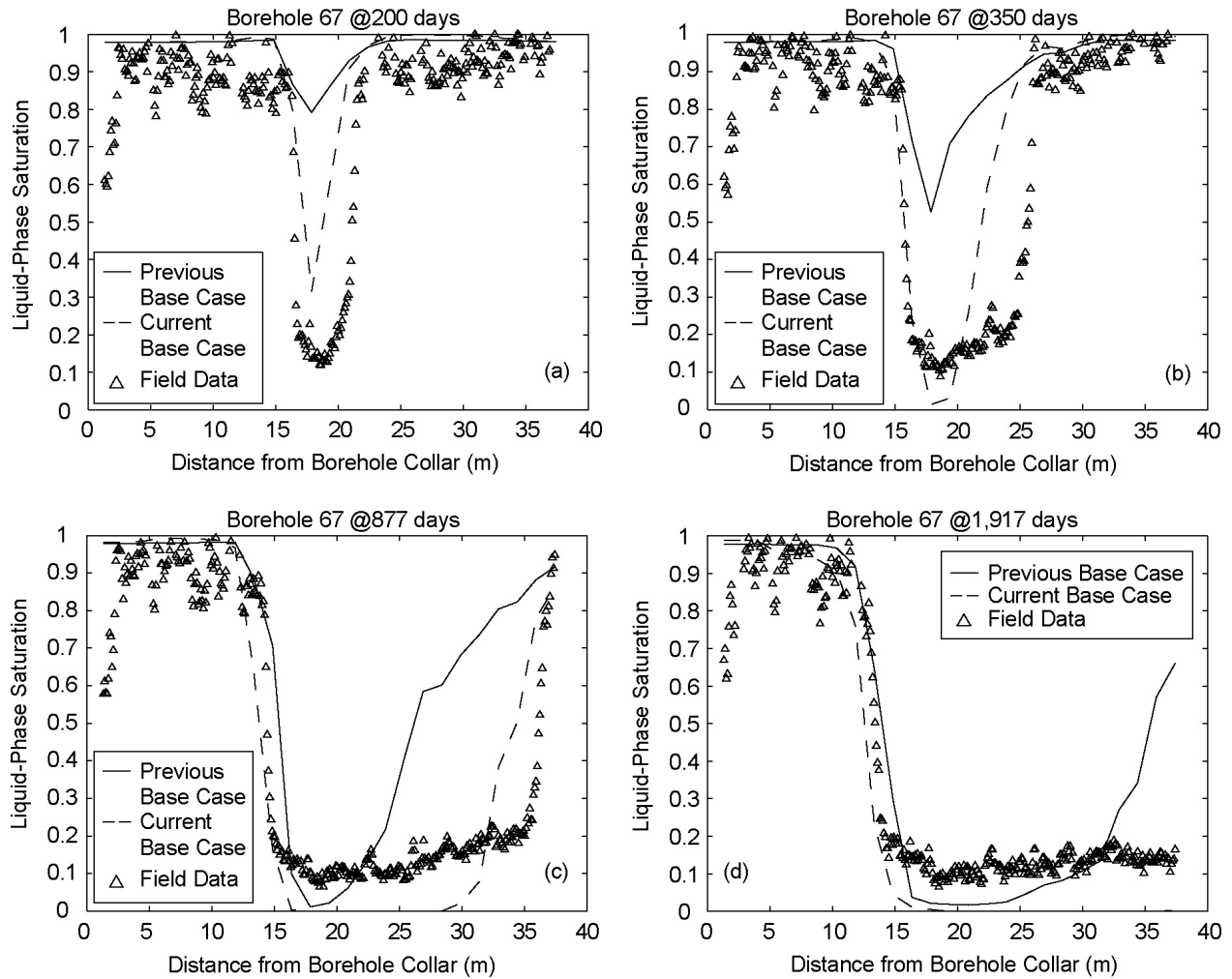
NOTE: HD = Heated Drift. The indicated orientation is relative to the Heated Drift. The source of the coordinates is given in Table 4-1 of CRWMS M&O 1998 [DIRS 111115] (collar coordinates used).



Source: Output DTN: LL0705PA032MST.028; see Table 4.4-2 of the parent report for field data DTNs.

NOTE: The NUFT simulations are for the two indicated cases. The “current base case” uses the updated thermal and hydrologic properties used in the current MSTHM calculations supporting TSPA. The “previous base case” is the base case from Section 7.4.4 of the parent report.

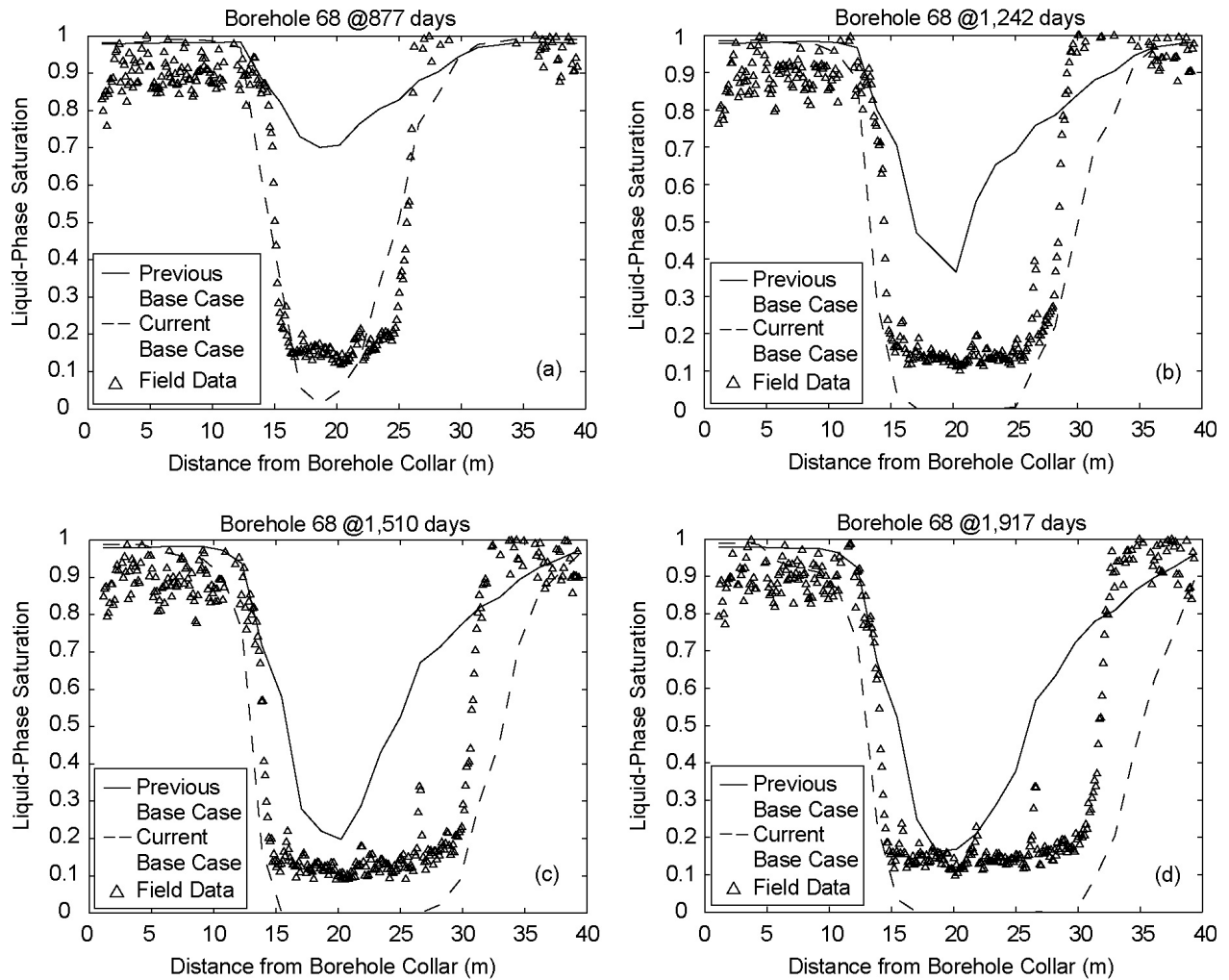
Figure 7.4-33[a]. NUFT-Simulated and Measured Liquid-Phase Saturations in the Matrix Compared along Borehole 66 at (a) 877 Days, (b) 1,242 Days, (c) 1,510 Days, and (d) 1,917 Days



Source: Output DTN: LL0705PA032MST.028; see Table 4.4-2 of the parent report for field data DTNs.

NOTE: The NUFT simulations are for the two indicated cases. The “current base case” uses the updated thermal and hydrologic properties used in the current MSTHM calculations supporting TSPA. The “previous base case” is the base case from Section 7.4.4 of the parent report.

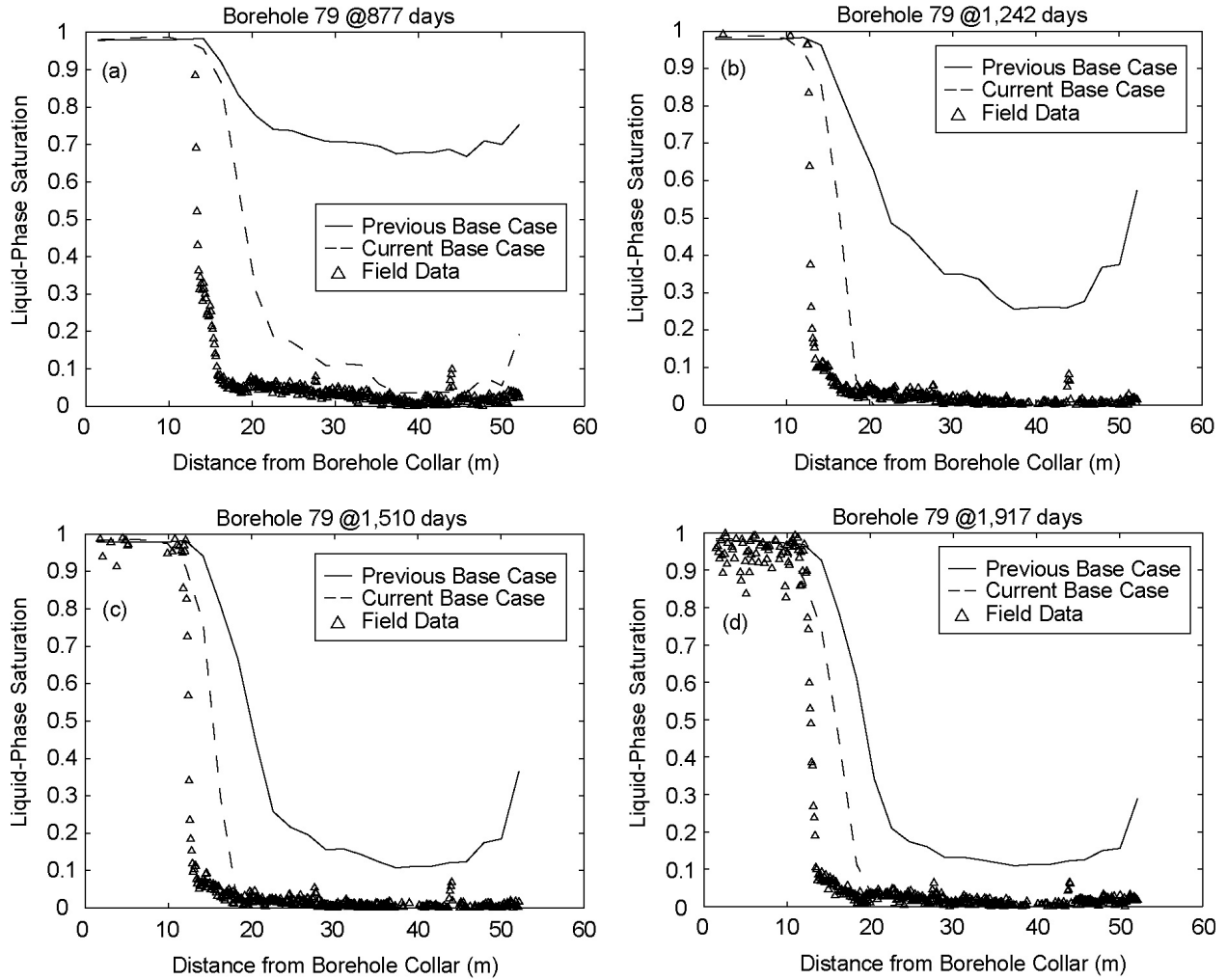
Figure 7.4-34[a]. NUFT-Simulated and Measured Liquid-Phase Saturations in the Matrix Compared along Borehole 67 at (a) 200 Days, (b) 350 Days, (c) 877 Days, and (d) 1,917 Days



Source: Output DTN: LL0705PA032MST.028; see Table 4.4-2 of the parent report for field data DTNs.

NOTE: The NUFT simulations are for the two indicated cases. The “current base case” uses the updated thermal and hydrologic properties used in the current MSTHM calculations supporting TSPA. The “previous base case” is the base case from Section 7.4.4 of the parent report.

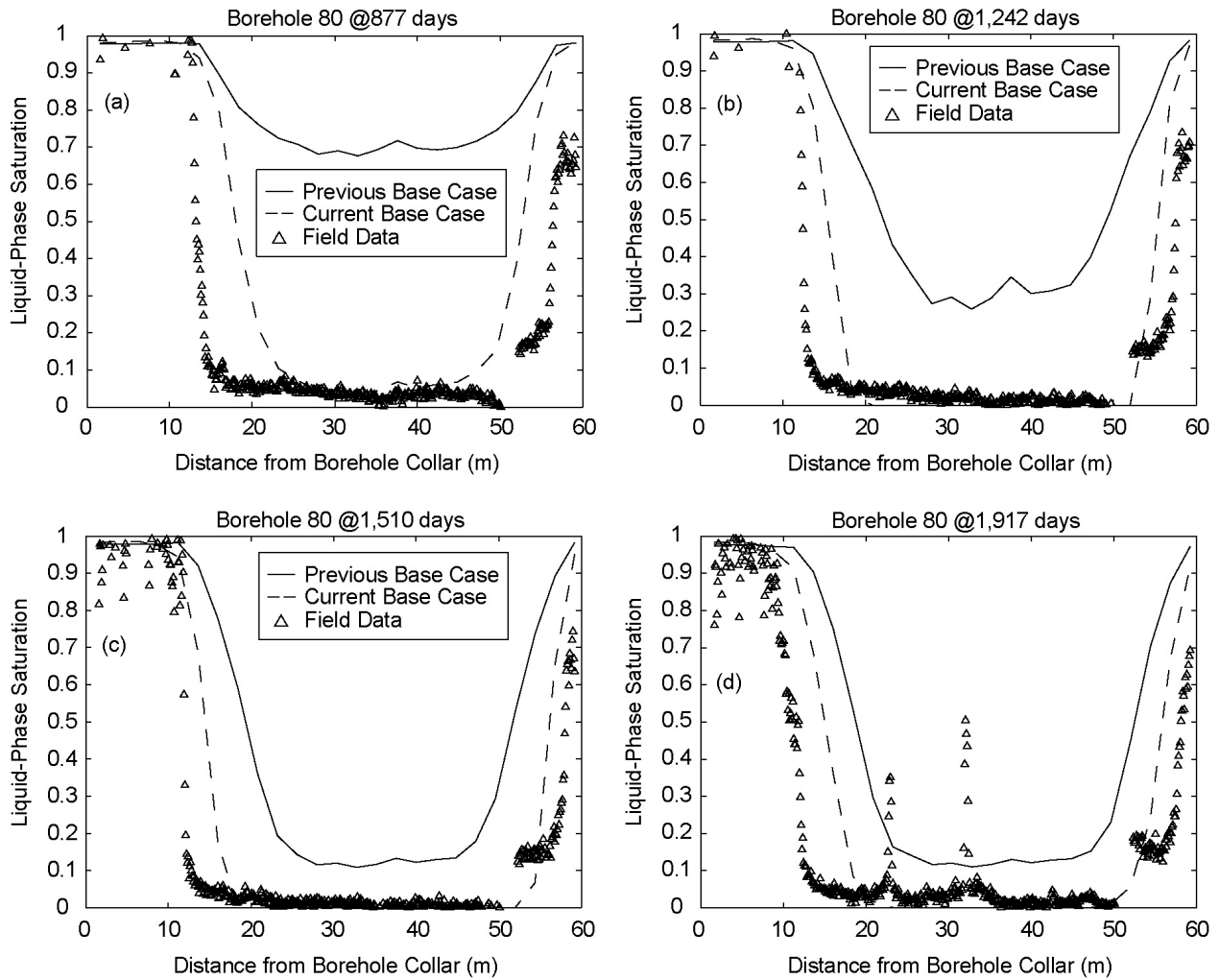
Figure 7.4-35[a]. NUFT-Simulated and Measured Liquid-Phase Saturations in the Matrix Compared along Borehole 68 at (a) 877 Days, (b) 1,242 Days, (c) 1,510 Days, and (d) 1,917 Days



Source: Output DTN: LL0705PA032MST.028; see Table 4.4-2 of the parent report for field data DTNs.

NOTE: The NUFT simulations are for the two indicated cases. The “current base case” uses the updated thermal and hydrologic properties used in the current MSTHM calculations supporting TSPA. The “previous base case” is the base case from Section 7.4.4 of the parent report.

Figure 7.4-36[a]. NUFT-Simulated and Measured Liquid-Phase Saturations in the Matrix Compared along Borehole 79 at (a) 877 Days, (b) 1,242 Days, (c) 1,510 Days, and (d) 1,917 Days



Source: Output DTN: LL0705PA032MST.028; see Table 4.4-2 of the parent report for field data DTNs.

NOTE: The NUFT simulations are for the two indicated cases. The “current base case” uses the updated thermal and hydrologic properties used in the current MSTHM calculations supporting TSPA. The “previous base case” is the base case from Section 7.4.3 of the parent report.

Figure 7.4-37[a]. NUFT-Simulated and Measured Liquid-Phase Saturations in the Matrix Compared along Borehole 80 at (a) 877 Days, (b) 1,242 Days, (c) 1,510 Days, and (d) 1,917 Days

7.4.8[a] Updated Summary of Model Validation Using DST Data

The comparison between NUFT-simulated and field-measured temperatures and liquid-phase saturations is updated by applying the thermal and hydrologic properties used in the current MSTHM calculations supporting the TSPA to the 3-D TH model of the DST. The use of updated thermal and hydrologic properties results in better agreement between the simulated and field-measured temperatures and liquid-phase saturations. The primary cause of this better agreement is the larger matrix permeability in the Ttpmn (tsw34), which is the host-rock unit in which the DST was conducted. Where field-measured temperatures are at or above the boiling point (96°C), the updated 3-D TH model (called the current base case) predicts lower temperatures, which are in better agreement with the field-measured temperatures, than are predicted by the previous base-case 3-D TH model of the DST. The current base case also predicts more rapid rock dry out, and ultimately drier liquid-phase saturations, than are predicted by the previous base case. The more rapid dry out is in better agreement with measured liquid-phase saturation histories.

As discussed in Section 7.4 of the parent report, the agreement between NUFT-simulated and field-measured temperatures and liquid-phase saturations obtained in the previous comparison was sufficient to support the adequacy and accuracy of the MSTHM for its intended use. Improved agreement obtained in the updated comparison further strengthens the validation of the MSTHM, thereby strengthening the case for the adequacy and accuracy of the MSTHM for its intended use in TSPA. This application of data from the DST is consistent with the DOE's position with respect to the Key Technical Issue agreement for *Thermal Effects on Flow (TEF)* 2.01 (Williams 2002 [DIRS 171270]). Whereas limitations on the DST are recognized (e.g., the observed lack of drift seepage) the influence of heat and mass losses through bulkhead is accounted for, and the DST is the largest directly applicable field-scale experiment ever conducted. Note that the Large Block Test is also included in the multiscale thermal-hydrologic model validation (Section 7.3 of the parent report).

7.5[a] COMPARISON OF THE MSTHM RESULTS AGAINST A MONOLITHIC THREE-DIMENSIONAL THERMAL-HYDROLOGIC MODEL

Applicable to this addendum, with the following correction. In the parent report (p. 7-67), the following sentence should refer to Figure 7.5-5 (not Figure 7.5-6), "At the edge, comparison of the MSTHM with case 3 shows relatively small differences (6.5°C to 17.1°C) in peak drip-shield temperature (Figure 7.5-5)."

7.6[a] COMPARISON OF THE MSTHM-PREDICTED IN-DRIFT TEMPERATURE DIFFERENCES AGAINST THOSE PREDICTED BY THE FLUENT CODE

Applicable to this addendum, with no changes required.

7.7[a] VALIDATION SUMMARY

Applicable to this addendum, with updates discussed in Section 7.9[a].

7.8[a] COMPARISON OF THE MSTHM RESULTS AGAINST A THREE-DIMENSIONAL PILLAR-SCALE THERMAL-HYDROLOGICAL MODEL

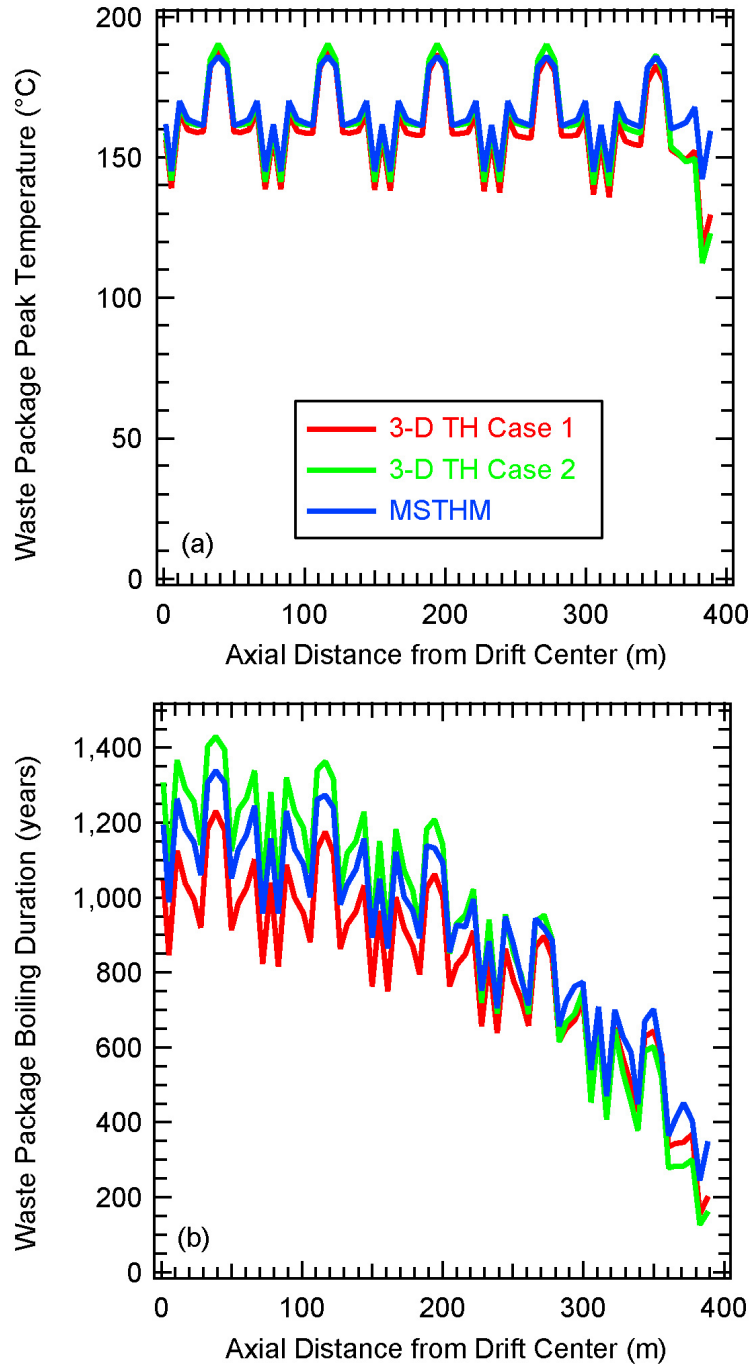
In Section 7.5[a] of the parent report, the MSTHM is validated against a monolithic 3-D TH model for a three-drift model validation test problem, where the emplacement drift half-length is 121.5 m. Because typical emplacement drifts have a half-length of about 400 m, it was decided to conduct a model confidence-building exercise of the MSTHM for a pillar-scale problem where the emplacement drift half-length is on the order of 400 m. Because of the computational expense of conducting TH model calculations with discrete waste packages and drip shields, the three-drift model validation in the parent report lumps the waste package and drip shield into a monolithic heat source, as shown in Figure 7.5-1 of the parent report. The availability of software NUFT v4.0 (Section 3.1.17[a]), which can be run on massively parallel CPU clusters, enables conducting TH model calculations for larger, more computationally demanding problems. Thus, it is now possible to conduct 3-D TH model calculations for problems that include a large number of discretely represented waste packages and drip shields, as is done in the DDT submodel (Section 6.2.17[a]). The cross-sectional geometry is that shown in Figure 6.2-8 of the parent report. Consequently, the pillar-scale model confidence-building test problem includes 71 waste packages (70 full waste packages and a single half waste package) along a drift with a heated half-length of 391.57 m. More specifically, the pillar-scale test problem represents the eight waste packages listed in Table 6.2-6[a], repeating that sequence ten times. The pillar-scale test problem utilizes symmetry in the longitudinal direction, by modeling half of the length of a 783.15-m emplacement drift. It utilizes lateral symmetry by modeling from the midline of the drift to the midline of the pillar, which is 40.5 m away from the drift midline. A half pwr1-1 waste package (Table 6.2-6[a]) is located at the repository center. The waste package sequence in the DDT submodel is reflected ten times from the repository center to the repository edge, with the last waste package being a full pwr1-1 waste package. Thus, the waste package inventory in the pillar-scale test problem includes ten of each of the following waste packages: dhlw-11, pwr2-1, bwr1-1, bwr2-1, dhlw-s1, and pwr1-2; five pwr1-3 waste packages, and five plus one half pwr1-1 waste packages.

The pillar-scale model confidence-building test problem is also conducted with the thermal and hydrologic property values used to conduct the MSTHM calculations supporting the TSPA, which are described in Section 6.3.16[a]. Therefore, both the MSTHM calculations and 3-D pillar-scale TH model calculations apply the drift-scale calibrated property set for the 30th percentile infiltration map (DTN: LB0610UZDSCP30.001 [DIRS 179180]). The test problem also applies the mean host-rock thermal conductivity values from Output DTN: MO0612MEANTHER.000. The pillar-scale test problem applies the thermal and hydrologic stratigraphy used in the LDTH submodel at the g_9 UZ flow model column location, which is close to the repository center in drift P3W-13 (Figure 6.2-17[a]), uniformly throughout the model domain. It also applies the P10 percolation flux conditions for the g_9 location. The P10 percolation flux case at this location is representative of a typical location in the center of the repository for the following reasons. It is within the predominant host-rock unit, which is the Tptpl1 (tsw35) unit, close to the center of the repository area. Moreover, the local P10 percolation flux values, which are 3.6, 6.8, 13.6, and 17.8 mm/yr for the present-day, monsoonal, glacial-transition, and post-10,000-year climates, respectively, are close to the repository-wide averages (4.1, 7.8, 12.2, and 15.9 mm/yr) for the P10 percolation flux case (see Table 6.2-5[a]).

As was done with the three-drift model-validation test problem, heat transfer in the drift by thermal radiation and natural convection are represented with the use of a calibrated effective thermal conductivity versus time relationship. As discussed in Section 6.3.18[a], a 2-D DDTH model, which has a discretely represented waste package and drip shield, is used for the calibration. Because this model produces “target” results, it is called the “target” 2-D DDTH model. The target model represents thermal radiation between the drip shield and drift wall and between the waste package and drip shield and utilizes an effective thermal conductivity for air, which represents the influence of natural convection, on the basis of correlations from the FLUENT-code thermal model in *In-Drift Natural Convection and Condensation* (SNL 2007 [DIRS 181648], Appendix J). The corresponding 2-D DDTH model with calibrated effective (equivalent) thermal conductivity is called the “calibration” model. The agreement in temperature predicted by the target and calibration models demonstrates the effective (equivalent) in-drift thermal conductivity to be a good approximation of the combined influences of thermal radiation and natural convection. This equivalent thermal conductivity relationship is applied to both the 3-D pillar-scale TH model and the DDT submodel used in the MSTHM calculations of the pillar-scale test problem. Both the 3-D pillar-scale TH model and the corresponding DDT submodel utilize the same discretization, which includes one grid-block column per waste package in the longitudinal direction. All of the MSTHM submodels—SMT, SDT, LDTH, and DDT, as well as the 3-D pillar-scale TH model—apply the same constant-temperature boundary condition at the water table. Note that for the MSTHM calculations that support TSPA, the LDTH, SDT, and SMT submodels do not fix the temperature at the water table. For the sake of this test problem, this difference is not significant.

The 3-D pillar-scale TH model is run for two cases. Case 1 allows advective and diffusive vapor transport in the longitudinal direction along the drift. Case 2 does not allow advective and diffusive vapor transport in the longitudinal direction along the drift; however, it does allow advective and diffusive vapor transport in the vertical and lateral directions in the drift. The reason for including Case 2 is to isolate the influence of in-drift longitudinal vapor transport on TH conditions. As discussed in Section 5.7 of the parent report, it is assumed that longitudinal vapor transport has an insignificant effect on TH conditions along emplacement drifts. Case 2 enables the quantification of the influence of this assumption.

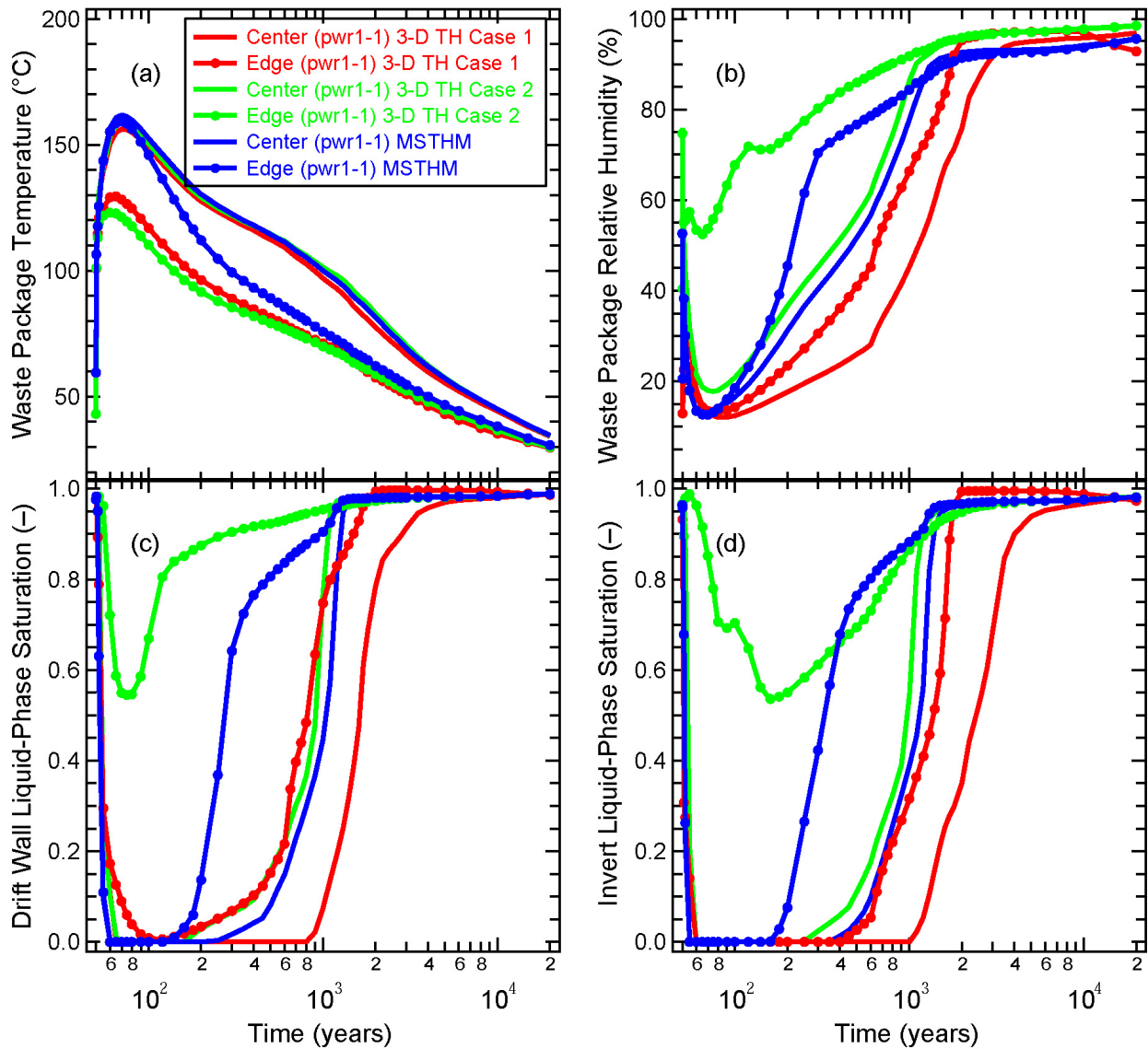
Figure 7.8-1[a] plots the peak waste package temperature and time when boiling ceases on the waste package for all 71 waste packages in the pillar-scale test problem. Figures 7.8-2[a] through 7.8-9[a] plot the TH conditions for all eight waste package types at the repository center and edge. A comparison of Case 1 and 2 in Figure 7.8-1[a] shows the influence of vapor transport along the drift. Vapor is transported from the hotter repository center to the cooler repository edge, where it condenses, resulting in latent heat transport from center to edge. Consequently, latent heat transport causes peak waste package temperatures to be slightly lowered at the repository center and for most of the drift, while slightly increasing peak waste package temperatures for the outermost two waste packages (Figure 7.8-1a[a]). The same pattern is seen along the drift for the time when boiling ceases on the waste package (Figure 7.8-1b[a], comparing the Case 1 and Case 2 curves). The influence of latent heat transport along the drift is even stronger for the boiling duration than for peak temperature.



Source: Output DTN: LL0705PA032MST.028.

NOTE: For the 3-D pillar-scale TH model, Case 1 allows advective and diffusive vapor transport along the drift, while Case 2 does not. These results are for 71 waste packages along an emplacement drift with a heated half-length of 391.57 m. The sequence listed in Table 6.2-6[a] is repeated ten times, starting with the pwr1-1 waste package at the repository center and ending with the pwr1-1 waste package at the repository edge.

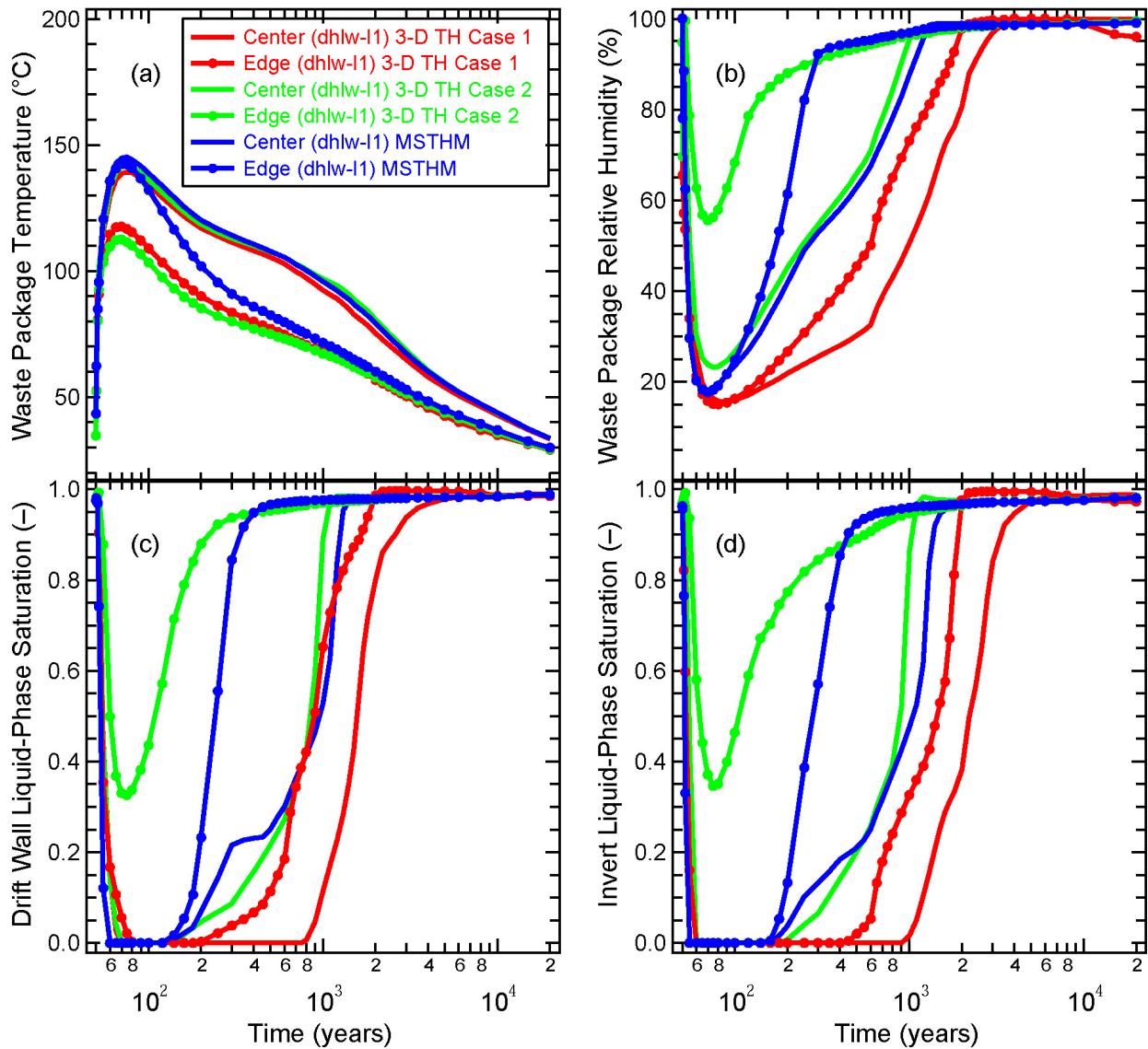
Figure 7.8-1[a]. Thermal-Hydrologic Conditions Predicted by the MSTHM and 3-D Pillar-Scale TH Model Compared along the Drift, Including (a) Peak Waste Package Temperature and (b) Time When Boiling Ceases on the Waste Package



Source: Output DTN: LL0705PA032MST.028.

NOTE: For the 3-D pillar-scale TH model, Case 1 allows advective and diffusive vapor transport along a drift, while Case 2 does not. These results are for the pwr1-1 waste packages located at the repository center and edge. At the repository edge, the pwr1-1 is the outermost waste package.

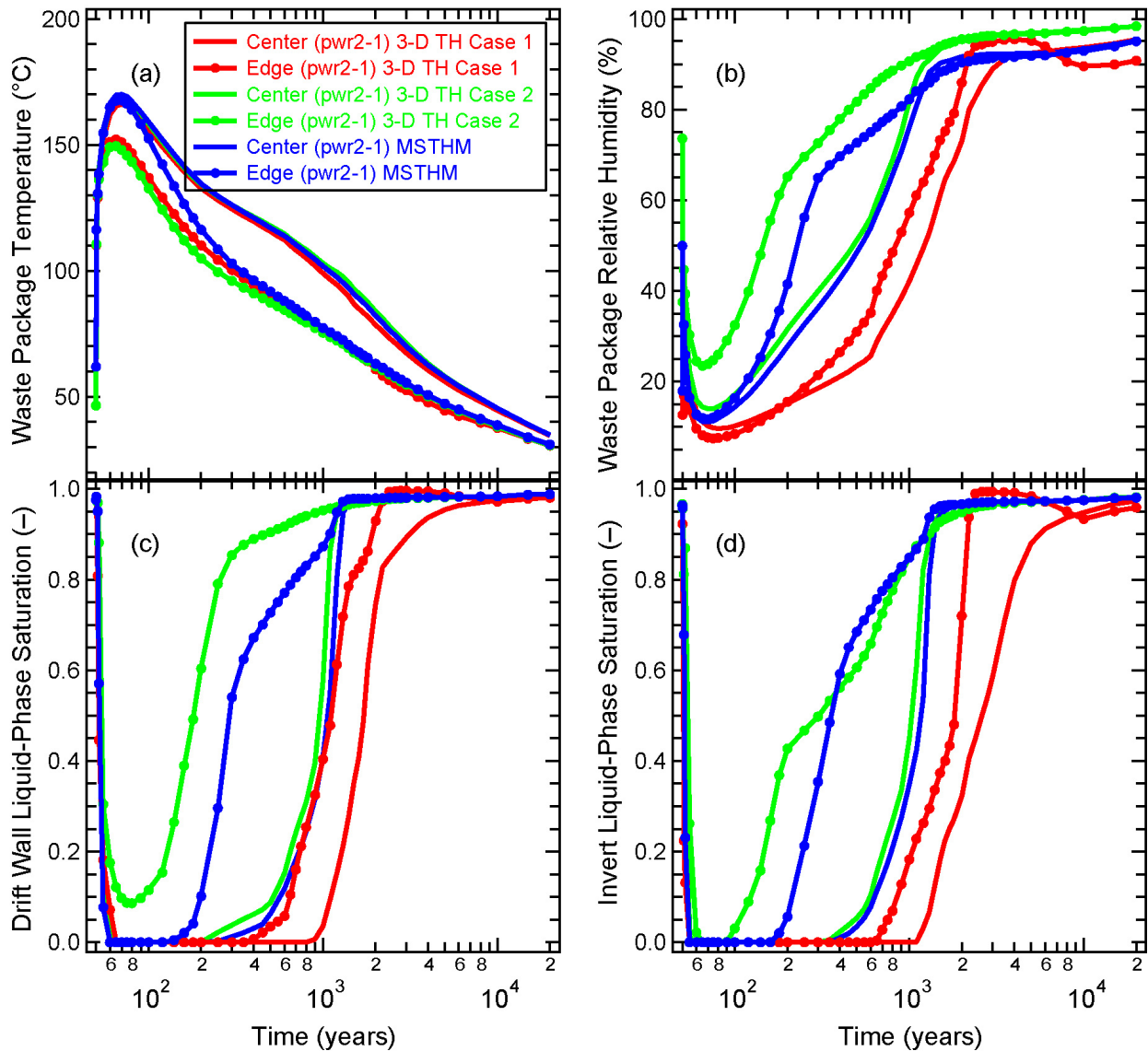
Figure 7.8-2[a]. Thermal-Hydrologic Conditions Predicted by the MSTHM and 3-D Pillar-Scale TH Model Compared at the Repository Center and Edge for the pwr1-1 Waste Package, Including Waste Package (a) Temperature and (b) Relative Humidity, and Liquid-Phase Saturation at the (c) Drift Wall and in the (d) Invert



Source: Output DTN: LL0705PA032MST.028.

NOTE: For the 3-D pillar-scale TH model, Case 1 allows advective and diffusive vapor transport along a drift, while Case 2 does not. These results are for the dhlw-11 waste packages located at the repository center and edge. At the repository edge, the dhlw-11 is the second waste package from the edge.

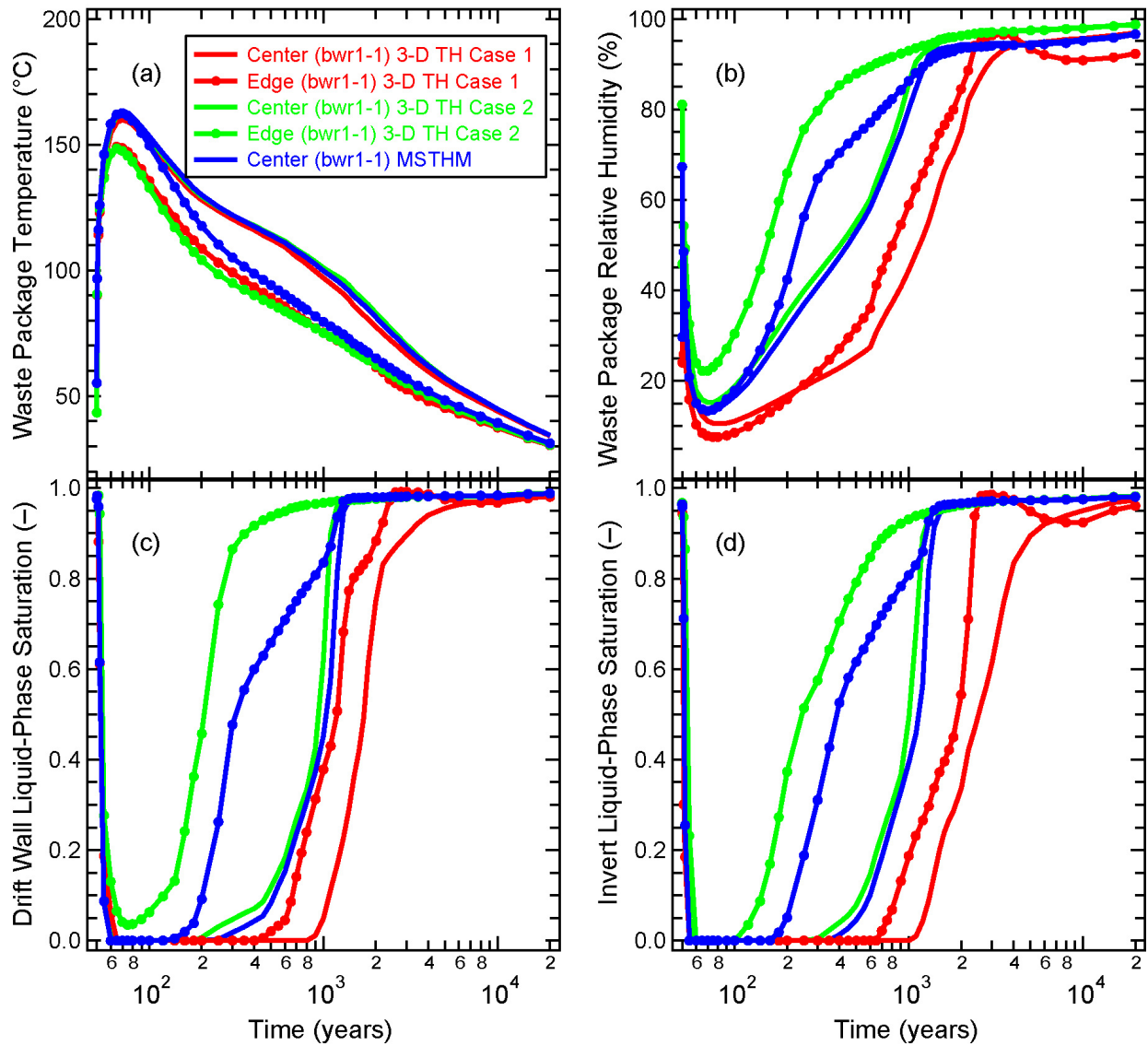
Figure 7.8-3[a]. Thermal-Hydrologic Conditions Predicted by the MSTHM and 3-D Pillar-Scale TH Model Compared at the Repository Center and Edge for the dhlw-11 Waste Package, Including Waste Package (a) Temperature and (b) Relative Humidity, and Liquid-Phase Saturation at the (c) Drift Wall and in the (d) Invert



Source: Output DTN: LL0705PA032MST.028.

NOTE: For the 3-D pillar-scale TH model, Case 1 allows advective and diffusive vapor transport along a drift, while Case 2 does not. These results are for the pwr2-1 waste packages located at the repository center and edge. At the repository edge, the pwr2-1 is the third waste package from the edge.

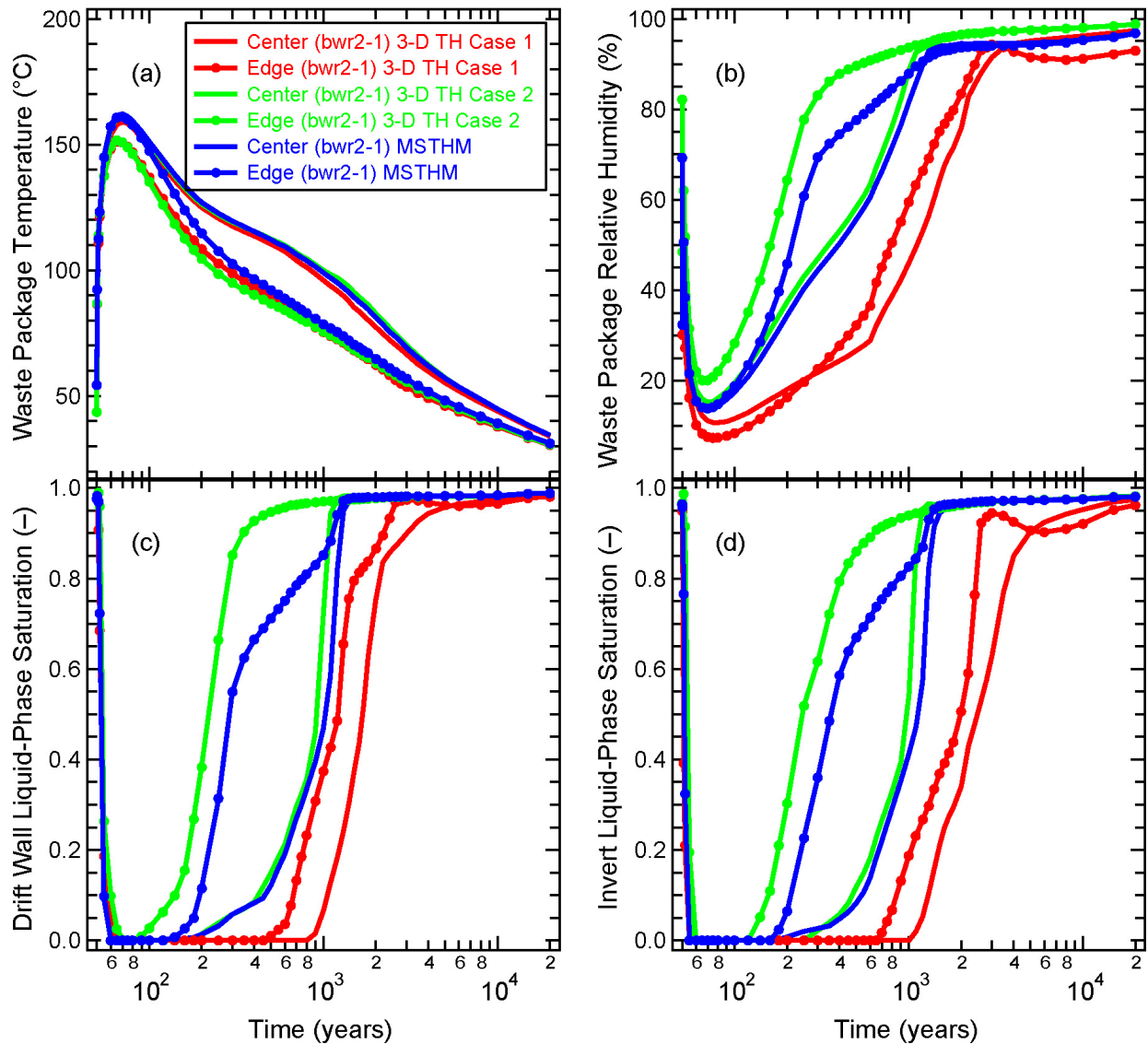
Figure 7.8-4[a]. Thermal-Hydrologic Conditions Predicted by the MSTHM and 3-D Pillar-Scale TH Model Compared at the Repository Center and Edge for the pwr2-1 Waste Package, Including Waste Package (a) Temperature and (b) Relative Humidity, and Liquid-Phase Saturation at the (c) Drift Wall and in the (d) Invert



Source: Output DTN: LL0705PA032MST.028.

NOTE: For the 3-D pillar-scale TH model, Case 1 allows advective and diffusive vapor transport along a drift, while Case 2 does not. These results are for the bwr1-1 waste packages located at the repository center and edge. At the repository edge, the bwr1-1 is the fourth waste package from the edge.

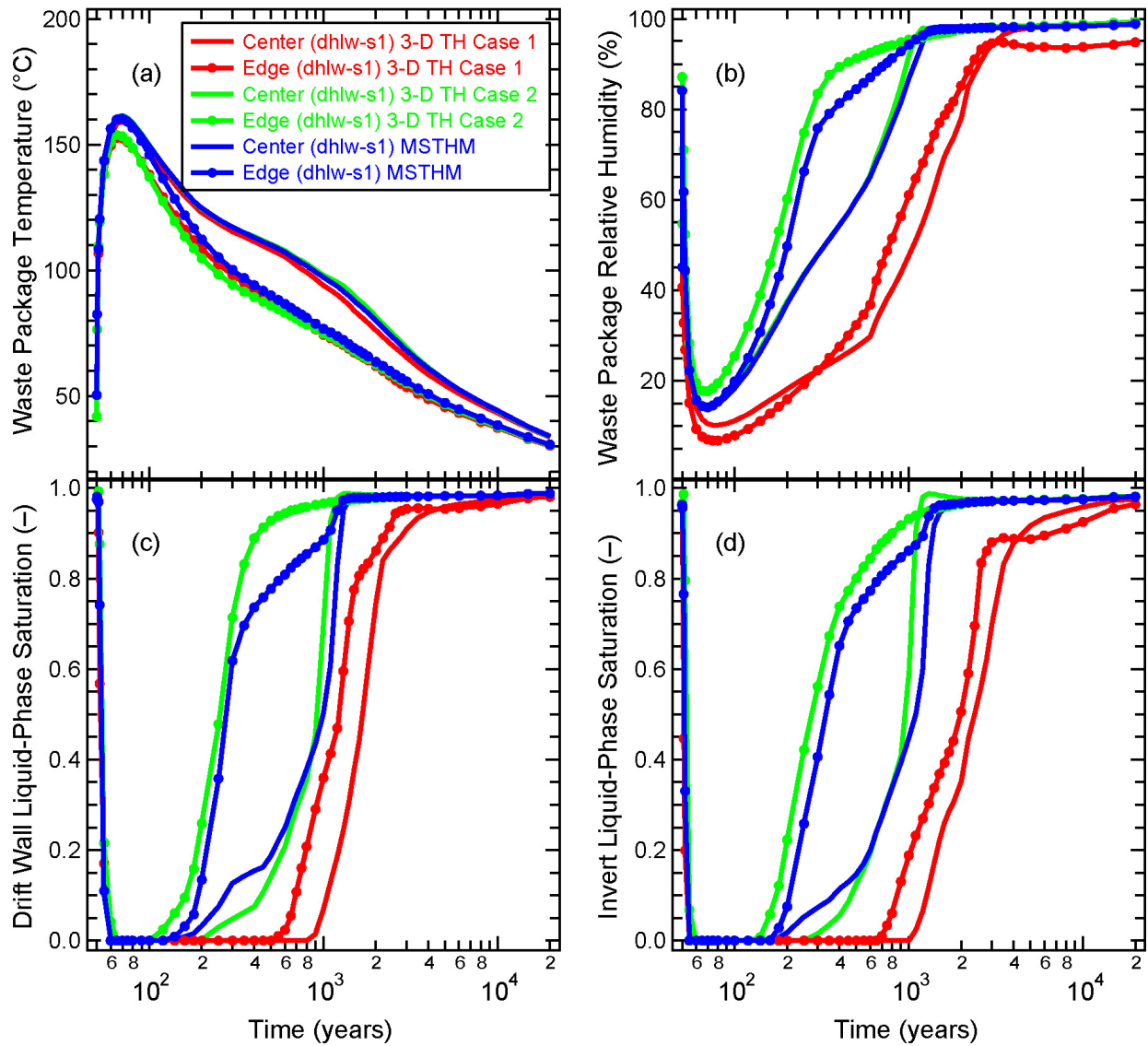
Figure 7.8-5[a]. Thermal-Hydrologic Conditions Predicted by the MSTHM and 3-D Pillar-Scale TH Model Compared at the Repository Center and Edge for the bwr1-1 Waste Package, Including Waste Package (a) Temperature and (b) Relative Humidity, and Liquid-Phase Saturation at the (c) Drift Wall and in the (d) Invert



Source: Output DTN: LL0705PA032MST.028.

NOTE: For the 3-D pillar-scale TH model, Case 1 allows advective and diffusive vapor transport along a drift, while Case 2 does not. These results are for the bwr2-1 waste packages located at the repository center and edge. At the repository edge, the bwr2-1 is the fifth waste package from the edge.

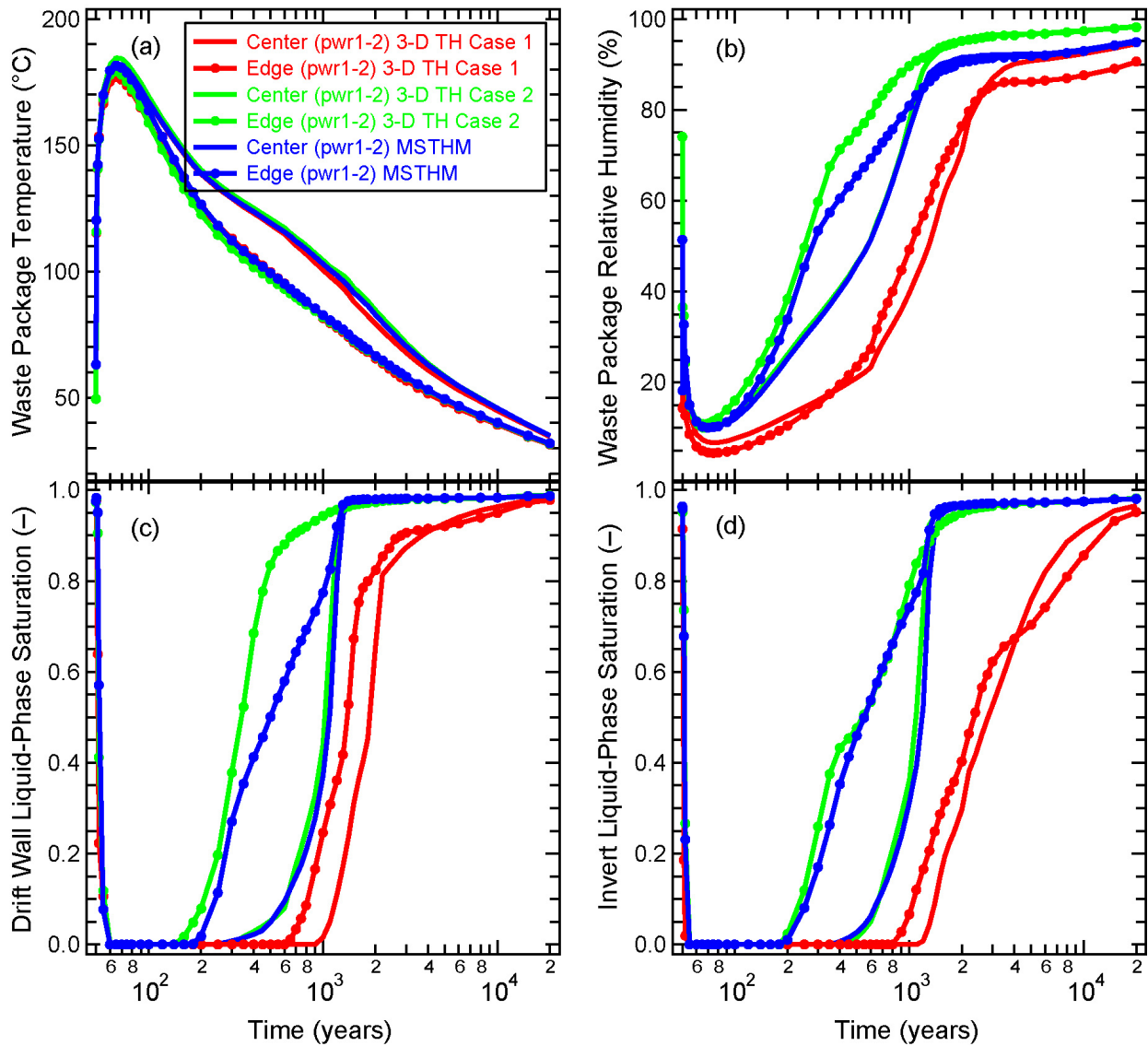
Figure 7.8-6[a]. Thermal-Hydrologic Conditions Predicted by the MSTHM and 3-D Pillar-Scale TH Model Compared at the Repository Center and Edge for the bwr2-1 Waste Package, Including Waste Package (a) Temperature and (b) Relative Humidity, and Liquid-Phase Saturation at the (c) Drift Wall and in the (d) Invert



Source: Output DTN: LL0705PA032MST.028.

NOTE: For the 3-D pillar-scale TH model, Case 1 allows advective and diffusive vapor transport along a drift, while Case 2 does not. These results are for the dhlw-s1 waste packages located at the repository center and edge. At the repository edge, the dhlw-s1 is the sixth waste package from the edge.

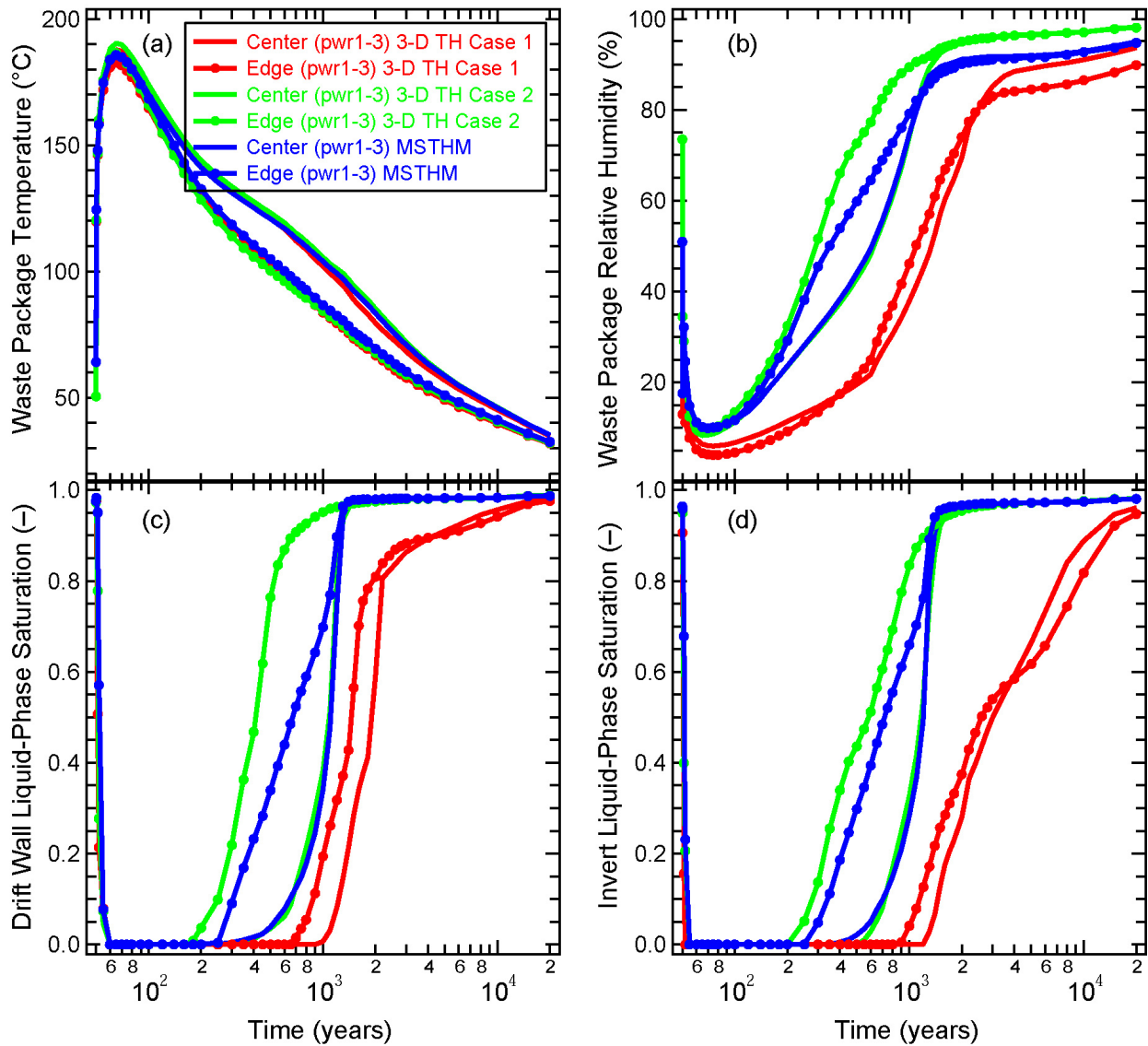
Figure 7.8-7[a]. Thermal-Hydrologic Conditions Predicted by the MSTHM and 3-D Pillar-Scale TH Model Compared at the Repository Center and Edge for the dhlw-s1 Waste Package, Including Waste Package (a) Temperature and (b) Relative Humidity, and Liquid-Phase Saturation at the (c) Drift Wall and in the (d) Invert



Source: Output DTN: LL0705PA032MST.028.

NOTE: For the 3-D pillar-scale TH model, Case 1 allows advective and diffusive vapor transport along a drift, while Case 2 does not. These results are for the pwr1-2 waste packages located at the repository center and edge. At the repository edge, the pwr1-2 is the seventh waste package from the edge.

Figure 7.8-8[a]. Thermal-Hydrologic Conditions Predicted by the MSTHM and 3-D Pillar-Scale TH Model Compared at the Repository Center and Edge for the pwr1-2 Waste Package, Including Waste Package (a) Temperature and (b) Relative Humidity, and Liquid-Phase Saturation at the (c) Drift Wall and in the (d) Invert



Source: Output DTN: LL0705PA032MST.028.

NOTE: For the 3-D pillar-scale TH model, Case 1 allows advective and diffusive vapor transport along a drift, while Case 2 does not. These results are for the pwr1-3 waste packages located at the repository center and edge. At the repository edge, the pwr1-3 is the eighth waste package from the edge.

Figure 7.8-9[a]. Thermal-Hydrologic Conditions Predicted by the MSTHM and 3-D Pillar-Scale TH Model Compared at the Repository Center and Edge for the pwr1-3 Waste Package, Including Waste Package (a) Temperature and (b) Relative Humidity, and Liquid-Phase Saturation at the (c) Drift Wall and in the (d) Invert

Figure 7.8-1[a] (panel “b”) also indicates that for much of the drift, the MSTHM predicts a boiling duration that lies between Case 1 and Case 2. Note that in Case 1, the value of gas-phase dispersivity is 2.5 times greater than the value used in Section 7.5[a]. This was done in an attempt to bound the influence of turbulent natural-convective mixing along the drift. It is possible that further calibration studies with computational fluid dynamics models will better define both the value and time-dependency of the gas-phase dispersivity. When this is done, it likely will result in TH behavior lying between that of Cases 1 and 2 in Figure 7.8-1[a]. Using the current values of dispersivity, Figure 7.8-1[a] shows that the MSTHM is in reasonably close agreement with the 3-D pillar-scale TH model for most of the drift interval, with the MSTHM predicting higher temperatures for the outermost several waste packages. As discussed in Section 7.5 of the parent report, the cause of this overprediction of temperature at the repository edge is the dimensionality of the DDT submodel. The use of an additional, more complex DDT submodel with an unheated portion in the axial direction (i.e., beyond the outermost waste package) would capture the influence of axial heat flow for the outermost two to three waste packages. The implementation of such a DDT submodel in the MSTHM would result in closer agreement in temperatures between the MSTHM and the 3-D pillar-scale TH model.

Figures 7.8-2[a] through 7.8-9[a] show the same relationship between the MSTHM and 3-D pillar-scale TH model. For all eight waste packages, good agreement in temperature is obtained between the MSTHM and 3-D TH model at the repository center. A close inspection of Figures 7.8-2[a] through 7.8-9[a] shows that for the fourth or fifth waste package from the edge, the MSTHM and 3-D TH model are in good agreement. For the outermost three to four waste packages, the MSTHM predicts higher temperatures for early time (including when temperatures peak); however, the agreement improves with time, resulting in good agreement by the time that boiling ceases. From the fourth or fifth waste package from the edge, all the way to the repository center, the relative humidity and liquid-phase saturation histories predicted by the MSTHM agree reasonably well with those of the 3-D TH model for Case 2. However, for the 3-D TH model for Case 1 predicts drier conditions than the MSTHM, which shows the influence of vapor transport, and moisture loss from the heated portion of the emplacement drift. These results show that the assumption concerning longitudinal vapor transport and condensation, which is discussed in Section 5.7 of the parent report, is justified with respect to temperature. However, vapor transport may result in drier conditions than those predicted by the MSTHM.

7.9[a] UPDATED VALIDATION SUMMARY

The intended use of the MSTHM is to predict a reasonable range of possible thermal-hydrologic conditions within emplacement drifts. To do this, the MSTHM range includes the influence of waste package-to-waste package heat output variability relevant to the license application design, as well as the influence of parametric uncertainty and variability in the geologic and hydrologic conditions relevant to predicting the thermal-hydrologic response in emplacement drifts. This goal is quite different from the goal of a model developed to predict a single expected thermal-hydrologic response. Accordingly, the determination of the adequacy and accuracy of the MSTHM is evaluated with respect to its intended purpose, which is to predict a reasonable range of possible thermal-hydrologic conditions within emplacement drifts.

The comparison of the MSTHM with the 3-D pillar-scale TH model strengthens the case for validation of the MSTHM, thereby strengthening the case for its adequacy and accuracy for its intended purpose, because of the following reasons:

- The pillar-scale model confidence-building test case involves a full-scale emplacement drift.
- The pillar-scale model confidence-building test case utilizes the current thermal and hydrologic properties used in the MSTHM calculations supporting TSPA.
- The pillar-scale model confidence-building test case employs a discrete representation of waste packages and drip shields for an entire drift.
- Peak waste package temperatures are in good agreement for most of the drift and reasonably bounded by the MSTHM for the outermost waste packages at the repository edge.
- The time when boiling ceases is in good agreement for most of the drift and in reasonably good agreement for the outermost waste packages at the repository edge.
- Vapor transport along the drift may result in drier conditions than predicted by the MSTHM, which is beneficial with respect to the potential onset of drift seepage.

The updated comparison between the 3-D TH model and the measured data from the DST strengthens the case for validation of the MSTHM, thereby strengthening the case for its adequacy and accuracy for its intended purpose, because of the following reasons:

- The updated TH model used in the comparison with the DST measurements utilizes the current thermal and hydrologic properties used in the MSTHM calculations supporting TSPA.
- The agreement between simulated and measured temperatures is improved since the previous comparison made in the parent report.
- The agreement between simulated and measured liquid-phase saturations is improved since the previous comparison made in the parent report.

In summary, the validation activities performed for the MSTHM establish its adequacy and accuracy for its intended purpose in TSPA.

8[a]. CONCLUSIONS

8.1[a] ANALYSIS AND MODELING CONCLUSIONS

Applicable to this addendum, with no changes required.

8.2[a] MODEL VALIDATION, UNCERTAINTIES, AND LIMITATIONS

Applicable to this addendum, with no changes required.

8.3[a] MODEL OUTPUTS

Applicable to this addendum, with no changes required with the exception of the new output DTNs presented in Table 8-1[a].

Table 8-1[a]. Data Tracking Numbers Associated with the Output Produced by This Addendum

DTN	Title
LL0702PA013MST.068	Input and Output Files for the SMT, SDT and DDT Submodels and MSTHAC Extract Output Files Used in ANL-EBS-MD-000049 Multiscale Thermohydrologic Model
LL0702PA014MST.069	Input and Output Files for the LDTH Submodels and MSTHAC Extract Output Files Used in ANL-EBS-MD-000049 Multiscale Thermohydrologic Model for the Mean Host-Rock Thermal Conductivity, 10-Percentile Percolation Flux Case
LL0702PA015MST.070 ^a	Output for ANL-EBS-MD-000049 Multiscale Thermohydrologic Model for the Mean Host-Rock Thermal Conductivity, 10-Percentile Percolation Flux Case
LL0702PA016MST.071	Input and Output Files for the LDTH Submodels and MSTHAC Extract Output Files Used in ANL-EBS-MD-000049 Multiscale Thermohydrologic Model for the Mean Host-Rock Thermal Conductivity, 30-Percentile Percolation Flux Case
LL0702PA017MST.072 ^a	Output for ANL-EBS-MD-000049 Multiscale Thermohydrologic Model for the Mean Host-Rock Thermal Conductivity, 30-Percentile Percolation Flux Case
LL0702PA018MST.073	Input and Output Files for the LDTH Submodels and MSTHAC Extract Output Files Used in ANL-EBS-MD-000049 Multiscale Thermohydrologic Model for the Mean Host-Rock Thermal Conductivity, 50-Percentile Percolation Flux Case
LL0702PA019MST.074 ^a	Output for ANL-EBS-MD-000049 Multiscale Thermohydrologic Model for the Mean Host-Rock Thermal Conductivity, 50-Percentile Percolation Flux Case
LL0702PA020MST.075	Input and Output Files for the LDTH Submodels and MSTHAC Extract Output Files Used in ANL-EBS-MD-000049 Multiscale Thermohydrologic Model for the Mean Host-Rock Thermal Conductivity, 90-Percentile Percolation Flux Case
LL0702PA021MST.076 ^a	Output for ANL-EBS-MD-000049 Multiscale Thermohydrologic Model for the Mean Host-Rock Thermal Conductivity, 90-Percentile Percolation Flux Case
LL0702PA022MST.077	Input and Output Files for the LDTH Submodels and MSTHAC Extract Output Files Used in ANL-EBS-MD-000049 Multiscale Thermohydrologic Model for the Low Host-Rock Thermal Conductivity, 10-Percentile Percolation Flux Case
LL0702PA023MST.078 ^a	Output for ANL-EBS-MD-000049 Multiscale Thermohydrologic Model for the Low Host-Rock Thermal Conductivity, 10-Percentile Percolation Flux Case
LL0702PA024MST.079	Input and Output Files for the LDTH Submodels and MSTHAC Extract Output Files Used in ANL-EBS-MD-000049 Multiscale Thermohydrologic Model for the High Host-Rock Thermal Conductivity, 90-Percentile Percolation Flux Case

Table 8-1[a]. Data Tracking Numbers Associated with the Output Produced by This Addendum (Continued)

DTN	Title
LL0702PA025MST.080 ^a	Output for ANL-EBS-MD-000049 Multiscale Thermohydrologic Model for the High Host-Rock Thermal Conductivity, 90-Percentile Percolation Flux Case
LL0702PA026MST.081	Input and Output Files for LDTH and DDT Submodels, and Corresponding MSTHAC Extract Files, for Mean Host-Rock Thermal Conductivity, 10-Percentile Percolation Flux, Collapsed-Drift, High and Low Rubble Thermal Conductivity Cases in ANL-EBS-MD-000049 Multiscale Thermohydrologic Model Calculations
LL0702PA027MST.082	Output for ANL-EBS-MD-000049 Multiscale Thermohydrologic Model for the Mean Host-Rock Thermal Conductivity, 10-Percentile Percolation Flux, Collapsed-Drift, High and Low Rubble Thermal Conductivity Cases
LL0702PA028MST.083	Input and Output Files for the LDTH Submodels and the Corresponding MSTHAC Extract Output Files for the High Host-Rock Thermal Conductivity (HKT), 10-Percentile Percolation (P10H) Case Used in ANL-EBS-MD-000049 Multiscale Thermohydrologic Model Calculations. Submittal date: 02/15/2007
LL0702PA029MST.084 ^a	Output for ANL-EBS-MD-000049 Multiscale Thermohydrologic Model for the Low Host-Rock Thermal Conductivity, 10-Percentile Percolation Flux Case
LL0702PA030MST.085	Plots of MSTHAC Output Files and of LDTH-, SDT-, SMT-, and DDT-Submodel Output Files from ANL-EBS-MD-000049 Multiscale Thermohydrologic Model
LL0703PA011MST.006 ^a	Output for ANL-EBS-MD-000049 REV 04 Multiscale Thermohydrologic Model for the Mean Host-Rock Thermal Conductivity, 10-Percentile Percolation Flux Case
LL0703PA012MST.007 ^a	Output for ANL-EBS-MD-000049 REV 04 Multiscale Thermohydrologic Model for the Mean Host-Rock Thermal Conductivity, 30-Percentile Percolation Flux Case
LL0703PA013MST.008 ^a	Output for ANL-EBS-MD-000049 REV 04 Multiscale Thermohydrologic Model for the Mean Host-Rock Thermal Conductivity, 50-Percentile Percolation Flux Case
LL0703PA014MST.009 ^a	Output for ANL-EBS-MD-000049 REV 04 Multiscale Thermohydrologic Model for the Mean Host-Rock Thermal Conductivity, 90-Percentile Percolation Flux Case
LL0703PA015MST.010 ^a	Output for ANL-EBS-MD-000049 REV 04 Multiscale Thermohydrologic Model for the Low Host-Rock Thermal Conductivity, 10-Percentile Percolation Flux Case
LL0703PA016MST.011 ^a	Output for ANL-EBS-MD-000049 REV 04 Multiscale Thermohydrologic Model for the High Host-Rock Thermal Conductivity, 90-Percentile Percolation Flux Case
LL0703PA017MST.012 ^a	Output for ANL-EBS-MD-000049 REV 04 Multiscale Thermohydrologic Model for the High Host-Rock Thermal Conductivity, 10-Percentile Percolation Flux Case
LL0703PA026MST.013	Weighting Factors for Low (10th-percentile), Mean and High (90th-percentile) Host-Rock Thermal Conductivity Cases from ANL-EBS-MD-000049 Multiscale Thermohydrologic Model
LL0703PA034MST.016 ^a	Output for ANL-EBS-MD-000049 Multiscale Thermohydrologic Model for the Low Host-Rock Thermal Conductivity, 90-Percentile Percolation Flux (P90L) Case
LL0703PA035MST.017 ^a	Output for ANL-EBS-MD-000049 Multiscale Thermohydrologic Model for the High Host-Rock Thermal Conductivity, 30-Percentile Percolation Flux (P30H) Case
LL0703PA036MST.018 ^a	Output for ANL-EBS-MD-000049 Multiscale Thermohydrologic Model for the Low Host-Rock Thermal Conductivity, 50-Percentile Percolation Flux (P50L) Case
LL0703PA037MST.019 ^a	Output for ANL-EBS-MD-000049 Multiscale Thermohydrologic Model for the High Host-Rock Thermal Conductivity, 50-Percentile Percolation Flux (P50H) Case
LL0703PA038MST.020 ^a	Output for ANL-EBS-MD-000049 Multiscale Thermohydrologic Model for the Low Host-Rock Thermal Conductivity, 90-Percentile Percolation Flux (P90L) Case
LL0703PA053MST.021	Selecting the Most Representative Calculated MSTHM Uncertainty Cases to Serve as Surrogates for Non-Calculated MSTHM Uncertainty Cases for ANL-EBS-MD-000049 Multiscale Thermohydrologic Model (MSTHM)

Table 8-1[a]. Data Tracking Numbers Associated with the Output Produced by This Addendum (Continued)

DTN	Title
LL0704PA003MST.022	Input- and Output-File Preparation Scripts and Output-Plotting Scripts for NUFT Submodels and MSTHAC Calculations for ANL-EBS-MD-000049 Multiscale Thermohydrologic Model (MSTHM)
LL0705PA032MST.028	Model-Confidence Building and Sensitivity Studies for ANL-EBS-MD-000049 Multiscale Thermohydrologic Model (MSTHM)
LL0705PA038MST.030	Model Preparation and Analysis Files for ANL-EBS-MD-000049 Multiscale Thermohydrologic Model (MSTHM)
LL070701823122.083	Impact Analysis for ANL-EBS-MD-000049 Multiscale Thermohydrologic Model (MSTHM) for the mean host-rock thermal conductivity, 10-percentile (P10) percolation flux case
MO0505SPAROCKM.000	Rock Mass and Invert Properties for TSPA-LA
MO0612MEANTHER.000	Mean Thermal Conductivity of Yucca Mountain Repository Units
MO0702PAGLOBAL.000	Global 10th and 90th Percentile Mean Thermal Conductivity of Yucca Mountain Repository Units
MO0703PAHYTHRM.000	Hydrological and Thermal Properties of the Invert
MO0703PARUBBLE.000	Effective Thermal Conductivity for Rubble

^a The invert relative humidity is calculated by TSPA, similar to the MathCad calculation described in Appendix XV of the parent report (Equation XV-35), based on the MSTHM-predicted temperature and liquid-phase saturation in the invert.

8.4[a] YUCCA MOUNTAIN REVIEW PLAN ACCEPTANCE CRITERIA

The MSTHM report presents results that directly pertain to the quantity and chemistry of water contacting the engineered barriers and waste forms as described in *Yucca Mountain Review Plan, Final Report* (NRC 2003 [DIRS 163274], Section 2.2.1.3.3.3). The YMRP acceptance criteria for this category are:

8.4.1[a] Acceptance Criterion 1 – System Description and Model Integration Are Adequate

- (1) Total system performance assessment adequately incorporates important design features, physical phenomena, and couplings, and uses consistent and appropriate assumptions throughout the quantity and chemistry of water contacting engineered barriers and waste forms abstraction process.

This addendum implements the same design features, physical phenomena, and couplings as the parent report. The only difference is that two reports have been updated and their results applied to recalculated MSTHM results for *Simulation of Net Infiltration for Present-Day and Potential Future Climates* (SNL 2007 [DIRS 174294]) and *UZ Flow Models and Submodels* (SNL 2007 [DIRS 175177]). In addition, the Drift Scale Test validation comparison has been updated using new estimates of thermal and hydrologic properties of the rock (Section 7.4[a]) and a new, more realistic three-dimensional validation problem representing a full repository drift has been added (Section 7.8[a]). The new three-dimensional problem is qualified for use to represent transient condensation processes in *In-Drift Convection and Condensation* (SNL 2007 [DIRS 181648]). Model results subject to recent design changes are addressed in Section 6.3.19[a].

- (2) The abstraction of the quantity and chemistry of water contacting engineered barriers and waste forms uses assumptions, technical bases, data, and models that are appropriate and consistent with other related U.S. Department of Energy abstractions.

The assumptions, bases, data, and modeling approaches used in the MSTHM are consistent with other abstractions as described in Section 8.4 of the parent report.

- (3) Important design features, such as waste package design and material selection, backfill, drip shield, ground support, thermal loading strategy, and degradation processes, are adequate to determine the initial and boundary conditions for calculations of the quantity and chemistry of water contacting engineered barriers and waste forms.

The design features represented in the MSTHM are adequate to describe the quantity and chemistry of water contacting engineered barriers and waste forms as described in the parent report (Section 8.4 of the parent report). Model results subject to recent design changes are addressed in Section 6.3.19[a].

- (4) Spatial and temporal abstractions appropriately address physical couplings (thermal-hydrologic-mechanical-chemical).

The treatment of physical couplings in this addendum, as in the parent report, is consistent with the treatment of FEPs implemented in TSPA (SNL 2007 [DIRS 179476]).

- (5) Sufficient technical bases and justification are provided for total system performance assessment assumptions and approximations for modeling coupled thermal-hydrologic-mechanical-chemical effects on seepage and flow, the waste package chemical environment, and the chemical environment for radionuclide release. The effects of distribution of flow on the amount of water contacting the engineered barriers and waste forms are consistently addressed, in all relevant abstractions.

The assumptions and technical approaches used in the MSTHM for modeling coupled process effects on seepage and flow are consistent with other abstractions and with the treatment of FEPs for TSPA (SNL 2007 [DIRS 179476]).

- (6) The expected ranges of environmental conditions within the waste package emplacement drifts, inside the breached waste packages, and contacting the waste forms and their evolution with time are identified.

Information from the MSTHM, as updated in this addendum, is provided to TSPA for description of environmental conditions in the drifts and their evolution with time. Updated results are presented in Section 6.3[a].

- (7) The model abstraction for quantity and chemistry of water contacting engineered barriers and waste forms is consistent with the detailed information on engineered barrier design and other engineered features.

Important design features are included in the MSTHM as described in the parent report (Section 8.4). The impacts from certain deviations from the current repository design are evaluated in Sections 6.2.21[a] and 6.3.19[a].

- (8) Adequate technical bases are provided, including activities such as independent modeling, laboratory or field data, or sensitivity studies, for inclusion of any thermal-hydrologic-mechanical-chemical couplings and features, events, and processes.

This sub-criterion is addressed by the parent report, particularly in Section 7 (model validation). Additional validation information is presented in Section 7[a].

- (9) Performance-affecting processes that have been observed in thermal-hydrologic tests and experiments are included into the performance assessment.

Simulations of the Large Block Test and Drift Scale Test are presented in the parent report. In addition, this addendum updates the simulation of the Drift Scale Test using current estimates for thermal and hydrologic properties of the rock (Section 7.4[a]).

- (12) Guidance in NUREG-1297 and NUREG-1298 (Altman et al. 1988 [DIRS 103597]; Altman et al. 1988 [DIRS 103750]), or other acceptable approaches, is followed.

Data qualification status is addressed in this addendum (Section 4.1[a]) through application of the implementing procedure SCI-PRO-006.

8.4.2[a] Acceptance Criterion 2 – Data Are Sufficient for Model Justification

- (1) Geological, hydrological, and geochemical values used in the license application are adequately justified. Adequate description of how the data were used, interpreted, and appropriately synthesized into the parameters is provided.

This addendum extracts host-rock thermal conductivity values from a geostatistical model, evaluates the influence of thermal conductivity on predicted temperatures, and assigns weights for implementation in TSPA (Section 6.2.13.3[a]). In addition, improved values for effective thermal conductivity of drift-collapse rubble are developed (Appendix XI[a]). Hydrologic properties for the host-rock units are based on updated information from *UZ Flow Models and Submodels* (SNL 2007 [DIRS 175177]). Use of a simplified thermal and hydrologic stratigraphy in thermal-hydrologic modeling is justified in Section 6.2.16[a].

- (2) Sufficient data were collected on the characteristics of the natural system and engineered materials to establish initial and boundary conditions for conceptual models of thermal-hydrological-mechanical-chemical coupled processes that affect seepage and flow and the engineered barrier chemical environment.

The acquired data relied upon to represent characteristics of the natural system and engineered materials are unchanged from the parent report (Section 8.4).

- (3) Thermal-hydrologic tests were designed and conducted with the explicit objectives of observing thermal-hydrologic processes for the temperature ranges expected for repository conditions and making measurements for mathematical models. Data are sufficient to verify that thermal-hydrologic conceptual models address important thermal-hydrologic phenomena.

This addendum relies on the same thermal-hydrologic tests described in the parent report (Section 7) supplemented by additional analyses using updated rock properties (Section 7.4.8[a]).

- (4) Sufficient information to formulate the conceptual approach(es) for analyzing water contact with the drip shield, engineered barriers, and waste forms is provided.

As developed in the parent report (Section 6.3) the multiscale model provides temperature and humidity conditions used to describe the environments on the drip shield, waste forms, and other engineered barriers.

8.4.3[a] Acceptance Criterion 3 – Data Uncertainty Is Characterized and Propagated through the Model Abstraction

- (1) Models use parameter values, assumed ranges, probability distributions, and bounding assumptions that are technically defensible, reasonably account for uncertainties and variabilities, and do not result in an under-representation of the risk estimate.

As identified in the parent report (Section 6.3), the multiscale modeling approach represents the effects from key parameter uncertainties for thermal-hydrologic performance of the repository: the percolation flux and host-rock thermal conductivity. The important sources of variability are also represented, namely the proximity of waste package locations to the repository edges, and the local variability of heat output from package to package. These features of the multiscale model are unchanged from the parent report, except that updated percolation flux data are used (Section 4.1[a]), and a new procedure is used for choosing weighted values for host-rock thermal conductivity (Section 6.2.13.3[a]).

- (2) Parameter values, assumed ranges, probability distributions, and bounding assumptions used in the total system performance assessment calculations of quantity and chemistry of water contacting engineered barriers and waste forms are technically defensible and reasonable, based on data from the Yucca Mountain region (e.g., results from large block and drift-scale heater and niche tests), and a combination of techniques that may include laboratory experiments, field measurements, natural analog research, and process-level modeling studies.

This addendum presents improved derivation of values for the host-rock thermal conductivity (Section 6.2.13.3[a]) and rubble thermal conductivity (Section 6.2.13.5[a]) parameters. The applicability of key multiscale modeling assumptions pertaining to axial transport of water vapor in the drifts (Section 5.7 of the parent report) is further evaluated using an improved three-dimensional thermal-hydrologic model (Section 7.8[a]).

- (3) Input values used in the total system performance assessment calculations of quantity and chemistry of water contacting engineered barriers (e.g., drip shield and waste package) are consistent with the initial and boundary conditions and the assumptions of the conceptual models and design concepts for the Yucca Mountain site. Correlations between input values are appropriately established in the U.S. Department of Energy total system performance assessment. Parameters used to define initial conditions, boundary conditions, and computational domain in sensitivity analyses involving coupled thermal-hydrologic-mechanical-chemical effects on seepage and flow, the waste package chemical environment, and the chemical environment for radionuclide release, are consistent with available data. Reasonable or conservative ranges of parameters or functional relations are established.

Input values used in this addendum are consistent with other inputs used to represent the in-drift environment in TSPA. A notable example is the percolation flux information conveyed to TSPA by the multiscale model that is consistent with *UZ Flow Models and Submodels* (SNL 2007 [DIRS 175177]) with certain simplifications used to represent temperature and humidity conditions and far-field properties (Sections 6.2.12[a] and 6.3.15[a]). Other examples are the percolation flux, thermal loading, and host-rock thermal conductivity parameter sets used in the multiscale model, which are also used by the near-field chemistry model for representing seepage composition (SNL 2007 [DIRS 177404]).

- (4) Adequate representation of uncertainties in the characteristics of the natural system and engineered materials is provided in parameter development for conceptual models, process-level models, and alternative conceptual models. The U.S. Department of Energy may constrain these uncertainties using sensitivity analyses or conservative limits. For example, the U.S. Department of Energy demonstrates how parameters used to describe flow through the engineered barrier system bound the effects of backfill and excavation-induced changes.

Uncertainties in host-rock thermal conductivity are propagated to TSPA (Section 6.2.13.3[a]). Simplifications in representing unsaturated-zone stratigraphy are justified using sensitivity analyses (Section 6.2.12[a]). Invert properties are represented using point values for thermal and hydrologic properties, based on sensitivity analyses (Sections 6.2.13.2[a] and 6.3.14[a]; Appendix X[a]). A conservative range is used to represent uncertainty in the effective thermal conductivity of drift-collapse rubble (Appendix XI[a]).

8.4.4[a] Acceptance Criterion 4 – Model Uncertainty Is Characterized and Propagated through the Model Abstraction

- (1) Alternative modeling approaches of features, events, and processes are considered and are consistent with available data and current scientific understanding, and the results and limitations are appropriately considered in the abstraction.

This addendum presents model output based on the same approach to propagation of uncertainty developed in the parent report.

- (2) Alternative modeling approaches are considered and the selected modeling approach is consistent with available data and current scientific understanding. A description that includes a discussion of alternative modeling approaches not considered in the final analysis and the limitations and uncertainties of the chosen model is provided.

Alternative modeling approaches are used in the multiscale validation strategy (Section 7 of the parent report). These results are updated in this addendum with the use of an improved three-dimensional thermal-hydrologic simulation (Section 7.8[a]).

- (3) Consideration of conceptual-model uncertainty is consistent with available site characterization data, laboratory experiments, field measurements, natural analog information and process-level modeling studies; and the treatment of conceptual-model uncertainty does not result in an under-representation of the risk estimate.

This addendum relies on the same approach to conceptual model uncertainty developed in the parent report.

- (4) Adequate consideration is given to effects of thermal-hydrologic-mechanical-chemical coupled processes in the assessment of alternative conceptual models.

The treatment of thermally driven coupled processes in this addendum is consistent with the parent report, and also with the screening of FEPs for TSPA (SNL 2007 [DIRS 179476]).

- (5) If the U.S. Department of Energy uses an equivalent continuum model for the total system performance assessment abstraction, the models produce conservative estimates of the effects of coupled thermal-hydrologic-mechanical-chemical processes on calculated compliance with the postclosure public health and environmental standards.

The equivalent continuum modeling approach is not used in the multiscale model results presented in this addendum or in the parent report.

8.4.5[a] Acceptance Criterion 5 – Model Abstraction Output Is Supported by Objective Comparisons

- (1) The models implemented in this total system performance assessment abstraction provide results consistent with output from detailed process-level models and/or empirical observations (laboratory and field testing and/or natural analogs).

This addendum compares the multiscale approach with an improved three-dimensional thermal-hydrologic numerical validation problem (Section 7.8[a]), supplementing the alternative model comparisons provided in the parent report (Section 7 of the parent report).

- (3) Accepted and well-documented procedures are used to construct and test the numerical models that simulate coupled thermal-hydrologic-mechanical-chemical effects on seepage and flow, engineered barrier chemical environment, and the chemical environment for radionuclide release. Analytical and numerical models are appropriately supported. Abstracted model results are compared with different mathematical models, to judge robustness of results.

This addendum and the parent report implement thermal-hydrologic modeling concepts that have been developed and published over a period of more than 10 years (Buscheck 1996 [DIRS 100658]; Buscheck et al. 2002 [DIRS 160749]; Buscheck et al. 2003 [DIRS 164638]). Thermal-hydrologic simulation technology has been used extensively to model geothermal systems (BSC 2005 [DIRS 174101]). The NUFT software used in this work (Section 3.1.1.9[a]) has been tested and documented in accordance with accepted software qualification procedures.

8.5[a] MSTHM CONDITION REPORTS

8.5.1[a] CR-6521 – Incorrect Waste Package Heating for the Discrete-heat-source, Drift-scale, Thermal-conduction (DDT) Submodels of the MSTHM

The condition identified by CR-6521 was corrected in MSTHM runs produced for TSPA-LA. This was done in conjunction with updates to all the waste package thermal output histories in the DDT submodel, to implement changes associated with the use of TAD canisters for CSNF.

8.5.2[a] CR-6543 – Selecting Representative Waste Packages for TSPA Percolation Bins

The condition identified by CR 6543 was corrected in the software used to produce MSTHM output for TSPA-LA. The software reformat_EXT_to_TSPA v2.0 (see Section 3.1.1.10[a] and Table 3-1[a]) was changed for compatibility with output from MSTHAC V7.0 (see Section 3.1.1.3[a] and Table 3-1[a]). Thus, the identification of typical waste packages for TSPA-LA is based on the selection algorithm of the parent report (Appendix VIII).

8.5.3[a] CR-6730 – Improve TSPA-Multiscale Temperature Abstraction

The condition identified by CR-6730 has been addressed in software reformat_EXT_to_TSPA v2.0 (see Section 3.1.1.10[a] and Table 3-1[a]), which allows selection of “typical” waste packages to be performed using any value of the percentile on the thermal measure. The base-case files provided for TSPA-LA are generated for the 50th percentile, but other sets of hotter or colder waste packages can now be generated using the same software.

8.5.4[a] CR-7191 – RIT Action Items Associated with AMR ANL-EBS-MD-000049, Multiscale Thermohydrologic Model

This CR tracks eight review comments from the Regulatory Integration Team (RIT) in 2004 that were saved for further consideration. The disposition of those comments is as follows:

1. RIT item PLI-041504-171355-09: The model validation comparison discussed in this comment was improved in the parent report (Section 7.5.3), and is discussed further in this addendum (Section 7[a]).

2. RIT item PLI-041604-141550-72: The alternative conceptual model comparison to the model of Haukwa et al. (1998 [DIRS 117826]) is retained in the multiscale report. The newer mountain-scale thermal-hydrology model (BSC 2005 [DIRS 169866]) was very similar, such that updating the comparison is considered to be of limited value. Comparison of MSTHM output to temperature predictions from conduction-only models is not necessary because three of the four major submodel types in the MSTHM methodology are conduction-only models.
3. RIT item PLI-042904-172804-60: This comment on possible future needs to justify or defend MSTHM model output and features, through additional MSTHM calculations or use of other models, is addressed by the parent report (Section 7.5), and in this addendum (Section 7.8[a]). The MSTHM computational efficiency would facilitate further sensitivity analyses, and the MSTHM has already been compared with alternative three-dimensional thermal-hydrologic simulations.
4. RIT item PLI-050604-144546-53: Two different three-dimensional cases have been produced for MSTHM validation in the parent report (Section 7.5) and in Section 7.8[a] of this addendum. The MSTHM has also been compared with key output from *In-Drift Natural Convection and Condensation* (SNL 2007 [DIRS 181648]).
5. RIT item PLI-050604-145212-19: Thermal conductivity information used in the MSTHM is based on systematic evaluation of the full output of the geostatistical model for conductivity of the host rock (BSC 2004 [DIRS 169854]; Section 6[a] of this addendum). The in-situ thermal conductivity tests described in this comment were determined to be appropriate for validation of the thermal conductivity model, and were used for that purpose.
6. RIT item PLI-051004-182154-50: Thermal effects from drift collapse are important when collapse occurs during the thermal period. Collapse is a consequence of strong ground motion that is relatively rare. The approach developed by the MSTHM for use in TSPA represents the greatest possible consequence (complete collapse) but not the full complexity of the transient partial-collapse condition, which is most likely to occur well after the thermal period.
7. RIT item PLI-060204-090647-27: In the parent report (Section 6.2.3.2), the text identifies where a radiative coupling term would be added in Equation 8, for those local applications of the energy balance equation which adjoin air spaces in the model domain.
8. RIT item PLI-070204-150712-65: Various improvements have been implemented in the traceability and transparency of MSTHM feeds to TSPA-LA. These improvements were made in the parent report unless indicated otherwise. They include (but are not limited to): (1) redevelopment of the TSPA-LA feeds and the associated MSTHM output DTNs; (2) preparation of an MSTHM TSPA Data Input Package as a preview of TSPA-LA feeds; (3) clarification in Section 1 of the parameters actually used by TSPA; (4) redevelopment of explanations and instructions

for use of MSTHM output DTNs; and (5) review and checking of qualification status for MSTHM inputs used to prepare TSPA-LA feeds.

8.5.5[a] CR-7892 – Prediction of the Effective Thermal Conductivity of Granular Material

This CR has been addressed in this addendum (Appendix XI[a]) using a predictive model for effective thermal conductivity (including thermal radiation) of granular media. The model was selected from a review of pertinent technical literature, including a survey article on the topic. This predictive model, with uncertainty, has been implemented in the simulations of drift collapse.

8.5.6[a] CR-7969 – Lack of Documentation on Temperature Limit(s)

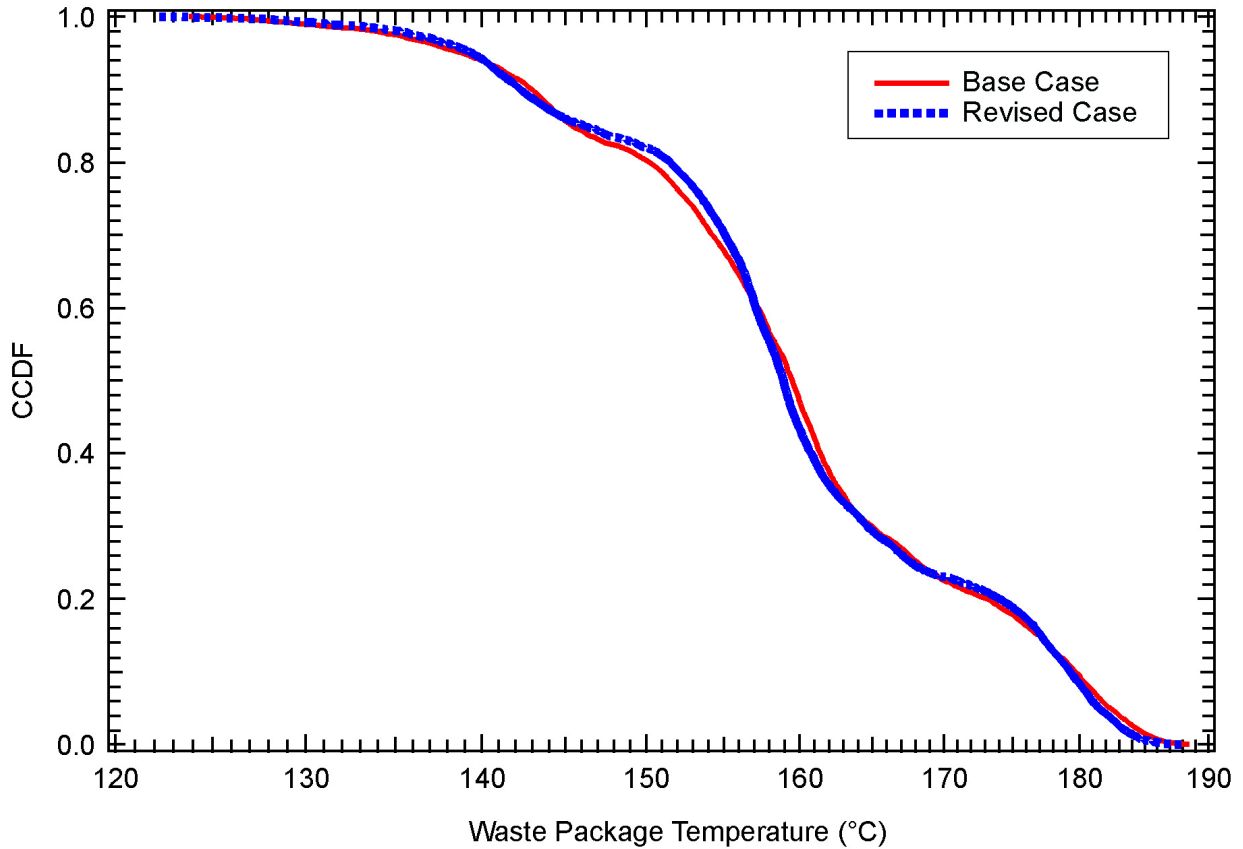
This CR addresses the technical basis particularly for the drift wall temperature limit of 200°C. This limit and the other postclosure temperature limits are addressed by *Post-Closure Analysis of the Range of Design Thermal Loadings* (SNL 2007 [DIRS 179962], Section 6.1).

8.5.7[a] CR-10733 – Qualified DTN: LL050500323122.060 Was Calculated Using Unqualified Data

Output DTN: LL0705PA032MST.028, which uses qualified data (see Section 6.3.18[a]), is available for in-drift vapor flow and condensation rates. Consequently, DTN: LL050500323122.060 [DIRS 181005] is no longer required for the purpose of providing in-drift vapor flow and condensation rates.

8.5.8[a] CR-10846 – Reversed Ventilation Direction in LDTH/SDT Submodels

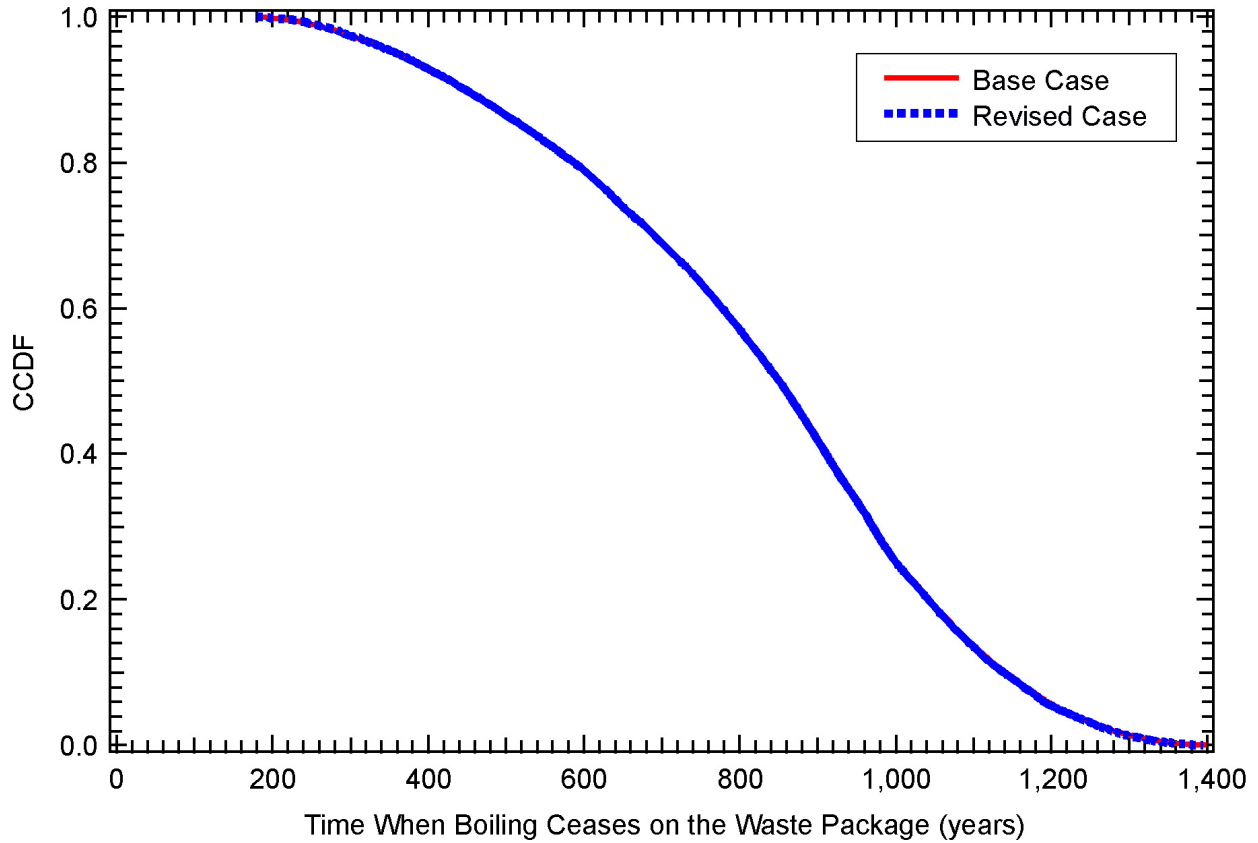
An impact analysis has been conducted by rerunning the MSTHM for an additional case for the P10 percolation flux/host-rock thermal conductivity case, which is the most likely of the seven percolation flux/host-rock thermal conductivity cases (Table 6.3-47[a]). This additional case (Output DTN: LL070701823122.083) involves rerunning the LDTH/SDT submodel pairs with the corrected ventilation direction for Panels 2 and 4 (Figure 6.2-19[a]). Figure 8.5-1[a] compares the CCDF of peak waste package temperature for the base case and revised case with the corrected ventilation direction in the LDTH/SDT submodel pairs. Figure 8.5-2[a] compares the CCDF of the time when boiling ceases on the waste package. It is important to note that the differences in peak temperature and in the time when boiling ceases, between the base and revised cases, are well within the range in peak waste package temperature resulting from parametric uncertainty. For the median waste package, the range in peak temperature arising from parametric uncertainty is on the order of 30°C (Figure 6.3-77[a] and Table 6.3-49[a]), while the impact of the reversed ventilation direction is on the order of 1°C (Figure 8.5-1[a]). For the median waste package, the range in the time when boiling ceases is on the order of 500 years (Figure 6.3-78[a] and Table 6.3-50[a]), while the impact of the reversed ventilation direction is on the order of 1 year (Figure 8.5-2[a]). Therefore, the influence of the reversed ventilation direction is insignificant.



Source: Output DTNs: LL0702PA015MST.070 and LL070701823122.083.

NOTE: Each of the CCDF plots represents 26,112 values, which is the product of eight different waste package types at 3,264 locations across the repository. Two cases are compared, including the base case, where the ventilation direction is reversed for the LDTH/SDT submodel pairs for Panels 2 and 4, and the revised case where the ventilation direction has been corrected.

Figure 8.5-1[a]. CCDF for Peak Waste Package Temperature for the P10 Percolation Flux/Host-Rock Thermal Conductivity Case



Source: Output DTNs: LL0702PA015MST.070 and LL070701823122.083.

NOTE: Each of the CCDF plots represents 26,112 values, which is the product of eight different waste package types at 3,264 locations across the repository. Two cases are compared, including the base case, where the ventilation direction is reversed for the LDTH/SDT submodel pairs for Panels 2 and 4, and the revised case where the ventilation direction has been corrected.

Figure 8.5-2[a]. CCDF for the Time When Boiling Ceases on the Waste Package for the P10 Percolation Flux/Host-Rock Thermal Conductivity Case

INTENTIONALLY LEFT BLANK

9[a]. INPUTS AND REFERENCES**9.1[a] DOCUMENTS CITED**

- 103750 Altman, W.D.; Donnelly, J.P.; and Kennedy, J.E. 1988. *Qualification of Existing Data for High-Level Nuclear Waste Repositories: Generic Technical Position*. NUREG-1298. Washington, D.C.: U.S. Nuclear Regulatory Commission. TIC: 200652.
- 103597 Altman, W.D.; Donnelly, J.P.; and Kennedy, J.E. 1988. *Peer Review for High-Level Nuclear Waste Repositories: Generic Technical Position*. NUREG-1297. Washington, D.C.: U.S. Nuclear Regulatory Commission. TIC: 200651.
- 104507 Arya, L.M. and Paris, J.F. 1981. "A Physicoempirical Model to Predict the Soil Moisture Characteristic from Particle-Size Distribution and Bulk Density Data." *Soil Science Society of America Journal*, 45, (5), 1023-1030. Madison, Wisconsin: Soil Science Society of America. TIC: 245978.
- 176802 Arya, L.M.; Leij, F.J.; and van Genuchten, M.Th. 1999. "Relationship Between Particle-Size Distribution and Soil Water Retention." *Proceedings of the International Workshop on Characterization and Measurement of the Hydraulic Properties of Unsaturated Porous Media, Part 2, Riverside, California, October 22-24, 1997*. van Genuchten, M.Th.; Leij, F.J.; and Wu, L., eds. Pages 931-946. Riverside, California: University of California. TIC: 247322.
- 108417 ASME (American Society of Mechanical Engineers) 1995. "Materials." Section II of *1995 ASME Boiler and Pressure Vessel Code*. New York, New York: American Society of Mechanical Engineers. TIC: 245287.
- 154108 Azizi, S.; Moyne, C.; and Degiovanni, A. 1988. "Approche Experimentale et Theorique de la Conductivite Thermique des Milieux Poreux Humides—I. Experimentation." *International Journal of Heat and Mass Transfer*, 31, (11), 2305-2317. New York, New York: Pergamon Press. TIC: 243729.
- 103524 Bird, R.B.; Stewart, W.E.; and Lightfoot, E.N. 1960. *Transport Phenomena*. New York, New York: John Wiley & Sons. TIC: 208957.
- 169855 BSC (Bechtel SAIC Company) 2004. *Development of Numerical Grids for UZ Flow and Transport Modeling*. ANL-NBS-HS-000015 REV 02. Las Vegas, Nevada: Bechtel SAIC Company. ACC: DOC.20040901.0001.
- 166107 BSC 2004. *Drift Degradation Analysis*. ANL-EBS-MD-000027 REV 03. Las Vegas, Nevada: Bechtel SAIC Company. ACC: DOC.20040915.0010; DOC.20050419.0001; DOC.20051130.0002; DOC.20060731.0005.

- 168138 BSC 2004. *Estimation of Mechanical Properties of Crushed Tuff for Use as Ballast Material in Emplacement Drifts*. 800-CYC-SSE0-00100-000-00A. Las Vegas, Nevada: Bechtel SAIC Company. ACC: ENG.20040309.0023; ENG.20050817.0009; ENG.20050829.0017.
- 170003 BSC 2004. *Heat Capacity Analysis Report*. ANL-NBS-GS-000013 REV 01. Las Vegas, Nevada: Bechtel SAIC Company. ACC: DOC.20041101.0003.
- 169866 BSC 2004. *Mountain-Scale Coupled Processes (TH/THC/THM) Models*. MDL-NBS-HS-000007 REV 02. Las Vegas, Nevada: Bechtel SAIC Company. ACC: DOC.20041108.0001.
- 170033 BSC 2004. *Thermal Conductivity of Non-Repository Lithostratigraphic Layers*. MDL-NBS-GS-000006 REV 01. Las Vegas, Nevada: Bechtel SAIC Company. ACC: DOC.20041022.0004.
- 169854 BSC 2004. *Thermal Conductivity of the Potential Repository Horizon*. MDL-NBS-GS-000005 REV 01. Las Vegas, Nevada: Bechtel SAIC Company. ACC: DOC.20040928.0006.
- 169861 BSC 2004. *UZ Flow Models and Submodels*. MDL-NBS-HS-000006 REV 02. Las Vegas, Nevada: Bechtel SAIC Company. ACC: DOC.20041101.0004; DOC.20050629.0003.
- 172232 BSC 2005. *Drift-Scale Coupled Processes (DST and TH Seepage) Models*. MDL-NBS-HS-000015 REV 02. Las Vegas, Nevada: Bechtel SAIC Company. ACC: DOC.20050114.0004; DOC.20051115.0002.
- 174101 BSC 2005. *Mountain-Scale Coupled Processes (TH/THC/THM) Models*. MDL-NBS-HS-000007 REV 03. Las Vegas, Nevada: Bechtel SAIC Company. ACC: DOC.20050825.0007.
- 178297 BSC 2006. *Technical Work Plan for: Additional Multiscale Thermohydrologic Modeling*. TWP-MGR-PA-000036 REV 02. Las Vegas, Nevada: Bechtel SAIC Company. ACC: DOC.20060825.0001.
- 100658 Buscheck, T. 1996. "Hydrothermal Modeling." Chapter 1.0 of *Near-Field and Altered-Zone Environment Report*. Wilder, D.G., ed. UCRL-LR-124998, Volume II. Livermore, California: Lawrence Livermore National Laboratory. ACC: MOL.19961212.0121.
- 164638 Buscheck, T.A.; Glascoe, L.G.; Lee, K.H.; Gansemer, J.; Sun, Y.; and Mansoor, K. 2003. "Validation of the Multiscale Thermohydrologic Model Used for Analysis of a Proposed Repository at Yucca Mountain." *Journal of Contaminant Hydrology*, 62-63, 421-440. New York, New York: Elsevier. TIC: 254205.

- 160749 Buscheck, T.A.; Rosenberg, N.D.; Gansemer, J.; and Sun, Y. 2002. "Thermohydrologic Behavior at an Underground Nuclear Waste Repository." *Water Resources Research*, 38, (3), 10-1 through 10-19. Washington, D.C.: American Geophysical Union. TIC: 253566.
- 113426 Crane, R.A.; Vachon, R.I.; and Khader, M.S. 1977. "Thermal Conductivity of Granular Materials - A Review." *Proceedings of the Seventh Symposium on Thermophysical Properties, held at National Bureau of Standards, Gaithersburg, Maryland, May 10-12, 1977*. Cezairliyan, A., ed. Pages 109-123. New York, New York: American Society of Mechanical Engineers. TIC: 246057.
- 111115 CRWMS M&O 1998. *Drift Scale Test As-Built Report*. BAB000000-01717-5700-00003 REV 01. Las Vegas, Nevada: CRWMS M&O. ACC: MOL.19990107.0223.
- 100439 de Marsily, G. 1986. *Quantitative Hydrogeology: Groundwater Hydrology for Engineers*. San Diego, California: Academic Press. TIC: 208450.
- 154172 Degiovanni, A. and Moyne, C. 1987. "Conductivite Thermique de Materiaux Poreux Humides: Evaluation Theorique et Possibilite de Mesure." *International Journal of Heat and Mass Transfer*, 30, (11), 2225-2245. New York, New York: Pergamon Journals. TIC: 249489.
- 180715 DOE (U.S. Department of Energy) 2002. *The Nuclear Waste Policy Act, as Amended, with Appropriations Acts Appended*. DOE/RW-0438, Rev. 2. Washington, D.C.: U.S. Department of Energy, Office of Civilian Radioactive Waste. ACC: MOL.20020305.0402.
- 181178 DOE 2006. *User Information for: reformat_EXT_to_TSPA V2.0*. Document ID: 11061-UID-2.0-00. Las Vegas, Nevada: Department of Energy. ACC: MOL.20060123.0007.
- 102009 Fetter, C.W. 1993. *Contaminant Hydrogeology*. Upper Saddle River, New Jersey: Prentice Hall. TIC: 240691.
- 164602 Francis, N.D., Jr.; Webb, S.W.; Itamura, M.T.; and James, D.L. 2003. *CFD Modeling of Natural Convection Heat Transfer and Fluid Flow in Yucca Mountain Project (YMP) Enclosures*. SAND2002-4179. Albuquerque, New Mexico: Sandia National Laboratories. ACC: MOL.20030906.0165.
- 169628 Green, R.T.; Prikryl, J.D.; and Hill, M.E. 1999. "Assessment of Heat Flow Through Bulk Geologic Material." *Thermal Conductivity 24, Proceedings of the 24th International Thermal Conductivity Conference, October 26-29, 1997, Pittsburgh, Pennsylvania*. Pages 715-730. Lancaster, Pennsylvania: Technomic. TIC: 255845.

- 117826 Haukwa, C.; Wu, Y.S.; Hinds, J.J.; Zhang, W.; Ritcey, A.C.; Pan, L.H.; Simmons, A.M.; and Bodvarsson, G.S. 1998. *Results of Sensitivity Studies of Thermo-Hydrologic Behavior Conducted on Hydrologic Parameter Sets*. Milestone SP3CK5M4. Berkeley, California: Lawrence Berkeley National Laboratory. ACC: MOL.19980918.0001.
- 108184 Incropera, F.P. and DeWitt, D.P. 1996. *Fundamentals of Heat and Mass Transfer*. 4th Edition. New York, New York: John Wiley & Sons. TIC: 243950.
- 102010 Jury, W.A.; Gardner, W.R.; and Gardner, W.H. 1991. *Soil Physics*. 5th Edition. New York, New York: John Wiley & Sons. TIC: 241000.
- 153166 Kunii, D. and Smith, J.M. 1960. "Heat Transfer Characteristics of Porous Rocks." *American Institute of Chemical Engineers Journal*, 6, (1), 71-78. New York, New York: American Institute of Chemical Engineers. TIC: 249321.
- 101876 Lide, D.R., ed. 1995. *CRC Handbook of Chemistry and Physics*. 76th Edition. Boca Raton, Florida: CRC Press. TIC: 216194.
- 161435 McAdams, W.H. 1954. *Heat Transmission*. 3rd Edition. New York, New York: McGraw-Hill. TIC: 242359.
- 163054 Michel, H. 1999. "Bernold Sheets." Letter from H. Michel (Bernold AG) to M. Grigore (MK), July 2, 1999, with enclosures. ACC: MOL.20030506.0321.
- 154107 Moyne, C.; Batsale, J-C.; and Degiovanni, A. 1988. "Approche Experimentale et Theorique de la Conductivite Thermique des Milieux Poreux Humides—II. Theorie." *International Journal of Heat and Mass Transfer*, 31, (11), 2319-2329. New York, New York: Pergamon Press. TIC: 249402.
- 100474 Nitao, J.J. 1998. *Reference Manual for the NUFT Flow and Transport Code, Version 2.0*. UCRL-MA-130651. Livermore, California: Lawrence Livermore National Laboratory. ACC: MOL.19980810.0391.
- 163274 NRC (U.S. Nuclear Regulatory Commission) 2003. *Yucca Mountain Review Plan, Final Report*. NUREG-1804, Rev. 2. Washington, D.C.: U.S. Nuclear Regulatory Commission, Office of Nuclear Material Safety and Safeguards. TIC: 254568.
- 181244 SNL (Sandia National Laboratories) 2007. *Abstraction of Drift Seepage*. MDL-NBS-HS-000019 REV 01 ADD 01. Las Vegas, Nevada: Sandia National Laboratories. ACC: DOC.20041103.0003; DOC.20070807.0001.
- 177404 SNL 2007. *Drift-Scale THC Seepage Model*. MDL-NBS-HS-000001 REV 05. Las Vegas, Nevada: Sandia National Laboratories.
- 177407 SNL 2007. *EBS Radionuclide Transport Abstraction*. ANL-WIS-PA-000001 REV 03. Las Vegas, Nevada: Sandia National Laboratories.

- 177412 SNL 2007. *Engineered Barrier System: Physical and Chemical Environment*. ANL-EBS-MD-000033 REV 06. Las Vegas, Nevada: Sandia National Laboratories.
- 179476 SNL 2007. *Features, Events, and Processes for the Total System Performance Assessment*. ANL-WIS-MD-000026 REV 00. Las Vegas, Nevada: Sandia National Laboratories.
- 181648 SNL 2007. *In-Drift Natural Convection and Condensation*. MDL-EBS-MD-000001 REV 00, AD 01. Las Vegas, Nevada: Sandia National Laboratories. ACC: DOC.20041025.0006; DOC.20050330.0001; DOC.20051122.0005.
- 180472 SNL 2007. *Initial Radionuclides Inventory*. ANL-WIS-MD-000020 REV 01 ADD 01. Las Vegas, Nevada: Sandia National Laboratories. ACC: DOC.20040921.0003; DOC.20050927.0005; DOC.20070801.0001.
- 179962 SNL 2007. *Postclosure Analysis of the Range of Design Thermal Loadings*. ANL-NBS-HS-000057 REV 00. Las Vegas, Nevada: Sandia National Laboratories.
- 174294 SNL 2007. *Simulation of Net Infiltration for Present-Day and Potential Future Climates*. MDL-NBS-HS-000023 REV 01. Las Vegas, Nevada: Sandia National Laboratories. ACC: DOC.20070530.0014.
- 179567 SNL 2007. *Total System Performance Assessment Data Input Package for Requirements Analysis for DOE SNF/HLW and Navy SNF Waste Package Overpack Physical Attributes Basis for Performance Assessment*. TDR-TDIP-ES-000009 REV 00. Las Vegas, Nevada: Sandia National Laboratories.
- 179354 SNL 2007. *Total System Performance Assessment Data Input Package for Requirements Analysis for EBS In-Drift Configuration*. TDR-TDIP-ES-000010 REV 00. Las Vegas, Nevada: Sandia National Laboratories.
- 179466 SNL 2007. *Total System Performance Assessment Data Input Package for Requirements Analysis for Subsurface Facilities*. TDR-TDIP-PA-000001 REV 00. Las Vegas, Nevada: Sandia National Laboratories.
- 179394 SNL 2007. *Total System Performance Assessment Data Input Package for Requirements Analysis for TAD Canister and Related Waste Package Overpack Physical Attributes Basis for Performance Assessment*. TDR-TDIP-ES-000006 REV 00. Las Vegas, Nevada: Sandia National Laboratories.
- 175177 SNL 2007. *UZ Flow Models and Submodels*. MDL-NBS-HS-000006 REV 03. Las Vegas, Nevada: Sandia National Laboratories.
- 171270 Williams, N.H. 2002. "Contract No. DE-AC28-01RW12101 - Key Technical Issue (KTI) Agreement Item Thermal Effects on Flow (TEF) 2.01." Letter from N.H. Williams (BSC) to J.D. Ziegler (DOE/ORD), December 18, 2002, MZ:mm-1217025488, with enclosures. ACC: MOL.20030213.0147.

170330 Yagi, S. and Kunii, D. 1957. "Studies on Effective Thermal Conductivities in Packed Beds." *AIChE Journal*, 3, (3), 373-381. New York, New York: American Institute of Chemical Engineers. TIC: 255847.

9.2[a] CODES, STANDARDS, REGULATIONS, AND PROCEDURES

178394 70 FR 53313. Implementation of a Dose Standard After 10,000 Years. Internet Accessible.

103515 ASTM G 1-90 (Reapproved 1999). 1999. *Standard Practice for Preparing, Cleaning, and Evaluating Corrosion Test Specimens*. West Conshohocken, Pennsylvania: American Society for Testing and Materials. TIC: 238771.

IM-PRO-003, Rev. 02, ICN 0. *Software Management*. Washington, D.C.: U.S. Department of Energy, Office of Civilian Radioactive Waste Management. ACC: DOC.20070228.0002.

SCI-PRO-004, Rev. 05, ICN 0. *Managing Technical Product Inputs*. Washington, D.C.: U.S. Department of Energy, Office of Civilian Radioactive Waste Management. ACC: DOC.20070810.0002.

SCI-PRO-006, Rev. 05, ICN 0. *Models*. Washington, D.C.: U.S. Department of Energy, Office of Civilian Radioactive Waste Management. ACC: DOC.20070810.0004.

9.3[a] SOURCE DATA, LISTED BY DATA TRACKING NUMBER

152932 GS000483351030.003. Thermal Properties Measured 12/01/99 to 12/02/99 Using the Thermolink Soil Multimeter and Thermal Properties Sensor on Selected Potential Candidate Backfill Materials Used in the Engineered Barrier System. Submittal date: 11/09/2000.

163107 GS020183351030.001. Uncompacted Bulk Density for Analyses Performed 02/02/00 to 05/23/00 on Potential Backfill Materials Used in the Engineered Barrier System. Submittal date: 01/22/2002.

119916 GS980808312242.015. Water Retention and Unsaturated Hydraulic Conductivity Measurements for Various Size Fractions of Crushed, Sieved, Welded Tuff Samples Measured Using a Centrifuge. Submittal date: 08/21/1998.

159525 LB0205REVUZPRP.001. Fracture Properties for UZ Model Layers Developed from Field Data. Submittal date: 05/14/2002.

161243 LB0208UZDSCPMI.002. Drift-Scale Calibrated Property Sets: Mean Infiltration Data Summary. Submittal date: 08/26/2002.

- 162354 LB03023DKMGRID.001. UZ 3-D Site Scale Model Grids. Submittal date: 02/26/2003.
- 180502 LB0610UZDSCP10.001. Drift-Scale Calibrated Property Set for the 10-Percentile Infiltration Map. Submittal date: 11/02/2006.
- 179180 LB0610UZDSCP30.001. Drift-Scale Calibrated Property Set for the 30-Percentile Infiltration Map. Submittal date: 11/02/2006.
- 179150 LB0612PDPTNTSW.001. Vertical Flux at PTN/TSW Interface for Present-Day Climate of 10th, 30th, 50th, and 90-Percentile Infiltration Maps. Submittal date: 12/19/2006.
- 179153 LB0701GTPTNTSW.001. Vertical Flux at PTN/TSW Interface for Glacial Transition Climate of 10th, 30th, 50th, and 90th-Percentile Infiltration Maps. Submittal date: 01/03/2007.
- 179156 LB0701MOPTNTSW.001. Vertical Flux at PTN/TSW Interface for Monsoon Climate of 10th, 30th, 50th and 90th-Percentile Infiltration Maps. Submittal date: 01/03/2007.
- 179283 LB0701PAWFINFM.001. Weighting Factors for Infiltration Maps. Submittal date: 01/25/2007.
- 179332 LB0702UZPTN10K.002. Vertical Flux at PTN/TSW Interface for Post-10K-Year Climate Infiltration Maps. Submittal date: 02/15/2007.
- 146894 LB991201233129.001. The Mountain-Scale Thermal-Hydrologic Model Simulations for AMR U0105, "Mountain-Scale Coupled Processes (TH) Models". Submittal date: 12/03/1999.
- 181005 LL050500323122.060. Comparison of the Differences Between the Multiscale Thermohydrologic Model (MSTHM) and a Corresponding Three-Dimensional Monolithic Thermal-Hydrologic Model (THM) with the Range of Conditions Resulting from Parametric Uncertainty. Submittal date: 05/25/2005.
- 156696 MO0109EBSAEQST.009. Engineered Barrier System Average Emissivity/Reflectivity Measurements of Materials Used at Different Temperatures in Quarter Scale Tests. Submittal date: 09/19/2001.
- 179085 MO0701VENTCALC.000. Analytical Ventilation Calculation for the Base Case Analysis with a 1.45 KW/M Initial Line Load. Submittal date: 01/23/2007.
- 179925 MO0702PASTREAM.001. Waste Stream Composition and Thermal Decay Histories for LA. Submittal date: 02/15/2007.

- 182472 MO0707TH2D3DDC.000. 2-D and 3-D Thermal-Hydrologic Analysis. Submittal date: 08/15/2007.
- 162401 SN0303T0503102.008. Revised Thermal Conductivity of the Non-Repository Layers of Yucca Mountain. Submittal date: 03/19/2003.
- 164196 SN0307T0510902.003. Updated Heat Capacity of Yucca Mountain Stratigraphic Units. Submittal date: 07/15/2003.
- 169129 SN0404T0503102.011. Thermal Conductivity of the Potential Repository Horizon Rev 3. Submittal date: 04/27/2004.
- 181200 SN0704T0502206.047. Recharge Estimates Used to Validate the Massif Model of Net Infiltration at Yucca Mountain. Submittal date: 04/19/2007.

9.4[a] OUTPUT DATA, LISTED BY DATA TRACKING NUMBER

LL0702PA013MST.068. Input and Output Files for the SMT, SDT and DDT Submodels and MSTHAC Extract Output Files Used in ANL-EBS-MD-000049 Multiscale Thermohydrologic Model. Submittal date: 04/26/2007.

LL0702PA014MST.069. Input and Output Files for the LDTH Submodels and MSTHAC Extract Output Files Used in ANL-EBS-MD-000049 Multiscale Thermohydrologic Model for the Mean Host-Rock Thermal Conductivity, 10-Percentile Percolation Flux Case. Submittal date: 02/23/2007.

LL0702PA015MST.070. Output for ANL-EBS-MD-000049 Multiscale Thermohydrologic Model for the Mean Host-Rock Thermal Conductivity, 10-Percentile Percolation Flux Case. Submittal date: 02/22/2007.

LL0702PA016MST.071. Input and Output Files for the LDTH Submodels and MSTHAC Extract Output Files Used in ANL-EBS-MD-000049 Multiscale Thermohydrologic Model for the Mean Host-Rock Thermal Conductivity, 30-Percentile Percolation Flux Case. Submittal date: 02/14/2007.

LL0702PA017MST.072. Output for ANL-EBS-MD-000049 Multiscale Thermohydrologic Model for the Mean Host-Rock Thermal Conductivity, 30-Percentile Percolation Flux Case. Submittal date: 02/14/2007.

LL0702PA018MST.073. Input and Output Files for the LDTH Submodels and MSTHAC Extract Output Files Used in ANL-EBS-MD-000049 Multiscale Thermohydrologic Model for the Mean Host-Rock Thermal Conductivity, 50-Percentile Percolation Flux Case. Submittal date: 02/14/2007.

LL0702PA019MST.074. Output for ANL-EBS-MD-000049 Multiscale Thermohydrologic Model for the Mean Host-Rock Thermal Conductivity, 50-Percentile Percolation Flux Case. Submittal date: 02/14/2007.

LL0702PA020MST.075. Input and Output Files for the LDTH Submodels and MSTHAC Extract Output Files Used in ANL-EBS-MD-000049 Multiscale Thermohydrologic Model for the Mean Host-Rock Thermal Conductivity, 90-Percentile Percolation Flux Case. Submittal date: 02/14/2007.

LL0702PA021MST.076. Output for ANL-EBS-MD-000049 Multiscale Thermohydrologic Model for the Mean Host-Rock Thermal Conductivity, 90-Percentile Percolation Flux Case. Submittal date: 02/14/2007.

LL0702PA022MST.077. Input and Output Files for the LDTH Submodels and MSTHAC Extract Output Files Used in ANL-EBS-MD-000049 Multiscale Thermohydrologic Model for the Low Host-Rock Thermal Conductivity, 10-Percentile Percolation Flux Case. Submittal date: 02/14/2007.

LL0702PA023MST.078. Output for ANL-EBS-MD-000049 Multiscale Thermohydrologic Model for the Low Host-Rock Thermal Conductivity, 10-Percentile Percolation Flux Case. Submittal date: 02/14/2007.

LL0702PA024MST.079. Input and Output Files for the LDTH Submodels and MSTHAC Extract Output Files Used in ANL-EBS-MD-000049 Multiscale Thermohydrologic Model for the High Host-Rock Thermal Conductivity, 90-Percentile Percolation Flux Case. Submittal date: 02/14/2007.

LL0702PA025MST.080. Output for ANL-EBS-MD-000049 Multiscale Thermohydrologic Model for the High Host-Rock Thermal Conductivity, 90-Percentile Percolation Flux Case. Submittal date: 02/14/2007.

LL0702PA026MST.081. Input and Output Files for LDTH and DDT Submodels, and Corresponding MSTHAC Extract Files, for Mean Host-Rock Thermal Conductivity, 10-Percentile Percolation Flux, Collapsed-Drift, High and Low Rubble Thermal Conductivity Cases in ANL-EBS-MD-000049 Multiscale Thermohydrologic Model Calculations. Submittal date: 02/15/2007.

LL0702PA027MST.082. Output for ANL-EBS-MD-000049 Multiscale Thermohydrologic Model for the Mean Host-Rock Thermal Conductivity, 10-Percentile Percolation Flux, Collapsed-Drift, High and Low Rubble Thermal Conductivity Cases. Submittal date: 02/15/2007.

LL0702PA028MST.083. Input and Output Files for the LDTH Submodels and the Corresponding MSTHAC Extract Output Files for the High Host-Rock Thermal Conductivity (HKT), 10-Percentile Percolation (P10H) Case Used in ANL-EBS-MD-000049 Multiscale Thermohydrologic Model Calculations. Submittal date: 02/15/2007.

LL0702PA029MST.084. Output for ANL-EBS-MD-000049 Multiscale Thermohydrologic Model for the Low Host-Rock Thermal Conductivity, 10-Percentile Percolation Flux Case. Submittal date: 02/15/2007.

LL0702PA030MST.085. Plots of MSTHAC Output Files and of LDTH-, SDT-, SMT-, and DDT-Submodel Output Files from ANL-EBS-MD-000049 Multiscale Thermohydrologic Model. Submittal date: 02/15/2007.

LL0703PA011MST.006. Output for ANL-EBS-MD-000049 REV 04 Multiscale Thermohydrologic Model for the Mean Host-Rock Thermal Conductivity, 10-Percentile Percolation Flux Case. Submittal date: 03/07/2007.

LL0703PA012MST.007. Output for ANL-EBS-MD-000049 REV 04 Multiscale Thermohydrologic Model for the Mean Host-Rock Thermal Conductivity, 30-Percentile Percolation Flux Case. Submittal date: 03/13/2007.

LL0703PA013MST.008. Output for ANL-EBS-MD-000049 REV 04 Multiscale Thermohydrologic Model for the Mean Host-Rock Thermal Conductivity, 50-Percentile Percolation Flux Case. Submittal date: 03/13/2007.

LL0703PA014MST.009. Output for ANL-EBS-MD-000049 REV 04 Multiscale Thermohydrologic Model for the Mean Host-Rock Thermal Conductivity, 90-Percentile Percolation Flux Case. Submittal date: 03/13/2007.

LL0703PA015MST.010. Output for ANL-EBS-MD-000049 REV 04 Multiscale Thermohydrologic Model for the Low Host-Rock Thermal Conductivity, 10-Percentile Percolation Flux Case. Submittal date: 03/13/2007.

LL0703PA016MST.011. Output for ANL-EBS-MD-000049 REV 04 Multiscale Thermohydrologic Model for the High Host-Rock Thermal Conductivity, 90-Percentile Percolation Flux Case. Submittal date: 03/13/2007.

LL0703PA017MST.012. Output for ANL-EBS-MD-000049 REV 04 Multiscale Thermohydrologic Model for the High Host-Rock Thermal Conductivity, 10-Percentile Percolation Flux Case. Submittal date: 03/13/2007.

LL0703PA026MST.013. Weighting factors for low (10th-percentile), mean and high (90th-percentile) host-rock thermal conductivity cases from ANL-EBS-MD-000049 Multiscale Thermohydrologic Model. Submittal date: 03/28/2007.

LL0703PA034MST.016. Output for ANL-EBS-MD-000049 Multiscale Thermohydrologic Model for the Low Host-Rock Thermal Conductivity, 90-Percentile Percolation Flux (P90L) Case. Submittal date: 03/22/2007.

LL0703PA035MST.017. Output for ANL-EBS-MD-000049 Multiscale Thermohydrologic Model for the High Host-Rock Thermal Conductivity, 30-Percentile Percolation Flux (P30H) Case. Submittal date: 03/22/2007.

LL0703PA036MST.018. Output for ANL-EBS-MD-000049 Multiscale Thermohydrologic Model for the Low Host-Rock Thermal Conductivity, 50-Percentile Percolation Flux (P50L) Case. Submittal date: 03/22/2007.

LL0703PA037MST.019. Output for ANL-EBS-MD-000049 Multiscale Thermohydrologic Model for the High Host-Rock Thermal Conductivity, 50-Percentile Percolation Flux (P50H) Case. Submittal date: 03/22/2007.

LL0703PA038MST.020. Output for ANL-EBS-MD-000049 Multiscale Thermohydrologic Model for the Low Host-Rock Thermal Conductivity, 90-Percentile Percolation Flux (P90L) Case. Submittal date: 03/22/2007.

LL0703PA053MST.021. Selecting the Most Representative Calculated MSTHM Uncertainty Cases to Serve as Surrogates for Non-Calculated MSTHM Uncertainty Cases for ANL-EBS-MD-000049 Multiscale Thermohydrologic Model (MSTHM). Submittal date: 03/22/2007.

LL0704PA003MST.022. Input- and Output-File Preparation Scripts and Output-Plotting Scripts for NUFT Submodels and MSTHAC Calculations for ANL-EBS-MD-000049 Multiscale Thermohydrologic Model (MSTHM). Submittal date: 04/12/2007.

LL0705PA032MST.028. Model-Confidence Building and Sensitivity Studies for ANL-EBS-MD-000049 Multiscale Thermohydrologic Model (MSTHM). Submittal date: 08/23/2007.

LL0705PA038MST.030. Model Preparation and Analysis Files for ANL-EBS-MD-000049 Multiscale Thermohydrologic Model (MSTHM). Submittal date: 07/17/2007.

LL070701823122.083. Impact Analysis for ANL-EBS-MD-000049 Multiscale Thermohydrologic Model (MSTHM) for the mean host-rock thermal conductivity, 10-percentile (P10) percolation flux case. Submittal date: 08/20/2007.

MO0505SPAROCKM.000. Rock Mass and Invert Properties for TSPA-LA. Submittal date: 05/23/2005.

MO0612MEANTHER.000. Mean Thermal Conductivity of Yucca Mountain Repository Units. Submittal date: 04/27/2007.

MO0702PAGLOBAL.000. Global 10th and 90th Percentile Mean Thermal Conductivity of Yucca Mountain Repository Units. Submittal date: 02/22/2007.

MO0703PAHYTHRM.000. Hydrological and Thermal Properties of the Invert. Submittal date: 07/19/2007.

MO0703PARUBBLE.000. Effective Thermal Conductivity for Rubble. Submittal date: 03/26/2007.

9.5[a] SOFTWARE CODES

- 164275 boundary_conditions V. 1.0. 2003. Sun, Sun OS 5.8. 11042-1.0-00.
- 164281 extractBlocks_EXT V. 1.0. 2003. Sun, SUN O.S. 5.8. 11040-1.0-00.
- 164276 Heatgen_ventTable_emplace V. 1.0. 2003. Solaris 8. STN: 11039-1.0-00.
- 164274 MSTHAC V. 7.0. 2002. SUN O.S. 5.8. STN: 10419-7.0-00.
- 164541 NUFT V. 3.0s. 2002. Sun O.S. 5.8. STN: 10088-3.0s-02.
- 180382 NUFT V. 4.0. 2007. SUN O.S. 5.8, AIX 5.2, AIX 5.3, CHAOS 3.1. STN: 11228-4.0-00.
- 164273 RADPRO V. 4.0. 2002. SUN O.S. 5.8. STN: 10204-4.0-00.
- 164542 readsUnits V. 1.0. 2002. SUN O.S. 5.5.1. STN: 10602-1.0-00.
- 180261 reformat_EXT_to_TSPA V. 2.0. 2006. OS 5.8. STN: 11061-2.0-00.
- 163892 rme6 V. 1.2. 2003. SUN, SOLARIS 8. 10617-1.2-00.
- 148638 XTOOL V. 10.1. 2000. Sun O.S. 5.6.1. STN: 10208-10.1-00.
- 163894 YMESH V. 1.54. 2003. SUN, SOLARIS 8. 10172-1.54-00.

APPENDIX I[a]
BUILDING NUFT SUBMODELS

To build the NUFT submodels, the 14 steps in the parent report must be completed. The only steps not changed were Steps 1, 2, and 7.

Step 1 – Reformat the mesh from UZ Flow Models and Submodels (BSC 2004 [DIRS 169861]) using rme6 v1.2.

Applicable to this addendum, with no changes required.

Step 2 – Expand the reformatted mountain-scale mesh using xw v1.0.

Applicable to this addendum, with no changes required.

Step 3 – Create the SDT, LDTH submodel “.dat” files.

The first step in building the NUFT LDTH and SDT submodels (also called chimney submodels) input files is to create the chimney location “.dat” files containing the vertical grid dimensions and associated UZ model layers at each LDTH/SDT submodel location. The “.dat” files are constructed by taking the user-defined vertical grid discretization format (for SDT or LDTH submodel) and inserting the Nevada Central coordinates for the specified LDTH/SDT submodel locations (Output DTNs: LL0702PA013MST.068 and LL0702PA014MST.069).

Step 4 – Create the SDT, LDTH submodel “.col” and “.nft” files (software routine YMESH v1.54).

Once the “.dat” files have been created, YMESH v1.54 is used to create the “User Column Description” files that contain the vertical dimensions of the grid, along with the vertical distribution of UZ model layers. This file contains the definition of each gridblock layer including its thickness and material type (i.e., UZ model layer). To create these files, YMESH v1.54 is started and the expanded World Mesh is read. Next, a “.dat” file is opened and a “.col” file is saved by selecting the “User Column Description” save option in the YMESH File/Save menu. This process is repeated at each chimney submodel location and for each of the SDT and LDTH submodels.

The output “.nft” file is a NUFT genmsh table as defined in the NUFT user’s manual (Nitao 1998 [DIRS 100474]). To create these files, YMESH v1.54 is started and the expanded World Mesh is read as input (using the “Open data file” command). Next, a “.dat” file is opened and a “.nft” file is saved by selecting the “User NUFT genmsh” save option in the YMESH v1.54 File/Save menu. This process is repeated at each chimney submodel location and for each of the SDT and LDTH submodels.

software routine:

YMESH v1.54

inputs:

LBL2003-LA-YMESH-expand_qualified (output from xw v1.0) (Output DTN: LL0702PA013MST.068) for SDT submodel
“.dat” files for each SDT submodel (chimney-submodel) location (Output DTN: LL0702PA013MST.068)

LBL2003-LA-YMESH-expand_qualified-2006 for LDTH submodel. (Note: This file is constructed from LBL2003-LA-YMESH-expand_qualified by renaming the elements which are to be lumped together as either “uz1” or “uz2” with using UNIX command “sed”.)

“.dat” files for each LDTH submodel (chimney submodel) location (Output DTN: LL0702PA014MST.069)

outputs:

“.col” file for each SDT submodel (chimney submodel) location (Output DTN: LL0702PA013MST.068)

“.nft” file for each SDT submodel (chimney submodel) location (Output DTN: LL0702PA013MST.068)

“.col” file for each LDTH submodel (chimney submodel) location (Output DTN: LL0702PA014MST.069)

“.nft” file for each LDTH submodel (chimney submodel) location (Output DTN: LL0702PA014MST.069)

methodology:

- (1) Start YMESH v1.54
- (2) Open data file: World Grid
- (3) Open data file: chimney “*.dat” file
- (4) Save data file: User NUFT genmsh file (“*.nft”)
- (5) Save data file: User Column Description file (“*.col”)
- (6) Repeat Substeps 3 to 5 for all chimney submodel locations and for each of the SDT, and LDTH submodels.

Step 5 – Create the SDT submodel files.

Once the “.nft” files have been created for the SDT submodel “chimney submodel” files (Step 4), the following substeps are carried out. For each chimney submodel location, two output files are created. The first output file is a “.nft.dkm” file that adds the atm, wt, wp, and sz1-6 and bsmnt blocks (for atmosphere, water table, waste package, and blocks below the water table, respectively) to the input NUFT gensmsh “.nft” file; this file is used for the SDT submodel runs with repository heating. A second file is also created that is a duplicate of the “.nft.dkm” file except there is no wp block present. The second file is called “.nft.dkm0”; this file is used for the SDT submodel initialization runs that have no repository heating. Note that because the file-naming convention is parallel with that used for the LDTH submodels (discussed below), the suffix “dkm” is used for the SDT submodels, as well as for the LDTH submodels. This naming convention does not mean that the SDT submodels use the dual-permeability model (DKM).

inputs (Output DTN: LL0702PA013MST.068)

“.nft” file for each SDT submodel (chimney-submodel) location

output files: (Output DTN: LL0702PA013MST.068)

“.nft.dkm” file: adds the atm, wt, wp, and sz1-6 and bsmnt gridblocks to the input “.nft” file for each chimney-submodel location

“.nft.dkm0” file: adds the atm, wt, and sz1-6 and bsmnt gridblocks to the input “.nft” file for each chimney-submodel location

Step 6 – Create the LDTH submodel DKM files.

Once the “.nft” files have been created, the DKM versions of these files are created for each LDTH submodel (chimney submodel) location. There are four output files created for each chimney submodel location. The input files are modified to include the atmosphere and water table boundary gridblocks, to define the gridblocks within the emplacement drifts that represent the engineered barrier system components (e.g., invert), and to define the matrix and fracture continua. The specific elements added to each of the four types of output files are detailed below. Note that the files with the string “dkm” are used in the LDTH submodel runs with repository heating. The files with the string “dkm0” are used in the LDTH submodel initialization runs that have no repository heating. For the LDTH submodels which are located in fault zones, the “dkm” and “dkm0” files generated for the neighboring non-fault UZ flow model grid column location are used in the LDTH submodel. There are 39 UZ flow model grid column locations that fall within fault zones, listed in the file *fault.names*, which is found in Output DTN: LL0702PA013MST.068 (directory: /meshGeneration/SDT-03). This file lists the prefix of the SDT/LDTH-submodel file name, which includes the name of the repository panel/drift and the UZ flow model grid column location. This file is generated by visually inspecting the original “.dkm” files and identifying those for which the repository horizon resides within fault zones.

inputs: (Output DTN: LL0702PA014MST.069)
“.nft” file for each LDTH submodel (chimney submodel) location

output files (a total of four files for each chimney submodel location): (Output DTN: LL0702PA014MST.069)

- “*.nft.msh.dkm0.f”:
adds the atm and wt fracture boundary gridblocks to the input “.nft” file. All blocks are prepended with “f-” to represent the fractures.
- “*.nft.msh.dkm.f”:
adds the atm, wt, drift, wp, invert, and hstrk fracture gridblocks to the input “.nft” file. All blocks are prepended with “f-” to represent the fractures.
- “*.nft.msh.dkm0.m”:
adds the atm and wt matrix boundary gridblocks to the input .nft file. All blocks are prepended with “m-” to represent the matrix.
- “*.nft.msh.dkm.m”:
adds the atm, wt, drift, wp, invert, and hstrk matrix gridblocks to the input .nft file. All blocks are prepended with “m-” to represent the matrix.

Step 8 – Calculate LDTH submodel percolation flux values.

- 1. Determine the present-day, monsoonal, and glacial-transition climate PTn-to-TSw percolation flux value for each LDTH submodel location**

All the three-dimensional site-scale UZ model grid columns within the repository footprint are identified, and each of them corresponds to one LDTH submodel (chimney submodel) location. Note that the identity of the UZ model grid column is given after the string “WORLD COLUMN” in the LDTH submodel input file. For each LDTH submodel location, the identity of the world column is used to find the corresponding the present-day, monsoonal, and glacial-transition climate PTn-to-TSw percolation fluxes calculated by the three-dimensional site-scale UZ flow model (DTNs: LB0612PDPTNTSW.001 [DIRS 179150], LB0701MOPTNTSW.001 [DIRS 179156], and LB0701GTPTNTSW.001 [DIRS 179153]). This is repeated for the 10th percentile, 30th percentile, 50th percentile, and 90th percentile percolation flux cases. Note that there are 12 percolation flux maps produced by the three-dimensional site-scale UZ flow model, corresponding to the three climate states and four percolation flux cases.

2. Calculate the scaled post-10k percolation flux value for each LDTH submodel location

- i. A weighted average of the glacial-transition percolation flux values for all LDTH submodel locations (or UZ model grid columns) that fall inside of the repository footprint is calculated. The weighting factors are determined by: (1) counting the number of SMT gridblocks in each LDTH submodel location, then (2) the weighting factors equate to the number of SMT gridblocks assigned to a given LDTH submodel location divided by the total number of SMT gridblocks within the repository footprint.
- ii. The weighting factors are applied to all LDTH submodel locations to obtain the averaged repository glacial-transition percolation flux.
- iii. The scaling factor is calculated by dividing the repository-averaged post-10k target percolation flux by the repository-averaged glacial-transition percolation flux. The average post-10k target percolation flux values are 15.9, 23.6, 35.2, and 52.4 mm/yr, respectively for the 10th percentile, 30th percentile, 50th percentile, and 90th percentile percolation flux cases. For further explanation see Section 6.2.16[a].
- iv. The scaled post-10k percolation flux value at each LDTH submodel location is obtained by multiplying the glacial-transition percolation flux value by the scaling factor. This process is repeated for the 10th percentile, 30th percentile, 50th percentile, and 90th percentile percolation flux cases.

Step 9 – Determine the identity of the world column (from the three-dimensional site-scale UZ flow model) for each LDTH-SDT submodel pair.

The “.col” files created in Step 4 include the name of the world column into which an LDTH/SDT submodel pair falls. These world column names are recorded from the “.col” files for the LDTH and SDT submodels. It should be noted that for the LDTH submodels that are located in fault zones, the “.col” files generated for the neighboring non-fault UZ flow model grid column location are used in the LDTH submodel.

Step 10 – Compute SMT, SDT, and LDTH submodel boundary conditions.

Applicable to this addendum, with the following changes.

For the SMT and SDT submodels, software routine `boundary_conditions v1.0` generates ground surface temperatures in NUFT-input format. For the SMT submodel, `boundary_conditions v1.0` generates boundary temperatures 1,000 m below the water table. See Appendix II[a] for details on the SMT submodel boundary condition construction. For the SDT submodels, the lower boundary temperatures are taken from those of the SMT submodel at the corresponding locations.

For the LDTH submodels, `boundary_conditions v1.0` generates a table of boundary conditions at the ground surface, including temperature, gas-phase pressure, air mass fraction, and specific enthalpy of water at the ground-surface conditions in NUFT-input format. Also generated for LDTH submodels are gas-phase pressure boundary conditions at the water table, in NUFT-input format. The temperature at the water table is provided as a function of time from the corresponding SDT submodel.

Step 11 – Compute SMT, SDT, LDTH and DDT submodel heat-generation curves.

Using a reference heat-generation-versus-time table, as well as a table of ventilation-heat-removal efficiency as a function of time and distance from the ventilation inlet, `heatgen_ventTable_emplace v1.0` produces files of heat-generation-versus-time tables in NUFT-heatgen format. These heat-generation files have the influence of reduced heat-generation rates during the 50-year ventilation preclosure period and full-power heating during the postventilation postclosure period. See Appendix III[a] for details on building the heat generation curves. See Appendix V[a] for the assembly of NUFT input files.

Step 12 – Compile natural- and engineered-system properties.

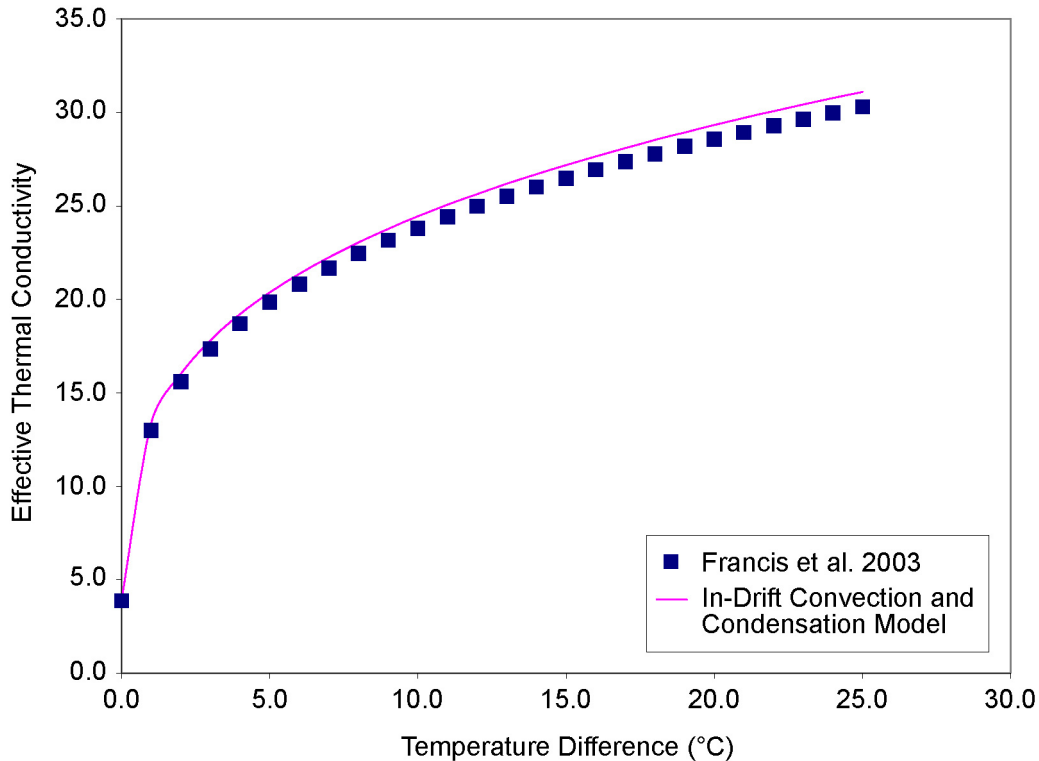
Using several DTNs containing material-property values of the natural system and several information exchange drawings containing material-property values of the engineered system, material-property files (called NUFT rocktab files) are constructed. These files are in the NUFT rocktab format; they are read in as “include” files in the SMT, SDT, LDTH, and DDT submodel NUFT input files. See Appendix IV[a] for details on assembling the rocktab files that contain the material property values for the respective submodels.

Step 13 – Compute effective thermal conductivity.

To account for heat transfer by natural convection in the emplacement drift, correlations have been developed (Francis et al. 2003 [DIRS 164602], Table 6) for the relationship between drift wall, waste package, and drift air temperatures and an effective thermal conductivity K_{eff} of the air in the emplacement drift cavity that represents the influence of heat transfer by natural convection. This process is conducted for the cavity between the drip shield and drift wall in the LDTH submodels and DDT submodels. This process is also conducted for the cavity between the waste package and drip shield in the DDT submodels.

It should be noted that the correlations for the in-drift effective thermal conductivity, which were obtained from Table 6 of the report by Francis et al. (2003 [DIRS 164602]), have been updated

in *In-Drift Natural Convection and Condensation* (SNL 2007 [DIRS 181648], Table 6.4.7-3), resulting in very small changes to the coefficients. The small changes to the coefficients in the correlations are negligible, as shown in Figure I-1[a] for the effective thermal conductivity between the drip shields and drift wall at an average fluid temperature of 95°C.



NOTE: The in-drift effective thermal conductivity between the drip shield and drift wall as a function of the temperature difference between those surfaces is plotted from the correlation in Table 6 of the report by Francis et al. (2003 [DIRS 164602]) and in Table 6.4.7-3 of *In-Drift Natural Convection and Condensation* (SNL 2007 [DIRS 181648]).

Figure I-1[a]. Plot of In-Drift Effective Thermal Conductivity between the Drip Shield and Drift Wall as a Function of Temperature Difference

The effective thermal conductivity K_{eff} is determined by running a NUFT submodel (either LDTH or DDT) starting with an initial guess for K_{eff} for the gas-filled cavities in the drift. The appropriate formula from Table 6 of the report by Francis et al. (2003 [DIRS 164602]) is used to compute K_{eff} in the gas-filled cavities and the NUFT submodel is rerun with the new value of K_{eff} . Each time a new NUFT-submodel run is completed, the value of K_{eff} is computed and compared with the previous iteration. After the value of K_{eff} has converged (between successive iterations), the iterative process is completed. The effective thermal conductivity K_{eff} is a time-varying parameter and the formula in Table 6 of the report by Frances et al. (2003 [DIRS 164602]) involves computing temperatures averaged over the gridblocks representing the gas-filled cavities in the emplacement drift. To carry out this iterative process, the software routine `extractBlocks_EXT v1.0` was used previously to generate the input DTN. This software, which is described in Section 3.1.14 of the parent report, takes a list of gridblocks, extracts the required information from the NUFT submodel output, applies the appropriate formula from Table 6 of the report by Frances et al. (2003 [DIRS 164602]), and produces a time history of calculated K_{eff} .

For the DDT submodels, Output DTN: LL0705PA038MST.030 contains the input and output files for the determination of the K_{eff} history for each of the eight different waste package types. For the preclosure period, which is prior to the emplacement of the drip shields, eight K_{eff} histories are determined for the cavity between the waste packages and drift wall. For the postclosure period, which is after the drip shields have been emplaced, eight K_{eff} histories are determined for the cavity between the waste package and drip shield and eight K_{eff} histories are determined for the cavity between the drip shields and drift wall.

In Output DTN: LL0705PA038MST.030, K_{eff} histories for the preclosure period and for the postclosure period up to 20,100 years are the same as those used in the parent report. For the current DDT submodels, K_{eff} histories are required out to 1,000,000 years. Using a MATLAB v6.1.0.450 (R12.1) script, which is in Output DTN: LL0705PA038MST.030, the K_{eff} histories are extrapolated from 20,100 years to 1,000,000 years on the basis of the heat output for each of the respective waste packages.

For the LDTH submodels, the K_{eff} histories for the preclosure and postclosure period up to 20,100 years are the same as those used in the parent report, which are contained in Output DTN: LL030704623122.031(output from the parent report). For the current LDTH submodels, K_{eff} histories are required out to 1,000,000 years. Using a MATLAB v6.1.0.450 (R12.1) script, which is in Output DTN: LL0705PA038MST.030, the K_{eff} histories are extrapolated from 20,100 years to 1,000,000 years on the basis of the line-averaged heat generation rate.

Step 14 – Create SMT submodel mesh.

To create the SMT submodel mesh used for the MSTHM calculations in this report, one must carefully perform the following steps. The files for generating the SMT submodel mesh are contained in Output DTN: LL0702PA013MST.068 in the directory \meshGeneration, subdirectory \SMT. Note that one must be using the qualified version of YMESH v1.54 and Solaris OS 5.8 UNIX operating system.

- a. Execute YMESH v1.54
ymesh
- b. Pull down *File* tab on YMESH v1.54 and *Open* the data file. In the *Select Input File* popup highlight the file “LBL2003-LA-YMESH-expand_qualified” (from NUFT submodel Building Step 2) and click *OK*
- c. Pull down *Edit* tab and highlight *Extend World Columns*. Make certain the *Above* tab is active. Enter the following:

Material *atm*
Thickness *200.*
click *OK* button

- d. Remain in the *Extended World Columns* but now make the *Below* tab active. Enter the following:

Material *sz1*
Thickness 30.
click *OK* button

Material *sz2*
Thickness 60.
click *OK* button

Material *sz3*
Thickness 70.
click *OK* button

Material *sz4*
Thickness 120.
click *OK* button

Material *sz5*
Thickness 240.
click *OK* button

Material *sz6*
Thickness 480.
click *OK* button

Material *bsmnt*
Thickness 0.1
click *OK* button

- e. Click *CLOSE* button on *Extend World Columns* popup
- f. Open *File* pulldown from YMESH v1.54 menu and select *Open data file*
- g. In the *Select Input File* popup, select file “tspa07.grid03-150w” and click *OK* button

Note that this is the input file that controls how YMESH is to construct the SMT submodel mesh. This file contains the lateral and longitudinal gridblock dimensions that are to be incorporated in the mesh file that is constructed by YMESH. This file also contains the specifications about how the vertical gridblock dimensions are to be constructed by YMESH, including either specific vertical dimensions or maximum vertical dimensions, as a function of distance from the repository horizon. This file also contains the coordinates of the corner of the SMT submodel mesh and the slope of the repository horizon plane.

- h. Highlight *Options* pulldown from YMESH v1.54 menu and select *Trim Top Boundary*

- i. In *Ending Conditions* popup menu, enter the following:

Material *atm*
Thickness *0.1*
click *Apply* button
click *Close* button

- j. Highlight *Edit* pulldown from YMESH v1.54 menu and select *Element Names*

- k. In *Rename Elements* popup window, follow these steps:

- i. Select *Material* button and enter

Prefix *atm*
Material *atm*
Click *Apply* button

Prefix *bsm*

Material *bsmnt*

Click *Apply* button

- ii. Select *PrefixIndexFile* button

In the *PrefixIndexRangeFile* space enter
heatBlockIndicesPane_1_2_3e_3w_4-TSPA07.data
Click *Apply* button
Click *Close* button

- l. Highlight the *File* pulldown menu and select *Save data file*

In the *Save File* popup window type the *Selection* space enter
tspa07.mesh03-150w
Click *OK* button

Note that this saves the mesh file that is read in by the SMT submodel. This file has two parts. The first part, which begins with the keyword “*elc*,” has the gridblock volumes and coordinates for each gridblock. The second part, which begins with the keyword “*conne*” gives the connected distances between the respective gridblocks.

- m. Return to a UNIX command prompt and type the following UNIX commands

```
grep P1 tspa07.mesh03-150w > P1.list  
grep P2 tspa07.mesh03-150w > P2.list  
grep P3E tspa07.mesh03-150w > P3E.list  
grep P3W tspa07.mesh03-150w > P3W.list  
grep P4 tspa07.mesh03-150w > P4.list
```

- n. Using a text editor, open the five files just created: *P1.list*, *P2.list*, *P3E.list*, *P3W.list*, and *P4.list* (Output DTN: LL0705PA038MST.030)

- o. Edit the five files by removing all gridblock connections information (which is the last 70% of the file), saving only the element information (which is the first 30% of the file)
- p. Save the five files with the above names
- q. Return to a UNIX command prompt and type the following UNIX command

```
cat P1.list P2.list P3E.list P3W.list P4.list > P1-P2-P3E-  
P3w-P4-TSPA07.list
```

File P1-P2-P3E-P3W-P4-TSPA07.list is found in Output DTN: LL0705PA038MST.030. Files tspa07.grid03-150w and tspa.mesh03-150w are found in Output DTN: LL0702PA013MST.068. Note that any mistake made by the user in executing the YMESH v1.54 steps forces the user to return to the beginning and redo the YMESH v1.54 steps.

APPENDIX II[a]
BUILDING BOUNDARY CONDITIONS FOR SUBMODELS

The software routine `boundary_conditions v1.0` generates upper and lower boundary conditions for the LDTH, SMT, and SDT submodels (see Step 10 of Appendix I[a]). The boundary conditions were originally derived from *Mountain-Scale Coupled Processes (TH/THC/THM) Models* (BSC 2004 [DIRS 169866]) (DTN: LB991201233129.001 [DIRS 146894]). Data are extracted from the three-dimensional site-scale UZ flow model grid being used in TSPA (DTN: LB03023DKMGRID.001 [DIRS 162354]), as well as from *Mountain-Scale Coupled Processes (TH/THC/THM) Models* (BSC 2004 [DIRS 169866]), including the boundary conditions (file `INCON_thm_s32.dat` in DTN: LB991201233129.001 [DIRS 146894]) and the corresponding three-dimensional mountain-scale grid (file `MESH_rep.VF` in DTN: LB991201233129.001 [DIRS 146894]). It should be noted that the three-dimensional mountain-scale grid used in *Mountain-Scale Coupled Processes (TH/THC/THM) Models* (BSC 2004 [DIRS 169866]) has a horizontal water table at an elevation of 730 m, while the three-dimensional site-scale UZ flow model grid used in the TSPA (DTN: LB03023DKMGRID.001 [DIRS 162354]) has a sloping boundary representing the water table. The software routine `boundary_conditions v1.0` uses linear interpolation to determine the water-table boundary conditions at the sloping water-table surface in the three-dimensional site-scale UZ flow model grid used in the TSPA (DTN: LB03023DKMGRID.001 [DIRS 162354]). The software routine `boundary_conditions v1.0` reads input files containing the following information, respectively: (1) the SMT submodel grid, (2) the UZ model grid and (3) initial conditions from *Mountain-Scale Coupled Processes (TH/THC/THM) Models* (BSC 2004 [DIRS 169866]), (4) the grid centers and ground-surface and water-table elevations of the World Columns in the three-dimensional site-scale UZ flow model, (5) coordinates of the LDTH/SDT submodel locations, and (6) the values of wet thermal conductivity of the UZ model layers.

For item (4) above, `colCen v1.0` was previously used to develop the input DTN in the parent report where the grid centers for all World Columns in the three-dimensional site-scale UZ flow model were specified.

Boundary conditions are generated by `boundary_conditions v1.0` at all World Columns (from the three-dimensional site-scale UZ flow model) and at all LDTH/SDT submodel locations. For the LDTH submodels, `boundary_conditions v1.0` generates a table of boundary conditions at the ground surface, including temperature, gas-phase pressure, air mass fraction, and specific enthalpy of water at the ground-surface conditions in NUFT-input format. Also generated for LDTH submodels are gas-phase pressure boundary conditions at the water table, in NUFT-input format. The temperature at the water table is provided as a function of time from the corresponding SDT submodel.

For the SMT and SDT submodels, software routine `boundary_conditions v1.0` generates ground-surface temperatures in NUFT-input format. For the SMT submodel, `boundary_conditions v1.0` generates boundary temperatures 1,000 m below the water table. For the SDT submodels, the lower boundary temperatures are identical to those of the SMT submodel at the corresponding locations.

Prior to determining the boundary conditions, Steps 1 and 2 of Appendix I[a], which result in an expanded three-dimensional mountain-scale mesh (called the expanded World Grid for YMESH v1.54), must be executed. This expanded three-dimensional mountain-scale mesh (also called the expanded World Grid) is used as an input to `boundary_conditions v1.0`, which

subsequently outputs all of the boundary condition files to be used for all of the submodels (see Appendix V[a] for the assembly of NUFT input files).

Create boundary condition files for all submodels.

The software routine `boundary_conditions v1.0` was used to create the boundary conditions for all submodels.

software routine:

`boundary_conditions`

input files (Output DTN: LL0702PA013MST.068)

`tspa07.mesh03-150w` (SMT submodel mesh file in NUFT meshfile input format, which includes the coordinates of each grid block.)

`MESH_rep.VF` of DTN: LB991201233129.001 [DIRS 146894] (Mesh file for BSC 2004 [DIRS 169866].)

`INCON_thm_s32.dat` of DTN: LB991201233129.001 [DIRS 146894] (Initial conditions for BSC 2004 [DIRS 169866].)

`grid_column_centers` (Ground-surface and water-table elevations and coordinates of World Columns of the three-dimensional site-scale UZ flow model grid, which is file `LBL2003-YMESH-expand_qualified`; this input information was generated previously in the parent report with `colCen v1.0`; see above.)

`chimneyLocation` (Coordinates of each of the 560 LDTH/SDT submodels pairs, which are established by identifying the heated gridblock from file `tspa07.mesh03-150w` that is closest to the coordinates of the corresponding World Column in file `LBL2003-YMESH-expand_qualified`. These coordinates are reported in the comment lines at the top of the respective LDTH and SDT submodel input files.)

`tcond.dat` (Thermal conductivity of UZ model layers.)

output files (Output DTN: LL0702PA013MST.068)

`chimSurfBC.dat` (LDTH submodel ground-surface boundary conditions: temperature, gas pressure, air mass fraction in gas phase, and specific enthalpy of water, which is parsed out into the files `Tatm.dat`, `Patm.dat`, `Xatm.dat`, and `enthalpy.dat` for use in the LDTH, and, for temperature only, for use in the SDT submodels.)

`chimLowerBC.dat` (LDTH submodel water table boundary conditions: temperature and gas pressure, which is parsed into the files `Twt.data` and `Pwt.dat`; note that the water table temperature is only used by the LDTH initialization submodels, while the post-emplacement LDTH submodels are

supplied a time-dependent water-table temperature from the corresponding SDT submodel.)

smtUpperBC.dat (Ground-surface boundary temperature for SMT submodel in NUFT input format.)

smtLowerBC.dat (Lower boundary temperature for SMT submodel in NUFT input format, which is also called the “basement,” 1,000 m below the water table, is parsed into the file *Tbs.dat* for use in the SDT submodels.)

execution process

To start, type:

boundary_conditions

Enter output file extension:

out

Enter thermal cond. of material below water table, SMT submodel:

1.2

Enter value of added thickness below water table, SMT submodel:

1000

Enter name of SMT submodel mesh file:

Hit return with no entry to use default file, smtMesh

SMTMESHTEST

Enter name of the Mountain-Scale Coupled Process (TH/THC/THM) Models (BSC 2004 [DIRS 169866]) mesh file:

Hit return with no entry to use default file, MESH_rep.VF

MESH_rep.VF

Enter name of the Mountain-Scale Coupled Process (TH/THC/THM) Models (BSC 2004 [DIRS 169866]) file with init.cond.:

Hit return with no entry to use default file, INCON_thm_s32.dat

INCON_thm_s32.dat

Enter name of file with World Column data from the 3-D site-scale UZ flow model:

Hit return with no entry to use default file, grid_column_centers

GRID_COLUMN_CENTERS

Enter name of file with LDTH-/SDT submodel "chimney" locations:

Hit return with no entry to use default file, chimneyLocation

CHIMNEYLOCATION

Enter name of file with thermal cond. data:

Hit return with no entry to use default file, tcond.dat

TCOND.DAT

Note that the boundary conditions in the LDTH and SDT ".dat" files appear in the same order as the list of 560 LDTH/SDT locations given in file *chimneyLocation* from Output DTN: LL0702PA013MST.068.

APPENDIX III[a]
HEAT GENERATION FOR SUBMODELS

To produce the heat generation for the SMT, SDT, DDT, and LDTH submodels (Step 11 in Appendix I[a]), the following instructions must be followed. The software routine `heatgen_ventTable_emplace v1.0` is used for this purpose.

The software routine `heatgen_ventTable_emplace v1.0` is used to incorporate the influence of ventilation heat-removal efficiency on the net heat generation available for heating the host rock. The source of the ventilation heat-removal efficiency is DTN: `MO0701VENTCALC.000 [DIRS 179085]`. This is accomplished using a net-available-heat-generation fraction, which is equal to 1 minus the heat-removal-efficiency fraction, and which is given as a function of time and distance from the ventilation inlet. This software routine requires a control file that provides names of the locations (within the repository) at which heat-generation files should be created along with the distance of that location from the ventilation inlet. The output of `heatgen_ventTable_emplace v1.0` is a series of files of heat-generation-rate-versus-time tables that account for the heat-removal efficiency of forced-convection ventilation of the emplacement drifts during the preclosure period. The output files from `heatgen_ventTable_emplace v1.0` are in NUFT `heatgen` format.

Creating Heat Generation Curves for the SDT and LDTH submodels

software routine

`heatgen_ventTable_emplace v1.0`

inputs: (Output DTN: `LL0702PA013MST.068`)

SDT: string indicating to the software routine that this is an SDT/LDTH submodel
heatgen file

`multi-package_7WP_Segment_Info_SDT_LDTH_TSPA03`: default SDT/LDTH submodel
heat-generation table with nominal loading and no ventilation

`LA_ventilation_table_50yr.rfm`: ventilation table with ventilation efficiency as a function of time and distance from the ventilation inlet.

`ventilation_time.reform`: file giving the name and distance from the ventilation inlet for each LDTH-/SDT submodel “chimney” location.

outputs: (heatgen file) (Output DTN: `LL0702PA013MST.068`)

`P*_LDTH-SDT` output heatgen file for each LDTH-/SDT submodel “chimney” location

Creating Heat Generation Curves for the DDT submodels

software routine

`heatgen_ventTable_emplace`

inputs: (Output DTN: `LL0705PA038MST.030`)

DDT: string indicating to the software routine that this is a DDT heatgen file
`DDT_TSPA07` is the default DDT heat generation table with nominal loading and no ventilation.

`LA_ventilation_table_50yr.rfm`: ventilation table with ventilation efficiency as a function of time and distance from the ventilation inlet.

ventilation_time.reform: file giving the name and distance from the ventilation inlet for each LDTH/SDT submodel “chimney” location.

outputs: (heatgen file) (Output DTN: LL0705PA038MST.030)

P*_DDT output heatgen file for each LDTH/SDT submodel “chimney” location

As discussed in Section 6.2.17[a], the time-dependent ventilation heat-removal efficiency for the DDT submodel is slightly different from that described in Section 6.2.8.4 of the parent report. The previous DDT submodel used the heat-generation curve pertaining to the g₉ UZ flow model LDTH/SDT submodel location (Figure 6.2-17[a]). The heat-generation curve for the current DDT submodel is based on an area-weighted average for the heat-generation curves for the 560 LDTH/SDT submodel locations, which are determined as described above. The average heat-generation curve is given in file *DDT_AVG_TSPA07* from Output DTN: LL0702PA013MST.068.

Creating Heat Generation Curves for the SMT submodel

software routine

heatgen_ventTable_emplace

inputs: (Output DTN: LL0702PA013MST.068)

SMT: string indicating to the software routine that this is an SMT submodel heatgen file

SMT_TSPA03: default SMT submodel heat-generation-versus-time table with nominal loading and no ventilation

LA_ventilation_table_50yr.rfm: ventilation table with ventilation efficiency as a function of time and distance from the ventilation inlet.

ventilation_time.rfm: file giving the name and distance from the ventilation inlet for each LDTH/SDT submodel “chimney” location.

outputs: (heatgen file) (Output DTN: LL0702PA013MST.068)

SMT_TSPA03_P* output heatgen file for each SMT submodel location

The heatgen files are then used as inputs to the NUFT input files; see Appendix V[a] for details on the assembly of NUFT input files. Note that the software heatgen_ventTable_emplace v1.0 generates heat-generation tables with a sharply defined transition from ventilated to unventilated conditions. For the 50-year ventilation period, it defines the transition occurring between 49.99999 and 50.00000 years.

APPENDIX IV[a]
BUILDING SUBMODEL MATERIAL PROPERTY FILES

LDTH Submodel DKM Properties

Hydrologic properties of Tptpmn (tsw34) and Tptpll (tsw35), which are listed in Table IV-4[a], are obtained from DTN: LB0610UZDSCP30.001 [DIRS 179180] and are applied to the LDTH submodels for all four percolation flux cases (P10, P30, P50, and P90). These data were distilled into file *SDT-IDds-06* in Output DTN: LL0702PA0131455.068 where the following parameters can be found: permeability (matrix and fracture in Table IV-3b[a]), porosity (matrix and fracture), van Genuchten properties (matrix and fracture), and residual saturation (matrix and fracture). See also DTN: LB0208UZDSCPMI.002 [DIRS 161243].

Thermal properties are taken from Output DTNs: MO0612MEANTHER.000 and MO0702PAGLOBAL.000, from DTNs SN0303T0503102.008 [DIRS 162401] and SN0307T0510902.003 [DIRS 164196], and from Table 7-10 of DTN: SN0404T0503102.011 [DIRS 169129] (file: *ReadMe Summary.doc*). The mean bulk thermal conductivity (for both wet and dry conditions) of the repository UZ model layers (host-rock units) was obtained from Output DTN: MO0612MEANTHER.000. The bulk thermal conductivity (for both wet and dry conditions) of the host-rock units for the low and high host-rock thermal conductivity cases was obtained from Output DTN: MO0702PAGLOBAL.000. Bulk thermal conductivity K_{th} (for both wet and dry conditions) and bulk density of the nonrepository GFM2000 layers was obtained from DTN: SN0303T0503102.008 [DIRS 162401]. The bulk density ρ_b of the host-rock units was obtained from Table 7-10 of DTN: SN0404T0503102.011 [DIRS 169129] (file: *ReadMe Summary.doc*). The specific heat capacity of the mineralogical model layers is taken from DTN: SN0307T0510902.003 [DIRS 164196]. The source input data for bulk density and bulk thermal conductivity is summarized in Table IV-3a[a].

The following parameters were calculated by hand using parameters obtained in the files listed above: (1) grain density, (2) matrix density and fracture density, (3) matrix and fracture contact length factors, and (4) thermal conductivity relations for matrix and fracture. Table IV-3b[a] shows the results of calculating the density and thermal conductivity for the matrix and fracture continua. It should be noted that the vitric units have no fractures, but for the DKM to work, values must be assigned to a “pseudo-fracture” continuum for vitric units. This is accomplished by simply assigning matrix properties to the fracture continuum for the vitric units (tsw9v, ch1v, ch2v, ch3v, ch4v, ch5v, and ch6v). The specific details of the hand calculations are listed below.

1. The grain density ρ_g is calculated as:

$$\rho_g = \frac{\rho_b}{1 - \phi_m},$$

where ϕ_m is matrix porosity and ρ_b is bulk density.

2. The grain density ρ_g is partitioned to the matrix and fracture continuum according to the fracture porosity, ϕ_f . The matrix and fracture densities, $\rho_{g,m}$ and $\rho_{g,f}$, are calculated as:

$$\begin{aligned}\rho_{g,m} &= \rho_g (1 - \phi_f), \\ \rho_{g,f} &= \rho_g \phi_f.\end{aligned}$$

Because the vitric units do not have fractures, the grain density for the fracture and matrix continuum is calculated slightly differently. The matrix porosity is apportioned 50% to the matrix continuum and 50% to the pseudo-fracture continuum. The bulk density is also apportioned 50% to the matrix continuum and 50% to the pseudo-fracture continuum. Thus, the grain densities for the fracture and matrix continuum are calculated as:

$$\rho_{g,m} = \rho_{g,f} = \frac{\rho_b}{2\left(1 - \frac{\phi_m}{2}\right)},$$

where ϕ_m is the total matrix porosity and ρ_b is the total bulk density. Table IV-3b[a] shows the result of this hand calculation for the vitric units.

3. The matrix-contact-length factor is calculated as $1/(6N)$, where N is the fracture frequency from DTN: LB0205REVUZPRP.001 [DIRS 159525] (Table IV-5[a]) and 6 accounts for the distance between the center of the matrix block and the fractures for Type #1 fractures as described in *Development of Numerical Grids for UZ Flow and Transport Modeling* (BSC 2004 [DIRS 169855], Equation 6-4). The fracture-contact-length factor is always 0 (BSC 2004 [DIRS 169855], Equation 6-3). The matrix-contact-length factor and the fracture-contact-length factor affect disequilibrium between the matrix and fracture continuum in the LDTH submodels.
4. The thermal conductivity for the matrix $K_{th,m}$ and fracture $K_{th,f}$ (both dry and wet) are calculated as a function of fracture porosity ϕ_f for the given wet and dry bulk thermal conductivities K_{th} :

$$K_{th,m}^{dry} = K_{th}^{dry} (1 - \phi_f),$$

$$K_{th,f}^{dry} = K_{th}^{dry} \phi_f,$$

$$K_{th,m}^{wet} = K_{th}^{wet} (1 - \phi_f),$$

$$K_{th,f}^{wet} = K_{th}^{wet} \phi_f.$$

These properties are written into a “rocktab” file (an example of which is listed at the bottom of this appendix) for the NUFT input file (see Appendix V[a]). All transport and partitioning parameters (e.g., K_d and $K_{d,Factor}$ in the rocktab file) are set to zero because sorption is not considered for any of the calculations of this report. The uncertainty of the wet and dry thermal conductivity values of the host-rock units is addressed with values from Output DTN: MO0702PAGLOBAL.000.

Note that de Marsily (1986 [DIRS 100439], p. 233) gives a range of tortuosity from 0.1 for clays to 0.7 for sands. The value of 0.2 for the matrix continuum is used because the pore sizes for the matrix are closer to those of clays than to those of sands. A value of 0.7 is assumed for the fracture in Section 5.3.1.9 of the parent report.

As described in Section 6.2.13.4[a], the thermal properties of the nonrepository units are averaged (i.e., lumped). The nonrepository units lying above the host-rock units are lumped in the uz1 unit, while the nonrepository units lying below the host-rock units are lumped in the uz2 unit. Section 6.3.14[a] justifies the reasonableness of this approach. The lumped uz1 and uz2 units are defined as the following two groups of nonrepository units:

1. uz1 = [tcw11, tcw12, tcw13, ptn21, ptn22, ptn23, ptn24, ptn25, ptn26, tsw31, tsw32]
2. uz2 = [tsw38, tsw39, tsw39v, ch1z, ch1v, ch2v, ch3v, ch4v, ch5v, ch6v, ch2z, ch3z, ch4z, ch5z, ch6z, pp4, pp3, pp2, pp1, bf3, bf2].

Host-rock units tsw33, tsw34, tsw35, and tsw36 remain unchanged (note that tsw37 is equivalent to tsw36). The process of lumping the thermal properties for the uz1 and uz2 units is as follows:

- Calculate area-weighting factors based of the 560 UZ flow model columns. The area-weighting factor for a given UZ flow model column is determined by the number of heated SMT submodel gridblocks within that column, divided by 3,264, which is the total number of heated SMT submodel gridblocks within the repository footprint.
- At each UZ flow model column, calculate the arithmetic mean values of solid density and specific heat for the uz1 and uz2 units on the basis of the unit thicknesses.
- At each UZ flow model column, calculate the harmonic mean values of thermal conductivity for the uz1 and uz2 units on the basis of the unit thicknesses.
- Calculate the arithmetic mean values of solid density, specific heat, and thermal conductivity for the uz1 and uz2 units, using the area-weighting factors described above.
- Thermal properties of each nonrepository unit are replaced with the calculated lumped values for the uz1 and uz2 units as appropriate.
- As described in Section 6.2.16[a], the hydrologic properties of the uz1 unit are those of the tsw33 unit, while the hydrologic properties of the uz2 unit are those of the tsw34 unit.

Note that with respect to the thermal properties, the lumped uz1 and uz2 units are also applied to the DDT submodels.

LDTH Submodel In-Drift, DKM Properties

Invert Properties

The invert properties for the matrix continuum (i.e., the intragranular porosity) are obtained from DTN: LB0610UZDSCP30.001 [DIRS 179180], and those for the fracture continuum (i.e., the intergranular porosity) are from Appendix X[a]. Section 5.3.1.8 of the parent report discusses the assumption about the intergranular permeability of the crushed-tuff invert material. The van Genuchten alpha for the fracture continuum from Table X-7[a] of Appendix X[a] is 624 bar^{-1} ($6.24 \times 10^{-3} \text{ Pa}^{-1}$). The input parameters that require hand calculations are:

(1) intragranular porosity (ϕ_m), (2) the thermal conductivity for the fracture and matrix continuum, and (3) the grain density of the matrix and of the fracture continuum.

Invert Porosity

The matrix porosity or intergranular porosity of the crushed-tuff grains in the invert, ϕ_m , is taken from DTN: LB0208UZDSCPMI.002 [DIRS 161243] and is equal to 0.131, which is the matrix porosity of the Tptpl1 (tsw35) unit. The intergranular porosity of the crushed-tuff invert material is obtained from Table X-7[a] of Appendix X[a] and is equal to 0.22. The porosity of the fracture continuum in the invert, ϕ_f , which is called the intergranular porosity, is a bulk quantity. Because the porosity of the matrix continuum in the invert, which is called the intragranular porosity, $\phi_{g,m}$, is also a bulk quantity, the intragranular porosity of the crushed-tuff invert material is given by:

$$\phi_{g,m} = \phi_m(1 - \phi_f).$$

Thus, the intragranular porosity (or matrix-continuum porosity) of the crushed-tuff invert material used in the LDTH submodels is equal to 0.1022.

Invert Thermal Conductivity

The bulk thermal conductivity of the crushed-tuff invert material is partitioned 99% to the matrix continuum and 1% to the fracture continuum, as follows:

$$\begin{aligned}K_{th,f} &= 0.01K_{th}, \\K_{th,m} &= 0.99K_{th}.\end{aligned}$$

This partitioning is done because the majority of the thermal mass in the invert resides in the matrix continuum.

Invert Grain Density

The bulk grain density of the crushed-tuff invert material is partitioned 99% to the matrix continuum and 1% to the fracture continuum, as follows:

$$\begin{aligned}\rho_{g,m} &= 0.99 \frac{\rho_b}{1 - \phi_m}, \\ \rho_{g,f} &= 0.01 \frac{\rho_b}{1 - \phi_f},\end{aligned}$$

where $\rho_{g,m}$ is the grain density of the matrix continuum, $\rho_{g,f}$ is the grain density of the fracture continuum, and ρ_b is the bulk density of the crushed-tuff invert material, as determined from the following:

$$\rho_b = \rho_{tsw35}^b (1 - \phi_{tsw35}^f) (1 - \phi_f),$$

where ρ_{tsw35}^b is the bulk density of tsw35 obtained from Table IV-3a[a], ϕ_m is the matrix-continuum porosity of the crushed-tuff invert material, and ϕ_m is the intergranular (fracture-continuum) porosity of the crushed-tuff invert. This partitioning is done because the majority of the thermal mass in the invert resides in the matrix continuum.

Waste Package and Drip Shield Properties

Due to grid resolution limitations in the drift, the geometry of the waste package and drip shield is lumped into a monolithic heat source in the LDTH submodels (see Figure 6.2-6). Waste package density, drip shield density, and thermal conductivity should be averaged into this lumped approximation. The half-area (called $A_{1/2}$) of the waste package and drip shield is represented in the LDTH submodel as a group of finite difference blocks with an area calculated as:

$$A_{1/2} = 0.242 \times 0.58 + 0.40 \times (0.40 + 0.37) + (0.759 + 0.760 + 0.425) \times (0.58 + 0.37 + 0.3025) = 2.9552 \text{ m}^2.$$

These dimensions are obtained from the gridblock spacings in the LDTH submodels, which are shown in Figure 6.2-6 of the parent report. Note that for the purpose of calculating the thermal properties of the monolithic heat source, the dimensions and weights of the waste packages from the parent report are used. Table 4-1 from the parent report gives the nominal number of waste packages in the repository: (1) 4,299 21-PWR AP waste packages, (2) 2,831 44-BWR AP waste packages, and (3) 11,184 total waste packages. Therefore, the majority of waste packages (64%) will be either 21-PWR AP waste packages or 44-BWR AP waste packages; both of these waste packages weigh 43,000 kg and are 5.165 m in length, which is given in Table 4-1 of the parent report. After adding 0.1 m for the waste package spacing (Table 4-1[a]) to the length of the waste package, the weight per unit length of the majority of waste packages is 43,000 kg divided by 5.265 m (5.165 m + 0.1 m), or 8,200 kg/m. This is taken to be representative of the average waste package in the repository. The lineal weight per unit length of drip shield is equal to the weight of the drip shield (5,000 kg, given in Table 4-1[a]) divided by the drip shield length (6.105 m, given in Table 4-1[a]), which is equal to 820 kg/m.

The lineal weights per unit length of the average waste package and drip shield are 8,200 kg/m and 820 kg/m, respectively, yielding a total lineal weight of 9,020 kg/m. The equivalent density, ρ_{equiv} , of the LDTH waste package and drip shield is calculated as:

$$\rho_{equiv} = \frac{9,020 \frac{\text{kg}}{\text{m}}}{2A_{1/2}} = 1,526.1 \frac{\text{kg}}{\text{m}^3}.$$

The value of ρ_{equiv} is rounded to 1,530 kg/m³.

The thermal conductivity of the waste package and drip shield is the sum of the thermal conductivity values weighted by the relative weight of the respective materials:

$$K_{th,equiv} = K_{th,ds} \frac{820}{9,020} + K_{th,wp} \frac{8,200}{9,020}.$$

SDT/DDT Submodel Thermal Properties

The thermal properties are taken from DTNs: SN0303T0503102.008 [DIRS 162401], SN0307T0510902.003 [DIRS 164196], and SN0404T0503102.011 [DIRS 169129] (Table 7-10, file: *readme_Summary.doc*). Bulk thermal conductivity and bulk density of the GFM2000 nonrepository layers are obtained from DTN: SN0303T0503102.008 [DIRS 162401]. Bulk thermal conductivity of the host-rock units is obtained from Output DTN: MO0612MEANTHER.000. As explained in Sections 6.3.14[a], 6.3.15[a], and 6.3.17[a], only the wet thermal conductivity values are used in the SMT, SDT, and DDT submodels. Bulk density of the host-rock units is obtained from Table 7-10 of DTN: SN0404T0503102.011 [DIRS 169129] (file: *readme_Summary.doc*). The specific heat capacity of the mineralogical model units is obtained from DTN: SN0307T0510902.003 [DIRS 164196]. The input data from these DTNs are summarized in Table IV-3a[a]. The SDT, DDT, and SMT submodels use the bulk density and bulk thermal conductivity values and do not require that these values be partitioned into the fracture and matrix continuum. Note that because NUFT uses the grain density (also called solid density), the matrix porosity, which is obtained from DTN: LB0208UZDSCPMI.002 [DIRS 161243], is also required as input to the input files for the SDT, DDT, and SMT submodels.

The only parameter requiring a hand calculation for the SDT and DDT submodel near-field properties is the grain density (or solid density) ρ_g , which is calculated as:

$$\rho_g = \frac{\rho_b}{1 - \phi_m}.$$

DDT Submodel In-Drift Thermal Properties

The material properties for the DDT submodel are the same as the corresponding bulk thermal properties in the drift for the LDTH submodel. There is a difference with how the waste package and drip shield are accounted for in the DDT submodel, however, as the DDT submodel represents each waste package separately and discretizes the drip shield.

Waste Package and Drip Shield Thermal Properties

For the DDT submodel, the weights of each waste package are discretely represented, not lumped, into an average representation of the drip shield and waste package, as was done for the LDTH submodel. Due to limitations of grid resolution in the drift of the DDT submodels, all waste packages are modeled as though they have the same diameter (see Section 5.4.1[a]) even though the actual diameters are not the same (see Table 4-1[a]). An effective mass density ρ_{eff} is calculated for each of the respective waste packages so that the mass of each waste package is properly represented in the DDT submodels. The effective density ρ_{eff} is equal to the mass of the waste package (SNL 2007 [DIRS 179394], Table 4-3), divided by volume of the waste package as it is represented in the DDT submodel.

Using the waste package dimensions (SNL 2007 [DIRS 179394], Tables 4-3, 4-8, and 4-9)), effective waste package specific heat, $C_{p,WP}$, of the DDT submodel is calculated for each waste package using a volumetric average of the corresponding materials:

$$C_{p,WP} = \frac{C_{p,outer}(d_3^2 - d_2^2) + C_{p,inner}(d_2^2 - d_1^2) + C_{p,internal}d_1^2}{d_3^2},$$

where d_3 is the outer diameter of the outer barrier, d_2 is the outer diameter of the inner vessel, and d_1 is the inner diameter of the inner vessel; $C_{p,outer}$ is the specific heat of the outer barrier, $C_{p,inner}$ is the specific heat of the inner vessel, and $C_{p,internal}$ is the specific heat of the internal cylinder. This value of specific heat is rounded to 480 J/kg·K, applied to each of the waste packages in the DDT submodels.

Using the waste package dimensions (SNL 2007 [DIRS 179394], Tables 4-3, 4-8, and 4-9)), the effective waste package thermal conductivity, $K_{th,WP}$, also uses a volumetric average:

$$K_{th,WP} = \frac{K_{th,outer}(d_3^2 - d_2^2) + K_{th,inner}(d_2^2 - d_1^2) + K_{th,internal}d_1^2}{d_3^2}.$$

The waste package thermal conductivity only influences longitudinal heat flow along the axis of the drift in the DDT submodel. In other words, radial heat flow (from the center of the waste package to the outer surface) is not predicted in the DDT submodel. Therefore, only the axial component of $K_{th,WP}$ is required in the DDT submodel. Because the materials in the waste package are concentrically arranged, the volumetric average of $K_{th,WP}$ of the respective components of the waste package is the appropriate manner in which to determine the effective waste package thermal conductivity. The value of effective waste package thermal conductivity is rounded to 2.1 W/m·K, applied to each of the waste packages in the DDT submodels.

Using the weight, thickness, and length of the drip shield (SNL 2007 [DIRS 179394], Tables 4-1 and 4-2)), as well as the cross-sectional representation of the drip shield in the DDT submodels, the mass density of the drip shield is calculated (and rounded) to be 7,580 kg/m³.

The thermal parameters for the drip shield (Table 4-1[a]) were taken directly from Table TCD of *1995 ASME Boiler and Pressure Vessel Code* (ASME 1995 [DIRS 108417], Section II). The thermal parameters required in the NUFT submodels necessitate the calculations described below for titanium.

Thermal Properties for Stainless Steel Type 316 and Titanium

Several of the direct inputs available for determining waste package and drip shield thermal properties require interpolation (to a reference temperature) and/or require simple calculations to the input parameters required by the DDT submodel. The thermal conductivity of Stainless Steel Type 316, which is used in the inner cylinder of the waste packages, requires interpolation to 100°C. Furthermore, the specific heat for Stainless Steel Type 316 was calculated on the basis

of thermal diffusivity and thermal conductivity, which are direct inputs. Similarly, the thermal conductivity of titanium, which is used in the drip shield, also requires interpolation to a temperature of 100°C while the specific heat for titanium was calculated on the basis of thermal diffusivity and thermal conductivity, which are direct inputs. The following steps were used to obtain the required parameter values.

1. Mass density of Stainless Steel Type 316

$$7.98 \text{ g/cm}^3 = 7,980 \text{ kg/m}^3 = 498.175 \text{ lb/ft}^3$$

The bold value above is taken from Table XI of ASTM G 1-90 [DIRS 103515].

2. Thermal conductivity of Stainless Steel Type 316 ($T = 100^\circ\text{C}$)

Table IV-1[a]. Interpolation of Thermal Diffusivity and Thermal Conductivity Outlined for Stainless Steel Type 316

Temperature (°F)	Temperature (°C)	Thermal Diffusivity (ft ² /hr)	Thermal Conductivity (BTU/hr-ft-°F)	Thermal Conductivity (W/m-K)
200	93.33	0.141	8.4	14.54
250	121.11	0.143	8.7	15.06
212	100.00	0.1415	8.472	14.665
Conversion Factor			1.0	1.730734666

NOTE: The conversion of these parameters from English units to SI units is also shown. The bold values are from Table TCD of 1995 ASME Boiler and Pressure Vessel Code (ASME 1995 [DIRS 108417]).

$$0.1415 = \mathbf{0.141} + (\mathbf{0.143} - \mathbf{0.141}) \times \frac{212 - 200}{250 - 200}$$

$$8.472 = \mathbf{8.4} + (\mathbf{8.7} - \mathbf{8.4}) \times \frac{212 - 200}{250 - 200}$$

$$14.655 = 14.54 + (15.06 - 14.54) \times \frac{212 - 200}{250 - 200}$$

$$14.663 = 1.730734666 \times 8.472$$

3. Specific heat of Stainless Steel Type 316 ($T = 100^\circ\text{C}$)

$$\begin{aligned} \text{Specific Heat (BTU/lb-}^\circ\text{F)} &= \frac{\text{Thermal Conductivity (BTU/hr-ft-}^\circ\text{F)}}{\text{Density (lb/ft}^3\text{) Thermal Diffusivity(ft}^2\text{/hr)}} \\ &= \frac{8.472}{498.175 \times 0.1415} = 0.1202 \text{ (BTU/lb-}^\circ\text{F)} \\ &= 503.19 \text{ (J/kg-}^\circ\text{K)}. \end{aligned}$$

4. Density of titanium

$$\mathbf{0.163} \text{ lb/in}^3 = 4521 \text{ kg/m}^3 = 281.675 \text{ lb/ft}^3$$

The bold value above is taken from Section II, Table NF-2 of *1995 ASME Boiler and Pressure Vessel Code* (ASME 1995 [DIRS 108417]).

5. Thermal conductivity of titanium ($T = 100^\circ\text{C}$)

Table IV-2[a]. Interpolation of Thermal Diffusivity and Thermal Conductivity Outlined for Titanium

Temperature (°F)	Temperature (°C)	Thermal Diffusivity (ft ² /hr)	Thermal Conductivity (BTU/h-ft-°F)	Thermal Conductivity (W/m-K)
200	93.33	0.331	12.00	20.7688
250	121.11	0.322	11.85	20.5092
212	100.00	0.3288	11.964	20.7065

NOTE: The conversion of these parameters from English units to SI units is also shown. The bold values are taken from Section II, Table NF-2 of *1995 ASME Boiler and Pressure Vessel Code* (ASME 1995 [DIRS 108417]).

$$0.3288 = \mathbf{0.331} + (\mathbf{0.332} - \mathbf{0.331}) \times \frac{212 - 200}{250 - 200}$$

$$11.964 = \mathbf{12.0} + (\mathbf{11.85} - \mathbf{12.0}) \times \frac{212 - 200}{250 - 200}$$

6. Specific heat of titanium ($T = 100^\circ\text{C}$)

$$\begin{aligned} \text{Specific Heat (BTU/lb-}^\circ\text{F)} &= \frac{\text{Thermal Conductivity (BTU/h-ft-}^\circ\text{F)}}{\text{Density (lb/ft}^3\text{) Thermal Diffusivity(ft}^2\text{/h)}} \\ &= \frac{11.964}{281.675 \times 0.3288} = 0.1292 \text{ (BTU/lb-}^\circ\text{F)} \\ &= 540.85 \text{ (J/kg-K)}. \end{aligned}$$

These simple calculations used the following conversion factors:

1. Heat Capacity: $1.0 \text{ Btu/(lb-}^\circ\text{F)} = 4186.8 \text{ J/(kg}\cdot\text{K)}$
2. Thermal Conductivity: $1.0 \text{ Btu/(h-ft-}^\circ\text{F)} = 1.730734666 \text{ W/(m}\cdot\text{K)}$
3. Density: $1.0 \text{ g/cm}^3 = 62.427960576 \text{ lb/ft}^3$
4. Density: $1.0 \text{ lb/in}^3 = 27,679.904710203 \text{ kg/m}^3$.

Invert Thermal Properties

For the DDT submodels, the invert has the same bulk thermal properties as the bulk thermal properties in the LDTH submodels. That is, the thermal conductivity, specific heat, and mass density in the DDT submodels are the same as the bulk thermal conductivity, specific heat capacity, and bulk mass density of the invert in the LDTH submodels. As discussed in Section 6.2.13.2[a], the DDT submodels use the same invert bulk density ($1,270 \text{ kg/m}^3$) used in the parent report, from DTN: GS020183351030.001 [DIRS 163107], while the LDTH submodels use an updated value ($1,530 \text{ kg/m}^3$), which is from DTN: SN0404T0503102.011 [DIRS 169129], adjusted for the updated invert porosity of 0.22. Because heat flow changes so slowly in the model, heat storage effects on temperature are negligible, and thus difference in invert bulk density has no impact on in-drift and near-field temperature histories.

SMT Submodel Thermal properties

Only fault and saturated zone thermal properties need to be specifically calculated for the SMT submodel thermal properties. Otherwise, the SMT submodel uses the same thermal properties as the SDT submodels.

Fault-Zone Thermal Properties

The density of the fault zone is simply the average of all of the units that make up the fault zone:

$$\begin{aligned}\rho_{\text{tcwfl}} &= (\rho_{\text{tcw11}} + \rho_{\text{tcw12}} + \rho_{\text{tcw13}})/3 \\ \rho_{\text{ptnfl}} &= (\rho_{\text{ptn21}} + \rho_{\text{ptn22}} + \rho_{\text{ptn23}} + \rho_{\text{ptn24}} + \rho_{\text{ptn25}} + \rho_{\text{ptn26}})/6 \\ \rho_{\text{tsw}} &= (\rho_{\text{tsw31}} + \rho_{\text{tsw32}} + \rho_{\text{tsw33}} + \rho_{\text{tsw34}} + \rho_{\text{tsw35}} + \rho_{\text{tsw36}} + \rho_{\text{tsw37}} + \rho_{\text{tsw38}} + \rho_{\text{tsw9v}} + \rho_{\text{tsw9z}})/10 \\ \rho_{\text{ch1fl}} &= (\rho_{\text{ch1v}} + \rho_{\text{ch1z}})/2 \text{ (similar for ch2fl, ch3fl, ch4fl, ch5fl, ch6fl)} \\ \rho_{\text{pp4fl}} &= \rho_{\text{pp4}} \text{ (similar for pp3, pp2, pp1, bf3, bf2, tr3, tr2)}\end{aligned}$$

The same process is used to determine the fault-zone properties for thermal conductivity, specific heat, and porosity.

Saturated Zone Thermal Properties

The saturated zone intersects 14 UZ model layers (ch1z, ch2z, ch3z, ch4z, ch5z, ch6z, pp4, pp3, pp2, pp1, bf3, bf2, tr3, and tr2). The saturated zone density, thermal conductivity, specific heat, and porosity are simply calculated as the sum of the properties for those units divided by 14.

Rocktab File Example

Listed below is a part of an example rocktab file (DKM-aFc-1Dds-vgm-P30-H35-06-05) that would be called in a NUFT input file (see Appendix V[a]). Of note is that several material properties are listed each delineated by the line “; End of the material.” Specific details of the rocktab file properties are found in the NUFT user’s manual (Nitao 1998 [DIRS 100474], p. 41).

```
(atm
  (cont-len-fac 1.00e+00) (cont-area-fac 2.00e+00)
  (exfac-adv (liquid 1.00e+00) (gas 1.00e+00))
  (solid-density 1.00e+08) (porosity 0.99)
  (Kd          (water 0.0) (air 0.0))
  (KdFactor   (water 0.0) (air 0.0))
  (Cp 1.00e+08)
  (tcond tcondLin (solid 1.00e+02) (liquid 1.00e+02) (gas 1.00e+02))
  (K0 1.00e-08) (K1 1.00e-08) (K2 1.00e-08)
  (tort (gas 1.00e+00) (liquid 0.00e+00))
  (kr (liquid krlLinear (Sr 0.00e+00) (Smax 1.0))
      (gas krgLinear   (Sr 0.00e+00) (Smax 1.0)))
  (pc (liquid 0.0))
  (krMC (liquid krMCintrinsic) (gas krMCintrinsic))
) ;;End of the material

(m-uz1
  (cont-len-fac 5.27e-02) (cont-area-fac 9.68e+00)
  (exfac-adv (liquid 1.00e+00) (gas 1.00e+00))
  (solid-density 2258.11) (porosity 0.131)
  (Kd          (water 0.0) (air 0.0))
  (KdFactor   (water 0.0) (air 0.0))
  (Cp 9.41e+02)
  (tcond tcondLin (solid 0.81147) (liquid 1.40442) (gas 0.81147))
  (K0 1.11e-17) (K1 1.11e-17) (K2 1.11e-17)
  (tort (gas 2.00e-01) (liquid 0.00e+00))
  (kr (liquid krlVanGen (Sr 1.20e-01) (m 2.16e-01) (Smax 1.0))
      (gas krgVanGenMinus (Sr 1.20e-01) (m 2.16e-01) (Smax 1.0)))
  (pc (liquid pcVanGen (Sr 1.20e-01) (m 2.16e-01)
                      (Sj 4.04e-01) (alpha 3.38e-06) (Smax1.0)))
  (krMC (liquid krMCintrinsic) (gas krMCintrinsic))
) ;;End of the material
```

[SECTION SKIP]

```
(f-uz1

  (cont-len-fac 0.00e+00) (cont-area-fac 1.00e+00)
  (exfac-adv (liquid 1.00e+00) (gas 1.00e+00))
  (solid-density 21.89) (porosity 9.60e-03)
  (Kd          (water 0.0) (air 0.0))
  (KdFactor   (water 0.0) (air 0.0))
  (Cp 9.41e+02)
  (tcond tcondLin (solid 0.00901) (liquid 0.01559) (gas 0.00901))
  (K0 9.10e-13) (K1 9.10e-13) (K2 9.10e-13)
  (tort (gas 7.00e-01) (liquid 0.00e+00))
  (kr (liquid krlVanGen (Sr 1.00e-02) (m 6.33e-01) (Smax 1.0) (gamma 4.00e-01))
      (gas krgVanGenMinus (Sr 1.00e-02) (m 6.33e-01) (Smax 1.0)))
  (pc (liquid pcVanGen (Sr 1.00e-02) (m 6.33e-01) (alpha 5.75e-04)
                      (Smax 1.0) (gamma 4.00e-01)))
  (krMC (liquid krMCactiveFrac (gamma 4.00e-01) (Sr 1.00e-02))
      (gas krMCactiveFrac (gamma 4.00e-01) (Sr 0.0)))
) ;;End of the material
```

[SECTION SKIP]

```
(f-tsw36
  (cont-len-fac 0.00e+00) (cont-area-fac 1.00e+00)
  (exfac-adv (liquid 1.00e+00) (gas 1.00e+00))
  (solid-density 20.57) (porosity 8.50e-03)
  (Kd          (water 0.0) (air 0.0))
  (KdFactor    (water 0.0) (air 0.0))
  (Cp 9.30e+02)
  (tcond tcondLin (solid 0.01872) (liquid 0.02743) (gas 0.01872))
  (K0 3.30e-13) (K1 3.30e-13) (K2 3.30e-13)
  (tort (gas 7.00e-01) (liquid 0.00e+00))
  (kr (liquid krlVanGen (Sr 1.00e-02) (m 6.33e-01) (Smax 1.0) (gamma 4.00e-01))
      (gas krgVanGenMinus (Sr 1.00e-02) (m 6.33e-01) (Smax 1.0)))
  (pc (liquid pcVanGen (Sr 1.00e-02) (m 6.33e-01) (alpha 3.16e-04)
      (Smax 1.0) (gamma 4.00e-01)))
  (krMC (liquid krMCactiveFrac (gamma 4.00e-01) (Sr 1.00e-02))
        (gas      krMCactiveFrac (gamma 4.00e-01) (Sr 0.0)))
) ;;End of the material
```

Table IV-3a[a]. Specific Heat Capacity, Thermal Conductivity (dry and wet), and Bulk Density for the GFM2000 Units

Material Name Used in LDTH Submodels	GFM2000 Layer	Mineralogic Model Unit	Bulk Density kg/m ³	Thermal Conductivity, Dry W/m-K	Thermal Conductivity, Wet W/m-K	Specific Heat Capacity J/g-K
tcw11	Tpcp	Tpc_un	2,190	1.30	1.81	0.93
tcw12	Tpcp		2,190	1.30	1.81	0.93
	TpcLD		2,190	1.30	1.81	0.93
tcw13	Tpcpv3	Tcppv3 –	2,310	0.688	0.796	0.95
	Tpcpv2	Tpcpv2	1,460	0.490	1.06	0.95
ptn21	Tpcpv1	PTn ^f	1,460	0.490	1.06	0.96
ptn22	Tpbt4		1,460	0.490	1.06	0.96
	Tpy (Yucca)		1,460	0.490	1.06	0.96
ptn23	Tpbt3		1,460	0.490	1.06	0.96
ptn24	Tpy		1,460	0.490	1.06	0.96
	Tpbt3		1,460	0.490	1.06	0.96
ptn25	Tpp (Pah)		1,460	0.490	1.06	0.96
ptn26	Tpbt2		1,460	0.490	1.06	0.96
	Tptrv3		1,460	0.490	1.06	0.96
	Tptrv2		1,460	0.490	1.06	0.96
tsw31	Tptrv1	Tptrv1	2,310	0.688	0.796	0.95
	Tptrn	Tptrn –	2,190	1.30	1.81	0.93
tsw32	Tptrn	Tptrl –	2,190	1.30	1.81	0.93
tsw33	Tptrl	Tptf	2,190	1.22 ^a	1.78 ^a	0.93
	Tptpul	Tptul	1,830			0.93
tsw34	Tptpmn	Tptpmn	2,150	1.39 ^a	2.06 ^a	0.93
tsw35	Tptpll	Tptpll	1,980	1.24 ^a	1.87 ^a	0.93
tsw36	Tptpln	Tptpln	2,210	1.44 ^a	2.11 ^a	0.93
tsw37	Tptpln		2,210	1.44 ^a	2.11 ^a	0.93
tsw38	Tptpv3	Tptpv3	2,310	0.688	0.796	0.98
tsw9v	Tptpv2	Tptpv2	1,460	0.490	1.06	0.96
tsw9z	Tptpv2		1,460	0.490	1.06	0.98
ch1v	Tptpv1	Tptpv1 –	1,460	0.490	1.06	0.96
	Tpbt1	Tpbt1	1,460	0.490	1.06	0.96
ch1z	Tptpv1	Tpbt1	1,460	0.490	1.06	1.08
	Tpbt1		1,460	0.490	1.06	1.08
ch2v	Tac (Calico)	Tac (4 layers)	1,670	0.595	1.26	0.96
ch3v	Tac (Calico)		1,670	0.595	1.26	0.96
ch4v	Tac (Calico)		1,670	0.595	1.26	0.96
ch5v	Tac (Calico)		1,670	0.595	1.26	0.96
ch2z	Tac (Calico)		1,670	0.595	1.26	1.07
ch3z	Tac (Calico)		1,670	0.595	1.26	1.07

Table IV-3a[a]. Specific Heat Capacity, Thermal Conductivity (Dry and Wet) and Bulk Density for the GFM2000 Units (Continued)

Material Name Used in LDTH Submodels	GFM2000 Layer	Mineralogic Model Unit	Bulk Density kg/m ³	Thermal Conductivity, Dry W/m-K	Thermal Conductivity, Wet W/m-K	Specific Heat Capacity J/g-K
ch4z	Tac (Calico)		1,670	0.595	1.26	1.07
ch5z	Tac (Calico)	Tac (Cont.)	1,670	0.595	1.26	1.07
ch6v	Tacbt (Calicobt)	Tacbt	1,670	0.595	1.26	0.97
ch6z	Tacbt (Calicobt)		1,670	0.595	1.26	1.02
pp4	Tcpuv (Prowuv)	Tcpuv	1,790	0.569	1.13	1.04
pp3	Tcpuc (Prowuc)	Tcpuc – Tcplc	1,790	0.569	1.13	0.93
pp2	Tcpmd (Prowmd)		2,070	1.06	1.63	0.93
	Tcplc (Prowlc)		1,790	0.569	1.13	0.93
pp1	Tcplv (Prowlv)	Tcplv – Tcbuv	1,790	0.569	1.13	1.10
	Tcpbt (Prowbt)		1,790	0.569	1.13	1.10
	Tcbuv (Bullfroguv)	1,880	0.658	1.19	1.10	
bf3	Tcbuc (Bullfroguc)	Tcbuc –	1,880	0.658	1.19	0.93
	Tcbmd (Bullfrogmd)	Tcblc	2,260	1.30	1.81	0.93
	Tcblc (Bullfroglc)		1,880	0.658	1.19	0.93
bf2	Tcblv (Bullfroglv)	Tcblv –	1,880	0.658	1.19	1.05
	Tcbbt (Bullfrogbt)	Tctuv	1,880	0.658	1.19	1.05
	Tctuv (Tramuv)		1,760	0.535	1.10	1.05
tr3	Tctuc (Tramuc)	Tctuc –	1,760	0.535	1.10	0.94
	Tctmd (Trammd)	Tctlc	2,140	1.06	1.63	0.94
	Tctlc (Tramlc)		1,760	0.535	1.10	0.94
tr2	Tctlv (Tramlv)	Tctlv –	1,760	0.535	1.10	0.94
	Tctbt (Trambt)	Tctbt	1,760	0.535	1.10	0.94

^a Based on Output DTN: MO0612MEANTHER.000.

NOTE: The values for the nonrepository layers are from DTN: SN0303T0503102.008 [DIRS 162401]. The thermal conductivity and bulk density values for the repository layers (tsw33, tsw34, tsw35, tsw36, and tsw37) are from Table 7-10 of DTN: SN0404T0503102.011 [DIRS 169129] (files: *Tptpl1.zip*, *tptpl2.zip*, *tptpl3.zip*, *tptpln1.zip*, *tptpln2.zip*, *tptpln3.zip*, *tptpmn1.zip*, *tptpmn2.zip*, *tptpmn3.zip*, *tptpul1.zip*, *tptpul2.zip*, and *tptpul3.zip*), with density values rounded. The GFM2000 layers shown in red italics pertain to data obtained from Table 7-10 of DTN: SN0404T0503102.011 [DIRS 169129] (file: *ReadMe Summary.doc*). Some bulk density values shown in green from DTN: SN0404T0503102.011 [DIRS 169129] (file: *ReadMe Summary.doc*) have been rounded to be consistent with the bulk density values from DTN: SN0303T0503102.008 [DIRS 162401]. Mineralogic model units are from *Heat Capacity Analysis Report* (BSC 2004 [DIRS 170003], Tables 6-1 and 6-7). The specific heat capacity for all layers is from DTN: SN0307T0510902.003 [DIRS 164196] for the temperature range of 25°C to 325°C. The values of specific heat capacity, thermal conductivity, and bulk density for the layers with multiple GFM2000 layers (e.g., pp1) are the arithmetic average of the corresponding GFM2000 layer values. Table IV-3b[a] gives the result of this averaging for bulk density and bulk thermal conductivity.

Table IV-3b[a]. Thermal Properties for the UZ Model Layers

Material Name	Porosity			Density				Thermal Conductivity					
	ϕ_m	ϕ	ρ_b kg/m ³	ρ_G kg/m ³	ρ_{G,m^3} kg/m ³	ρ_{G,f^3} kg/m ³	$K_{th,b}$ wet W/m ² °C	$K_{th,m}$ wet W/m ² °C	$K_{th,f}$ wet W/m ² °C	$K_{th,b}$ dry W/m ² °C	$K_{th,m}$ dry W/m ² °C	$K_{th,f}$ dry W/m ² °C	
tcw11	0.241	2.40E-02	2,190	2,890	2,820.64	69.36	1.81	1.767	4.34E-02	1.30	1.269	3.12E-02	
tcw12	0.088	1.70E-02	2,190	2,400	2,359.20	40.80	1.81	1.779	3.08E-02	1.30	1.278	2.21E-02	
tcw13	0.200	1.30E-02	1,890	2,360	2,329.32	30.68	0.93	0.918	1.21E-02	0.59	0.582	7.67E-03	
ptn21	0.387	9.20E-03	1,460	2,380	2,358.10	21.90	1.06	1.050	9.75E-03	0.49	0.485	4.51E-03	
ptn22	0.428	1.00E-02	1,460	2,550	2,524.50	25.50	1.06	1.049	1.06E-02	0.49	0.485	4.90E-03	
ptn23	0.233	2.10E-03	1,460	1,900	1,896.01	3.99	1.06	1.058	2.23E-03	0.49	0.489	1.03E-03	
ptn24	0.413	1.00E-02	1,460	2,490	2,465.10	24.90	1.06	1.049	1.06E-02	0.49	0.485	4.90E-03	
ptn25	0.498	5.50E-03	1,460	2,910	2,894.00	16.00	1.06	1.054	5.83E-03	0.49	0.487	2.69E-03	
ptn26	0.490	3.10E-03	1,460	2,860	2,851.13	8.87	1.06	1.057	3.29E-03	0.49	0.488	1.52E-03	
tsw31	0.054	5.00E-03	2,250	2,380	2,368.10	11.90	1.30	1.294	6.50E-03	0.99	0.985	4.95E-03	
tsw32	0.157	8.30E-03	2,190	2,600	2,578.42	21.58	1.81	1.795	1.50E-02	1.30	1.289	1.08E-02	
tsw33	0.155	5.80E-03	2,010	2,380	2,366.20	13.80	1.78	1.770	1.03E-02	1.22	1.213	7.08E-03	
tsw34	0.111	8.50E-03	2,150	2,420	2,399.43	20.57	2.06	2.042	1.75E-02	1.39	1.378	1.18E-02	
tsw35	0.131	9.60E-03	1,980	2,280	2,258.11	21.89	1.87	1.852	1.80E-02	1.24	1.228	1.19E-02	
tsw36	0.103	1.30E-02	2,210	2,460	2,428.02	31.98	2.11	2.083	2.74E-02	1.44	1.421	1.87E-02	
tsw37	0.103	1.30E-02	2,210	2,460	2,428.02	31.98	2.11	2.083	2.74E-02	1.44	1.421	1.87E-02	
tsw38	0.043	1.10E-02	2,310	2,410	2,383.49	26.51	0.80	0.791	8.80E-03	0.69	0.682	7.59E-03	
tsw9v	0.115 ^a	0.115 ^a	1,460	1,890 ^b	824.39 ^c	824.39 ^c	1.06	1.060	N/A	0.49	0.490	N/A	
tsw9z	0.275	4.30E-03	1,460	2,010	2,001.36	8.64	1.06	1.055	4.56E-03	0.49	0.488	2.11E-03	
ch1v	0.166 ^a	0.166 ^a	1,460	2,180 ^b	874.78 ^c	874.78 ^c	1.06	1.060	N/A	0.49	0.490	N/A	
ch1z	0.285	1.60E-04	1,460	2,040	2,039.67	0.33	1.06	1.060	1.70E-04	0.49	0.490	8.00E-05	
ch2v	0.173 ^a	0.173 ^a	1,670	2,550 ^b	1,009.67 ^c	1009.67 ^c	1.26	1.260	N/A	0.60	0.600	N/A	
ch3v	0.173 ^a	0.173 ^a	1,670	2,550 ^b	1,009.67 ^c	1009.67 ^c	1.26	1.260	N/A	0.60	0.600	N/A	
ch4v	0.173 ^a	0.173 ^a	1,670	2,550 ^b	1,009.67 ^c	1009.67 ^c	1.26	1.260	N/A	0.60	0.600	N/A	
ch5v	0.173 ^a	0.173 ^a	1,670	2,550 ^b	1,009.67 ^c	1009.67 ^c	1.26	1.260	N/A	0.60	0.600	N/A	

Table IV-3b[a]. Thermal Properties for the UZ Model Layers (Continued)

Material Name	Porosity		Density				Thermal Conductivity					
	ϕ_m	ϕ	ρ_b kg/m ³	ρ_g kg/m ³	$\rho_{g,m}$ kg/m ³	$\rho_{g,f}$ kg/m ³	$K_{th,b}$ wet W/m ² °C	$K_{th,m}$ wet W/m ² °C	$K_{th,f}$ wet W/m ² °C	$K_{th,b}$ dry W/m ² °C	$K_{th,m}$ dry W/m ² °C	$K_{th,f}$ dry W/m ² °C
ch2z	0.322	3.70E-04	1,670	2,460	2,459.09	0.91	1.26	1.260	4.70E-04	0.60	0.600	2.20E-04
ch3z	0.322	3.70E-04	1,670	2,460	2,459.09	0.91	1.26	1.260	4.70E-04	0.60	0.600	2.20E-04
ch4z	0.322	3.70E-04	1,670	2,460	2,459.09	0.91	1.26	1.260	4.70E-04	0.60	0.600	2.20E-04
ch5z	0.322	3.70E-04	1,670	2,460	2,459.09	0.91	1.26	1.260	4.70E-04	0.60	0.600	2.20E-04
ch6v	0.166 ^a	0.166 ^a	1,670	2,550 ^b	1,000.60 ^c	1000.60 ^c	1.26	1.260	N/A	0.60	0.600	N/A
ch6z	0.271	1.60E-04	1,670	2,290	2,289.63	0.37	1.26	1.260	2.00E-04	0.60	0.600	1.00E-04
pp4	0.321	3.70E-04	1,790	2,640	2,639.02	0.98	1.13	1.130	4.20E-04	0.57	0.570	2.10E-04
pp3	0.318	9.70E-04	1,790	2,620	2,617.46	2.54	1.13	1.129	1.10E-03	0.57	0.569	5.50E-04
pp2	0.221	9.70E-04	1,930	2,480	2,477.59	2.41	1.38	1.379	1.34E-03	0.81	0.809	7.90E-04
pp1	0.297	3.70E-04	1,820	2,590	2,589.04	0.96	1.15	1.150	4.30E-04	0.60	0.600	2.20E-04
bf3	0.175	9.70E-04	2,010	2,440	2,437.63	2.37	1.40	1.399	1.36E-03	0.87	0.869	8.40E-04
bf2	0.234	3.70E-04	1,840	2,400	2,399.11	0.89	1.16	1.160	4.30E-04	0.62	0.620	2.30E-04
tr3	0.175	9.70E-04	1,890	2,290	2,287.78	2.22	1.28	1.279	1.24E-03	0.71	0.709	6.90E-04
tr2	0.234	3.70E-04	1,760	2,300	2,299.15	0.85	1.10	1.100	4.10E-04	0.54	0.540	2.00E-04

^a Vitric units have matrix porosity partitioned 50% to the matrix continuum and 50% to the pseudo-fracture continuum.

^b Value not used in LDTH submodel.

^c Vitric units have grain density partitioned 50% to the matrix continuum and 50% to the pseudo-fracture continuum.

NOTES: The subscripts *m*, *f*, *b*, and *g* stand for matrix, fracture, bulk, and grain, respectively. The bulk density ρ_b and bulk thermal conductivity $K_{th,b}$ (wet and dry) are obtained from Table IV-3a[a], with averaging applied to UZ model layers with multiple GFM2000 layers. The density and thermal conductivity for the matrix and fracture continua are calculated by hand on the basis of fracture porosity.

Porosity values are from DTN: LB0208UZDSCPM1.002 [DIRS 161243], file: *drift-scale calibrated properties for mean infiltration2.xls*, worksheet: "Drift-scale Cal. Hydro Props."

Table IV-4[a]. Matrix and Fracture Properties for the Drift-Scale Calibrated Property Set for the 30th Percentile Infiltration Map

Model Layer	K_M (m ²)	α_M (1/Pa)	m_M (-)	K_F (m ²)	α_F (1/Pa)	m_F (-)	γ (-)
tcw11	3.88E-15	1.22E-05	0.388	3.0E-11	4.99E-03	0.633	0.400
tcw12	1.15E-19	2.88E-06	0.280	5.3E-12	2.18E-03	0.633	0.400
tcw13	4.39E-16	2.61E-06	0.259	4.5E-12	1.85E-03	0.633	0.400
ptn21	2.13E-14	9.82E-05	0.245	3.2E-12	2.68E-03	0.633	0.001
ptn22	1.28E-11	1.22E-04	0.219	3.0E-13	1.37E-03	0.633	0.001
ptn23	4.06E-14	2.41E-05	0.247	3.0E-13	1.22E-03	0.633	0.001
ptn24	7.64E-12	7.44E-04	0.182	3.0E-12	2.94E-03	0.633	0.001
ptn25	9.63E-13	6.28E-05	0.300	1.7E-13	1.09E-03	0.633	0.001
ptn26	1.86E-11	8.11E-04	0.126	2.2E-13	9.51E-04	0.633	0.001
tsw31	3.21E-17	2.90E-05	0.218	8.1E-13	2.08E-05	0.633	0.088
tsw32	3.01E-16	1.59E-05	0.290	7.1E-13	5.65E-05	0.633	0.400
tsw33	1.86E-17	6.56E-06	0.283	7.8E-13	1.58E-03	0.633	0.400
tsw34	3.16E-18	1.71E-06	0.317	3.3E-13	3.16E-04	0.633	0.400
tsw35	1.11E-17	3.38E-06	0.216	9.1E-13	5.75E-04	0.633	0.400
tsw36	3.16E-18	7.32E-07	0.442	1.3E-12	1.09E-03	0.633	0.400
tsw37	3.16E-18	7.32E-07	0.442	1.3E-12	1.09E-03	0.633	0.400
tsw38	1.27E-17	3.11E-06	0.286	8.1E-13	8.87E-04	0.633	0.400
tswz (zeolitic portion of tsw39)	3.50E-17	4.61E-06	0.059	8.1E-13	1.50E-03	0.633	0.250
tswv (vitric portion of tsw39)	2.23E-13	4.69E-05	0.293	8.1E-13	1.50E-03	0.633	0.250
ch1z	3.50E-17	2.12E-07	0.349	2.5E-14	1.40E-03	0.633	0.250
ch1v	2.59E-12	1.11E-04	0.240	2.2E-13	2.10E-03	0.633	0.250
ch2v	6.77E-11	3.33E-04	0.158	2.2E-13	1.90E-03	0.633	0.250
ch3v	6.77E-11	3.33E-04	0.158	2.2E-13	1.90E-03	0.633	0.250
ch4v	6.77E-11	3.33E-04	0.158	2.2E-13	1.90E-03	0.633	0.250
ch5v	6.77E-11	3.33E-04	0.158	2.2E-13	1.90E-03	0.633	0.250
ch6v	2.71E-13	1.84E-05	0.147	2.2E-13	1.90E-03	0.633	0.250
ch2z	5.20E-18	2.25E-06	0.257	2.5E-14	8.90E-04	0.633	0.250
ch3z	5.20E-18	2.25E-06	0.257	2.5E-14	8.90E-04	0.633	0.250
ch4z	5.20E-18	2.25E-06	0.257	2.5E-14	8.90E-04	0.633	0.250
ch5z	5.20E-18	2.25E-06	0.257	2.5E-14	8.90E-04	0.633	0.250
ch6z	8.20E-19	1.56E-07	0.499	2.5E-14	1.40E-03	0.633	0.250
pp4	3.51E-17	6.31E-06	0.474	2.5E-14	2.82E-04	0.633	0.400
pp3	1.02E-13	1.48E-05	0.407	2.2E-13	1.65E-03	0.633	0.400
pp2	1.69E-15	3.89E-06	0.309	2.2E-13	1.65E-03	0.633	0.400
pp1	2.57E-17	3.16E-05	0.272	2.5E-14	1.58E-04	0.633	0.400
bf3	6.31E-14	6.18E-05	0.193	2.2E-13	1.65E-03	0.633	0.400
bf2	8.10E-17	1.18E-07	0.617	2.5E-14	8.90E-04	0.633	0.250

Source DTN: LB0610UZDSCP30.001 [DIRS 179180], file: *Calibrated Parameter_R113_30%.doc*

NOTE: Bold indicates calibrated parameters.

Table IV-5[a]. Fracture Frequency and Fracture-to-Matrix Interface Area

Material Name	Fracture Frequency (m^{-1})	Interface Area (m^2/m^3)
tcw11	0.92	1.56
tcw12	1.91	13.39
tcw13	2.79	3.77
ptn21	0.67	1.00
ptn22	0.46	1.41
ptn23	0.57	1.75
ptn24	0.46	0.34
ptn25	0.52	1.09
ptn26	0.97	3.56
tsw31	2.17	3.86
tsw32	1.12	3.21
tsw33	0.81	4.44
tsw34	4.32	13.54
tsw35	3.16	9.68
tsw36	4.02	12.31
tsw37	4.02	12.31
tsw38	4.36	13.34
tsw39 (tsw9v)	N/A ^a	N/A ^a
tsw39 (tsw9z)	0.96	2.95
ch1VI (ch1v)	N/A ^a	N/A ^a
ch1Ze (ch1z)	0.04	0.11
ch2VI (ch2v)	N/A ^a	N/A ^a
ch3VI (ch3v)	N/A ^a	N/A ^a
ch4VI (ch4v)	N/A ^a	N/A ^a
ch5VI (ch5v)	N/A ^a	N/A ^a
ch2Ze (ch2z)	0.14	0.43
ch3Ze (ch3z)	0.14	0.43
ch4Ze (ch4z)	0.14	0.43
ch5Ze (ch5z)	0.14	0.43
ch6VI (ch6v)	N/A ^a	N/A ^a
ch6 (ch6z)	0.04	0.11
pp4	0.14	0.43
pp3	0.20	0.61
pp2	0.20	0.61
pp1	0.14	0.43
bf3	0.20	0.61
bf2	0.14	0.43
tr3	0.20	0.61
tr2	0.14	0.43

Source: DTN: LB0205REVUZPRP.001 [DIRS 159525], file: *FRACTURE PROPERTY.xls*, worksheet: "Table 1. Fracture Properties."

^a Vitric units (those units ending with a "VI" or a "v") do not have fractures; therefore, fracture properties do not pertain to those units.

NOTE: In parentheses are the material names used in the LDTH submodels of the MSTHM.

APPENDIX V[a]
BUILDING SUBMODEL INPUT FILES

SMT Submodel

The SMT submodel has the following information in this order:

1. Time information (start time, stop time, timestepsize)
2. Material properties (in the form of a rocktab file; see Appendix IV[a])
3. Output information (for “.ext” time-history output; this is readable by XTOOL v10.1)
4. Heat generation information (in the form of a heatgen file; see Appendix III[a])
5. Restart file information
6. Boundary conditions
7. Initial conditions
8. SMT submodel mesh file (in the form of an SMT submodel mesh file; see Appendix I[a])
9. Run control parameters.

All parameter values are taken directly from inputs or calculations described in other appendices. An example of an SMT submodel NUFT usnt-option input file follows below. For more information, see the NUFT documentation (Nitao 1998 [DIRS 100474]). The SMT submodel input and output files are found in Output DTN: LL0702PA013MST.068.

```
(usnt
  (title "* YMP Site-Scale 3D Model, Conduction-Only Post-Emplacement Run")
  ;; AML = 55 MTU/acre ;; ventilation + post-closure run for MSTHM for the License
Application
  ;; rotated mesh explicitly representing emplacement drifts
  ;; Includes all of Panels 1, 2, 3E, 3W, and 4
  ;; conduction only
  (modelname usnt)
  (include-pkg "thermcon.pkg") ;; single-comp (air), single-phase (gas) pkg for cond-
only run
  (tstop 1000000y)
  (time 0)
  (stepmax 1000000)
  (dtmax 1.0e25)
  (dt 1e2)
  ;; include thermal properties
  (rocktab
    (include "SDT-1Dds-06") ;; read rocktab data
    (include "SMT-1Dds-fl-07") ;; read rocktab data
  ) ;; end rocktab
  ;;
  *****
  **
  ;; *****

  (output
    (extool (variables T) ;; repository node temperatures
      (file-ext ".lvl.ext") (range "##*:1")
      (outtimes
        (include "outputTimes-SMT-01L")
      )
    )
  ) ;; end output
```

```

;; *****
;; include heat curves in srctab
;; (srctab
   (include "SMT_LA_includes")
;; ) ;; end srctab
;; *****
;; read restart file
   (read-restart
     (file "SMT55-07-03-150w_t-i.rst")
     (time 1.0e6y))
;; *****
(bctab
  (top
    (range "at*")
    (clamped))
  (bottom
    (range "bs*")
    (clamped))
) ;; end bctab
;; *****
;; set initial conditions
;; (state
;; (P by-key ("*" 1.0e5))
;; (T by-key
   (include "smtUpperBC.dat")
   (include "smtLowerBC.dat")
;; )
;; ) ;; end state

;; *****
(mesh-file "tspa07.mesh03-150w") ;; read mesh and connection data
;; *****

(include "run_control_param_SMT-v01")
) ;; end of model

```

LDTH submodel

For the LDTH submodel input files, a calculation (in addition to those described in other appendices) must be made to convert the percolation flux from mm/yr to kg/m²/sec. An example of this calculation is:

$$J=4.1884 \text{ mm/yr} (1 \text{ day}/86,400 \text{ sec})(1 \text{ yr}/365.25 \text{ days})(\text{m}/1,000 \text{ mm})(1,000 \text{ kg}/\text{m}^3) = 1.3274 \times 10^{-7} \text{ kg}/\text{m}^2/\text{sec}$$

The LDTH submodel has the following information in this order:

1. Header information (lines preceded by a semicolon)
2. Time information (start time, stop time, timestepsize)
3. Convergence tolerance information
4. Output file (for “.ext” time-history output; this is readable by XTOOL v10.1)
5. Material properties (in the form of rocktab files; see Appendix IV[a])
6. Percolation flux information (see the flux conversion mm/yr to kg/m²/sec noted above)
7. Heat generation information (in the form of a heatgen file; see Appendix III[a])

8. Boundary conditions
9. Restart conditions (optional)
10. Initial conditions (optional)
11. Mesh information for matrix continuum
12. Radcon information for matrix continuum (in the form of a file for doing thermal-radiation connections; see Appendix VI[a])
13. Mesh information for fracture continuum
14. Run control parameters.

All parameter values are taken directly from inputs or calculations described in other appendices. An example of an DDT submodel NUFT usnt-option input file follows. For more information, see the NUFT documentation (Nitao 1998 [DIRS 100474]). LDTH submodel input files follow the naming convention P#-D#-UZGC-LDTH(aml)-PK.in, where P# stands for panel number, D# stands for drift number, UZGC stands for UZ flow model grid column, and PK stands for percolation flux, thermal conductivity case. There are 2,800 input files, which includes 560 initialization runs and 2,240 postemplacement runs for each of the seven MSTHM uncertainty cases (P10, P30, P50, P90, P10L, P10H, and P90H). See Figure 6.3-73[a] for complete list of LDTH submodel DTNs.

```
;; This model was produced on
;; Fri Jan 12 09:56:38 PST 2007
;; Implicit DKM with active fracture concept (AFC)
;; NBS material properties from 1D drift-scale infiltration flux property set
;; AML = 54.82 MTU/acre; half drift spacing = 40.5 m

;; P3W-13-g_9.col.units

;; COLUMN INFORMATION (x,y = 170754.578, 234921.031) WORLD COLUMN g_9

;; unit      thickness (m)
;; _____

;; uz1       146.982
;; tsw33     85.281
;; tsw34     32.906
;; tsw35     104.766
;; tsw36     38.696
;; uz2       180.420

;; repository elevation (m):          1052.874
;; host rock:                          tsw35

;; meters of host rock (tsw35) above repository:  45.375
;; meters of host rock (tsw35) below repository:  59.391

;; overburden thickness (m):          310.544
;; distance from repository plane to top of water table (m):  278.506

(usnt
  (title "3.610000e+00mm_yr,line-load,AML=55mtu_acre,LDTH55")
  (modelname usnt)

  (tstop 1e6y)
```

```

(time 0)
(stepmax 1000000)
(dtmax 1.000e+25)
(dt 1e2)

(tolerconv (P 5000.) (S 0.005) (X 0.005) (T 0.5))
;; absolute NR conv. tolerance
(reltolerconv (P 0.005) (S 0.0) (X 0.0) (T 1.e-3))

(tolerdt (P 2.e4) (S 0.35) (X 0.25) (T 10.))
(reltolerdt (P 0.1) (S 0.0) (X 0.0) (T 0.0))

;; trying with harmonic mean everywhere which means turning off the geometric before
vtough.pkg
;; gets called.
(diffusion-geo-mean off)
;; for imp-DKM do not have this so that it will default to harmonic for fract-matrix
interaction
;; (mult-cont-diff-harmonic off)
;; following has to come after tolerances
(rmstolerconv 1e-4)
(include-pkg "vtough.pkg")
(check-mult-con off )

;;
*****
*****
(output
  (extool (continuum f)
    (variables T S.liquid X.air.gas RH Pc.liquid P.gas qPhChg.water.gas QPhChg.water.gas
      q.liquid q.water.gas q.air.gas)
    (file-ext ".f.EBS.ext") (range "*hstrk*.f*" "dr*.f*" "*in*.f*" "*wp*.f*")
    (outtimes
      (include "outputTimes-LDTH-SDT-DDT-55-01L")
    )
  )
  (extool (continuum m)
    (variables T S.liquid X.air.gas RH Pc.liquid P.gas qPhChg.water.gas QPhChg.water.gas
      q.liquid q.water.gas q.air.gas)
    (file-ext ".m.EBS.ext") (range "*hstrk*.m*" "dr*.m*" "*in*.m*" "*wp*.m*")
    (outtimes
      (include "outputTimes-LDTH-SDT-DDT-55-01L")
    )
  )
) ;; create the restart file for main runs
;; (restart (file-ext ".res") (outtimes 600y 2000y 10000y))

) ;; end output

;;
*****
*****
(rocktab
  (include "DKM-afc-1Dds-vgm-P30-H34-H35-06-05")
  (include "dkm-afc-EBS-P30-06")
) ;; close rocktab
(include "modpropTSPA07_01_55")
;;
*****
*****
;; This srctab is adjusted to allocate percolation to just the fracture.
(srctab
  (compflux

```

```

        (comp water)
        (name infil)
        (range "*.f*:*:2")
        (mult-by-area z)
        (allocate-by-element ("*" 1.0))
        (table 0.0 1.143940e-07 600.0y 1.143940e-07 ;; 3.610000e+00 mm/yr
              600.001y 2.157959e-07 2000.0y 2.157959e-07 ;; 6.810000e+00 mm/yr
              2000.001y 4.309580e-07 10000.0y 4.309580e-07 ;; 1.360000e+01 mm/yr
              10000.001y 5.636125e-07 1.0e30 5.636125e-07) ;; 1.778626e+01 mm/yr
        (enthalpy 0.0 7.0987600e+04 1.0e30 7.0987600e+04 )
        )

        (include "P3W-13-g_9_LDTH-SDT")
    ) ;; end srctab

    ;; set boundary conditions
    (bctab
    (atmos
    (range "at*")
    (basephase gas)
    (tables
    (T 0.0 1.6906000e+01 1.0e30 1.6906000e+01)
    (S.liquid 0.0 0.0 1.0e30 0.0 )
    (P 0.0 8.5627312e+04 1.0e30 8.5627312e+04)
    (X.air 0.0 9.8588460e-01 1.0e30 9.8588460e-01)
    )
    )

    (gwater
    (range "wt*")
    (basephase liquid)
    (tables
    ;; (T 0.0 2.8348000e+01 1.0e30 2.8348000e+01)
    (include "P3W-13-g_9-SDT55-01.wtTable")
    (S.liquid 0 1.0 1.0e30 1.0)
    (P 0 9.1553594e+04 1.0e30 9.1553594e+04)
    (X.air 0 1.0e-6 1.0e30 1.0e-6)
    )
    )

    ;; SET PHASEFACTOR GAS TO 0, AND LIQUID TO 1 (JOHN)
    (phasefactor
    (gas 0 0.0 1.0e30 0.0)
    (liquid 0 1.0 1.0e30 1.0)
    )

    )
    ) ;; end bctab

    ;; set initial conditions.
    (read-restart (time 3.15576e20)
    (file "P3W-13-g_9-LDTH55-P10-01i.res"))
    (overwrite-restart
    (X.air by-key ("dr*" 1.0) ("*wp*" 1.0) ("*in*" 1.0))
    (S.liquid by-key ("dr*" 0.0) ("*wp*" 0.0) ("*in.m*" 0.9) ("*in.f*" 0.1))
    ) ;; end overwrite

    ;;This is for a unit symmetry cell with a half drift and half pillar
    ;;between drifts.
    (genmsh
    (anisotropic)
    (down 0. 0. 1.0)
    (coord rect)
    (multi-continua
    (type rocktab)

```

Multiscale Thermohydrologic Model

```

        (continuum (name m)
; ; 54.82 MTU/acre
(dx 0.580 0.370 0.3165 0.4082 0.4222 0.350 0.3031 0.35 0.5 0.9 1.0 1.5 2.5 4.0 6.0 9.0
12.00)
(dy 1.0)
(dz
uz1      1.0e-30  26.982  30.000  30.000  30.000 ; ; 1- 5:      atm      uz1
uz1      uz1      uz1
tsw33    30.000  18.281  20.000  15.000  10.000 ; ; 6- 10:     uz1      tsw33
tsw33    tsw33    tsw33
tsw33    10.000  6.000  6.000  4.453  4.453 ; ; 11- 15:    tsw33    tsw33
tsw33    tsw34    tsw34
tsw34    6.000  6.000  6.000  6.000  3.375 ; ; 16- 20:    tsw34    tsw34
tsw34    tsw34    tsw35
tsw35    6.000  6.000  6.000  3.000  3.000 ; ; 21- 25:    tsw35    tsw35
tsw35    tsw35    tsw35
tsw35    3.000  3.000  1.500  2.000  1.000 ; ; 26- 30:    tsw35    tsw35
tsw35    tsw35    tsw35
tsw35    1.000  0.500  0.300  0.200  0.200 ; ; 31- 35:    tsw35    tsw35
tsw35    tsw35    tsw35
tsw35    0.200  0.200  0.200  0.200  0.200 ; ; 36- 40:    tsw35    tsw35
tsw35    tsw35    tsw35
tsw35    0.200  0.200  0.200  0.200  0.108 ; ; 41- 45:    tsw35    tsw35
tsw35    tsw35    tsw35
tsw35    0.242  0.400  0.759  0.760  0.425 ; ; 46- 50:    tsw35    tsw35
tsw35    tsw35    tsw35
tsw35    0.403  0.403  0.800  1.200  1.500 ; ; 51- 55:    tsw35    tsw35
tsw35    tsw35    tsw35
tsw35    2.500  3.000  3.000  6.000  6.000 ; ; 56- 60:    tsw35    tsw35
tsw35    tsw35    tsw35
tsw35    6.000  6.000  6.000  6.000  6.000 ; ; 61- 65:    tsw35    tsw35
tsw35    tsw35    tsw35
tsw36    5.391  6.000  6.000  6.000  6.000 ; ; 66- 70:    tsw35    tsw36
tsw36    tsw36    tsw36
tsw36    6.000  4.348  4.348  10.000  10.000 ; ; 71- 75:    tsw36    tsw36
tsw36    uz2      uz2
uz2      15.000  20.000  30.000  30.000  30.000 ; ; 76- 80:    uz2      uz2
uz2      uz2      uz2
wt       30.000  5.420  1.0e-30          ; ; 81- 83:    uz2      uz2
wt
)
(mat
(atm      atm      1 nx 1 ny 1 1)
(uz1      m-uz1    1 nx 1 ny 2 6)
(tsw33    m-tsw33  1 nx 1 ny 7 13)
(tsw34    m-tsw34  1 nx 1 ny 14 19)
(tsw35    m-tsw35  1 nx 1 ny 20 66)
(tsw36    m-tsw36  1 nx 1 ny 67 73)
(uz2      m-uz2    1 nx 1 ny 74 82)
(wt       m-uz2    1 nx 1 ny 83 83)
(hstrk    m-tsw35  1 nx 1 ny 28 55)
(dr       m-dr     1 1 1 ny 35 35)
(dr       m-dr     1 3 1 ny 36 36)
(dr       m-dr     1 4 1 ny 37 38)
(dr       m-dr     1 5 1 ny 39 40)
(dr       m-dr     1 6 1 ny 41 43)
(dr       m-dr     1 7 1 ny 44 48)
(dr       m-dr     1 6 1 ny 49 49)
(dr       m-dr     1 5 1 ny 50 50)
(wp       lsnf     1 1 1 ny 46 46)
(wp       lsnf     1 2 1 ny 47 47)
(wp       lsnf     1 3 1 ny 48 50)
(in       m-invert1 1 4 1 ny 51 51)
(in       m-invert2 1 2 1 ny 52 52)
)

```

```

)
(radcon
  (surface-offset 0 0 0)
  (include "ldth0_300m.radcon")
) ;; close radcon

) ;; end continuum
(continuum (name f)
  (flow-area-density ("*.f*" 1.0))
  (LenFirst ("*.f*" 1.0)) ;; same as y-direction
                          ;; half-width of matrix block
  (Len ("*.f*" 1.0)) ;; same as y-direction
                          ;; half-width of fracture
);; LenFirst and Len values are doubled here since 50% of cont-len-fac
);; is used in rocktab file
);; 54.82 MTU/acre
(dx 0.580 0.370 0.3165 0.4082 0.4222 0.350 0.3031 0.35 0.5 0.9 1.0 1.5 2.5 4.0 6.0 9.0
12.00)
(dy 1.0)
(dz
uz1      1.0e-30   26.982   30.000   30.000   30.000 ;; 1- 5:   atm      uz1
uz1      uz1      uz1
tsw33    30.000   18.281   20.000   15.000   10.000 ;; 6- 10:   uz1      tsw33
tsw33    tsw33   tsw33
tsw33    10.000   6.000    6.000    4.453    4.453 ;; 11- 15:  tsw33   tsw33
tsw33    tsw34   tsw34
tsw33    6.000    6.000    6.000    6.000    3.375 ;; 16- 20:  tsw34   tsw34
tsw34    tsw34   tsw35
tsw34    6.000    6.000    6.000    3.000    3.000 ;; 21- 25:  tsw35   tsw35
tsw35    tsw35   tsw35
tsw35    3.000    3.000    1.500    2.000    1.000 ;; 26- 30:  tsw35   tsw35
tsw35    tsw35   tsw35
tsw35    1.000    0.500    0.300    0.200    0.200 ;; 31- 35:  tsw35   tsw35
tsw35    tsw35   tsw35
tsw35    0.200    0.200    0.200    0.200    0.200 ;; 36- 40:  tsw35   tsw35
tsw35    tsw35   tsw35
tsw35    0.200    0.200    0.200    0.200    0.108 ;; 41- 45:  tsw35   tsw35
tsw35    tsw35   tsw35
tsw35    0.242    0.400    0.759    0.760    0.425 ;; 46- 50:  tsw35   tsw35
tsw35    tsw35   tsw35
tsw35    0.403    0.403    0.800    1.200    1.500 ;; 51- 55:  tsw35   tsw35
tsw35    tsw35   tsw35
tsw35    2.500    3.000    3.000    6.000    6.000 ;; 56- 60:  tsw35   tsw35
tsw35    tsw35   tsw35
tsw35    6.000    6.000    6.000    6.000    6.000 ;; 61- 65:  tsw35   tsw35
tsw35    tsw35   tsw35
tsw35    5.391    6.000    6.000    6.000    6.000 ;; 66- 70:  tsw35   tsw36
tsw36    tsw36   tsw36
tsw36    6.000    4.348    4.348    10.000   10.000 ;; 71- 75:  tsw36   tsw36
tsw36    uz2     uz2
tsw36    15.000   20.000   30.000   30.000   30.000 ;; 76- 80:   uz2     uz2
uz2      uz2     uz2
uz2      30.000   5.420    1.0e-30           ;; 81- 83:   uz2     uz2
wt
)
(mat
  (atm      atm      1 nx 1 ny 1 1)
  (uz1      f-uz1    1 nx 1 ny 2 6)
  (tsw33    f-tsw33  1 nx 1 ny 7 13)
  (tsw34    f-tsw34  1 nx 1 ny 14 19)
  (tsw35    f-tsw35  1 nx 1 ny 20 66)
  (tsw36    f-tsw36  1 nx 1 ny 67 73)
  (uz2      f-uz2    1 nx 1 ny 74 82)
)

```

```

(wt          f-uz2          1 nx  1  ny  83  83)
(hstrk      f-tsw35        1 nx  1  ny  28  55)
(dr         f-dr           1  1  1  ny  35  35)
(dr         f-dr           1  3  1  ny  36  36)
(dr         f-dr           1  4  1  ny  37  38)
(dr         f-dr           1  5  1  ny  39  40)
(dr         f-dr           1  6  1  ny  41  43)
(dr         f-dr           1  7  1  ny  44  48)
(dr         f-dr           1  6  1  ny  49  49)
(dr         f-dr           1  5  1  ny  50  50)
(wp         lsnf           1  1  1  ny  46  46)
(wp         lsnf           1  2  1  ny  47  47)
(wp         lsnf           1  3  1  ny  48  50)
(in         f-invert1      1  4  1  ny  51  51)
(in         f-invert2      1  2  1  ny  52  52)
)
) ;; end continuum
) ;; end multi-continua
) ;; end genmsh

;; *****Down stream
weighting*****
;; #include DWSWT

;; ***** Solver options
*****
(include "run_control_param_LDTH-v09")

) ;; end of model input

;; ***** Done
!*****

```

SDT submodel

The SDT submodel has the following information in this order:

1. Header information (lines preceded by a semicolon)
2. Time information (start time, stop time, timestepsize)
3. Output information (for “.ext” time-history output; this is a readable by XTOOL v10.1)
4. Material properties (in the form of a rocktab file; see Appendix IV[a])
5. Heat generation information (in the form of a heatgen file; see Appendix III[a])
6. Boundary conditions
7. Initial conditions (“state” command)
8. SDT submodel mesh file (in the form of an SDT submodel mesh file, see Appendix I[a]).

All parameter values are taken directly from inputs or calculations described in other appendices. An example of an SDT submodel NUFT input file follows. For more information, see the NUFT documentation (Nitao 1998 [DIRS 100474]). SDT submodel input files follow the naming convention P#-D#-UZGC-SDT(aml).in where P# stands for panel number, D# stands for drift

number, and UZGC stands for UZ flow model grid column. Note that only one set of SDT submodels is required to address all seven MSTHM uncertainty cases (P10, P30, P50, P10L, P10H, and P90H). Thus, there are 2,800 input files, which includes 560 initialization runs and 2,240 post-emplacement runs. These files are found in Output DTN: LL0702PA013MST.068.

```
;; /home2/TSPA06/sdt_mesh/data/P3W-13-g_9-SDT55-02.in was produced on
;; Tue Jan 16 09:30:16 PST 2007
;; Conduction-only for smeared-heat-source cases
;; AML = 55 MTU/acre; half drift spacing = 40.50 m
;; use tcond_wet for both solid and gas pgases.

;; P3W-13-g_9.col.units

;; COLUMN INFORMATION (x,y = 170754.578, 234921.031) WORLD COLUMN g_9

;; unit      thickness (m)
;; _____
;; uz1        146.982
;; tsw33       85.281
;; tsw34       32.906
;; tsw35      104.766
;; tsw36       38.696
;; uz2        180.420

;; repository elevation (m):          1052.874
;; host rock:                          tsw35

;; meters of host rock (tsw35) above repository:  45.375
;; meters of host rock (tsw35) below repository:  59.391

;; overburden thickness (m):          310.544
;; distance from repository plane to top of water table (m):  278.506

(usnt
  (title "AML=55mtu_acre,SDT55")
  (modelname usnt)

(include-pkg "thermcon.pkg") ;; single-comp (air), single-phase (gas) pkg for cond-
only run
  (tstop 1.0e6y)
  (time 0)
  (stepmax 1000000)
  (dtmax 1.728e+18)
  (dt 1e2)

;;
*****
*****

(output
  (extool (variables T)
    (file-ext ".ext") (range "**")
    (outtimes
      (include "/home2/TSPA07/outputTimes/outputTimes-LDTH-SDT-DDT-55-01L")
    )
  )
  (history
    (file-ext ".wt")
    (variable T)
    (element "wt#1:1:66")
  )
)
```

```

)
)

;*****
*****
  (rocktab
  (include "/home2/TSPA06/physical_properties/SDT-1Dds-06")
  ) ;; close rocktab
;*****
*****

;;   There is no percolation for the conduction-only case
  (srctab
  (include "/home2/TSPA07/heatgen/SDT_LDTH_blocks/50yr/P3W-13-g_9_LDTH-SDT")
  ) ;; end srctab
;*****
*****

;; set boundary conditions
(bctab
  (atmos
    (range "at*")
    (clamped)
  )
  (bsmnt
    (range "bs*")
    (clamped)
  )
) ;; end bctab

;*****
*****
  (state
  (include "/home2/TSPA07/SDT/SDT66/01i/P3W-13-g_9-SDT-01i.ztable")
  ) ;; end state
;*****
*****
  (genmsh
    (down 0. 0. 1.0)
    (coord rect)
    (dx 40.50)
    (dy 1.0)
    (dz
      1.0e-30 20.244 4.014 7.207 5.596 ;; 1 - 5: atm tcw12 tcw13 ptn21
ptn22
      2.021 12.510 6.504 30.000 11.250 ;; 6 - 10: ptn23 ptn24 ptn25 ptn25
ptn26
      2.021 15.557 30.000 18.311 20.000 ;; 11 - 15: tsw31 tsw32 tsw32 tsw33
tsw33
      15.000 10.000 10.000 6.000 6.000 ;; 16 - 20: tsw33 tsw33 tsw33 tsw33
tsw33
      4.453 4.453 6.000 6.000 6.000 ;; 21 - 25: tsw34 tsw34 tsw34 tsw34
tsw34
      6.000 4.359 6.000 6.000 6.000 ;; 26 - 30: tsw34 tsw35 tsw35 tsw35
tsw35
      6.000 6.000 5.500 5.500 6.000 ;; 31 - 35: tsw35 tsw35 tsw35 tsw35
tsw35
      6.000 6.000 6.000 6.000 6.000 ;; 36 - 40: tsw35 tsw35 tsw35 tsw35
tsw35
      6.000 6.000 6.000 5.391 6.000 ;; 41 - 45: tsw35 tsw35 tsw35 tsw35
tsw36
      6.000 6.000 3.891 3.891 6.000 ;; 46 - 50: tsw36 tsw36 tsw36 tsw36
tsw37
    )
  )

```


Multiscale Thermohydrologic Model

```

        6.914    10.000    10.000    1.934    6.592 ;; 51 - 55: tsw37 tsw38 tsw38 tsw38
tsw9z
        15.039   20.000    0.293    20.273   20.303 ;; 56 - 60:  ch1z  ch2z  ch2z  ch3z
ch4z
        20.303   17.578   19.688   14.326    4.102 ;; 61 - 65:  ch5z  ch6z   pp4   pp3
pp2
        0.900    29.000    60.000    70.000  120.000 ;; 66 - 70:   pp2   sz1   sz2   sz3
sz4
        240.000  480.000    0.100                ;; 71 - 73:   sz5   sz6 bsmnt
    )
    (mat
      ( atm      atm  1 nx  1 ny  1  1)
      (tcw12    tcw12 1 nx  1 ny  2  2)
      (tcw13    tcw13 1 nx  1 ny  3  3)
      (ptn21    ptn21 1 nx  1 ny  4  4)
      (ptn22    ptn22 1 nx  1 ny  5  5)
      (ptn23    ptn23 1 nx  1 ny  6  6)
      (ptn24    ptn24 1 nx  1 ny  7  7)
      (ptn25    ptn25 1 nx  1 ny  8  9)
      (ptn26    ptn26 1 nx  1 ny 10 10)
      (tsw31    tsw31 1 nx  1 ny 11 11)
      (tsw32    tsw32 1 nx  1 ny 12 13)
      (tsw33    tsw33 1 nx  1 ny 14 20)
      (tsw34    tsw34 1 nx  1 ny 21 26)
      (tsw35    tsw35 1 nx  1 ny 27 44)
      (tsw36    tsw36 1 nx  1 ny 45 49)
      (tsw37    tsw37 1 nx  1 ny 50 51)
      (tsw38    tsw38 1 nx  1 ny 52 54)
      (tsw9z    tsw9z 1 nx  1 ny 55 55)
      ( ch1z    ch1z  1 nx  1 ny 56 56)
      ( ch2z    ch2z  1 nx  1 ny 57 58)
      ( ch3z    ch3z  1 nx  1 ny 59 59)
      ( ch4z    ch4z  1 nx  1 ny 60 60)
      ( ch5z    ch5z  1 nx  1 ny 61 61)
      ( ch6z    ch6z  1 nx  1 ny 62 62)
      ( pp4     pp4   1 nx  1 ny 63 63)
      ( pp3     pp3   1 nx  1 ny 64 64)
      ( pp2     pp2   1 nx  1 ny 65 65)
      ( wt      pp2   1 nx  1 ny 66 66)
      ( sz1     sz1   1 nx  1 ny 67 67)
      ( sz2     sz2   1 nx  1 ny 68 68)
      ( sz3     sz3   1 nx  1 ny 69 69)
      ( sz4     sz4   1 nx  1 ny 70 70)
      ( sz5     sz5   1 nx  1 ny 71 71)
      ( sz6     sz6   1 nx  1 ny 72 72)
      (bsmnt    bsmnt 1 nx  1 ny 73 73)
      ( wp      tsw35 1 nx  1 ny 34 34)
    ) ) ;; end genmsh

;; Use this for the 1-D, 2-D cases
   (linear-solver d4vband)

);; end of model input

```

DDT submodel

The DDT submodel has the following information in this order:

1. Header information (lines preceded by a semicolon)
2. Time information (start time, stop time, timestepsize)
3. Output information (for “.ext” time-history output this is readable by XTOOL v10.1)
4. Material properties (in the form of a rocktab file; see Appendix IV of the parent report)
5. Heat generation information (in the form of a heatgen file; see Appendix III of the parent report)
6. Boundary conditions
7. Restart file information
8. Initial conditions
9. DDT mesh file
10. Radcon information (in the form of a file for doing thermal-radiation connections; see Appendix VI[a])
11. Run control parameters.

All parameter values are taken directly from inputs or calculations described in other appendices. An example of a DDT submodel input file follows. For more information, refer to the NUFT documentation (Nitao 1998 [DIRS 100474]) for specific details of this input file. DDT submodel input and output files are found in Output DTN: LL0702PA013MST.068.

```
;; Implicit DKM with active fracture concept (AFC)
;; NBS material properties from 1D drift-scale mean infiltration flux
property set assembled by Ken Lee
;; AML = 54.82 MTU/acre; half drift spacing = 40.5 m
;; represents 8 WPs: 6 full WPs and 2 half WPs
;; WP and drip-shield dimensions updated to correspond to FY07 MSTHM for
TSPA-LA Compliance Model

;; P3W-13-g_9.col.units

;; COLUMN INFORMATION (x,y = 170754.578, 234921.031) WORLD COLUMN g_9

;; unit thickness (m)
;; _____
;; uz1 146.982
;; tsw33 85.281
;; tsw34 32.906
;; tsw35 104.766
;; tsw36 38.696
;; uz2 180.420

;; repository elevation (m): 1052.874
```

```

;; host rock:                                     tsw35

;; meters of host rock (tsw35) above repository:  45.375
;; meters of host rock (tsw35) below repository:  59.391

;; overburden thickness (m):                     310.544
;; distance from repository plane to top of water table (m): 278.506

(usnt
  (title "line-load,AML=55mtu_acre,P3W-13-g_9-DDT55-01")
  (modelname usnt)

  (include-pkg "thermcon.pkg") ;; single-comp (air), single-phase (gas) pkg for cond-
only run

  (tstop 1e6y)
  (time 50y)
  (stepmax 1000000)
  (dtmax 1.000e+25)
  (dt 1e2)
  (check-mult-con off)

;;
*****
*****
  (output
    (extool (variables T )
      (file-ext ".EBS.ext")(range "hstrk*" "dr*" "dhlw*" "bwr*" "pwr*" "in*"
"ds*")
      (outtimes
        (include "outputTimes-LDTH-SDT-DDT-55-01L")
      )
    )
  ) ;; end output

;;
*****
*****
  (rocktab
    (include "DDT-1Dds-07")
    (include "DDT-EBS-TSPA07")
  ) ;; close rocktab
    (include "modprop-DDT55_02i")
    (include "modprop-DDT55_02o")

;;
*****
*****

;; There is no percolation for the conduction-only case
  (srctab
    (include "DDT_AVG_TSPA07")
  ) ;; end srctab

;*****
*****

;; set boundary conditions
  (bctab
    (atmos
      (range "at*")
      (clamped)
    )
    (gwater

```

```

        (range "wt*")
          (clamped)
        )
      ) ;; end bctab

;*****
*****
; ; set initial conditions.
  (read-restart (time 50y)
    (file "P3W-13-g_9-DDT55-01v.res"))

;*****
*****
; ; This is for a unit symmetry cell with a half drift and half pillar
; ; between drifts.
  (genmsh
    (down 0. 0. 1.0)
    (coord rect)
; ; 54.82 MTU/acre
(dx 0.8900 0.3615 0.015 0.4082 0.4222 0.350 0.3031 0.35 0.5 0.9 1.0 1.5 2.5 4.0 6.0
9.0 12.00)
; ; the WP cross-sectional area is the same as for a blended WP with a diameter of
2.0085 m
; ; which results in a 1.78-m x 1.78-m WP
; ; the drip-shield width is 2.5330 m ; ; the drip-shield half-width is 1.2665 m
; ; the location the WP centerline above the invert is 1.2181 m
; ; the maximum height of drip shield is 2.886 m
; ; the location of the intersection of plate 1 and plate 2 is 1.891 m above invert
; ; the "average height of drip shield is (2.886 + 1.891)/2 = 2.3885 m
      (dy      1.462525 1.462525      ; ; 1/2 21-PWR TAD      2.92505 m j = 1-2
        0.1      ; ; gap      0.1 m      j = 3
      1.307000 2.614000 1.307000      ; ; CDSP 1L/5L      5.2280 m j = 4-6
        0.1      ; ; gap      0.1 m      j = 7
      1.462525 2.925050 1.462525      ; ; 21-PWR TAD (hot) 5.8501 m j = 8-10
        0.1      ; ; gap      0.1 m      j = 11
      1.462525 2.925050 1.462525      ; ; 44-BWR TAD      5.8501 m j = 12-14
        0.1      ; ; gap      0.1 m      j = 15
      1.462525 2.925050 1.462525      ; ; 44-BWR TAD (adj) 5.8501 m j = 16-18
        0.1      ; ; gap      0.1 m      j = 19
      0.920350 1.840700 0.920350      ; ; CDSP 1S/5S      3.6814 m j = 20-22
        0.1      ; ; gap      0.1 m      j = 23
      1.462525 2.925050 1.462525      ; ; 21-PWR TAD      5.8501 m j = 24-26
        0.1      ; ; gap      0.1 m      j = 27
      1.462525 1.462525      ; ; 1/2 21-PWR TAD      2.92505 m j = 28-29
    ) ;; total length of drift = 38.9199 m
    (dz
      1.0e-30 26.982 30.000 30.000 30.000 ; ; 1- 5:      atm      uz1
    uz1      uz1      uz1
      30.000 18.281 20.000 15.000 10.000 ; ; 6- 10:      uz1      tsw33
    tsw33    tsw33    tsw33
      10.000 6.000 6.000 4.453 4.453 ; ; 11- 15:      tsw33    tsw33
    tsw33    tsw34    tsw34
      6.000 6.000 6.000 6.000 3.375 ; ; 16- 20:      tsw34    tsw34
    tsw34    tsw34    tsw35
      6.000 6.000 6.000 3.000 3.000 ; ; 21- 25:      tsw35    tsw35
    tsw35    tsw35    tsw35
      3.000 3.000 1.500 2.000 1.000 ; ; 26- 30:      tsw35    tsw35
    tsw35    tsw35    tsw35
      1.000 0.500 0.300 0.200 0.200 ; ; 31- 35:      tsw35    tsw35
    tsw35    tsw35    tsw35
      0.200 0.200 0.200 0.200 0.200 ; ; 36- 40:      tsw35    tsw35
    tsw35    tsw35    tsw35
      0.200 0.200 0.200 0.200 0.3055 ; ; 41- 45:      tsw35    tsw35
    tsw35    tsw35    tsw35
  )

```

Multiscale Thermohydrologic Model

```

tsw35      0.015      0.2654      0.890      0.890      0.3281 ;; 46- 50:      tsw35      tsw35
tsw35      tsw35      tsw35
tsw35      0.403      0.403      0.800      1.200      1.500 ;; 51- 55:      tsw35      tsw35
tsw35      tsw35      tsw35
tsw35      2.500      3.000      3.000      6.000      6.000 ;; 56- 60:      tsw35      tsw35
tsw35      tsw35      tsw35
tsw35      6.000      6.000      6.000      6.000      6.000 ;; 61- 65:      tsw35      tsw35
tsw35      tsw35      tsw35
tsw36      5.391      6.000      6.000      6.000      6.000 ;; 66- 70:      tsw35      tsw36
tsw36      tsw36      tsw36
tsw36      6.000      4.348      4.348      10.000     10.000 ;; 71- 75:      tsw36      tsw36
tsw36      uz2       uz2
tsw36      15.000     20.000     30.000     30.000     30.000 ;; 76- 80:      uz2       uz2
uz2       uz2       uz2
uz2       30.000     5.420     1.0e-30           ;; 81- 83:      uz2       uz2
wt
)
(mat
(atm      atm      1 nx 1 ny 1 1)
(uz1     uz1     1 nx 1 ny 2 6)
(tsw33   tsw33   1 nx 1 ny 7 13)
(tsw34   tsw34   1 nx 1 ny 14 19)
(tsw35   tsw35   1 nx 1 ny 20 66)
(tsw36   tsw36   1 nx 1 ny 67 73)
(uz2     uz2     1 nx 1 ny 74 82)
(wt      uz2     1 nx 1 ny 83 83)
(hstrk   tsw35   1 nx 1 ny 28 55)
(dr      drift   1 1 1 ny 35 35)
(dr      drift   1 3 1 ny 36 36)
(dr      drift   1 4 1 ny 37 38)
(dr      drift   1 5 1 ny 39 40)
(dr      drift   1 6 1 ny 41 43)
(dr      drift   1 7 1 ny 44 48)
(dr      drift   1 6 1 ny 49 49)
(dr      drift   1 5 1 ny 50 50)
;; WP1 half 21-PWR PWR AP WP
(dro_wp1 dro_wp1 1 1 1 3 35 35)
(dro_wp1 dro_wp1 1 3 1 3 36 36)
(dro_wp1 dro_wp1 1 4 1 3 37 38)
(dro_wp1 dro_wp1 1 5 1 3 39 40)
(dro_wp1 dro_wp1 1 6 1 3 41 43)
(dro_wp1 dro_wp1 1 7 1 3 44 48)
(dro_wp1 dro_wp1 1 6 1 3 49 49)
(dro_wp1 dro_wp1 1 5 1 3 50 50)
(dri_wp1 dri_wp1 1 2 1 3 47 50)
(ds_pwr1-1 drpshld 1 3 1 2 46 46)
(ds_pwr1-1 drpshld 3 3 1 2 47 50)
(pwr1-1 pwr 1 1 1 2 48 49)
(dr      drift   1 1 3 3 48 49)
;; Gap1
(dr      drift   1 1 3 3 48 49)
(ds_gap1 drpshld 1 3 3 3 46 46)
(ds_gap1 drpshld 3 3 3 3 47 50)
;; WP2 full 5-DHLW Long WP
(dro_wp2 dro_wp2 1 1 4 7 35 35)
(dro_wp2 dro_wp2 1 3 4 7 36 36)
(dro_wp2 dro_wp2 1 4 4 7 37 38)
(dro_wp2 dro_wp2 1 5 4 7 39 40)
(dro_wp2 dro_wp2 1 6 4 7 41 43)
(dro_wp2 dro_wp2 1 7 4 7 44 48)
(dro_wp2 dro_wp2 1 6 4 7 49 49)
(dro_wp2 dro_wp2 1 5 4 7 50 50)
(dri_wp2 dri_wp2 1 2 4 7 47 50)
(ds_dhlw-11 drpshld 1 3 4 6 46 46)

```

```

(ds_dhlw-11 drpshld 3 3 4 6 47 50)
(dhlw-11 dhlw-1 1 1 4 6 48 49)
;; Gap2
(dr drift 1 1 7 7 48 49)
(ds_gap2 drpshld 1 3 7 7 46 46)
(ds_gap2 drpshld 3 3 7 7 47 50)
;; WP3 full 21-PWR AP Hot WP
(dro_wp3 dro_wp3 1 1 8 11 35 35)
(dro_wp3 dro_wp3 1 3 8 11 36 36)
(dro_wp3 dro_wp3 1 4 8 11 37 38)
(dro_wp3 dro_wp3 1 5 8 11 39 40)
(dro_wp3 dro_wp3 1 6 8 11 41 43)
(dro_wp3 dro_wp3 1 7 8 11 44 48)
(dro_wp3 dro_wp3 1 6 8 11 49 49)
(dro_wp3 dro_wp3 1 5 8 11 50 50)
(dri_wp3 dri_wp3 1 2 8 11 47 50)
(ds_pwr2-1 drpshld 1 3 8 10 46 46)
(ds_pwr2-1 drpshld 3 3 8 10 47 50)
(pwr2-1 pwr 1 1 8 10 48 49)
;; Gap3
(dr drift 1 1 11 11 48 49)
(ds_gap3 drpshld 1 3 11 11 46 46)
(ds_gap3 drpshld 3 3 11 11 47 50)
;; WP4 full 37-BWR AP WP
(dro_wp4 dro_wp4 1 1 12 15 35 35)
(dro_wp4 dro_wp4 1 3 12 15 36 36)
(dro_wp4 dro_wp4 1 4 12 15 37 38)
(dro_wp4 dro_wp4 1 5 12 15 39 40)
(dro_wp4 dro_wp4 1 6 12 15 41 43)
(dro_wp4 dro_wp4 1 7 12 15 44 48)
(dro_wp4 dro_wp4 1 6 12 15 49 49)
(dro_wp4 dro_wp4 1 5 12 15 50 50)
(dri_wp4 dri_wp4 1 2 12 15 47 50)
(ds_bwr1-1 drpshld 1 3 12 14 46 46)
(ds_bwr1-1 drpshld 3 3 12 14 47 50)
(bwr1-1 bwr 1 1 12 14 48 49)
;; Gap4
(dr drift 1 1 15 15 48 49)
(ds_gap4 drpshld 1 3 15 15 46 46)
(ds_gap4 drpshld 3 3 15 15 47 50)
;; WP5 full 37-BWR AP Adjusted WP
(dro_wp5 dro_wp5 1 1 16 19 35 35)
(dro_wp5 dro_wp5 1 3 16 19 36 36)
(dro_wp5 dro_wp5 1 4 16 19 37 38)
(dro_wp5 dro_wp5 1 5 16 19 39 40)
(dro_wp5 dro_wp5 1 6 16 19 41 43)
(dro_wp5 dro_wp5 1 7 16 19 44 48)
(dro_wp5 dro_wp5 1 6 16 19 49 49)
(dro_wp5 dro_wp5 1 5 16 19 50 50)
(dri_wp5 dri_wp5 1 2 16 19 47 50)
(ds_bwr2-1 drpshld 1 3 16 18 46 46)
(ds_bwr2-1 drpshld 3 3 16 18 47 50)
(bwr2-1 bwr 1 1 16 18 48 49)
;; Gap5
(dr drift 1 1 19 19 48 49)
(ds_gap5 drpshld 1 3 19 19 46 46)
(ds_gap5 drpshld 3 3 19 19 47 50)
;; WP6 full 5-DHLW Short WP
(dro_wp6 dro_wp6 1 1 20 23 35 35)
(dro_wp6 dro_wp6 1 3 20 23 36 36)
(dro_wp6 dro_wp6 1 4 20 23 37 38)
(dro_wp6 dro_wp6 1 5 20 23 39 40)
(dro_wp6 dro_wp6 1 6 20 23 41 43)
(dro_wp6 dro_wp6 1 7 20 23 44 48)

```

```

        (dro_wp6 dro_wp6 1 6 20 23 49 49)
        (dro_wp6 dro_wp6 1 5 20 23 50 50)
        (dri_wp6 dri_wp6 1 2 20 23 47 50)
        (ds_dhlw-s1 drpshld 1 3 20 22 46 46)
        (ds_dhlw-s1 drpshld 3 3 20 22 47 50)
        (dhlw-s1 dhlw-s 1 1 20 22 48 49)
;; Gap6
        (dr drift 1 1 23 23 48 49)
        (ds_gap6 drpshld 1 3 23 23 46 46)
        (ds_gap6 drpshld 3 3 23 23 47 50)
;; WP7 full 21-PWR AP WP
        (dro_wp7 dro_wp7 1 1 24 27 35 35)
        (dro_wp7 dro_wp7 1 3 24 27 36 36)
        (dro_wp7 dro_wp7 1 4 24 27 37 38)
        (dro_wp7 dro_wp7 1 5 24 27 39 40)
        (dro_wp7 dro_wp7 1 6 24 27 41 43)
        (dro_wp7 dro_wp7 1 7 24 27 44 48)
        (dro_wp7 dro_wp7 1 6 24 27 49 49)
        (dro_wp7 dro_wp7 1 5 24 27 50 50)
        (dri_wp7 dri_wp7 1 2 24 27 47 50)
        (ds_pwr1-2 drpshld 1 3 24 26 46 46)
        (ds_pwr1-2 drpshld 3 3 24 26 47 50)
        (pwr1-2 pwr 1 1 24 26 48 49)
;; Gap7
        (dr drift 1 1 27 27 48 49)
        (ds_gap7 drpshld 1 3 27 27 46 46)
        (ds_gap7 drpshld 3 3 27 27 47 50)
;; WP8 half 37-BWR AP WP
        (dro_wp8 dro_wp8 1 1 28 29 35 35)
        (dro_wp8 dro_wp8 1 3 28 29 36 36)
        (dro_wp8 dro_wp8 1 4 28 29 37 38)
        (dro_wp8 dro_wp8 1 5 28 29 39 40)
        (dro_wp8 dro_wp8 1 6 28 29 41 43)
        (dro_wp8 dro_wp8 1 7 28 29 44 48)
        (dro_wp8 dro_wp8 1 6 28 29 49 49)
        (dro_wp8 dro_wp8 1 5 28 29 50 50)
        (dri_wp8 dri_wp8 1 2 28 29 47 50)
        (ds_pwr1-3 drpshld 1 3 28 29 46 46)
        (ds_pwr1-3 drpshld 3 3 28 29 47 50)
        (pwr1-3 bwr 1 1 28 29 48 49)
        (in invert 1 4 1 ny 51 51)
        (in invert 1 2 1 ny 52 52)
    ) ;; end of material assignment
(radcon
    (surface-offset 0 0 -7)
    (include "P2WR5C10-DDT55-TSPA07-01-1e-13.radcon")
) ;; close radcon
) ;; end genmsh

;; ***** Solver options
*****
(include "run_control_param_SMT-v02")

);; end of model input

;; ***** Done
!*****

```

INTENTIONALLY LEFT BLANK

APPENDIX VI[a]

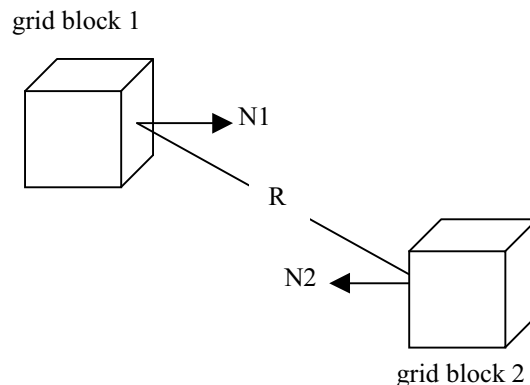
**LDTH AND DDT SUBMODEL THERMAL-RADIATION CONNECTION
CALCULATION**

The LDTH and DDT submodels include heat transfer by thermal radiation inside the drift. The LDTH and DDT submodels represent thermal-radiative heat transfer between the drip shield, drift wall, and invert surfaces. The DDT submodels also represent thermal-radiative heat transfer between the waste package, drip shield, and invert surfaces beneath the drip shield. The determination of the thermal-radiation coefficients requires one direct input, which is the emissivity of the surfaces. The emissivity of the drift wall and invert surfaces is taken to be 0.9, which is near the middle of the range given for rocks (0.88 to 0.95) in *Fundamentals of Heat and Mass Transfer* (Incropera and DeWitt 1996 [DIRS 108184], Table A.11). The process of determining thermal-radiation connections for the LDTH and the DDT submodels is done by hand, following these steps:

1. Compile a list of model gridblocks that have at least one face contacting air within the drift
2. For each pair of gridblocks in this list:
 - a. Determine if there is a clear path (line of sight between face centers) between the air contacting face of each block
 - b. If a clear path exists, calculate the thermal-radiation coefficient for that connection and write a “radcon” entry in NUFT format, which is given in *Reference Manual for the NUFT Flow and Transport Code, Version 2.0* (Nitao 1998 [DIRS 100474]). The coefficient c used in Equations 9 and 10 of Section 6.2.3.3 of the parent report, which is calculated by RADPRO v4.0 (Section 3.1.1.1[a]), is determined as follows:

$$c = \frac{\sigma \varepsilon (N_1 \times R)(-N_2 \times R) A_1 A_2}{\pi R^4}, \quad (\text{Eq. VI-1[a]})$$

where σ is Stefan’s constant, ε is emissivity, A_1 is the area of grid block face 1 (radiating), A_2 is the area of grid block face 2 (connecting), N_1 is the unit vector normal to face 1, N_2 is the unit vector normal to face 2, and R is the distance from the center of face 1 to center of face 2.



Radcon files are located in DTN: LL0702PA0131455.068. The file names are:

```
P2WR5C10-DDT55-01v.radcon
P2WR5C10-DDT55-TSPA07-01-1e-13.radcon
P2WR5C10-DDT55-TSPA07-01v.radcon
```

Determining Effective Emissivity for RADPRO Radcon Files

Equations 9 and 10 in Section 6.2.3.3 of the parent report apply to gray body-to-black body thermal radiation, where the heat receiving surface (A_2) is a perfect black body (i.e., ε equal to 1). The software routine RADPRO v4.0 (Section 3.1.1.1[a]), which calculates the coefficient c in Equation VI-1[a], also pertains to gray-body-to-black-body thermal radiation. However, all surfaces within the emplacement drifts are gray bodies, with values of emissivity less than 1. Therefore, the value of emissivity, ε , taken as input for RADPRO v4.0 is actually an *effective* emissivity, ε_{eff} , for the heat-emitting surface, which accounts for the fact that the heat-receiving surface is a gray body, rather than a black body. The value of effective emissivity, ε_{eff} , is determined by applying the solution from Bird et al. (1960 [DIRS 103524]) for radiative heat transfer between two long, gray coaxial cylinders by considering multiple reflections from the two sources:

$$Q_{12} = \frac{\sigma(T_1^4 - T_2^4)}{\frac{1}{A_1\varepsilon_1} + \frac{1}{A_2}\left(\frac{1}{\varepsilon_2} - 1\right)}. \quad (\text{Eq. VI-2[a]})$$

Multiplying the numerator and denominator by $A_1\varepsilon_1$ yields the following expression:

$$Q_{12} = \frac{A_1\varepsilon_1\sigma(T_1^4 - T_2^4)}{1 + \frac{A_1}{A_2}\left(\frac{\varepsilon_1}{\varepsilon_2} - \varepsilon_1\right)} \quad (\text{Eq. VI-3[a]})$$

Using an *effective* emissivity, ε_{eff} , results in the following expression:

$$Q_{12} = A_1\varepsilon_{\text{eff}}\sigma(T_1^4 - T_2^4), \quad (\text{Eq. VI-4[a]})$$

where ε_{eff} is:

$$\varepsilon_{\text{eff}} = \frac{\varepsilon_1}{1 + \frac{A_1\varepsilon_1}{A_2}\left(\frac{1}{\varepsilon_2} - 1\right)}. \quad (\text{Eq. VI-5[a]})$$

The effective emissivity, ε_{eff} , which is a direct input for RADPRO v4.0 input files (e.g., *P2WR5C10-DDT55-01v.radin*, *P2WR5C10-DDT55-TSPA07-01.radin*, *P2WR5C10-DDT55-TSPA07-01v.radin*), is simply ε_1 , multiplied by a coefficient C :

$$\varepsilon_{\text{eff}} = C\varepsilon_1, \quad (\text{Eq. VI-6[a]})$$

where the coefficient C is given by:

$$C = \frac{1}{1 + \frac{A_1 \epsilon_1}{A_2} \left(\frac{1}{\epsilon_2} - 1 \right)}. \quad (\text{Eq. VI-7[a]})$$

For the RADPRO v4.0 input, A_1 is taken to be equal to A_2 , resulting in the following expression:

$$C = \frac{1}{1 + \epsilon_1 \left(\frac{1}{\epsilon_2} - 1 \right)}. \quad (\text{Eq. VI-8[a]})$$

In the previous implementation of the MSTHM in the parent report, the surface of the drift wall was assumed to be a rock surface. The value of ϵ_{eff} between the drip shield and drift wall surface is determined for the LDTH and DDT submodels, using Equations VI-6[a] and VI-8[a] and the following values for emissivity on the drip shield ($\epsilon_1 = 0.63$, which is for titanium; see Lide 1995 [DIRS 101876], p. 10-298) and for emissivity on the drift wall (rock) surface ($\epsilon_2 = 0.9$, which is for rock and within the range of 0.88 to 0.95; see Incropera and DeWitt 1996 [DIRS 108184]).

This yields a value of 0.935 for the coefficient, C . As discussed in Section 6.2.13.6[a], the drift wall surface is covered with a liner of Stainless Steel Type 316, which has an emissivity of 0.28 at 75°F (24°C) and 0.57 at 450°F (232°C) (McAdams 1954 [DIRS 161435], p. 475). Interpolating to 140°C, which is a typical peak drift wall temperature, results in an emissivity of 0.44, which is the value applied to all of the current LDTH and DDT submodels. However, the average emissivity values for stainless steel range from 0.823 to 0.843 (with an average of 0.83), as reported in DTN: MO0109EBSAEQST.009 [DIRS 156696] (file: *s01143_001_002.pdf*). Therefore, the emissivity values from McAdams (1954 [DIRS 161435], p. 475) probably pertain to polished samples, while the values in DTN: MO0109EBSAEQST.009 [DIRS 156696] (file: *s01143_001_002.pdf*) pertain to a dull surface texture. Table VI-1[a] summarizes the value of the coefficient C for different values of emissivity (ϵ_2) at the drift wall.

Table VI-1[a]. Value of the Coefficient C from Equation VI-8[a] Calculated for Different Values of Emissivity at the Drift Wall

Emissivity at Drift Wall (ϵ_2)	C	$\frac{C}{C_{\text{orig}}}$
0.90	0.935	1.000
0.83	0.886	0.948
0.44	0.555	0.594

NOTE: These values pertain to radiation between the drip shields and drift wall, where emissivity on the drip shield (ϵ_1) is equal to 0.63.

C_{orig} is the value of C that was applied to determine ϵ_{eff} from the drip shield to the drift wall for the LDTH and DDT submodels, which was calculated using Equation VI-8[a] and is equal to 0.935.

For emissivity (ϵ_1) on the drip shield equal to 0.63 and emissivity (ϵ_2) at the drift wall ranging from 0.44 to 0.83, Equation VI-8[a] gives values of C ranging from 0.555 to 0.886. As discussed above, for the previous LDTH and DDT submodels, a value of 0.935 was calculated (using Equation VI-8[a]) for the coefficient C (called C_{orig} in Table VI-1[a]), which was used to determine the value ϵ_{eff} from the drip shield to drift wall. The ratio C/C_{orig} is listed in Table VI-1[a] to illustrate the relative change in ϵ_{eff} that would occur if this range of ϵ_2 were applied, compared to the value of ϵ_{eff} used in the LDTH and DDT submodels in the previous implementation of the parent report. Thus, relative to the emissivity value for rock, the value of ϵ_{eff} would be reduced by 5.2% to 40.6% for the range of emissivities reported for stainless steel.

Because thermal radiation depends on the difference of the respective temperatures each raised to the fourth power (Equation VI-4[a]), the influence of a 5.2% to 40.6% reduction in the value of ϵ_{eff} is small. Using the P10 case and the g_9 UZ flow model location, which is close to the center of the repository in Panel P3W, the peak drip shield temperature is 161.1°C when the emissivity of the drift wall is 0.44 (directory /LDTH-emissivity-test of Output DTN: LL0705PA032MST.028). When the drift wall emissivity is 0.9, the peak drip shield temperature is 157.5°C, which is a decrease of only 3.6°C (directory /LDTH-emissivity-test of Output DTN: LL0705PA032MST.028). Thus, a 40.6% decrease in drift wall emissivity only results in a 3.6°C increase in peak temperature of the drip shield. Linearly interpolating between emissivity values of 0.44 and 0.90 to an emissivity value of 0.83 results in a drip shield temperature change of 3.0°C, which is much smaller than the range of temperatures resulting from parametric uncertainty described in Section 6.3.16[a]. Therefore, an emissivity value of 0.44 for the drift wall is reasonable.

APPENDIX VII[a]

**EXTRACTION/MICRO-ABSTRACTION PROCESS FOR MSTHAC (BUILDING
VIRTUAL LDTH AND SDT “CHIMNEY” SUBMODELS)**

Extract MSTHAC v7.0 information from SMT, SDT, LDTH, and SDT submodel output

For the first stage of the multiscale thermohydrologic model abstraction process, MSTHAC v7.0 reads the NUFT output files for the SMT, SDT, LDTH, and DDT submodels, extracts the requested time histories, and saves them to a MSTHAC v7.0 “extraction” file. Detailed information on the extraction is provided in the MSTHAC v7.0 user’s manual.

Map LDTH and SDT “chimney” submodel output to the SMT submodel locations (virtual LDTH and SDT “chimney” submodel extraction files)

The virtual LDTH and SDT “chimney” submodels are built at each SMT submodel grid block. As discussed in Appendix I[a], 560 LDTH/SDT submodel locations correspond to 3,264 SMT submodel repository-gridblock locations. Therefore, one LDTH/SDT submodel may correspond to more than one virtual LDTH and SDT “chimney” submodel. The virtual chimney submodel extraction files at each SMT submodel location and for each AML (e.g., 66, 55, 27, and 14 MTU/acre) are obtained by copying the extraction files at the corresponding LDTH/SDT “chimney” submodel locations and renaming them. This process is only conducted for the SDT and LDTH submodels.

There are approximately 91,392 virtual LDTH submodel extraction files, and 2,240 virtual SDT submodel extraction files.

These files are found in the following Output DTNs:

- LL0702PA013MST.068
- LL0702PA014MST.069
- LL0702PA016MST.071
- LL0702PA018MST.073
- LL0702PA020MST.075
- LL0702PA022MST.077
- LL0702PA024MST.079
- LL0702PA028MST.083.

File names follow the conventions:

LDTH submodels:

(panel #)(*i* index):(j index)-LDTH(AML)-(Case ID)-02.m-f.EBS.ext.extract_LDTH_rev_14

SDT submodels:

(panel #)(*i* index):(j index)-SDT(AML)-03.ext.extract_SDT_rev_0

- Note that (panel #) represents the panel number, which are 1#, 2#, 3e#, 3w#, and 4# for Panel P1, P2, P3E, P3W, and P4, respectively.
- The (*i* index) and (*j* index) are *i* and *j* indices from the SMT submodel.
- (AML) stands for AML label (e.g. 14, 27, 55, and 66).

- (Case ID) is one of following labels:
 - P10, which stands for the mean host-rock thermal conductivity, 10th percentile percolation flux case
 - P10L, which stands for the low host-rock thermal conductivity, 10th percentile percolation flux case
 - P10H, which stands for the high host-rock thermal conductivity, 10th percentile percolation flux case
 - P30, which stands for the mean host-rock thermal conductivity, 30th percentile percolation flux case
 - P50, which stands for the mean host-rock thermal conductivity, 50th percentile percolation flux case
 - P90, which stands for the mean host-rock thermal conductivity, 90th percentile percolation flux case
 - P90H, which stands for the high host-rock thermal conductivity, 90th percentile percolation flux case.

Create *.in files for each virtual NUFT LDTH “chimney” submodel

For the purposes of micro-abstraction, MSTHAC v7.0 requires the following information:

- The coordinates of the LDTH “chimney” submodels
- The real number for the AML (e.g., the real number for an AML of 66 MTU/acre is 65.784 MTU/acre)
- The glacial-transition climate percolation fluxes for that LDTH submodel location.

Note that there are 3,264 virtual LDTH “chimney” submodels. To obtain this information, MSTHAC v7.0 reads a *.in file associated with each LDTH submodel. The format of the *.in file is specified by the MSTHAC v7.0 user’s manual. A “virtual” LDTH submodel *.in file is created for each SMT submodel repository-gridblock location.

It should be noted that the only purpose for the virtual LDTH submodel *.in files is to supply MSTHAC v7.0 with the percolation flux for the glacial-transition climate for each of the SMT submodel repository gridblock locations. The percolation flux values for the present-day and monsoonal climates are not required. The percolation flux value for the glacial-transition climate along with the coordinates of that location is edited into each of the virtual LDTH submodel *.in files with the use of scripts containing standard UNIX commands.

The names of these virtual LDTH submodel *.in files use the following convention:

(panel #)(i index):(j index)-LDTH(AML)-(Case ID)-02.in

Run MSTHAC v7.0 at all SMT submodel locations using virtual SDT and LDTH “chimney” submodel extraction files, in conjunction with DDT and SMT submodel extraction files

Once the virtual SDT and LDTH submodel extraction files and the virtual LDTH submodel *.in files have been created, MSTHAC v7.0 is run to generate the micro-abstraction output file at each SMT submodel location. This process also requires DDT submodel extraction files, as well as the SMT submodel extraction file.

The process is carried out by first creating an abstraction MSTHAC v7.0 input file, as defined in the MSTHAC v7.0 user’s manual. Once the input files are created, MSTHAC v7.0 is run with these files as input, and the micro-abstraction output files are generated at each SMT submodel location.

INTENTIONALLY LEFT BLANK

APPENDIX VIII[a]
BINNING CALCULATIONS

Bin Indexes

Bin indices were calculated for each SMT submodel location based on the rank of the percolation flux associated with the location. The general calculation procedure is as follows:

1. Sort SMT submodel locations by ascending values of percolation flux
2. Calculate quantile values for each sorted point according to the rank of the point in the sorted data set
3. Assign bin indices according to quantile intervals.

Glacial-transition climate state (median case) was specified as the percolation flux source. Binning was performed according to specifications provided by the Performance Assessment department as follows:

Bin Index	Quantile Range
Bin 1	<~5%
Bin 2	between ~5% and ~30%
Bin 3	between ~30% and ~70%
Bin 4	between ~70% and ~ 95%
Bin 5	>~95%

Bin indices were calculated for each of the 3,264 SMT submodel locations.

Bin the MSTHAC v7.0 output and reformat it for TSPA

After all 3,264 MSTHAC v7.0 microabstractions have been generated for a particular percolation case, the output is processed to yield the set of information required by TSPA. To facilitate TSPA analyses, the micro-abstraction requires possessing in two different ways: “WAPDEG” binning and “TSPA” binning. Note that WAPDEG is an analysis that uses MSTHM output. Because the WAPDEG is downstream of the MSTHM (with respect to model-to-model parameter flow), WAPDEG does not produce any output required by the MSTHM.

WAPDEG Binning

The first processing (WAPDEG binning) involves reporting the T_{wp}, RH_{wp}, T_{ds}, and RH_{ds} for each SMT submodel location and each waste package type. There are eight waste package types that comprise two waste package groups:

Group1: DHLW: dhlw-l1 and dhlw-s1

Group2: CSNF: pwr1-1, pwr2-1, bwr1-1, bwr2-1, pwr1-2, and pwr1-3

For WAPDEG binning, there are 3,264 locations × 8 waste package types = 26,112 typical waste packages reported because each repository location and each waste package type are needed.

Because WAPDEG binning yields a large number of output files, the files are concatenated using a UNIX shell script so that all locations falling within a bin and all waste packages of a given type (CSNF or DHLW) are included in a single file. This process generates 5 (# of bins) \times 2 (number of waste package groups) = 10 output files for delivery to TSPA. A second set of 10 files is provided in the WAPDEG format that only uses the “typical waste package” as explained below. Hence, a total of 20 WAPDEG files are provided for each case.

TSPA Binning

The second process (TSPA binning) involves determining the “typical” location given a set of locations that define a “bin.” For TSPA purposes, the analysis requires assessment of the “typical” waste package (see below) in a group/bin; therefore, there are 5 bins \times 2 groups = 10 typical waste packages reported. A bin is a set of SMT submodel locations that have similar percolation values as defined by the TSPA organization. For the purposes of processing, the waste packages are grouped into two waste package type groups (CSNF and DHLW). For each bin, two output files are created, one for the most typical CSNF package and one for the most typical DHLW package. There are 5 (# of bins) \times 2 (waste package groups) = 10 files generated for this type of processing.

Typical Waste Package Determination

The most typical package is selected by compiling (for each waste package type and bin member) the peak waste package temperature and boiling duration at the waste package. These data are sorted from low to high, and a percentile assigned to each. For each waste package type and location in the list, the typical packages are defined equal to the medians of the two parameter spaces.

To do this processing, the software code reformat_EXT_to_TSPA v2.0 is used. The software code reformat_EXT_to_TSPA v2.0 takes the name of an input file as its only input. The format of this file is defined in the reformat_EXT_to_TSPA v2.0 User’s Manual (DOE 2006 [DIRS 181178]).

Binning files are delivered as output from reformat_EXT_to_TSPA v2.0.

Binning Algorithm

For each location in a bin and waste package in a waste package group:

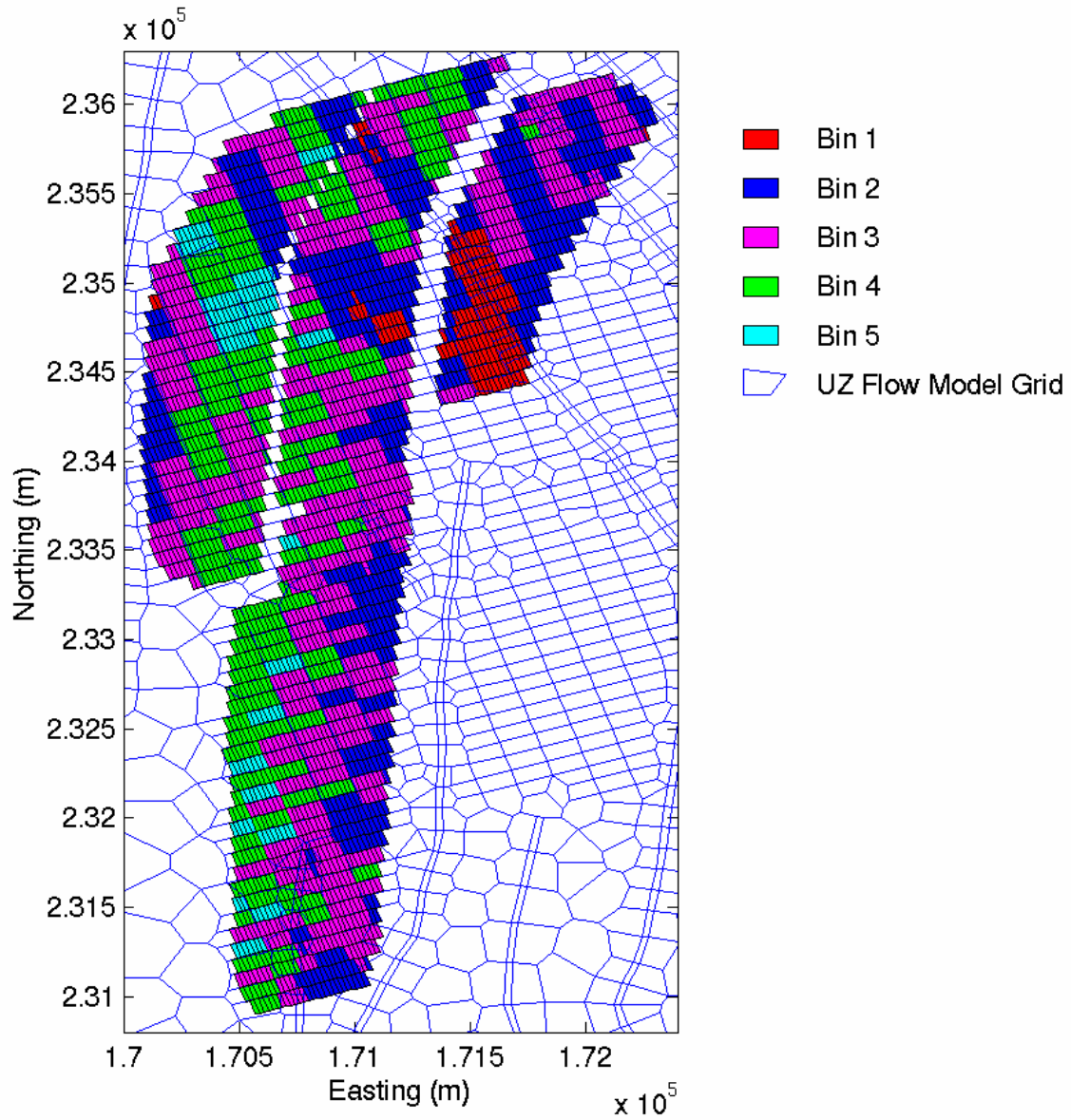
1. Calculate peak waste package temperature
2. Calculate boiling duration at the waste package
3. Sort peak waste package temperature from high to low
4. Sort boiling duration from low to high
5. Assign percentile rank to each waste package temperature
6. Assign percentile rank to each boiling duration.

For each included waste package type/location in the bin:

1. Calculate deviation of percentile rank from median (50%) for peak waste package temperature (e.g., if the current package type/location is ranked 47%, then the deviation = $0.50 - 0.47 = 0.03$).
2. Calculate deviation of percentile rank from median (50%) for boiling duration (e.g., if the current waste package type/location is ranked 54%, then the deviation = $0.50 - 0.54 = -0.04$).
3. Calculate sum of squared deviations from Steps 1 and 2 (e.g., $0.03^2 + 0.04^2 = 0.0025$).

For the current bin/waste package group, select the waste package type/location with the smallest squared deviation (this is the most typical package).

The results of percolation binning is shown in Figure VIII-1[a] where bins are overlain on the UZ flow model grid in the plan of the repository.



Source: DTN: LB03023DKMGRID.001 [DIRS 162354] and Output DTN: LL0702PA015MST.070.

NOTE: UZ flow model grid (SNL 2007 [DIRS 175177]) shown as blue mesh.

Figure VIII-1[a]. Color Plot of the Five Percolation Bins within the Heated Footprint of the Heated Repository Footprint in the SMT Submodel Mesh Overlain on the UZ Flow Model Grid

APPENDIX IX[a]

**MULTISCALE MODEL APPROACH TO THERMOHYDROLOGY AT YUCCA
MOUNTAIN**

No change (not applicable to the addendum).

INTENTIONALLY LEFT BLANK

APPENDIX X[a]

**HYDROLOGIC PROPERTIES FOR THE INTERGRANULAR POROSITY OF THE
INVERT**

X.1[a] Development of the Water Retention Characteristics for the Invert Ballast Material

This appendix develops hydrologic properties for the intergranular porosity of the invert ballast material (Sections X.1[a] and X.2[a]), and bulk thermal conductivity (Section X.3[a]). Intragranular properties are taken to be the same as for the matrix of the tsw35 unit (Ttptll, lower lithophysal), which will be the host unit for much of the repository. Intragranular properties used in MSTHM simulations are shown in Table 4-3[a].

Arya and Paris (1981 [DIRS 104507]) presented a physicoempirical approach for estimating the moisture characteristics of a particulate medium (e.g., soil) from its particle-size distribution and bulk density. The idea for the method emerged from observation of similarities between the shape of particle-size distribution curves and soil moisture characteristic curves. The approach for representing capillary behavior for pores in each size range by cylindrical pores (capillary bundles) is widely used in estimating capillary properties of geologic media (for example, see Jury 1991 [DIRS 102010], Section 3.3.3).

The cumulative particle-size distribution curve is used to divide the soil mass into n fractions and then reassemble the soil mass to represent a soil, summing contributions of the fractions to the water retention properties. The pore volume associated with each size fraction is expressed as (Arya and Paris 1981 [DIRS 104507], Equation 1):

$$V_{vi} = \left(\frac{W_i}{\rho_s} \right) e, \quad i=1,2,\dots,n, \quad (\text{Eq. X-1[a]})$$

where V_{vi} is the pore volume per unit sample mass associated with the solid particle in the i th particle size, W_i is the solid mass per unit sample in the i th particle-size range, ρ_s is the particle density, and e is the void ratio (volume of the voids divided by the volume of the solids).

By representing the solid mass in the i th particle range by n_i spherical particles, the total solid volume (V_{pi}) in the assemblage can be expressed as a function of the particle radius (R_i) and number of particles (n_i) (Arya and Paris 1981 [DIRS 104507], Equation 6):

$$V_{pi} = \frac{n_i 4\pi R_i^3}{3} = \frac{W_i}{\rho_s}. \quad (\text{Eq. X-2[a]})$$

Representing the porosity of each fraction as cylindrical pores with appropriate geometry, the associated pore volume per unit mass can be presented as (Arya and Paris 1981 [DIRS 104507], Equation 7):

$$V_{vi} = \pi r_i^2 h_i = \left(\frac{W_i}{\rho_s} \right) e, \quad (\text{Eq. X-3[a]})$$

where r_i is the mean pore radius and h_i is the total pore length. For a given assemblage of particles, the pore length is approximated as the number of particles that lie along the pore path times the length contributed by each particle. Thus, in a cubic close-packed assemblage of

uniformly sized spherical particles, the total pore length h_i will equal $2n_iR_i$ (Arya and Paris 1981 [DIRS 104507], p. 1,025).

In real materials, the total pore length will depend on actual particle shapes, sizes, and orientations. Let the number of natural particles required be n_i^λ , where $\lambda > 1$. The total pore length will then be equal to $n_i^\lambda 2R_i$ (Arya and Paris 1981 [DIRS 104507], p. 1,025).

Substitution for h_i in Equation X-3[a] and equating with Equation X-1[a] yields (Arya and Paris 1981 [DIRS 104507], Equation 9):

$$r_i = R_i \left[\frac{4en_i^{(1-\lambda)}}{6} \right]^{1/2}. \quad (\text{Eq. X-4[a]})$$

The equation of capillarity is used to obtain the soil water capillary pressure (ψ_i) (Arya and Paris 1981 [DIRS 104507], Equation 10):

$$\psi_i = \frac{2\sigma_w \cos \omega}{\rho g r_i}, \quad (\text{Eq. X-5[a]})$$

where ω is the contact angle, σ_w is the surface tension of water (dyne/cm), ρ is the density of water (gm/cm^3), g is the gravitational acceleration (cm/sec^2), and r_i is the radius of the i th capillary tube. A temperature of 25°C and a contact angle (ω) of 0° (strongly wetting) are used here because: (1) comparisons with measured property data are typically made at 25°C , (2) previous property estimation for the invert ballast used 25°C , and (3) silicate mineral surfaces are strongly wetting.

The calculations were done in an Excel workbook (Output DTN: MO0703PAHYTHRM.000, workbook: *arya_original_data_interpretation 4.xls*). The worksheets used within this workbook are summarized in Table X-1[a]. The LTBM-2 gradation in the engineering report *Estimation of Mechanical Properties of Crushed Tuff for Use as Ballast Material in Emplacement Drifts* (SNL 2007 [DIRS 179354], which directs the user to BSC 2004 [DIRS 168138], Table 5) was considered as the candidate invert ballast material. The minimum, average, and maximum material properties provided in this source (SNL 2007 [DIRS 179354]; see BSC 2004 [DIRS 168138], Table 5) are considered as the range of variation for the invert ballast material. Physical properties used in the water retention property estimation are summarized in Table 4-3[a].

The water retention curves developed using the method of Arya and Paris (1981 [DIRS 104507]) are plotted in Figure X-1[a]. These curves are generated in workbook *arya_original_data_interpretation 4.xls*, located in Output DTN: MO0703PAHYTHRM.000, as listed in Table X-2[a]. The results show that the LTBM-2 material falls within the range of the four single-particle-size curves used in the parent report for water content from approximately 5% up to full saturation. Thermal-hydrologic differences associated with the four curves previously calculated were found to be insignificant (see Appendix X of the parent report). At water content less than 5%, the LTBM-2 estimates are more realistic because they are based on graded

particle size rather than single-size particles. Hence, the average water retention for the LTBM-2 material is appropriate for use in multiscale model calculations supporting TSPA.

The van Genuchten characteristic function used in thermal-hydrologic models was fitted to the predicted water retention data for the LTBM-2 material in workbook *Van Genuchten Properties.xls* in Output DTN: MO0703PAHYTHRM.000. Details of this workbook are provided in Table X-3[a]. The resulting van Genuchten parameters for the LTBM-2 crushed tuff are listed in Table X-4[a].

X.2[a] Porosity and Residual Saturation for the Intergranular Porosity

The physical properties from *Estimation of Mechanical Properties of Crushed Tuff for Use as Ballast Material in Emplacement Drifts* (SNL 2007 [DIRS 179354]; see BSC 2004 [DIRS 168138], Table 5) apply to the total porosity of the crushed tuff invert. The multiscale model uses dual continuum properties for the invert, requiring estimates for unsaturated properties of the intergranular porosity between the crushed tuff particles. Properties for the intragranular porosity are obtained from values for the undisturbed host-rock matrix (Section 4.1[a]) from which the invert ballast material will be prepared.

The following discussion presents the relationships between the single- and dual-continuum properties. The porosity relationships are defined, then values for the intergranular porosity and residual moisture content are selected using measured data for crushed tuff from the Tptpmn (nonlithophysal) unit. Although the invert ballast may be constructed using crushed lithophysal tuff (e.g., from the Tptpll unit), the intergranular properties are dominated by the effects of crushing and size gradation, so matrix properties from the Tptpmn units are used in part of the analysis. The invert ballast is an engineered material, with controlled grading and compaction characteristics.

The total porosity (ϕ_T) is defined as the total pore volume (V_p) divided by the total or bulk volume (V_b):

$$\phi_T = \frac{V_p}{V_b}. \quad (\text{Eq. X-6[a]})$$

The intergranular porosity (ϕ_I) is defined as the intergranular pore volume (V_I) divided by the bulk volume (V_b):

$$\phi_I = \frac{V_I}{V_b}. \quad (\text{Eq. X-7[a]})$$

The intrinsic or intragranular porosity is defined on the basis of core properties for the tuff matrix and it equals the volume of intragranular pore water (V_{mp}) divided by the volume of particles (V_{mb}):

$$\phi_m = \frac{V_{mp}}{V_{mb}}. \quad (\text{Eq. X-8[a]})$$

Noting that the total pore volume (V_p) equals the sum of the intergranular and intragranular volumes and that the bulk volume equals the sum of the intergranular pore space and the particle volume:

$$V_p = V_I + V_{mp}, \quad (\text{Eq. X-9[a]})$$

$$V_b = V_I + V_{mb}. \quad (\text{Eq. X-10[a]})$$

Dividing Equation X-9[a] by the bulk volume (V_b), and using the definitions in Equations X-7[a] and X-8[a] yields:

$$\phi_T = \phi_I + \frac{V_{mp}}{V_{mb}} \frac{V_{mb}}{V_b}. \quad (\text{Eq. X-11[a]})$$

Solving Equation X-10[a] for V_{mb} and using the definitions presented in Equations X-7[a] and X-8[a] results in:

$$\phi_T = \phi_I + \phi_m(1 - \phi_I). \quad (\text{Eq. X-12[a]})$$

The total water content (θ_T) is defined to be the total water volume (V_w) divided by the bulk volume:

$$\theta_T = \frac{V_w}{V_b}. \quad (\text{Eq. X-13[a]})$$

The intergranular water content is defined to be the water volume in the intergranular pore space (V_{Iw}) divided by the bulk volume (V_b):

$$\theta_I = \frac{V_{Iw}}{V_b}. \quad (\text{Eq. X-14[a]})$$

The intrinsic intragranular water content is defined to be the water volume in the intragranular pore space (V_{mw}) divided by the bulk volume of the matrix:

$$\theta_m = \frac{V_{mw}}{V_{mb}}. \quad (\text{Eq. X-15[a]})$$

The total water saturation is defined to be the total water volume divided by the total pore volume:

$$S_T = \frac{V_w}{V_p} = \frac{\theta_T}{\phi_T}. \quad (\text{Eq. X-16[a]})$$

The intergranular water saturation is defined to be the intergranular water volume divided by the intergranular volume:

$$S_I = \frac{V_{Iw}}{V_I} = \frac{\theta_I}{\phi_I}. \quad (\text{Eq. X-17[a]})$$

The intragranular water saturation is defined to be the matrix water volume divided by the matrix pore volume:

$$S_m = \frac{V_{mw}}{V_{mp}} = \frac{\theta_m}{\phi_m}. \quad (\text{Eq. X-18[a]})$$

Noting that the sum of the water volumes in the intergranular and intragranular pore space equals the total water volume:

$$V_w = V_{Iw} + V_{mw}. \quad (\text{Eq. X-19[a]})$$

Dividing Equation X-19[a] by the bulk volume (V_b) and using the definitions for water contents presented in Equations X-13[a] and X-14[a]:

$$\theta_T = \theta_I + \frac{V_{mw}}{V_{mb}} \frac{V_{mb}}{V_b}. \quad (\text{Eq. X-20[a]})$$

Solving Equation X-20[a] for the matrix volume and using the definitions in Equations X-7[a] and X-15[a] yields:

$$\theta_T = \theta_I + \theta_m(1 - \phi_I). \quad (\text{Eq. X-21[a]})$$

Note that this equation agrees with Equation X-12[a] when the pore space is fully saturated with water ($\theta_m = \phi_m$ and $\theta_I = \phi_I$). This equation is also in agreement with Equation 6.5.3.3-11 of *EBS Radionuclide Transport Abstraction* (SNL 2007 [DIRS 177407]).

Using the definitions for the intergranular and intragranular saturations in terms of the intergranular and intragranular water contents:

$$\theta_T = S_I \phi_I + S_m \phi_m (1 - \phi_I), \quad (\text{Eq. X-22[a]})$$

and dividing this equation by Equation X-12[a] results in:

$$\frac{\theta_T}{\phi_T} = \frac{S_I \phi_I + S_m \phi_m (1 - \phi_I)}{\phi_I + \phi_m (1 - \phi_I)}. \quad (\text{Eq. X-23[a]})$$

For the LTBM-2 crushed tuff material, the total porosity (ϕ_T) is 0.31 (SNL 2007 [DIRS 179354]; see BSC 2004 [DIRS 168138], Table 5). The intragranular porosity (ϕ_m) for the matrix of the Tsw34 (Tptpmn) is 0.111 (Table 4-1[a]). Upon applying Equation X-21[a], the intergranular porosity for the crushed tuff invert is:

$$\phi_I = \frac{\phi_T - \phi_m}{1 - \phi_m} = \frac{0.31 - 0.111}{1 - 0.111} = 0.224. \quad (\text{Eq. X-24[a]})$$

Two approaches for estimating the van Genuchten residual saturation parameter value for the intergranular porosity are presented below. The residual saturation is a fitting parameter that is related to (but not necessarily equal to) the lower bound of liquid saturation in certain applications such as agricultural soils. Use of the van Genuchten equations does not mean that saturation cannot be driven to zero, for example by heating. The first option for the intergranular porosity is to adopt the residual saturation value of 1% that is used for the fractures of the host rock (Sections 4.1[a] and 5.3.1.11[a]). The invert ballast shares certain characteristics (such as particle size grading) with soils and other porous media, suggesting a similar approach for parameter estimation. However, the host-rock fracture continuum includes many fine fractures with strong water retention that are analogous to the contacts between larger particles present in the ballast.

A second option is to use limited available laboratory data on the water retention behavior of crushed-tuff aggregates, to independently derive a residual saturation value. The available data consist of water content measurements in samples of crushed tuff sorted in various size fractions up to 4 mm, and subjected to ultra-centrifugation (DTN: GS980808312242.015 [DIRS 119916]). The centrifuge apparatus included a low-flow pump that provided fluid to the sample through a rotating seal assembly. Residual water was determined by wetting the sample, then allowing it to drain to quasi-equilibrium in the centrifuge, and measuring the water content gravimetrically. For water potential down to -20 bar, the residual volumetric water content was approximately 5%, and variation about this value was minor (on the order of 50% or less of the measured residual) for the size fractions tested.

Adopting a value of 5% for the LTBM-2 material, the intergranular component is estimated by subtracting off the intragranular residual water content using tabulated properties for the Tptpmn rock matrix. The Tptpmn residual water saturation (Table 4-1[a]) is 0.19. Accordingly, the residual water content for the intergranular porosity (θ_{Ir}) of the LTBM-2 material is estimated using Equation X-21[a]:

$$\begin{aligned} \theta_{Ir} &= S_{Ir} \cdot \phi_I = \theta_{Tr} - S_{mr} \cdot \phi_m \cdot (1 - \phi_I) \\ &= 0.05 - 0.19 \cdot 0.111 \cdot (1 - 0.224) = 0.0336. \end{aligned} \quad (\text{Eq. X-25[a]})$$

The residual saturation (S_{Ir}) is determined by applying Equation X-17[a]:

$$S_{Ir} = \frac{\theta_{Ir}}{\phi_I} = \frac{0.0336}{0.224} = 0.150. \quad (\text{Eq. X-26[a]})$$

Ranges of values for the intergranular porosity, the intergranular residual water content, and intergranular residual water saturation for the LTBM-2 minimum and maximum gradations are presented in Table X-1[a].

Table X-1[a]. Intergranular Porosity, Intergranular Residual Water Content, and Intergranular Residual Water Saturation for the LTBM-2 Crushed Tuff

Case	Intergranular Porosity ^a	Intergranular Residual Water Content ^b	Intergranular Residual Water Saturation ^c	Total Porosity for the Tptpll Unit ^d
LTBM-2 minimum	0.179	0.0327	0.183	0.286
LTBM-2 maximum	0.314	0.0355	0.113	0.404
LTBM-2 average	0.224	0.0336	0.150	0.326

Source: Output DTN: MO0703PAHYTHRM.000, file: *Porosity Calculations 13Jul07.xmcd*.

^a The intergranular porosity is calculated from Equation X-12[a] using total porosities (ϕ_t) for the three cases from Table 4-1[a] with matrix porosity of 0.111 (Tptpmn unit), and solving for the intergranular porosity (ϕ_i).

^b The intergranular residual moisture content (θ_r) is determined from Equation X-25[a] for the three cases.

^c The intergranular residual saturation ($S_{r,i}$) is determined from Equation X-26[a] for the three cases.

^d The total porosity for the Tptpll unit is determined through application of Equation X-12[a] with a matrix porosity of 0.131 (Table 4-1[a]).

Sensitivity studies were conducted using the LDTH submodel to evaluate the sensitivity of multiscale thermal-hydrologic predictions to the value of intergranular residual saturation for the invert ballast (Section 6.3.14[a]). The results show no significant difference between the two options described above (1% or 15%) in terms of the extremes of invert saturation, or the timing of rewetting behavior. Considering these options, the laboratory-based approach yields a residual saturation that is probably too high, because the laboratory tests were limited in range of moisture potential to -20 bar, and because the crushed-tuff aggregate materials tested were too fine. Accordingly, the 1% value for intergranular residual liquid water saturation is used in the multiscale calculations for TSPA.

Note that the preceding calculations, based on measured and tabulated properties for the tsw34 rock unit (Tptpmn, nonlithophysal), produce estimates that are applicable to invert ballast containing crushed tuff prepared from the tsw35 unit (Tptpll, lithophysal). Table X-1[a] includes a calculation of the total porosity for the Tptpll unit. The matrix porosity for this unit is slightly greater (0.131; see Table 4-1[a]) than the matrix porosity from the Tptpmn unit (Table 4-1[a]) and results in a total porosity of 0.326. When substituted into Equations X-24[a] and X-25[a], this information yields intergranular property values very similar to those shown in Table X-1[a]. Brief descriptions of the calculations in Output DTN: MO0703PAHYTHRM.000 are provided in Table X-2[a] and X-3[a] with results presented in Table X-4[a].

Table X-2[a]. Description of the Spreadsheets in Workbook *arya_original data interpretation 4 17Jul07.xls*, Located in Output DTN: MO0703PAHYTHRM.000

Worksheet Name	Brief Description
LTBM-2, Average, revised	Calculation of the water retention characteristics for the LTBM-2 material with average property values
LTBM-2, Minimum, revised	Calculation of the water retention characteristics for the LTBM-2 material with minimum property values
LTBM-2, Maximum, revised	Calculation of the water retention characteristics for the LTBM-2 material with maximum property values

Table X-3[a]. Description of the Spreadsheets in Workbook *Van Genuchten Properties 17Jul07.xls*

Worksheet Name	Brief Description
Summary van Genuchten	Summary of the van Genuchten parameters for the average, minimum, and maximum LTBM-2 cases
LTBM-2, Average, Revised	Calculation of the van Genuchten parameters for the LTBM-2 material with average property values
LTBM-2, Minimum, Revised	Calculation of the van Genuchten parameters for the LTBM-2 material with minimum property values
LTBM-2, Maximum, Revised	Calculation of the van Genuchten parameters for the LTBM-2 material with maximum property values

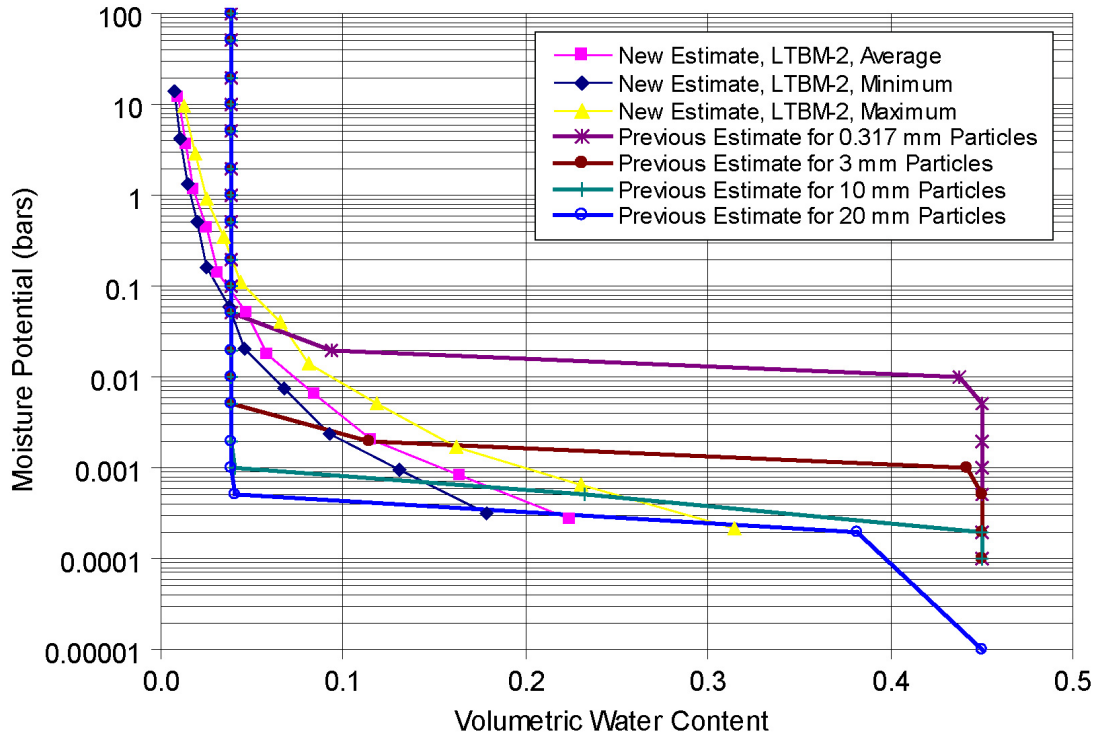
Source: Output DTN: MO0703PAHYTHRM.000, workbook: *Van Genuchten Properties 17Jul07.xls*.

Table X-4[a]. Best-Fit van Genuchten Parameters for the LTBM-2 Material

van Genuchten Parameters	LTBM-2 Average	LTBM-2 Minimum	LTBM-2 Maximum
α (1/bar)	1,780.59	1,764.52	2,565.25
n	1.39	1.38	1.37
m	0.283	0.273	0.273

Source: Output DTN: MO0703PAHYTHRM.000, workbook: *Van Genuchten Properties 17Jul07s.xls*.

The van Genuchten parameters calculated in Output DTN: MO0703PAHYTHRM.000 (file: *Van Genuchten Properties 17Jul07.xls*) are estimated using a least-squares fit between observed and predicted volumetric moisture content as a function of moisture potential using Excel's equation solver. Results yield van Genuchten parameters as listed in Table X-4[a] and the fit for the LTBM-2 average, minimum, and maximum are shown in Figure X-1[a].



Source: Figures X-3 through X-6 of the parent report.

Output DTN: MO0703PAHYTHRM.000, workbooks: *arya_original data interpretation 4 17Jul07.xls* and *Van Genuchten Properties 17Jul07.xls*.

NOTE: The different grain sizes are specifically discussed in Section 6.3.11 of the parent report as shown in Figure 6.3-65 of the parent report.

Figure X-1[a]. Comparison of the Developed Water Retention Relationship for the Invert Ballast Materials and the Relationship Provided to the MSTHM

X.3[a] Thermal Conductivity

The effective thermal conductivity of a granular medium increases as the size of the particle increases due to radiant heat transfer effects. The combined effects from thermal conduction and radiation on the effective thermal conductivity of a granular medium are included in work published by Kunii and Smith (1960 [DIRS 153166]). That approach is used here to estimate the conduction effect, and to evaluate whether thermal radiation will contribute significantly to heat transfer in the invert ballast. Although heat transfer in the invert has been demonstrated to be of limited importance to repository thermal-hydrology (see parent report) the radiative effect increases with temperature and has not been previously evaluated for the selected invert ballast material.

The parent report (Section XI.2[a]) documents the technical approach to calculating the effective thermal conductivity of the crushed tuff in the invert. The material to be used as invert ballast (LTBM-2) is crushed tuff with a maximum particle size of 50 mm with 50% passing 10 mm, as described in *Estimation of Mechanical Properties of Crushed Tuff for Use as Ballast Material in Emplacement Drifts* (SNL 2007 [DIRS 179354]; see BSC 2004 [DIRS 168138], Figure 2). Particle properties (wet/dry thermal conductivity values) are those of the rock matrix of the

Tptpll (lower lithophysal) host-rock unit, an appropriate approximation because this unit comprises most of the repository horizon. These values are then substituted into the effective thermal conductivity relationship presented by Kunii and Smith (1960 [DIRS 153166], Equation 8).

The total porosity (intragranular plus intergranular) of the compacted invert material will be in the range of 27% to 39%, with an average of 31% (SNL 2007 [DIRS 179354]; see BSC 2004 [DIRS 168138], Table 5). The Tptpmn matrix (intragranular) porosity is approximately 11% (Table IV-3b[a]), so the intergranular porosity of the compacted invert ballast will be approximately 20%. Table X-5[a] shows effective thermal conductivity values calculated by the method of Kunii and Smith (1960 [DIRS 153166]) for a well-sorted medium consisting of single-size (spherical) particles ranging in diameter from 1 to 100 mm, with particle thermal conductivity from the Tptpll unit, temperatures of 35°C and 50°C, and intergranular porosity (ϕ) values of 0.18, 0.22, and 0.31.

The characteristic void-to-void dimension of a single-particle-size packed bed is approximated based on spherical particle diameter (D_p) as $D_p/\sqrt{3}$ (Yagi and Kunii 1957 [DIRS 170330], p. 379). For particles 10 to 50 mm in diameter, this length is estimated to be 5.77 to 28.87 mm. The characteristic radius in the void space is approximately $0.077D_p$, so for the same particle diameters, this radius is 0.77 to 3.85 mm, or 1.54 to 7.70 mm in diameter. Recognizing that the specified particle-size distribution for the LTBM-2 invert material (SNL 2007 [DIRS 179354]; see BSC 2004 [DIRS 168138], Table 5) shows approximately 25% passing 2 mm (close to 1.6 mm) and 45% passing 8 mm (close to 7.6 mm), these particles will “fit” in between the larger 10- to 50-mm diameter particles. Therefore, the invert ballast material can be described as 2- to 8-mm diameter particles with respect to the characteristic void lengths.

Comparing these particle diameters (2 to 8 mm, averaging approximately 5 mm) to those in Table X-5[a] shows that thermal radiation effects range from small (at the 10-mm diameter size) to negligible (at 1- to 5-mm diameters). For invert ballast material with total porosity of 0.31, the estimated thermal conductivity (for 5-mm particles) is 0.21 W/m-K (for particle thermal conductivity of 2.0707 W/m-K). The uncertainty associated with these predicted effective thermal conductivities is 30%, as described in the parent report (Appendix XI).

The bulk thermal conductivity estimate for the well-graded LTBM-2 invert ballast material is similar to the values used in the parent report, Table IV-9). The 11 test data (from DTN: GS000483351030.003 [DIRS 152932]) listed in Table IV-9 of the parent report average to 0.16 W/m-K with a minimum of 0.14 W/m-K and a maximum of 0.17 W/m-K.

Table X-5[a]. Thermal Conductivity (W/m-K) for a Single-Sized Particle Medium as a Function of Particle Size, Porosity, and Temperature

Particle size (mm)	Temperature = 35°C			Temperature = 50°C		
	$\phi_l = 0.18$	$\phi_l = 0.22$	$\phi_l = 0.31$	$\phi_l = 0.18$	$\phi_l = 0.22$	$\phi_l = 0.31$
1	0.22	0.21	0.19	0.22	0.22	0.19
2	0.22	0.21	0.19	0.23	0.22	0.20
5	0.24	0.23	0.21	0.25	0.24	0.22
10	0.26	0.25	0.24	0.28	0.27	0.25
20	0.31	0.30	0.29	0.33	0.33	0.31
50	0.45	0.45	0.44	0.49	0.49	0.48
100	0.67	0.67	0.67	0.73	0.73	0.74

Source: Output DTN: MO0703PAHYTHRM.000, file: *thermalk_vc.xls*.

NOTE: Calculations based upon the technical approach of Kunii and Smith (1960 [DIRS 153166]) as presented in the parent report (Appendix XI).

X.4[a] Unsaturated Hydraulic Conductivity for the Crushed Tuff Invert

The following discussion presents the methodology for determining the relationship between unsaturated hydraulic conductivity (K_{us}) and capillary pressure from the retention curve using the two-parameter non-dimensional van Genuchten relationship for the crushed tuff. The well-known Kozeny-Carmen equation relates the intrinsic permeability to porosity (de Marsily 1986 [DIRS 100439], p. 62). The Excel workbook *Kozeny Rev0 13Jul071.xls* in Output DTN: MO0703PAHYTHRM.000 calculates the intrinsic permeability of the intergranular pore space of the invert and yields a value of $4.19 \times 10^{-12} \text{ m}^2$.

The relative permeability relationship is given by Fetter (1993 [DIRS 102009], p. 182, Equation 4.17) based the van Genuchten parameters and the conversion to hydraulic conductivity:

$$K_{ul} = \frac{\rho_w g}{\mu_w} k_{sl} \cdot \frac{\{1 - (\alpha_l \psi)^{n_l - 1} [1 + (\alpha_l \psi)^{n_l}]^{-m_l}\}^2}{[1 + (\alpha_l \psi)^{n_l}]^{\frac{m_l}{2}}} \quad (\text{Eq. X-27[a]})$$

where K_{ul} is the unsaturated hydraulic conductivity of water in the intragranular/intergranular pore space, ρ_w is the fluid density of water, μ_w is the absolute viscosity of water, g is acceleration due to gravity, α_l is the van Genuchten parameter for the intragranular/intergranular pore space, n_l is the van Genuchten parameter for the intragranular/intergranular pore space, m_l is the van Genuchten parameter for the intragranular/intergranular pore space, k_{sl} is the intrinsic permeability for the intragranular/intergranular pore space of the invert, and ψ is the moisture potential.

The calculations are summarized in Table X-6[a] over a range of moisture potentials.

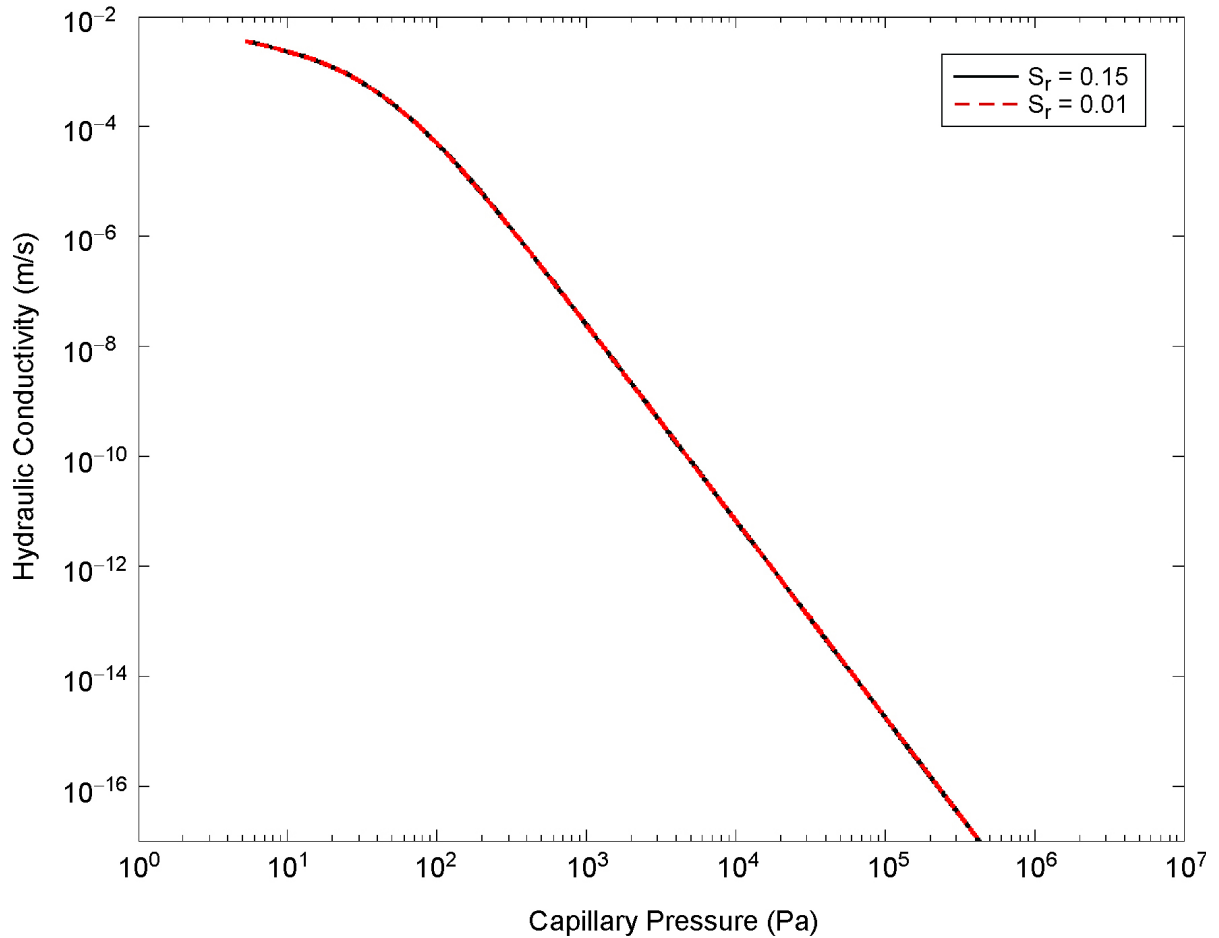
Table X-6[a]. Unsaturated Hydraulic Conductivity as a Function of Moisture Potential

Moisture Potential (ψ) (bars)	Hydraulic Conductivity (cm/sec)	
	Intragranular Pore Space	Intergranular Pore Space
1×10^{-5}	1.85×10^{-8}	4.71×10^{-3}
2×10^{-5}	1.82×10^{-8}	3.98×10^{-3}
5×10^{-5}	1.78×10^{-8}	2.83×10^{-3}
1×10^{-4}	1.75×10^{-8}	1.88×10^{-3}
2×10^{-4}	1.70×10^{-8}	1.00×10^{-3}
5×10^{-4}	1.63×10^{-8}	2.65×10^{-4}
1×10^{-3}	1.56×10^{-8}	6.20×10^{-5}
2×10^{-3}	1.48×10^{-8}	1.07×10^{-5}
5×10^{-3}	1.35×10^{-8}	8.14×10^{-7}
1×10^{-2}	1.24×10^{-8}	1.07×10^{-7}
2×10^{-2}	1.10×10^{-8}	1.37×10^{-8}
5×10^{-2}	9.00×10^{-9}	8.97×10^{-10}
1×10^{-1}	7.28×10^{-8}	1.14×10^{-10}
2×10^{-1}	5.47×10^{-9}	1.43×10^{-11}
5×10^{-1}	3.13×10^{-9}	9.31×10^{-13}
1	1.66×10^{-9}	1.18×10^{-13}
2	6.74×10^{-10}	1.48×10^{-14}
5	1.27×10^{-10}	9.63×10^{-16}
10	2.63×10^{-11}	1.22×10^{-16}
20	4.43×10^{-12}	1.54×10^{-17}

Source: Output DTN: MO0703PAHYTHRM.000, folder: /Residual Saturation of_.15, MathCad file: *Unsaturated Hydraulic Conductivity Rev03 13Jul07.xmcd*.

NOTE: The intergranular hydraulic conductivity values are based on 15% residual saturation. Difference from values calculated at 1% residual saturation (from MathCad file *Unsaturated Hydraulic Conductivity Rev03 17Jul07.xmcd*) is insignificant (less than 0.3%).

Capillary pressure in the invert is controlled by that of the surrounding host rock. The relationship between hydraulic conductivity and capillary pressure in the intergranular porosity, which is calculated using Equation X-27[a], is unaffected by the choice of residual liquid-phase saturation, as shown in Figure X-2[a]. This explains the lack of sensitivity to residual liquid-phase saturation as discussed in Section 6.3.14[a] and shown in Figure 6.3-72[a].



Source: Derived from Output DTN: LL0705PA032MST.028.

NOTE: The plots are generated by applying Equation X-27[a] and the invert hydrologic parameters obtained from file *dkm-afc-EBS-P30-06* for the $S_r = 0.01$ case from Output DTN: LL0702PA014MST.069, and file *dkm-afc-EBS-P30-06-07* for the $S_r = 0.15$ case from Output DTN: LL0705PA032MST.028. The values for the fluid density of water, ρ_w , and the absolute viscosity of water, μ_w , correspond to a temperature of 20°C.

Figure X-2[a]. Hydraulic Conductivity as a Function of Capillary Pressure for Residual Saturations of 0.15 (black curve) and 0.01 (dashed red curve) When Water Density is 987.88 kg/m^3 and Dynamic Viscosity is $5.46 \times 10^{-4} \text{ kg/m}\cdot\text{s}$

INTENTIONALLY LEFT BLANK

APPENDIX XI[a]

THERMAL CONDUCTIVITY OF THE COLLAPSED DRIFT ZONE

XI.1[a] Thermal Conductivity of Drift-Collapse Rubble

Drift collapse rubble is described in *Drift Degradation Analysis* (BSC 2004 [DIRS 166107], Section 6.4.2.5.1):

As the lithophysal rock mass fails, pre-existing and new fractures will break, forming block sizes of relatively small volume (estimated to be on the order of cm on a side). The falling rock blocks will come to rest on the invert of the tunnel and the drip shield. Because the fallen blocks do not perfectly fit together as they did in the in situ rock mass, there will be an overall increase in volume (termed “bulking”). Eventually, if the failure process continues, the tunnel will completely fill with bulked rock and will choke off further failure because the back pressure provided by the rubble will stabilize further yield.

In addition, *Drift Degradation Analysis* (BSC 2004 [DIRS 166107], Section 5.2.2) justifies an assumption that block size in lithophysal drift-collapse rubble is controlled by inter-lithophysal fracture density and lithophysal cavity spacing. Part of the justification is the observation of block sizes on the order of “a few inches in diameter” in the Enhanced Characterization of the Repository Block cross-drift.

Drift collapse with accumulation of rubble in amounts sufficient to affect heat transfer from waste packages is predicted to occur predominantly in the lithophysal tuff. In the nonlithophysal units, postclosure seismic events may produce “localized areas of rock failure sufficient to cover the drip shield” (BSC 2004 [DIRS 166107], p. ix), but drift collapse in the nonlithophysal units is not considered further here. This is justified because the extent of nonlithophysal rubble around the drip shield would not approach that predicted for collapse in lithophysal tuff. Also, the consequences from small incidence of collapse in nonlithophysal tuff are already encompassed by the full-collapse behavior modeled for lithophysal tuff (BSC 2004 [DIRS 166107], Section 6.3). Accordingly, the thermal conductivity (K_{th}) of rubble derived from nonlithophysal tuff is not considered further here.

Distinct-element simulations of drift collapse (BSC 2004 [DIRS 166107], Section 6.4.2.4.3.2) show that the diameter of the collapse is typically twice that of the original opening. The characteristics of drift-collapse rubble include inter-particle porosity on the order of 30%, which is consistent with a bulking factor of approximately 20%. The bulking factor is the ratio of original opening cross-sectional area (subtracting the area of the drip shield/waste package and of the invert) to the area of rock that collapses. The size of rubble particles is on the order of 10 cm, based on lithophysal cavity spacing (BSC 2004 [DIRS 166107], Section 6.1.4.1) and the potential for breakage on fractures between cavities. The thermal conductivity of the uncollapsed lithophysal (T_{tpll}) rock mass ranges from 1.071 (dry, 10th percentile) to 2.055 W/m·K (wet, 90th percentile) (see Table XI-1[a]).

Drift collapse rubble will have less thermal conductivity (in the sense of Fourier heat conduction) than the intact rock mass from which it forms; however, it can transfer heat as thermal radiation across open cavities, and therefore can have a greater effective thermal conductivity. Even with radiative heat transfer, the rubble will present more thermal resistance than the air space that it fills. This means that the temperatures of the drip shield, waste package, and waste form will increase after drift collapse (if radioactive waste heat is produced). The temperatures may

increase enough, and the voids in the rubble may be large enough, that thermal radiation becomes an important mode of heat transfer, relative to conduction alone. The effect from thermal radiation is an important uncertainty for the effective thermal conductivity of rubble (as defined for use in the MSTHM). To represent this uncertainty, the chosen modeling approach should span the range from conduction-dominated heat transfer to strongly radiative heat-transfer. This range could even be realized in a stratified rubble accumulation, with finer particles (and smaller voids) in the lower strata.

The effective thermal conductivity estimated here describes heat transfer by the processes of conduction and radiation. It does not include natural or forced convection, nor other effects associated with mass transfer. This is appropriate because the effective K_{th} parameter is intended for use in thermal-hydrologic models that explicitly represent convection, evaporation, and condensation (natural convection can be approximated where it is known to be important). In general, the K_{th} for drift-collapse rubble is uncertain because of particle size and distribution, the potential for variability in accumulated rubble, and because of uncertainty with respect to processes controlling heat transfer across voids and at elevated temperature.

XI.2[a] Published Literature on Heat Transfer in Granular Solids

There are many published accounts of experimental and theoretical work on thermal conductivity of granular materials, such as those used in packed beds. Such published sources are evaluated here for use in estimating the effective thermal conductivity of drift-collapse rubble. A review of the prediction of the thermal conductivity of granular materials was conducted by Crane et al. (1977 [DIRS 113426]). These authors investigated numerous models of the effective thermal conductivity of granular media, but radiant heat transfer is rarely, if ever, included in these models. It is useful to note from this paper that model–data comparisons typically agree to no better than $\pm 20\%$, even where radiation is not a factor, and sometimes the prediction error is much greater.

The most applicable model identified from published literature is that of Kunii and Smith (1960 [DIRS 153166]) and Yagi and Kunii (1957 [DIRS 170330]). The approach is applicable to drift-collapse rubble because it pertains to unconsolidated particles in loose packings, and includes thermal radiation as well as conduction. It thus includes the processes of interest, and is justified in the cited publications by comparison to experimental data. Yagi and Kunii (1957 [DIRS 170330]) cite experimental data for uniform particles with diameter up to approximately 11 mm, which is substantially less than the expected rubble particle size.

Green et al. (1999 [DIRS 169628]) measured the effective thermal conductivity of samples of Apache Leap Tuff that were broken to resemble rubble. Particle diameter ranged from 1.6 to 4.0 cm, with inter-particle porosity of 42%. They concluded that the effective thermal conductivity of the dry material was 0.26 W/m·K for thermal gradients up to approximately 600°C/m, and that of wet material containing water in the matrix pores was 0.49 W/m·K. They further concluded that thermal radiation is important only for thermal gradients greater than 500°C/m, and that the contributions of radiation and convection to the overall heat flux in unsaturated crushed tuff are secondary to conduction even at high thermal gradients. The measured values from Green et al. (1999 [DIRS 169628]) are used below to test the validity of the Kunii and Smith (1960 [DIRS 153166]) predictive model.

The general equation to predict the effective thermal conductivity for a granular particle layer, from Kunii and Smith (1960 [DIRS 153166], Equation 8), is:

$$\frac{k_e^o}{k_s} = \varepsilon \left[1 + \beta \frac{h_{rv} D_p}{k_g} \right] + \frac{\beta(1-\varepsilon)}{\frac{1}{\phi + \frac{D_p h_{rs}}{k_g}} + \gamma \left(\frac{k_g}{k_s} \right)}, \quad (\text{Eq. XI-1[a]})$$

where this equation applies to beds of unconsolidated particles. The parameter ϕ corresponds to the packing of spheres (choose loose packing for rubble). This parameter is illustrated in Figure 5 of Kunii and Smith (1960 [DIRS 153166]), but is calculated in the implementation of Equation XI-1[a] (rather than estimating graphically) in Output DTN: MO0703PARUBBLE.000

The effective thermal conductivity for the tuff material described by Green et al. (1997 [DIRS 169628]) is then evaluated using Equation XI-1[a]. The material was produced from Apache Leap Tuff, crushed and sorted to a size range of 1.6 to 4.0 cm. Particle size was 2.5 cm in the prediction, representing an average value skewed slightly toward smaller particles which fit between larger ones. The “loose” packing was chosen for parameter ϕ in the Kunii and Smith model in Output DTN: MO0703PARUBBLE.000. Predictions were made over the temperature range 25 to 90°C, for dry particles with thermal conductivity of 1.744 W/m·K, void fraction of 42%, and emissivity of 0.9 (values reported in Green et al. 1997 [DIRS 169628]). The prediction ranged from 0.27 to 0.37 W/m·K versus the measured value of 0.26 W/m·K (Output DTN: MO0703PARUBBLE.000, file: *thermalk_vc_rubble_MSTHM.xls*). For wet particles with thermal conductivity of 1.909 W/m·K the predicted range was 0.27 to 0.38 W/m·K, versus the measured value of 0.49 W/m·K.

Green et al. (1999 [DIRS 169628], p. 719) indicated that a guarded-heat flow meter was used with the heat source at the bottom and the heat sink at the top. This arrangement can induce convective heat and mass transfers that bias the results to higher values, especially with moisture (see Moyne et al. 1988 [DIRS 154107]; Degiovanni and Moyne 1987 [DIRS 154172]; and Azizi et al. 1988 [DIRS 154108]). This was likely a factor, because spatial variations in the state of wetting for individual samples were observed during the experiments (Green et al. 1999 [DIRS 169628], p. 723).

XI.3[a] Predicted Thermal Conductivity of Drift-Collapse Rubble

Ranges of uncertain thermal conductivity for dry and wet drift-collapse material are estimated using the Kunii and Smith (1960 [DIRS 153166]) model. For calculating peak temperature of the engineered barriers after drift collapse, dry conditions pertain because simulations have shown that the tuff readily dries out at temperatures greater than 96°C (see SNL 2007 [DIRS 177412], Figure 6.3-16). Particle size is the most sensitive independent variable of the model. It controls void size and thus the temperature difference across voids, and the effectiveness of radiative coupling. As a parameter of the model, particle size is varied over a range from 1 to 10 cm, as shown in Table XI-1[a]. The smaller value (1 cm) is an appropriate end-member because it involves little radiative coupling (verified by exercising the model). The larger value (10 cm) produces significant radiative coupling and is a reasonable typical

controlling dimension for voids between irregularly shaped, nominally 20-cm diameter particles (the Kunii and Smith model was developed for spheres). To generate a range of uncertain, temperature-dependent effective thermal conductivity for use in the MSTHM, the Kunii and Smith (1960 DIRS 153166)] model was exercised for the parameter combinations indicated in Table XI-1[a]. The results are plotted in Figures XI-1[a] and XI-2[a], for dry and wet particles, respectively. Although wet particles cannot occur at temperatures greater than approximately 96°C as discussed above, the NUFT code interpolates between dry and wet values, and requires the wet value in order to calculate dry values at all temperatures. The resulting selected ranges for use in TSPA are:

Lower Estimates: 1-cm particles; 30% void fraction; 10th percentile dry K_{th} ;
10th percentile wet K_{th}

Upper Estimates: 10-cm particles; 40% void fraction; 90th percentile dry K_{th} ;
90th percentile wet K_{th} .

Table XI-1[a]. Parameter Ranges for Calculation of Effective K_{th} for the MSTHM

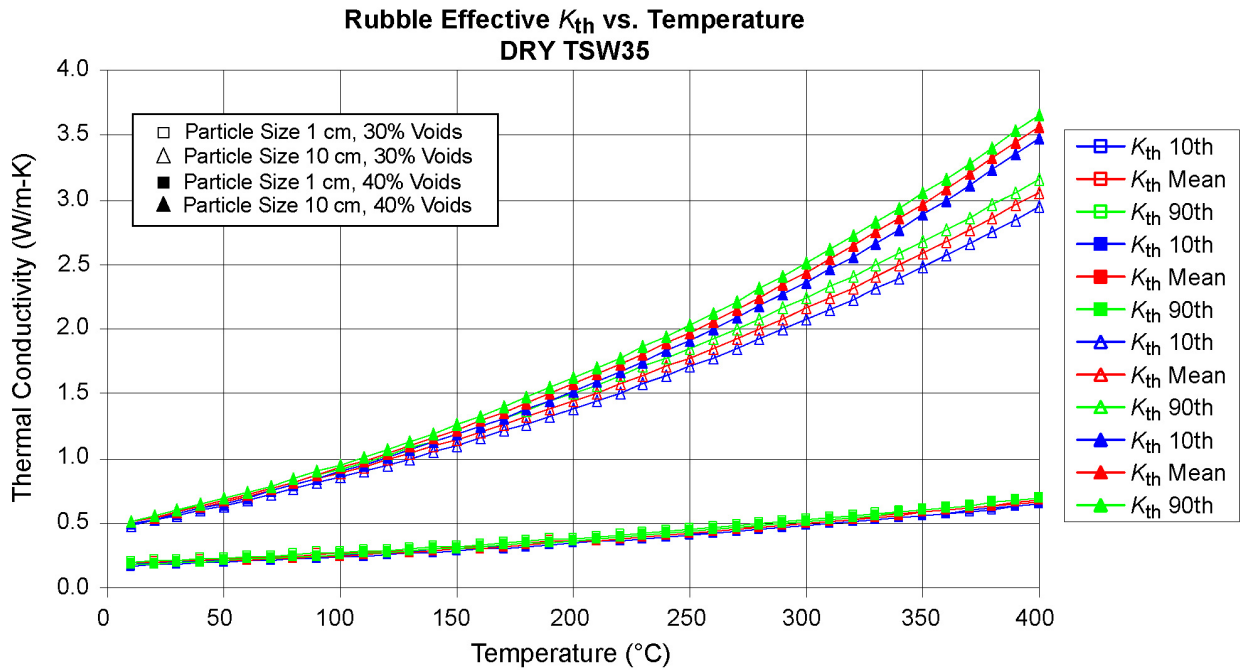
Particle Size (cm)	Host Rock Unit: Lower Lithophysal (tsw35)	
	Intact Rock Mass K_{th} Dry / Wet Values (W/m·K) ^a	Void Fraction
1	10th percentile: 1.071 / 1.690^b	0.3
		0.4
	Mean: 1.240 / 1.870	0.3
		0.4
	90th percentile: 1.414 / 2.055	0.3
10		0.4
	10th percentile: 1.071 / 1.690	0.3
		0.4
	Mean: 1.240 / 1.870	0.3
		0.4
	90th percentile: 1.414 / 2.055^b	0.3
		0.4
Other, fixed parameters:		
Emissivity	0.92	
Stephan-Boltzmann Constant	$5.67 \times 10^{-8} \text{ W/m}^2 \cdot \text{K}^4$	
Beta	1 (see Kunii and Smith 1960 [DIRS 153166], p. 72)	
Gamma	0.667 (see Kunii and Smith 1960 [DIRS 153166], p. 72)	

^a Thermal conductivity values from Output DTNs: MO0702PAGLOBAL.000 and MO0612MEANTHER.000.

^b Combinations selected as the lower and upper limits of the range of rubble K_{th} for TSPA-supporting calculations are shown in bold.

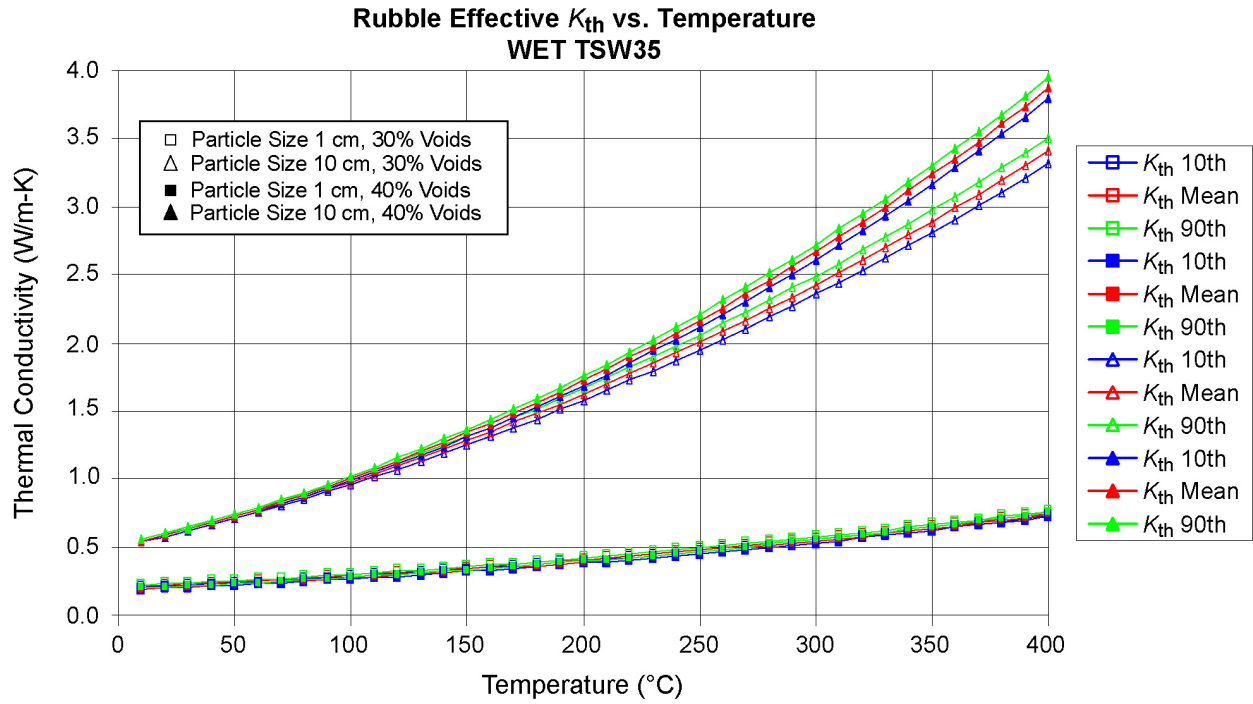
The results (Figures XI-1[a] and XI-2[a]) show strong temperature dependence; for small particles this is mainly because of the temperature dependence of K_{th} for air, while for larger particles this is caused by the nonlinear dependence of thermal radiation on absolute temperature. For the MSTHM, the needed (dry, wet) paired values were taken from the respective minimum of the dry values, and the maximum of the wet values, for results obtained with each particle size. Thus there is one set of temperature-dependent (dry, wet) functions for the 1-cm particle size, and another for the 10-cm particle size. These are intended to be weighted equally in

TSPA, representing uncertainty as to the uniformity and configuration of rubble in collapsed drifts, and the resulting effect on heat transfer from the drip shield/waste package.



Source: Output DTN: MO0703PARUBBLE.000, file: *thermalk_vc rubble_MSTHM.xls*, tab: "Results."

Figure XI-1[a]. Range of Effective K_{th} Calculated for Rubble with Dry Particles



Source: Output DTN: MO0703PARUBBLE.000, file: *thermalk_vc rubble_MSTHM.xls*, tab: "Results."

Figure XI-2[a]. Range of Effective K_{th} Calculated for Rubble with Wet Particles

APPENDIX XII[a]
COMPARISON OF PERCOLATION FLUXES

No change (not applicable to addendum).

INTENTIONALLY LEFT BLANK

APPENDIX XIII[a]

LIST OF DATA SOURCES FOR FIGURES AND TABLES

No change (not applicable to addendum).

INTENTIONALLY LEFT BLANK

APPENDIX XIV[a]
QUALIFICATION OF UNQUALIFIED PROJECT DATA

No change (not applicable to addendum).

INTENTIONALLY LEFT BLANK

APPENDIX XV[a]
PREDICTION OF RH IN THE INVERT

No change (not applicable to addendum).

INTENTIONALLY LEFT BLANK

APPENDIX XVI[a]
NUFT V4.0 EXECUTABLE INSTALL INFORMATION

XVI.1[a] NUFT v4.0 Install Information on LLNL Machine uP

The NUFT4.0 executables used on AIX5.3CSM1.5 operating system for SMT, DDT, and LDTH submodels, and MSTHM validation test and 3D-pillar model.

Note: nuft is NUFT4.0 serial executable
 nuft-par is NUFT4.0 parallel executable

directory listing:

```
total 39616
-r----- 1      1112 Sep 20 2006 README
-r----- 1         7 Sep 20 2006 Version
drwx----- 2      4096 Sep 20 2006 lsp
-r-x----- 1 6106262 Sep 20 2006 nuft
-r-x----- 1 7647974 Sep 20 2006 nuft-par
-r-x----- 1 6485254 Oct 06 2006 nuft-par0
drwx----- 2      4096 Sep 20 2006 pkg
./lsp:
total 304
-r----- 1      956 Sep 20 2006 biofil.lsp
-r----- 1      438 Sep 20 2006 connect.lsp
-r----- 1     3310 Sep 20 2006 init.lsp
-r----- 1     3412 Sep 20 2006 lin-elas.lsp
-r----- 1     8539 Sep 20 2006 macros.lsp
-r----- 1     3775 Sep 20 2006 num-proc.lsp
-r----- 1     3889 Sep 20 2006 prelude.lsp
-r----- 1    48806 Sep 20 2006 prep.lsp
-r----- 1     4471 Sep 20 2006 read-msh.lsp
-r----- 1      410 Sep 20 2006 trn-slot.lsp
-r----- 1    11986 Sep 20 2006 trn.lsp
-r----- 1     1896 Sep 20 2006 ucheader.lsp
-r----- 1     3358 Sep 20 2006 ucsat.lsp
-r----- 1     9790 Sep 20 2006 us.lsp
-r----- 1     3043 Sep 20 2006 us1c.lsp
-r----- 1     3301 Sep 20 2006 us1p.lsp
-r----- 1    13045 Sep 20 2006 usnt.lsp

./pkg:
total 56
-r----- 1     1888 Sep 20 2006 2p2ct.pkg
-r----- 1     1573 Sep 20 2006 rms.pkg
-r----- 1     2001 Sep 20 2006 rmsew.pkg
-r----- 1     1371 Sep 20 2006 thermcon.pkg
-r----- 1      220 Sep 20 2006 vt-rms.pkg
-r----- 1      415 Sep 20 2006 vt-rmsew.pkg
-r----- 1     3915 Sep 20 2006 vtough.pkg
```

The NUFT4.0 executables in the CD obtained from SCM

directory listing:

```
..
total 26952
-rw-r----- 1     1036 Jan  5 2007 README
```

```
-r--r----- 1      7 Jan  5 2007 Version
drwxr-xr-x   2    4096 Jan  5 2007 lsp
-r-xr--r--   1 6106262 Jan  5 2007 nuft
-r-xr--r--   1 7647974 Jan  5 2007 nuft-par
drwxr-xr-x   2    4096 Jan  5 2007 pkg
```

```
./lsp:
total 304
-r--r----- 1     956 Jan  5 2007 biofil.lsp
-r--r----- 1     438 Jan  5 2007 connect.lsp
-r--r----- 1    3310 Jan  5 2007 init.lsp
-r--r----- 1    3412 Jan  5 2007 lin-elas.lsp
-r--r----- 1    8539 Jan  5 2007 macros.lsp
-r--r----- 1    3775 Jan  5 2007 num-proc.lsp
-r--r----- 1    3889 Jan  5 2007 prelude.lsp
-r--r----- 1   48806 Jan  5 2007 prep.lsp
-r--r----- 1    4471 Jan  5 2007 read-msh.lsp
-r--r----- 1     410 Jan  5 2007 trn-slot.lsp
-r--r----- 1   11986 Jan  5 2007 trn.lsp
-r--r----- 1    1896 Jan  5 2007 ucheader.lsp
-r--r----- 1    3358 Jan  5 2007 ucsat.lsp
-r--r----- 1    9790 Jan  5 2007 us.lsp
-r--r----- 1    3043 Jan  5 2007 us1c.lsp
-r--r----- 1    3301 Jan  5 2007 us1p.lsp
-r--r----- 1   13045 Jan  5 2007 usnt.lsp
```

```
./pkg:
total 56
-r--r----- 1    1888 Jan  5 2007 2p2ct.pkg
-r--r----- 1    1573 Jan  5 2007 rms.pkg
-r--r----- 1    2001 Jan  5 2007 rmsew.pkg
-r--r----- 1    1371 Jan  5 2007 thermcon.pkg
-r--r----- 1     220 Jan  5 2007 vt-rms.pkg
-r--r----- 1     415 Jan  5 2007 vt-rmsew.pkg
-r--r----- 1    3915 Jan  5 2007 vtough.pkg
```

XVI.2[a] NUFT v4.0 Install Information on LLNL Machine Thunder

The NUFT4.0 executables used on AIX5.2PSSP3.5 operating system for SMT, DDT, and LDTH submodels, and MSTHM validation test and 3D-pillar model.

Note: nuft is NUFT4.0 serial executable
 nuft-par is NUFT4.0 parallel executable

directory listing 1:

```
total 24688
-rw----- 1    1036 Jan 05 2007 README
-r----- 1      7 Jan 05 2007 Version
drwx----- 2    4096 Jan 05 2007 lsp
-r-x----- 1 6109546 Jan 05 2007 nuft
-r-x----- 1 6486492 Jan 05 2007 nuft-par
drwx----- 2    4096 Jan 05 2007 pkg
./lsp:
total 312
-r----- 1     956 Jan 05 2007 biofil.lsp
```

```

-r----- 1      438 Jan 05 2007 connect.lsp
-r----- 1     3310 Jan 05 2007 init.lsp
-r----- 1     3412 Jan 05 2007 lin-elas.lsp
-r----- 1     8539 Jan 05 2007 macros.lsp
-r----- 1     3775 Jan 05 2007 num-proc.lsp
-r----- 1     3889 Jan 05 2007 prelude.lsp
-r----- 1    48806 Jan 05 2007 prep.lsp
-r----- 1     4471 Jan 05 2007 read-msh.lsp
-r----- 1      410 Jan 05 2007 trn-slot.lsp
-r----- 1    11986 Jan 05 2007 trn.lsp
-r----- 1     1896 Jan 05 2007 ucheader.lsp
-r----- 1     3358 Jan 05 2007 ucsat.lsp
-r----- 1     9790 Jan 05 2007 us.lsp
-r----- 1     3043 Jan 05 2007 us1c.lsp
-r----- 1     3301 Jan 05 2007 us1p.lsp
-r----- 1    13045 Jan 05 2007 usnt.lsp

```

./pkg:

total 56

```

-r----- 1     1888 Jan 05 2007 2p2ct.pkg
-r----- 1     1573 Jan 05 2007 rms.pkg
-r----- 1     2001 Jan 05 2007 rmsew.pkg
-r----- 1     1371 Jan 05 2007 thermcon.pkg
-r----- 1      220 Jan 05 2007 vt-rms.pkg
-r----- 1      415 Jan 05 2007 vt-rmsew.pkg
-r----- 1     3915 Jan 05 2007 vtough.pkg

```

directory listing 2:

total 24688

```

-rw----- 1     1036 Jan 05 2007 README
-r----- 1         7 Jan 05 2007 Version
drwx----- 2     4096 Jan 05 2007 lsp
-r-x----- 1   6109546 Jan 05 2007 nuft
-r-x----- 1   6486492 Jan 05 2007 nuft-par
drwx----- 2     4096 Jan 05 2007 pkg

```

./lsp:

total 312

```

-r----- 1      956 Jan 05 2007 biofil.lsp
-r----- 1      438 Jan 05 2007 connect.lsp
-r----- 1     3310 Jan 05 2007 init.lsp
-r----- 1     3412 Jan 05 2007 lin-elas.lsp
-r----- 1     8539 Jan 05 2007 macros.lsp
-r----- 1     3775 Jan 05 2007 num-proc.lsp
-r----- 1     3889 Jan 05 2007 prelude.lsp
-r----- 1    48806 Jan 05 2007 prep.lsp
-r----- 1     4471 Jan 05 2007 read-msh.lsp
-r----- 1      410 Jan 05 2007 trn-slot.lsp
-r----- 1    11986 Jan 05 2007 trn.lsp
-r----- 1     1896 Jan 05 2007 ucheader.lsp
-r----- 1     3358 Jan 05 2007 ucsat.lsp
-r----- 1     9790 Jan 05 2007 us.lsp
-r----- 1     3043 Jan 05 2007 us1c.lsp
-r----- 1     3301 Jan 05 2007 us1p.lsp
-r----- 1    13045 Jan 05 2007 usnt.lsp

```

```
./pkg:
total 56
-r----- 1      1888 Jan 05 2007 2p2ct.pkg
-r----- 1      1573 Jan 05 2007 rms.pkg
-r----- 1      2001 Jan 05 2007 rmsew.pkg
-r----- 1     1371 Jan 05 2007 thermcon.pkg
-r----- 1       220 Jan 05 2007 vt-rms.pkg
-r----- 1      415 Jan 05 2007 vt-rmsew.pkg
-r----- 1     3915 Jan 05 2007 vtough.pkg
```

The NUFT4.0 executables in the CD obtained from SCM

directory listing:

```
.:
total 24688
-rw-r----- 1     1036 Jan  5 2007 README
-r--r----- 1        7 Jan  5 2007 Version
drwxr-xr-x  2     4096 Jan  5 2007 lsp
-r-xr-xr-x  1 6109546 Jan  5 2007 nuft
-r-xr-xr-x  1 6486492 Jan  5 2007 nuft-par
drwxr-xr-x  2     4096 Jan  5 2007 pkg
```

```
./lsp:
total 304
-r--r----- 1     956 Jan  5 2007 biofil.lsp
-r--r----- 1     438 Jan  5 2007 connect.lsp
-r--r----- 1    3310 Jan  5 2007 init.lsp
-r--r----- 1    3412 Jan  5 2007 lin-elas.lsp
-r--r----- 1    8539 Jan  5 2007 macros.lsp
-r--r----- 1    3775 Jan  5 2007 num-proc.lsp
-r--r----- 1    3889 Jan  5 2007 prelude.lsp
-r--r----- 1   48806 Jan  5 2007 prep.lsp
-r--r----- 1    4471 Jan  5 2007 read-msh.lsp
-r--r----- 1     410 Jan  5 2007 trn-slot.lsp
-r--r----- 1   11986 Jan  5 2007 trn.lsp
-r--r----- 1    1896 Jan  5 2007 ucheader.lsp
-r--r----- 1    3358 Jan  5 2007 ucsat.lsp
-r--r----- 1    9790 Jan  5 2007 us.lsp
-r--r----- 1    3043 Jan  5 2007 us1c.lsp
-r--r----- 1    3301 Jan  5 2007 us1p.lsp
-r--r----- 1   13045 Jan  5 2007 usnt.lsp
```

```
./pkg:
total 56
-r--r----- 1     1888 Jan  5 2007 2p2ct.pkg
-r--r----- 1     1573 Jan  5 2007 rms.pkg
-r--r----- 1     2001 Jan  5 2007 rmsew.pkg
-r--r----- 1    1371 Jan  5 2007 thermcon.pkg
-r--r----- 1       220 Jan  5 2007 vt-rms.pkg
-r--r----- 1     415 Jan  5 2007 vt-rmsew.pkg
-r--r----- 1    3915 Jan  5 2007 vtough.pkg
```

XVI.3[a] NUFT v4.0 Install Information on LLNL Machine Snowbert

The NUFT4.0 executables used on CHAOS3.1 operating system for SMT, DDT, and LDTH submodels, and MSTHM validation test and 3D-pillar model.

Note: nuft is NUFT4.0 serial executable
 nuft-par is NUFT4.0 parallel executable

directory listing 1:

```

.:
total 29748
-rw----- 1      1036 Jan  5 16:34 README
-r----- 1         7 Jan  5 16:34 Version
drwx----- 2      4096 Apr  5 11:33 lsp
-r-x----- 1 12321722 Jan  5 16:34 nuft
-r-x----- 1 18091870 Jan  5 16:34 nuft-par
drwx----- 2      4096 Apr  5 11:33 pkg

./lsp:
total 152
-r----- 1     956 Jan  5 16:34 biofil.lsp
-r----- 1     438 Jan  5 16:34 connect.lsp
-r----- 1    3310 Jan  5 16:34 init.lsp
-r----- 1    3412 Jan  5 16:34 lin-elas.lsp
-r----- 1    8539 Jan  5 16:34 macros.lsp
-r----- 1    3775 Jan  5 16:34 num-proc.lsp
-r----- 1    3889 Jan  5 16:34 prelude.lsp
-r----- 1   48806 Jan  5 16:34 prep.lsp
-r----- 1    4471 Jan  5 16:34 read-msh.lsp
-r----- 1     410 Jan  5 16:34 trn-slot.lsp
-r----- 1   11986 Jan  5 16:34 trn.lsp
-r----- 1    1896 Jan  5 16:34 ucheader.lsp
-r----- 1    3358 Jan  5 16:34 ucsat.lsp
-r----- 1    9790 Jan  5 16:34 us.lsp
-r----- 1    3043 Jan  5 16:34 us1c.lsp
-r----- 1    3301 Jan  5 16:34 us1p.lsp
-r----- 1   13045 Jan  5 16:34 usnt.lsp

./pkg:
total 28
-r----- 1   1888 Jan  5 16:34 2p2ct.pkg
-r----- 1   1573 Jan  5 16:34 rms.pkg
-r----- 1   2001 Jan  5 16:34 rmsew.pkg
-r----- 1   1371 Jan  5 16:34 thermcon.pkg
-r----- 1    220 Jan  5 16:34 vt-rms.pkg
-r----- 1    415 Jan  5 16:34 vt-rmsew.pkg
-r----- 1   3915 Jan  5 16:34 vtough.pkg

```

directory listing 2:

```

.:
total 12068
-r----- 1         7 Jan 23 12:08 Version
drwx----- 2      4096 Jun  8 20:47 lsp
-r-x----- 1 12321722 Jan 23 12:08 nuft

```

```

drwx----- 2      4096 Jan 23 12:08 pkg

./lsp:
total 212
-r----- 1    956 Jan 23 12:08 biofil.lsp
-r----- 1    438 Jan 23 12:08 connect.lsp
-r----- 1   3310 Jan 23 12:08 init.lsp
-r----- 1   3412 Jan 23 12:08 lin-elas.lsp
-r----- 1   8539 Jan 23 12:08 macros.lsp
-r----- 1   3775 Jan 23 12:08 num-proc.lsp
-r----- 1   3889 Jan 23 12:08 prelude.lsp
-r----- 1  48806 Jan 23 12:08 prep.lsp
-r----- 1   4471 Jan 23 12:08 read-msh.lsp
-r----- 1  11986 Jan 23 12:08 trn.lsp
-r----- 1   1896 Jan 23 12:08 ucheader.lsp
-r----- 1   3358 Jan 23 12:08 ucsat.lsp
-r----- 1   9790 Jan 23 12:08 us.lsp
-r----- 1   3043 Jan 23 12:08 us1c.lsp
-r----- 1   3301 Jan 23 12:08 us1p.lsp
-r----- 1  13045 Jan 23 12:08 usnt.lsp

```

```

./pkg:
total 56
-r----- 1  1888 Jan 23 12:08 2p2ct.pkg
-r----- 1  1573 Jan 23 12:08 rms.pkg
-r----- 1  2001 Jan 23 12:08 rmsew.pkg
-r----- 1  1371 Jan 23 12:08 thermcon.pkg
-r----- 1   220 Jan 23 12:08 vt-rms.pkg
-r----- 1   415 Jan 23 12:08 vt-rmsew.pkg
-r----- 1  3915 Jan 23 12:08 vtough.pkg

```

The NUFT4.0 executables in the CD obtained from SCM

directory listing:

```

.:
total 59520
-rw-r----- 1    1036 Jan  5  2007 README
-r--r----- 1         7 Jan  5  2007 Version
drwxr-xr-x  2    4096 Jan  5  2007 lsp
-r-xr--r--  1 12321722 Jan  5  2007 nuft
-r-xr--r--  1 18091870 Jan  5  2007 nuft-par
drwxr-xr-x  2    4096 Jan  5  2007 pkg

./lsp:
total 304
-r--r----- 1    956 Jan  5  2007 biofil.lsp
-r--r----- 1    438 Jan  5  2007 connect.lsp
-r--r----- 1   3310 Jan  5  2007 init.lsp
-r--r----- 1   3412 Jan  5  2007 lin-elas.lsp
-r--r----- 1   8539 Jan  5  2007 macros.lsp
-r--r----- 1   3775 Jan  5  2007 num-proc.lsp
-r--r----- 1   3889 Jan  5  2007 prelude.lsp
-r--r----- 1  48806 Jan  5  2007 prep.lsp
-r--r----- 1   4471 Jan  5  2007 read-msh.lsp
-r--r----- 1    410 Jan  5  2007 trn-slot.lsp

```

```
-r--r----- 1 11986 Jan 5 2007 trn.lsp
-r--r----- 1 1896 Jan 5 2007 ucheader.lsp
-r--r----- 1 3358 Jan 5 2007 ucsat.lsp
-r--r----- 1 9790 Jan 5 2007 us.lsp
-r--r----- 1 3043 Jan 5 2007 us1c.lsp
-r--r----- 1 3301 Jan 5 2007 us1p.lsp
-r--r----- 1 13045 Jan 5 2007 usnt.lsp
```

./pkg:

total 56

```
-r--r----- 1 1888 Jan 5 2007 2p2ct.pkg
-r--r----- 1 1573 Jan 5 2007 rms.pkg
-r--r----- 1 2001 Jan 5 2007 rmsew.pkg
-r--r----- 1 1371 Jan 5 2007 thermcon.pkg
-r--r----- 1 220 Jan 5 2007 vt-rms.pkg
-r--r----- 1 415 Jan 5 2007 vt-rmsew.pkg
-r--r----- 1 3915 Jan 5 2007 vtough.pkg
```

INTENTIONALLY LEFT BLANK